Corrosion Testing and Modeling of Chloride-Induced Corrosion Deterioration of Concrete Bridge Decks

Soundar Sriram Govindarajan Balakumaran

Dissertation submitted to the faculty of the Virginia Polytechnic Institute and State University in partial fulfillment of the requirements for the degree of

Doctor of Philosophy

In

Civil Engineering

Richard E. Weyers, Chair
Michael C. Brown
Thomas E. Cousins
Carin L. Roberts-Wollmann

March 1, 2012

Blacksburg, VA

Keywords: corrosion, service life, bridge decks, modeling, deterioration, chloride diffusion, concrete, epoxy, overlay, LTBP

Corrosion Testing and Modeling of Chloride-Induced Corrosion Deterioration of Concrete Bridge Decks

Soundar Sriram Govindarajan Balakumaran

ABSTRACT

Modeling of chloride-induced deterioration of bridge decks by using Fick's Second Law of diffusion was performed. The objective of this study is to select suitable input parameters for the model to estimate the service life of bridge decks. Five bridge decks, one in each of the following states, Virginia, Florida, New Jersey, New York, and Minnesota were evaluated.

Data collection process involved visual inspections, damage surveys, corrosion testing including continuity, one-point resistivity, four-point resistivity, half-cell potentials, and three-electrode linear polarization, reinforcement cover depths, chloride samples. The Virginia bridge deck was built with epoxy-coated reinforcement as top reinforcement mat and black bar as the bottom mat. The Florida bridge is a segmental prestressed box girder structure built with black bar. The New Jersey bridge deck was overlaid with latex modified concrete. The New York bridge deck, which was built in 1990, is six inch concrete topping over prestressed adjacent box beams structure with epoxy-coated bar in the negative moment area. The Minnesota bridge was rebuilt in 1984. The deck was rebuilt with epoxy coated reinforcing steel in the top and bottom mats.

The probabilistic Fickian model requires reinforcement cover depths, surface chloride concentration, chloride initiation concentration, and diffusion coefficients as input parameters. The chloride initiation concentration was input via parametric bootstrapping, while the other parameters were input as simple bootstrapping. Chloride initiation concentration was determined from the chloride concentration at the reinforcement bar depths.

The modeling results showed that the deterioration of the Virginia bridge deck was corrosion controlled and the bridge will undergo increasingly severe damage in the future. Florida bridge deck is not undergoing corrosion and will not experience corrosion damage within 100 years. New Jersey bridge deck's service life has been most likely extended by the overlay. Deterioration of the New York bridge was not corrosion controlled, but was related to longitudinal cracking of the topping at match lines of adjacent box beams. Minnesota bridge deck is delaminated and contained a large number of cracks that should be included in service life modeling; otherwise the service life estimate is underestimated.

In addition to service life corrosion performance modeling, analyses were conducted on the relationships and interrelations of resistivity, corrosion potential, corrosion current and chloride at the reinforcing bar depth.

ACKNOWLEDGEMENTS

I am thankful to Dr. Richard Weyers, without whom this research was impossible. I am grateful for his kindness and support during the times when I messed up. I am not being appreciative enough when I say I owe everything I learnt during my masters and doctorate to him.

My committee has been extremely patient and supportive to me throughout the research. Without Dr. Michael Brown's help and guidance, this work would have been far harder. I am grateful to Dr. Cousins and Dr. Wollmann, who have been kind and sympathetic during the times of hardships.

Path to the PhD has been memorable and close to my heart, thanks to my friends and colleagues.

Without a need to say, I am thankful to my parents G. Balakumaran and Chandra Balakumaran, my sister Uma Swaminathan, my grandmother Pankajam, and relatives, who have been my moral support all the time.

நான் முனைவர் பட்டம் பெறுவதற்கு மனதளவில் உறுதுணையாய் இருந்த என் பெற்றொர் கோ. பாலகுமரன், சந்திரா பாலகுமரன், என் அக்கா உமா சுவாமிநாதன் மற்றும் என் பாட்டி பங்கஜம் அம்மாள் அவர்களுக்கும் என்னுடைய நன்றிகள். நண்பர்கள் மற்றும் உறவினர்களின் அன்பும், ஆலோசனைகளும் ஆதரவாய் அமைந்தது.

எப்பொருள் யார்யார்வாய்க் கேட்பினும் அப்பொருள்
மெய்ப்பொருள் காண்ப தறிவு.

குறள் 423

Though things diverse from divers sages' lips we learn,
'Tis wisdom's part in each the true thing to discern.

Thirukkural 423
G. U. Pope Translation.

TABLE OF CONTENTS

LIST OF TABLES

LIST OF FIGURES

INTRODUCTION

According to National Transportation Report in 2010, there are 603,259 bridges in the United States, where about 11.8 percent (71,177) of the bridges are structurally deficient and about 13.0 percent (78,477) of the bridges are functionally obsolete, as of December 2009. A bridge structure becomes functionally obsolete when it does not conform to the current building standards, and a structurally deficient bridge contains highly deteriorated load carrying elements that may need significant repair, rehabilitation or even replacement. Damages to load carrying elements are mostly attributed to the accelerated deterioration by chloride-induced corrosion, and other causes such as vehicle collisions, aging of structure increased by increased traffic demand, increased truck traffic, and severe weather conditions.

Bridge management systems and databases are being utilized in the scheduled maintenance activities by the state DOTs. Still, many unknown factors influence the bridge deterioration rates and the causes of which are to be addressed. Detailed service life models, improved life cycle cost prediction tools, better bridge health monitoring systems, and efficient inspection techniques are sought for supplementing the existing bridge maintenance protocols.

Federal Highway Administration (FHWA) launched a program called Long term Bridge Performance (LTBP), the focus of which is to better understand the performance of bridge structures and the factors affecting them. This research study, a part of the LTBP pilot study, focuses on the chloride-induced corrosion of bridge deck reinforcement and deterioration associated with it.

LITERATURE REVIEW

BRIDGE DECKS IN UNITED STATES

USDOT report states that, out of the highway bridges in the United States, as of 2006, approximately 75.5 percent are located in the rural areas. About 46.8 percent of the bridges were built before 1966, which were not built with special corrosion prevention techniques (FHWA Report 2008). Many corrosion protection methods were employed, starting in the 1970s, in order to extend the service life of bridge structures, such as using coated reinforcement, overlaying the deck with low permeability concrete, using cementitious pozzolons, installing cathodic protection systems, and using reinforcement materials with high corrosion resistance. Some of the corrosion protection methods, which will be addressed in this study, are discussed in the following chapters.

Epoxy-Coated Reinforcement

To prevent ever-increasing corrosion damages in bridge structures, epoxy-coated reinforcements were introduced as a corrosion prevention method in the late 1970s. Sufficient research was not conducted on the performance of epoxy-coated reinforcements (ECR) before replacing black bars in concrete (Zemajtis, J. et al. 1996). The use of ECR became popular partly due to the assumption that the environment to which the reinforcement steel were exposed was similar to other environments where the material was employed successfully, especially the pipeline industry (Ramniceanu, A. 2007).

Commonly used epoxy resin is made from Bisphenol-amine (Bisphenol-A or BPA, Molecular Formula: $C_{15}H_{16}O_2$). From the total amount of BPA produced, 20 percent was used for producing epoxy resins in US, as reported in the year 2007 (US Environmental Protection Agency). Production of epoxy resins, also called as ethoxyline resins, involves the condensation of BPA and epichlorohydrin (C_3H_5ClO) (Brown, M.C. 2002). The mechanical properties of BPA epoxy resin include high ductility, low shrinkage when curing, and moderate heat resistance, thus the material was found suitable for reinforcement coating (Manning, D.G. 1996). The epoxy resin can be applied to a reinforcement bar either in liquid state or powder.

The liquid epoxy resin is prepared by mixing epoxy resin and polyamine in a two-part system. It can be applied by immersing the reinforcement bar in a resin bath. Rough application of epoxy coating is possible by either brushing or spraying on the reinforcement, which is typically carried on in the field for rectifying any damage.

Most commonly, the epoxy coating is applied by fusion-bonded powder method. Powder resin, with an electrostatic charge, is applied on clean preheated reinforcement bar, at an application temperature of 204 C to 230 C (400 F to 446 F). The charged powder is attracted to the preheated steel and melts to form a continuous uniform coating. Then the coated bar is quenched to form a solid coating. This method of application ensures more uniformity and fewer faults than the liquid resin method.

Epoxy coating over the reinforcement should provide corrosion resistance because of its inherent physical-chemical properties. Corrosion resistance may increase by using coatings in one of the four mechanisms presented as follows (Revie, R.W. 2000).

1. Resistance inhibition – being an insulating material, epoxy coating inhibits the ionic movement towards the reinforcement. Thus, the moisture passing through the coating will have high electrical resistance.
2. Oxygen deprivation – oxygen diffusion is slowed down, resulting in slower corrosion reactions.
3. Cathodic protection – introducing a less noble metal or pigment in the coating can act as a sacrificial anode.
4. Inhibition or aestivation – material diffusing through the coating may result in the formation of protective passive layer over the reinforcement bar.

A study was conducted on the performance of ECR bars. The conclusions derived from this study are presented as follow (Ramniceanu, A. 2007).

1. Coatings extracted from the samples that were at least 15 years old showed more cracking than the new samples.
2. Frequency of cracks in the coatings correlated well with concentration of chlorides at the reinforcement level, residual adhesion, moisture content in the coating, and coating color.

3. Differential scanning calorimetry (DSC) method was used to determine the curing state of the coating. The measurements showed that both the extracted aged samples and new samples were not fully cured during the manufacturing process. Inadequate curing often results in higher number of holidays and moisture absorption.
4. Coating degree of curing indicated that the bars were inadequately and unevenly heated before the coating application.
5. As adhesion is lost between the coating and the reinforcement, corrosion will proceed unrestrained even with no chloride presence.

Adhesion loss was observed in a study conducted on ECR performance in 4-year-old bridge decks and the reason for the adhesion loss was found to be the accumulation of moisture rather than chlorides (Pyć, W.A. 1998).

A study was conducted on the effect of ultra-violet (UV) rays and aggressive environments, such as the presence of sulfuric acid, sodium chloride, and potassium hydroxide, on the epoxy coating performance (Kotnarowska, D. 1999). Sets of epoxy coatings were exposed to UV rays, 5% solutions of sulfuric acid, sodium chloride, and potassium hydroxide for 1008 hours. Conclusions drawn from the study are presented as follows.

1. Ageing with 5% potassium hydroxide and 5% sodium chloride solutions caused band-shaped (strips) cracks, while 5% sulfuric acid solution caused circle-shaped cracks around blisters.
2. UV radiation caused the heaviest destruction of epoxy material. It generated characteristic cracks called silver cracks, which are shiny due to the formation of pores. Silver cracks can develop into larger cracks causing fracture.
3. Ageing changes introduce reduction of mechanical properties of epoxy coating such as hardness, static and dynamic strength.

Brown concluded in the study of service life performance of ECR bars that the service life extension provided by ECR can be as little as 5 years longer than uncoated bar (Brown, M.C. 2002). The time for corrosion initiation to cracking of the surrounding concrete for uncoated reinforcement bars (UCS) is about 6 years (Liu, Y. 1996). Thus, the total time between corrosion initiation and cracking of the cover concrete could be estimated at about 11 years.

Bridge Decks with Uncoated Steel Reinforcement

As stated before, about 46.8 percent of all bridge decks in the US were constructed before 1966. Epoxy-coated reinforcements became one of the most popular corrosion prevention methods in bridge decks after about 1978 (Weyers et al. 1994). Prior to that period, the corrosion resistance methods were limited to conventional practices such as low permeable concrete, increased cover depths, and better drainage systems. Air entrainment was a common practice during that period, thus corrosion damage due to chloride diffusion often dominates (Weyers et al. 1994).

As a part of Strategic Highway Research Program (SHRP), a number of bridge decks were selected for analysis. About 47 decks from NY, 234 decks from PA, and 120 decks from VA were selected, where the average service was about 20 years. Figure 1 represents the mean service life of the decks from each state against the failure frequencies (Weyers et al. 1994).

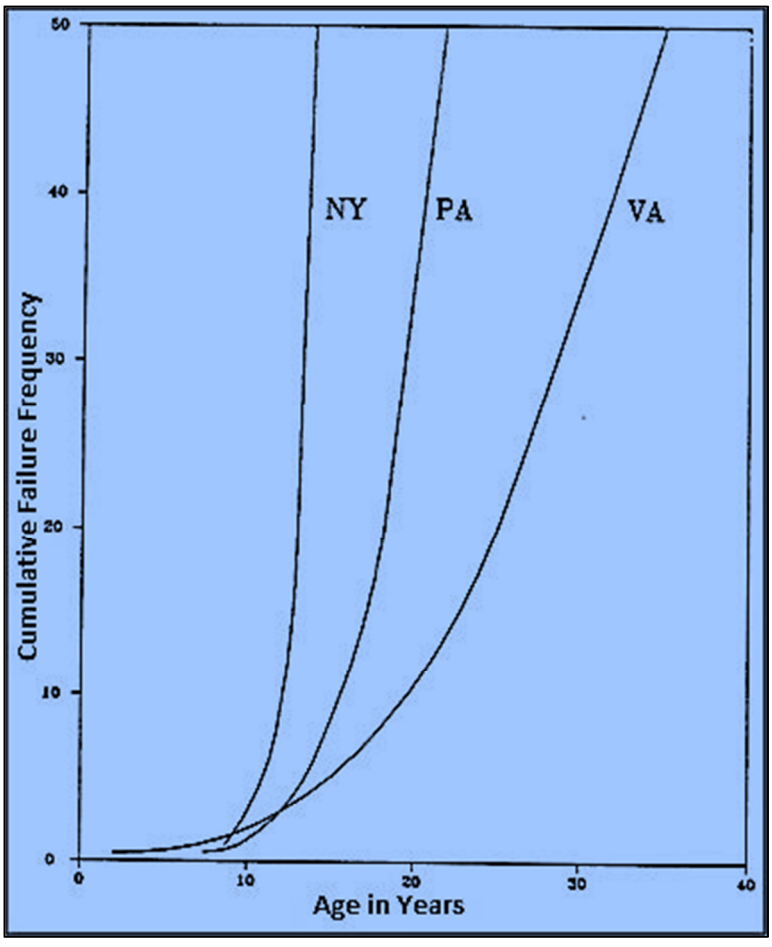

Figure 1 – Normalized Service Life Distributions for Bridge Decks with UCS

It is clear that the bridge decks of VA have higher life expectancy than PA bridges, and PA bridges have higher service life expectancy than NY bridges. Figure 2 shows the deicing salt usage per annum for the corresponding three states and associated mean service life (Weyers et al. 1994).

Figure 3 shows the relationship between mean service life and the mean snowfall per annum. As expected, comparing the plots show that with increasing snowfall comes increased salt usage, which results in shorter service life for the bridge decks. Importance of this relationship is that it can be stated quantitatively for such a wide range of bridge decks (Weyers et al. 1994). Thus, it may be possible to predict the service life of bridge decks in a different weather region.

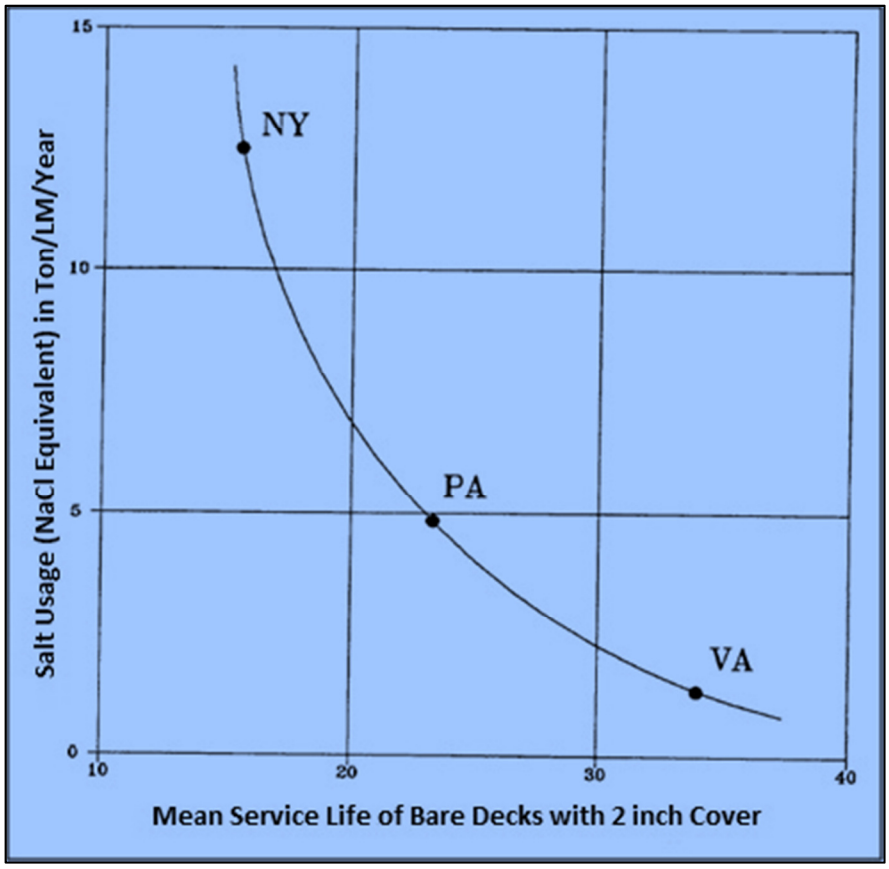

Figure 2 – Salt Usage and Service Life of Bridge Decks with UCS

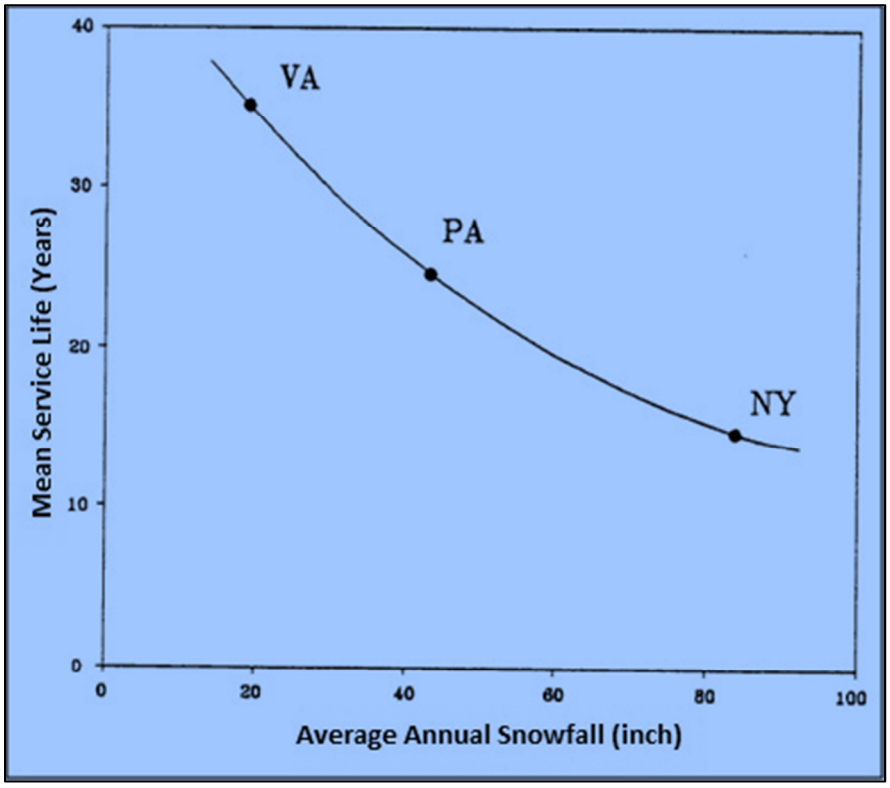

Figure 3 – Service Life vs. Mean Annual Snowfall for Bridge Decks with UCS

Overlaid Bridge Decks

Chloride diffusion is the primary mode by which the corrosion of bridge deck reinforcements initiates and cause significant damage to the structure. Overlaying the deck with a low-permeability, high-strength concrete is a corrosion protection method, which can significantly slow the diffusion of chlorides and other impurities to the level of reinforcement. Also, overlays are placed on the bridge decks in order to improve the skid resistance, riding quality, drainage, and appearance of the surface (Sprinkel, M.S. 2004). Deck overlays were generally used either as a method of maintenance or rehabilitation of the bridge decks.

When used as a repair, the deck overlay is placed on the existing sound concrete surface after surface cleaning. This is conducted in locations where significant bridge deck deterioration has not begun. The base concrete surface is cleaned by blasting and wetted before applying the overlay to ensure good bonding. If a bridge deck exhibits major damage then the damaged areas are addressed before overlaying with patching concrete, which is called as rehabilitation. Deck areas showing active corrosion or high deterioration must be removed, patched and then the overlay is

applied, otherwise the cause of the problem is left unaddressed. Following the overlaying of the deck during rehabilitation, it has been estimated that the service life added to the structure is up to 70 years (Weyers et al. 1993).

There are certain problems with overlays, which could potentially worsen the condition of the rehabilitated bridge. Problems may arise in one or more of the characteristics of overlays, such as bond strength, shrinkage crack formation, and permeability.

Bond Strength

According to historical data, major overlays have, in some cases, delaminated over large areas even before being opened to the traffic (Sprinkel, M.S. 2004). Delamination formations always point towards poor bond strengths between overlay concrete and base concrete, where poor bond strengths point towards inadequate surface preparation. Commonly used surface preparation techniques are milling, shot-blasting, grit-blasting, and hydro-blasting. While being the most economical method of concrete removal, milling may fracture the surface of the base concrete (Sprinkel, M.S. 2004). The fractured surface of base concrete reduces the bond strength and may result in delaminations near the interface of base concrete and overlay. Thus, it is recommended to use a blasting technique after milling has been conducted, to remove the fractured concrete.

Shrinkage Cracks

Shrinkage of concrete is a volumetric phenomenon that results in the overall reduction of dimensions. Being the hardest component of concrete, the coarse aggregates provide resistance to the volumetric shrinkage (Ramniceanu, A. et al. 2010). A study conducted by Buchanan P.M. on shrinkage of LMC overlays, and the factors affecting it resulted in the following conclusions (Buchanan, P. 2002).

1. Increase in the cement content of concrete results in the increase of shrinkage.
2. Latex content did not have a significant effect on the shrinkage.
3. Increasing the $^{w}/_{c}$ ratio of the concrete mixture significantly increases the shrinkage.
4. Moist curing duration did not have a significant effect on the shrinkage values.

5. Though no significant differences could be found in the shrinkage values of LMC and micro silica concrete (MSC), shrinkage cracking is more widespread and severe in the field MSC specimens.

Sprinkel states, “Overlays are rarely free of cracks” (Sprinkel, M.S. 2004).

Permeability

Deck overlays are expected to have considerably lower permeability and higher density than base concrete, in order to reduce the diffusion of chlorides and aggressive materials. Generally the use of pozzolons increases the resistance to diffusion. However, the overlay placement procedure can negatively affect the permeability of the concrete. A study conducted on deck overlays of bridge structures in Virginia, placed in 1996, has shown low to very low permeability after 4 years of service life (Sprinkel, M.S. and Ozyildirim, C. 2000).

Deck overlays can be either latex modified concrete (LMC), low-slump dense concrete (LSDC), polymer concrete (epoxy), micro-silica concrete (MSC), or hot mix asphalt concrete and membrane (HMAM) systems. Background information and properties of LMC and LSDC overlays will be discussed in the following chapters as these are the most used systems.

Latex Modified Concrete (LMC) Overlay

Latex is a colloidal dispersion of styrene butadiene in water (Kuhlmann, L.A. 1985). A stabilizer is introduced in order to increase the freeze-thaw resistance. Advantage of latex is that when added to concrete, water content can be reduced between 20 and 30 percent. Lower $^{w}/_{c}$ ratio ensures lower permeability and high strength, which is desired in a deck overlay concrete. Also, latex coats the micro cracks in concrete, due to its elasticity and high bond strength, which decreases the permeability of concrete and increases bond strength (Kuhlmann, L.A. 1985).

A study conducted by Weyers et al. included 136 bridge decks from 19 states, that had LMC overlay (Weyers et al. 1994). The analysis was conducted in two ways; all the data sets combined, called national data base analysis, and specific data sets, called agency studies or case studies.

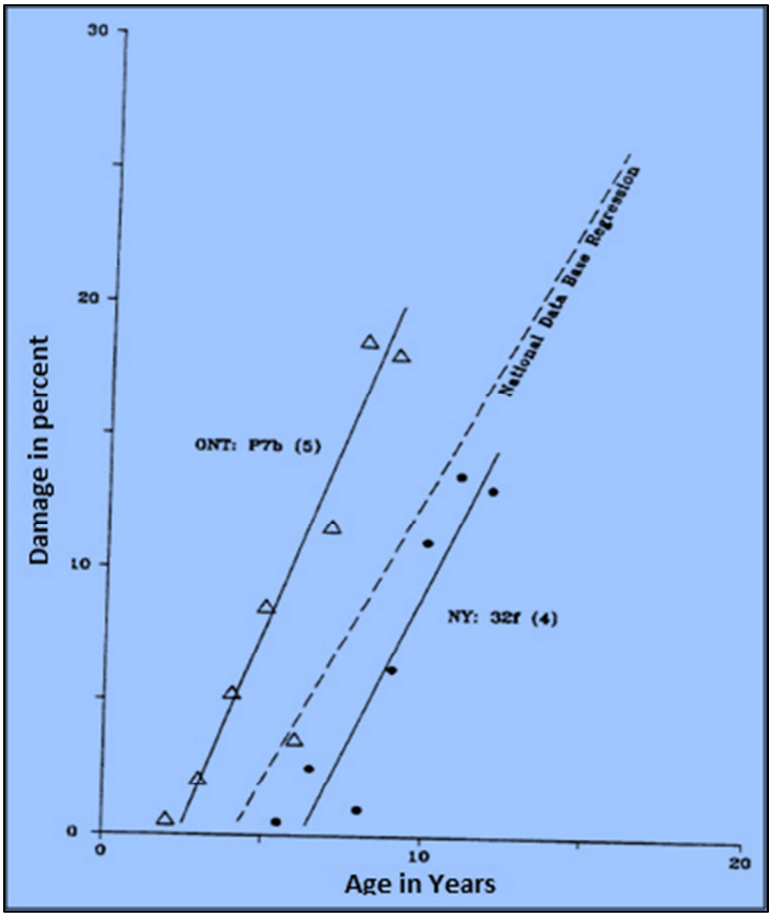

Figure 4 – Regression of Performance Data for Individual LMC Overlay Decks

Figure 4 presents the regression analysis of 2 data sets, and the national data base. It can be observed that the national data base predicts over 10% damage at 10 years, whereas specific locations have greater or lesser damage in 10 years. Damage percentage is the sum of the delaminated, spalled, and patched areas on the deck.

Low Slump Dense Concrete (LSDC) Overlay

LSDC is same as that of ordinary portland cement concrete, except that the slump is kept very low, generally less than one inch. Low slump indicates lower $^{w}/_{c}$ ratio, high strength, high density, low permeability, but low workability as well.

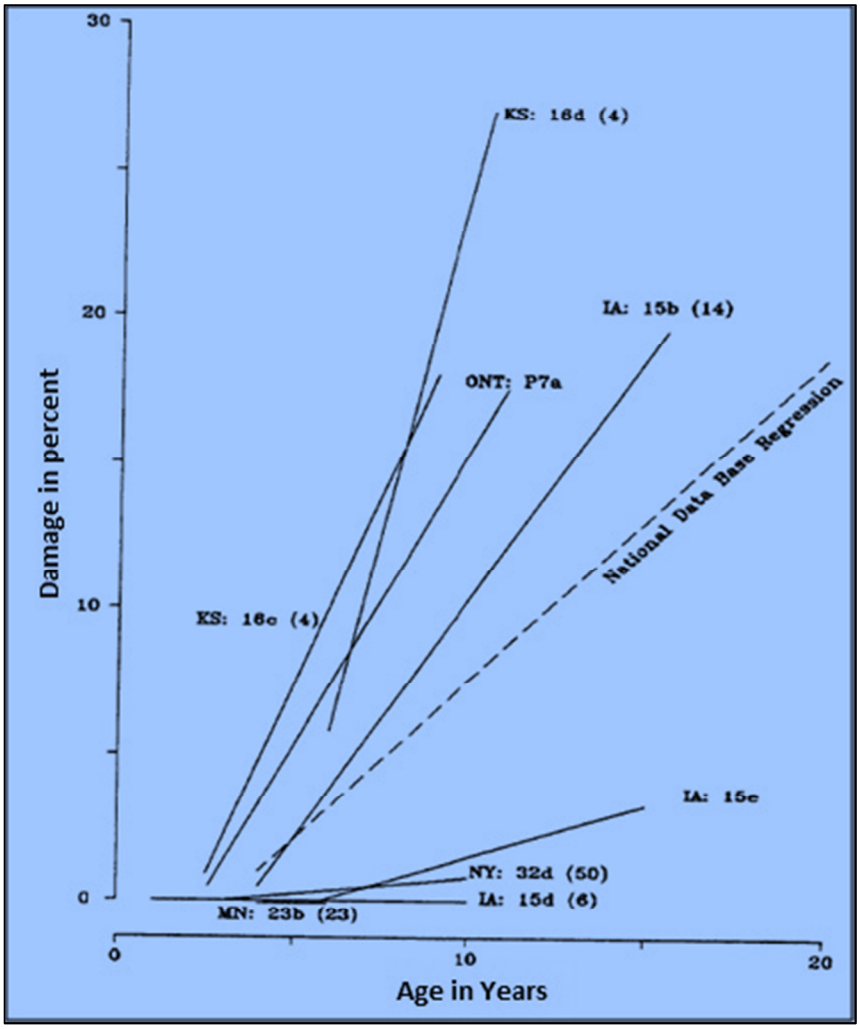

Figure 5 – Regression of Performance Data for Individual LSDC Overlay Decks

A study conducted by Weyers et al. included 155 bridge decks from 17 states that had LSDC overlay (Weyers et al. 1994). The analysis was conducted in two ways; all the data sets combined, called national data base analysis, and specific data sets, called agency studies or case studies. Most decks under study were located in moderate or severe environments based upon the mean annual snowfall and traffic. It was found by experience that spalling often lags the occurrence of delamination, at least for the first 15 to 20 years of their life (Weyers et al. 1994). A regression analysis was conducted by taking individual data sets and the national data base (Figure 5). It can be observed that the national data base shows less than 10 percent damage at the age of 10 years, which is slightly better than the performance of LMC overlays. Again, performance was dependant upon specific locations.

A comparison study between the LSDC and LMC decks was conducted, where all the LMC decks and those LSDC decks which have service life projections from 13 to 29 years, see Figure 6.

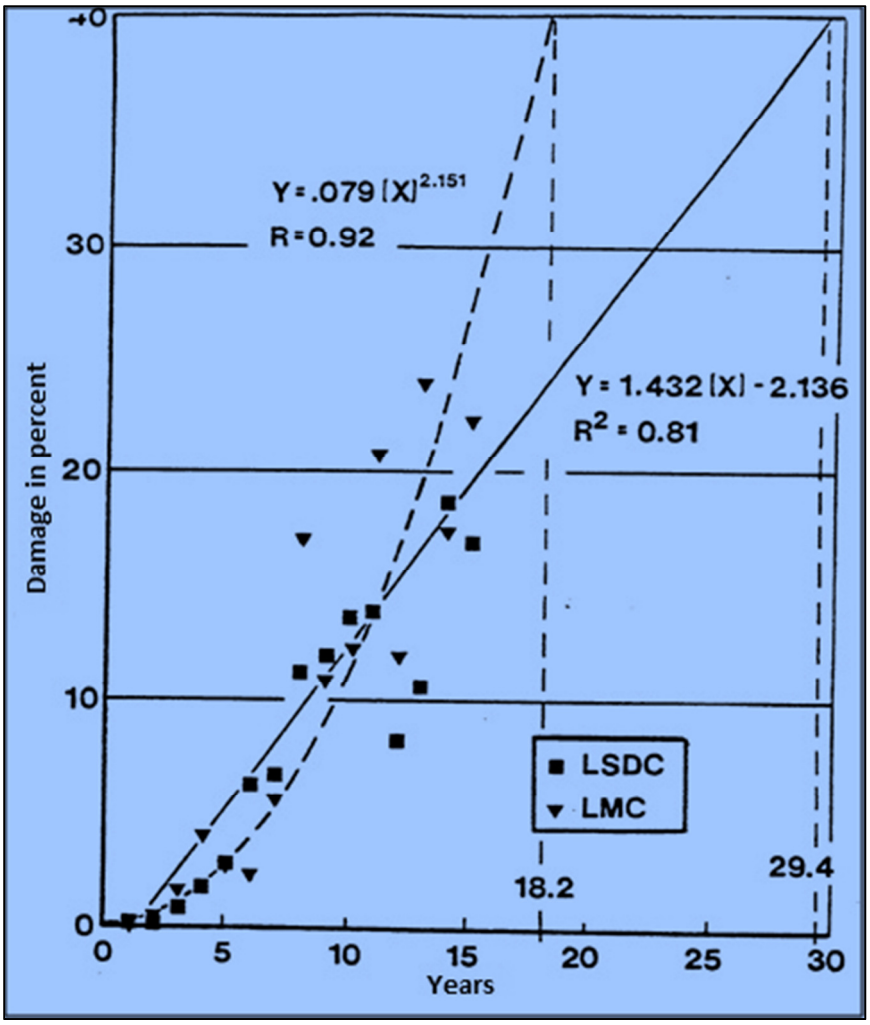

Figure 6 – Performance of LMC and Selected LSDC Decks

From Figure 6, it can be noted that there are no significant differences between LSDC and LMC decks, at least in the first 10 years where there are mode data points. Both straight and curved line fits are shown in the plot, since the overlay decay curve is unknown. The average of the two fits gives 24 years of service life for LSDC and LMC deck overlays (Weyers et al. 1994).

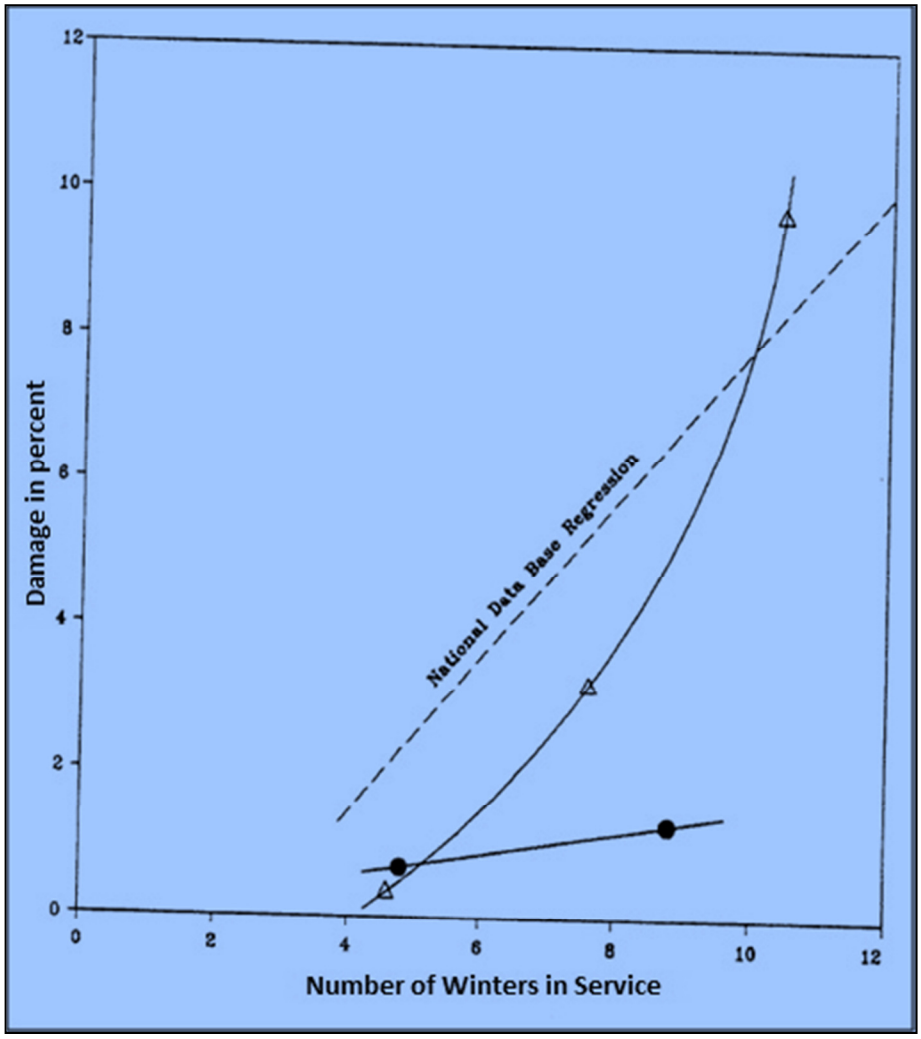

Figure 7 – Performance of LSDC Overlaid and Bare Bridge Decks of New York

A comparison plot between the LSDC overlaid decks and the bare decks is shown in Figure 6. The triangular marks indicate bare decks and the shaded circles indicate LSDC decks. It can be observed that before five winters of service, the bare decks exhibit lower damage than the LSDC decks. After five winters of service, the damage undergone by the bare decks increases exponentially, while the LSDC decks have experienced significantly lower damage rate (Weyers et al. 1994).

Polymer Concrete Overlay

Polymer concrete overlays, when laid, can reduce the diffusion of moisture and chloride into the deck and improve skid resistance. Commonly used binders for polymer concrete and mortars are epoxy, polyester styrene, and methacrylate. Similar to other overlays, polymer concrete overlays will not be effective over severely chloride contaminated cover concrete. Three forms of overlays

are used such as multiple-layer, slurry, and premixed (Weyers et al. 1994). Multiple-layer polymer overlay consists of two or more layers of polymer binder and broadcast angular-grained aggregate. Slurry overlay consists of polymer aggregate struck off with gauge rakes and covered with broadcast aggregate for skid resistance. Premixed overlay consists of concrete mixture struck off with a vibratory screed. Since the deterioration of the polymer concrete overlays is controlled by skid resistance, adhesion loss, corrosion-induced spalling, and chloride diffusion, the average daily traffic may have an influence on the overlay health.

The service life extension as a result of different forms of polymer concrete overlay through field evaluations are (Weyers et al 1994):

- Multiple-layer Epoxy 25 years
- Multiple-layer Epoxy-Urethane 25 years
- Premixed Polyester 25 years
- Methacrylate Slurry 18 years
- Multiple-layer Polyester 10 years
- Multiple-layer Methacrylate 15 years

Percent Damage Models

In order to predict damage in the bare, LMC overlaid, and LSDC overlaid bridge decks, over 530 models were investigated (Weyers et al. 1994). PRESS statistic, which indicates the extent to which any multiple regression model can be generalized, was utilized in comparing the deck damage models. Models were developed based on the either the total percent damage over the whole deck or the percent damage for the worst lane of each bridge. Four models were finalized for the whole deck percent damage and at least three models were finalized for the worst-lane percent damage. All the models involved one or more of the following predictor variables in the form of regression equations.

1. Percent damage as dependent variable,
2. Dummy variable to represent if the deck was overlaid or not,
3. Age of deck,
4. Age of overlay,
5. Average annual daily traffic volume,
6. Snowfall,

7. Reinforcement size,
8. Half-cell potentials,
9. 3LP corrosion rate,
10. Resistance of concrete,
11. Cover depth
12. Chloride content at reinforcement level,
13. Cumulative snow before rehabilitation (snowfall * age)

Best models among each group of models were selected, but a model that can represent a wide number of deck percent damage was not found. Even if a model was found with large R-squared values and low standard deviations, they required a large number of field measurements as input parameters (Weyers et al. 1994).

Corrosion Rate Models

In order to predict the corrosion rate of the bridge decks, over 330 models were investigated (Weyers et al. 1994). Two models were finalized from a group of models; one for bare bridge decks, and other for overlaid bridge decks combined. Model for predicting bare bridge deck 3LP corrosion rate is shown in Equation 1, which involves the half-cell potentials and the cumulative snowfall throughout the age of the bridge deck. The model has a standard deviation of 0.804 and sum of squared errors (SSE) of 5.17 and feasible predictor parameters.

$$i_{corr} = 0.00636 * Potential + 0.000959 * Snow\ Age \quad \text{Eqn. 1)}$$

Where, i_{corr} = average 3LP corrosion rate, mA/ft^2,
$Potential$ = average CSE half-cell potential, mV,
$Snow\ Age$ = average cumulative snow = age of bridge deck * average annual snowfall, in

Model for predicting 3LP corrosion rate of overlaid bridge decks is shown in Equation 2, which involves half-cell potentials, cumulative snow age, and concrete resistance (Larsen, E. 1993). The model has a standard deviation of 0.556, relatively high SSE of 8.3, and feasible predictor parameters.

$$i_{corr} = 0.00227 \cdot Potential + 0.000871 \cdot Snow\ Age + 0.639/Resistance \quad \text{Eqn. 2)}$$

Where, $Snow\ Age$ = cumulative snowfall from deck construction to time of rehabilitation, inch,

$Resistance$ = average concrete resistance, ohms

The 3LP corrosion rate can be predicted for bridge deck overlay systems with potentials ranging from an average of -91 to -333 mV CSE, resistances from an average of 580 to 6110 ohms, and total cumulative snow ranging from an average of 53 to 2520 inch (135 to 6400 cm) (Larsen, E. 1993).

Effect of Pozzolons

Pozzolons are siliceous materials which are used to replace part of cement in a concrete mixture to improve the qualities of concrete such as permeability and strength. Pozzolons do not possess cementitious properties on their own; however they can attain cement-like properties while used with portland cement in concrete. Since chloride diffusion to the reinforcement level has been identified as the primary source of concrete deck deterioration, the use of pozzolons must increase the corrosion resistance of concrete in general.

Williamson predicted the service life of bridge decks with pozzolons and with no pozzolons, as a validation of his service life model (Williamson, G. 2007). Input parameters for the model include diffusion constants, concrete cover depths, and surface chloride contents. Three bridge deck sets were selected with 0.45 $^{w}/_{c}$ ratio with no pozzolons, 0.45 $^{w}/_{c}$ ratio with pozzolons, and 0.47 $^{w}/_{c}$ ratio with no pozzolons. The averages of the input parameters are presented in the Table 1, along with variability (Williamson, G. 2007).

Table 1 – Input Parameters for Service Life Model

Parameter	0.45 $^{w}/_{c}$ ratio with no pozzolons	0.45 $^{w}/_{c}$ ratio with pozzolons	0.47 $^{w}/_{c}$ ratio with no pozzolons	Mean	Std. Dev.
Diffusion Coefficients ($mm^2/year$)	26.3	3.45	10.93	13.6	11.6
Surface Chlorides (kg/m^3)	3.47	3.95	3.53	3.65	0.26
Cover Depths (mm)	59.4	61.5	52.18	57.7	4.9

From Table 1, it can be observed that the diffusion constants are highly variable, while the surface chlorides and cover depths are not as variable. The service life estimates from the model are presented in Table 2 for the three bridge sets (Williamson, G. 2007).

Table 2 – Service Life Estimates of Pozzolons and No-Pozzolons Bridge Decks

	0.45 $^{w}/_{c}$ ratio with no pozzolons			**0.45 $^{w}/_{c}$ ratio with pozzolons**			**0.47 $^{w}/_{c}$ ratio with no pozzolons**		
	Time (year)	SD (year)	CV (%)	Time (year)	SD (year)	CV (%)	Time (year)	SD (year)	CV (%)
Time to 2% Initiation	21	0.4	1.9	169	4.8	2.8	31	1.5	5.0
Estimated Service Life	43	-	-	191	-	-	53	-	-

Time to 2 percent damage in the worst lane of a bridge deck is taken as the time for corrosion initiation in the model. It can be noted that the bridge decks with pozzolons have a significantly higher service life values than the bridge decks with no pozzolons. Also as a side note, it can be observed that the increase of $^{w}/_{c}$ ratio from 0.45 to 0.47 had little effect; in fact the higher $^{w}/_{c}$ ratio had negligible impact on the service life compared to the addition of pozzolons. Shorter service life of the 0.45 w/c specified decks compared to the concrete decks with 0.47 w/c is most likely related to construction quality procedures used in the newer 0.45 w/c decks (Williamson, G. 2007).

CORROSION CONDITION ASSESSMENT METHODS

Quantification of corrosion is a difficult task. However, various measurement techniques an integrative analysis may be conducted to assess the state of corrosion. Selection of test methods for the corrosion condition assessment depends upon the time, cost, and ease with which the test can be conducted (Berkeley, K. and Pathmanaban, S. 1990).

Electrical Potentials

Flow of electrons between anodes and cathodes occurs as a part of the corrosion mechanism. The electrical potential of the system will provide information about the presence of active corrosion. It will, however, not give any information on the rate of loss of metal. The test is preferred for field structures because a large number of measurements can be taken quickly, and thus inexpensively (Mehta, K.P. 2005).

ASTM C 876-09 presents the method for conducting the half-cell potential test either in the field or laboratory (ASTM C 876-09). Since corrosion is an electrochemical process, the potential of the ferrous environment of steel reinforcement can be found by connecting a standard reference half-cell and forming an electrochemical cell. A standard copper-copper sulfate (CSE) reference electrode is commonly used in the half-cell potential test. Other reference electrodes such as silver-silver chloride and mercury-mercury oxide may also be used.

Standard reference half-cell when placed on the concrete surface, after making electrical contact to the steel reinforcement, measures the potential difference, with a voltmeter connected in the circuit. The positive terminal of the voltmeter connects to the steel reinforcement and the negative terminal connects to the reference half-cell. A positive low-resistance connection method to the reinforcing steel must be made. One method used on bridge decks is to drill, tap, and screw in a stainless steel rod into the reinforcing steel at selected locations. Electrical continuity between the select locations must be established prior to making potential measurements. Figure 8 illustrates the CSE half-cell apparatus.

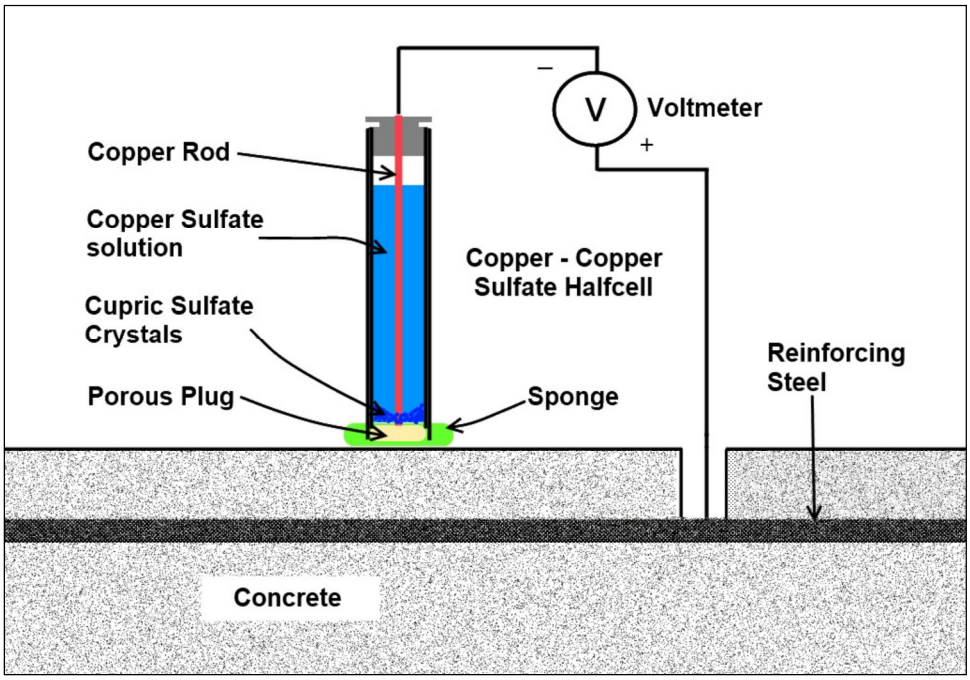

Figure 8 – Half-Cell Potential Apparatus

As setup in Figure 8, the corrosion potential readings are negative since ferrous ions have lower electrode potential than the standard copper-copper sulfate half-cell and the electrons flow from the negative steel to oxidizing standard half-cell (Broomfield, J.P. 2007). Less negative potentials generally indicate high passivity of steel, while higher negative potentials indicate possible break-down of the passive layer and corrosion initiation. Saturated condition in concrete can also result in highly negative potentials, where there is no corrosion activity due to the lack of oxygen. The electrical potential is a measure of the thermodynamics of the corrosion, not the corrosion rate (Broomfield, J.P. 2007). Table 3 presents a generally accepted interpretation of CSE potential values for reinforcing steel in concrete.

Half-cell potential mapping may be used to locate the positions for destructive testing such as core sampling, chloride sampling, and corrosion rate measurement. Moreover, the potential mapping can be used for identifying areas of bridge decks for repair works (Berkeley, K. and Pathmanaban, S. 1990).

Table 3 – Interpretation of Half-Cell Potentials against CSE Reference Electrode for Uncoated Bars

Measured Potential (mV vs. CSE)	Corrosion Probability
> -200	Low, less than 10%
-200 to -350	Uncertain
< -350	High, greater than 90%

ASTM C 876-09 states specifically that the half-cell potential test and its interpretation are for uncoated bars. In a study conducted by Balakumaran on corrosion of UCS, the test specimens were studied for 45 months by ponding with a chloride solution for corrosion initiation (Balakumaran 2010). Based on the corrosion test results, six test specimens were autopsied to check the correlation between the actual corrosion and the corrosion test results. Using the results of the aforementioned test, corrosion risk interpretation was formed for the measured CSE potential values, see Table 4.

Table 4 - Interpretation of Half-Cell Potentials against CSE Reference Electrode for Uncoated Bars

Measured Potential (mV vs. CSE)	Corrosion Risk
> -200	Low
-200 to -300	Moderate
< -300	High

Epoxy coating, being dielectric, is not expected to exhibit stable, interpretive half-cell readings. However, Ramniceanu has shown that half-cell potential test can be conducted on ECR bars that have been in service for sufficient time for epoxy to absorb moisture and become electrically conductive (Ramniceanu, A. 2004). Also, the half-cell potential readings were found to be stable on ECR bars and were normally distributed. But, no recommendations on interpretation of half-cell potentials over ECR bars are provided.

Linear Polarization

Linear polarization is a perturbation method of measurement, which includes controlled disturbance of an existing system by an external influence, thus is not a non-destructive method (Berkeley, K. and Pathmanaban, S. 1990). Perturbation is performed by either supplying varying external current called the galvanostatic method or by supplying small potential changes called the

potentiostatic method. A simplified method, called the polarization resistance method, involves application of around 20 mV voltage in known increments through counter electrodes and the input current is measured (Berkeley, K. and Pathmanaban, S. 1990).

Three-electrode linear polarization (3LP) method, which is a potentiostatic method, is one of the commonly used linear polarization methods to measure corrosion current. This technique requires the polarization of steel by passing electricity from a variable low voltage DC power supply (Broomfield, J.P. 2007).

The 3LP test method is based on the Stern-Geary characterization of a polarization curve for corrosion. The method utilizes three electrodes. The steel bar that is tested for corrosion rate is called the working electrode (Clear, K.C. 1989). The reference electrode is a standard half-cell, typically CSE, which is used for measuring the potential changes in the steel bar (Clear, K.C. 1989). The third electrode is called a counter electrode, which is a conductive metallic mesh used to introduce current into the concrete and the reinforcing steel (Clear, K.C. 1989). The counter electrode is placed over a sponge on the surface of the concrete directly above the reinforcing steel. A current is applied through the counter electrode into the concrete reinforcement and the corresponding potential change is sensed by standard half-cell and recorded. Using the Stern-Geary equation, the corrosion current (Icorr) is calculated.

Stern-Geary equation is as follows.

$$\boldsymbol{I_{corr}} = \frac{\Delta \boldsymbol{I_{appl}}}{\boldsymbol{2.3}\Delta\emptyset} . \frac{(\boldsymbol{\beta_a} . \boldsymbol{\beta_c})}{(\boldsymbol{\beta_a} + \boldsymbol{\beta_c})} \qquad \text{Eqn. 3)}$$

Where, I_{corr} = corrosion current, mA

I_{appl} = current required to polarize the rebar by different potential values

$\Delta\emptyset$ = absolute value of polarization potential minus the half cell potential

β_a = anodic tafel slope

β_c = cathodic tafel slope

$$R_p = \frac{B}{i_{corr}} \qquad \text{Eqn. 4)}$$

$$B = \frac{\beta_a . \beta_c}{2.3(\beta_a + \beta_c)} \qquad \text{Eqn. 5)}$$

Where, R_p = polarization resistance, ohms

i_{corr} = corrosion current density, µA/cm^2

B = constant value between 26 and 52 (mV), a value of 40 is used in the unguarded 3LP device (Clear, K.C. 1989)

Table 5 – Interpretation of Corrosion Current Density Values for Uncoated Bars

Corrosion Current Density ($\mu A/cm^2$)	Expected time for corrosion
i_{corr} < 0.2	No corrosion damage expected
i_{corr} = 0.2 to 1.0	Corrosion damage possible in 10-15 years
i_{corr} = 1.0 to 10	Corrosion damage expected in 2-10 years
i_{corr} > 10	Corrosion damage expected in 2 years or less

Table 5 presents the commonly accepted interpretation of corrosion current density values for bare reinforcing steel (Clear, K.E. 1989). In the study conducted on bare steel corrosion, corrosion risk interpretation was found as shown in Table 6 (Balakumaran, S. 2010).

Table 6 – Interpretation of Corrosion Current Density Values for Uncoated Bars

Corrosion Current Density ($\mu A/cm^2$)	Expected time for corrosion
i_{corr} < 1.0	Low
i_{corr} = 1.0 to 3.0	Moderate
i_{corr} > 3.0	High

The unguarded 3LP test was developed to be used on the uncoated steel bars alone. Epoxy coating, being dielectric, is not expected to let current pass through and polarize the steel bar. However, Ramniceanu has shown from limited data that 3LP tests can be conducted on ECR bars after several years in service (Ramniceanu, A. 2004). But no recommendations on interpretation of corrosion rates on ECR bars are provided. If the epoxy coating has a high resistance and is intact (no holes or breaks), then the polarization of the reinforcement may not be possible.

Resistivity

Corrosion, being an electrochemical process, will be affected by the electrical resistivity of the concrete. The ionic current flow (charged ions flowing through concrete pore water) from anodes to cathodes, a constituent reaction of corrosion, will depend on the resistivity of the concrete

(Broomfield, J.P. 2007). The aggressiveness of corrosion in the reinforcement steel depends on the ease with which the corrosion current flows through the concrete (Berkeley, K. and Pathmanaban, S. 1990). It is possible for the resistivity of concrete to vary significantly over a complete structure, due to varying site conditions from day to day. The level of ions in the concrete can be related directly to the diminution of resistance (Berkeley, K. and Pathmanaban, S. 1990).

Many techniques have been developed for measuring concrete resistance. Two field methods will be discussed; the most cited four-point resistivity and a developing one-point resistivity.

Four-Point Resistivity

Wenner four-point resistivity meter is used in measuring the four-point resistance of concrete. The device was originally designed to measure soil resistance. The resistance of the four-terminal conductor depends upon the distance between the electrodes and the resistivity of a sample space whose linear dimensions are the same as that of the distance between the outer electrodes (Wenner, F. 1915). Generally, the spacing between probes is kept larger than the maximum aggregate size so as to avoid measuring the resistance of the aggregates, which exceeds the resistance of concrete by a large amount (Broomfield, J.P. 2007). Resistance does not appreciably depend on the size of the electrodes and the kind of electrical connection they make with the sample space, but on the distance between the points (Wenner, F. 1915).

The equipment for concrete testing was modified as a spring-loaded instrument to avoid drilling holes in the concrete surface. The outer two probes pass current through the concrete, while the inner two probes read the potential difference. Wetted wooden plugs are placed at the end of the probes to increase conductivity, especially during field measurements (Broomfield, J.P. 2007). The probes are to be placed on the concrete surface while avoiding proximity with steel reinforcement, contact with exposed aggregates and concrete edges so as to prevent errors in the readings. When the steel reinforcement cannot be avoided, the probe is to be placed perpendicular to the reinforcement such that steel is not aligned with and not parallel with the conductive path of electrical current (Broomfield, J.P. 2007). Figure 9 presents the Wenner four-point testing apparatus.

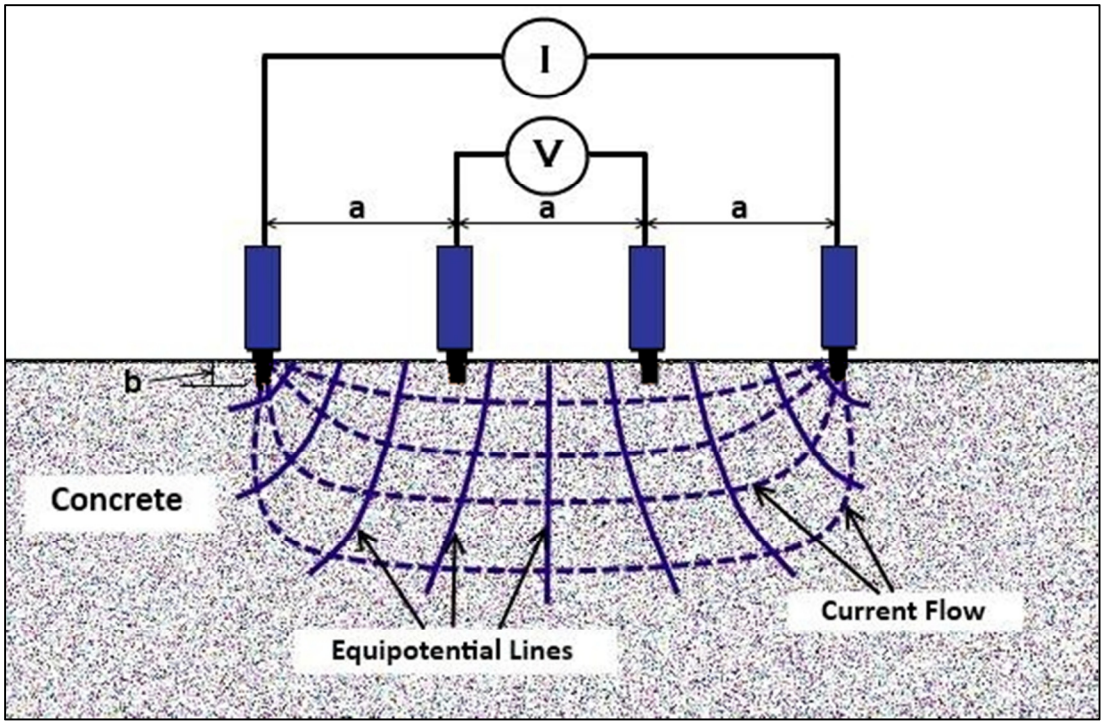

Figure 9 – Four-Point Resistivity Test Apparatus

If the surface of concrete is highly rugged or contains large amounts of impurities, it is common to drill holes for the four terminals to have better contact. Calculation of resistivity of the sample space is made using the following formula (Wenner, F. 1915).

$$\rho = \frac{4\pi aR}{1 + \frac{2a}{\sqrt{a^2 + 4b^2}} + \frac{2a}{\sqrt{4a^2 + 4b^2}}} \qquad \text{Eqn. 6)}$$

Where, ρ = resistivity, ohm-m

a = distance between the probes, m

b = depth of the holes, m

R = measured resistance, ohms.

If depth of holes is much greater than distance between the holes, then

$$\rho = 4\pi aR \qquad \text{Eqn. 7)}$$

If depth of holes is much smaller compared to the distance between the holes, then

$$\rho = 2\pi aR \qquad \text{Eqn. 8)}$$

Alternating current is used in the four-point resistivity measurement procedure, since using direct current will result in polarization, which might cause serious difficulties in the accuracy of the measurements (Wenner, F. 1915). However, since the earth and moist concrete act as electrolyte, an electromotive force occurs in the presence of two electrodes of four-point meter, and thus polarization occurs at any electrode through which considerable amount of current passes, even if it is alternating current. The polarization affects the accuracy of measurements, but high accuracy in the resistance measurements is not necessary (Wenner, F. 1915).

The resulting resistivity from the four-point instrument depends primarily upon the resistivity of the portion of the sample space, near and between the inner (potential) electrodes (Wenner, F. 1915). Also, the portion of sample space between the inner potential terminals has higher influence on the measured resistance. These influences on the resistivity are relying upon the condition that the four electrodes are approximately uniformly spaced (Wenner, F. 1915). An interpretation of the four-point resistivity for steel reinforced concrete supporting corrosion is presented in Table 7 (Langford and Broomfield, 1987).

Table 7 – Interpretation of Concrete Four-Point Resistivity Values

Concrete Resistivity (ohm – m)	Empirical Corrosion Rate
> 200	Negligible
100 – 200	Low
50 – 100	High
< 50	Very High

Table 8 – Interpretation of Concrete Four-Point Resistivity Values

Concrete Resistivity (ohm – m)	Empirical Corrosion Rate
< 400	High
400 to 650	Moderate
> 650	Low

Table 8 presents another interpretation formed from the laboratory study on bare steel corrosion (Balakumaran 2010). Significant drawback of the four-point resistivity method is that the result is

an average of the resistivities from concrete surface down to the depth regulated by the pin spacing (Berkeley, K. and Pathmanaban, S. 1990). Surface concrete affected by carbonation or by differential moisture content may result in higher or lower resistivity (Millard, S.G. and Gowers, K.R. 1992). Furthermore, the influence of differential moisture content and other chemical conditions on the flow of current in the concrete is not taken into account.

One-Point Resistivity

One-point resistivity method is operated by considering the reinforcement as a counter-electrode and using a single electrode on the surface (Feliu, S. *et al* 1996). A single disc shaped electrode is placed on the concrete surface where steel reinforcement is directly below the electrode. The current flow profile in the concrete is expected to be in a cylindrical form, extending from the single electrode towards the reinforcement. The one-point resistivity is calculated from the measured resistance using the following formula (Eqn. 9). The depth of interrogative volume is taken as the cover depth plus the half the reinforcement bar diameter. Figure 10 shows the one-point testing apparatus.

$$\rho = \frac{\pi {d_e}^2 R}{4 * \left(d_c + \frac{1}{2} d_b\right)} \qquad \text{Eqn. 9)}$$

Where, ρ = resistivity, ohm-m

R = measured resistance, ohms

d_e = diameter of single electrode, m

d_c = concrete cover depth, m

d_b = diameter of reinforcement bar, m

One advantage of one-point method over the four-point method is that the depth of the flow of current is known. Hence, the errors associated with the different chemical conditions, that affected current flow path, are avoided to some extent. The errors associated with the choice of current flow depth and the area through which the current flows will be overridden, if the values are kept constant for different measurements. The interpretation of the one-point resistivity recommended by Feliu is presented in Table 9 (Feliu, S. 1996). This interpretation is based on the following equation.

$$\rho = 2\,R\,D \qquad \text{Eqn. 10)}$$

Where, D = diameter of the sensor

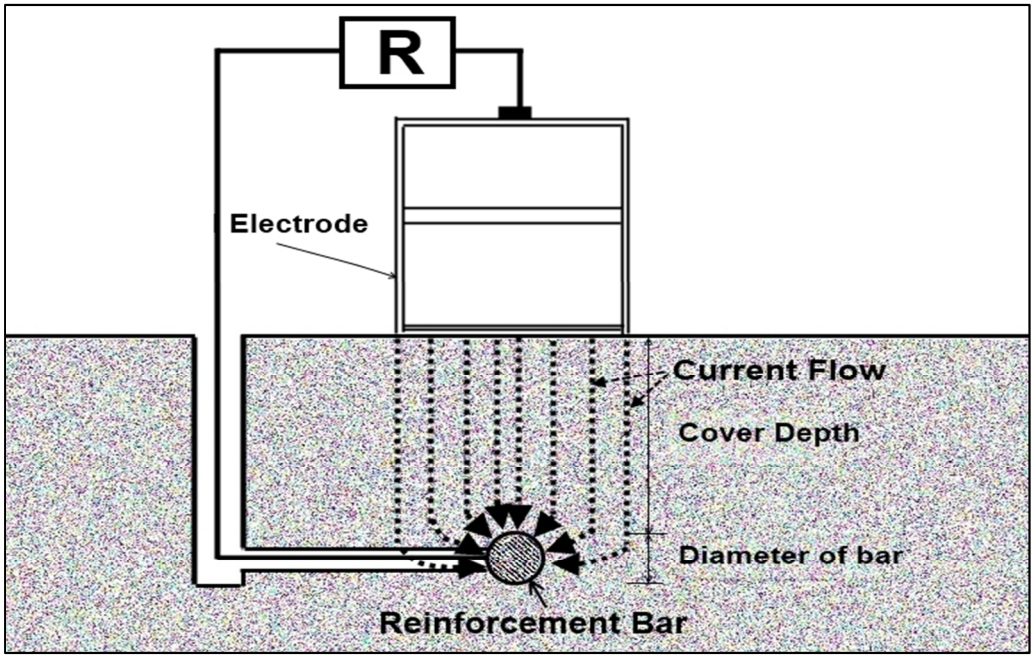

Figure 10 – One-Point Resistivity Schematic

Table 9 – Interpretation of One-Point Resistivity Values for Black Bars

Resistivity (ohm-m)	Risk Levels
> 1000 – 2000	Very low corrosion rates, even if carbonated or chloride contaminated
100 – 1000	Low to high corrosion rate
< 100	Resistivity is not the controlling parameter

Also, the study conducted by Feliu utilized GECOR device, with an alternating current (AC) of 1-5 KHz or current interruption technique (DC), for measuring resistance, which is not used in this study. Thus, the interpretation may not be applicable for the measurements taken in this study.

Another difference between four-point and one-point resistivity methods is that the four-point interpretation is the same regardless of the reinforcement type or corrosion state, since the

measurement is a function of the concrete material properties alone. However, the one-point resistivity measurement is conducted over a reinforcement bar as a counter electrode using a square wave form of AC current of 97 Hz. Subsequently, the resistivity of a reinforcement coating and corrosion condition may be included in the measurement. One-point resistivity conducted on coated bars, such as epoxy coated bars (ECR), may be affected by the coating resistance as well as the corrosion under the coating. Interpretation of one-point resistivity needs further evaluation.

Chloride Contents

Free chlorides present in the concrete, usually available through diffusion, react and result in the breakdown of the protective passive layer over the steel reinforcement. However, a critical amount of chloride is necessary for the depassivation of the reinforcement to begin. It is known from experiments and literature that the critical chloride content is not a constant value and it depends on electrochemical conditions such as potential, pH, and oxygen content at the steel surface, and humidity in concrete (Zimmerman L., Elsener B., and BÖhni 1999). So, chloride content in concrete is an important indication of the reinforcement corrosion conditions.

In order to determine the chloride contents in concrete, first step is to collect the concrete sample. Since concrete is an inhomogeneous material and free chlorides are generally present in the cement paste exclusively, chloride core diameter should not be less than 50 mm (1.97 inch) or, when dust drilling, diameter should not be less than 20 mm (0.79 inch) with minimum three depths so as to get a chloride depth profile (Berkeley, K. and Pathmanaban, S. 1990).

Chloride content is determined from the concrete sample by using acid-soluble or water-soluble method. The water-soluble method takes into account the free chloride alone, while the acid soluble method includes both free and background chlorides. Out of these methods, acid soluble method is recommended for routine analysis (Bertolini L. 2004). Results of chloride laboratory determination processes depend upon the concrete powder fineness, time to dissolution and other physical properties, so reproducibility is not guaranteed. Since acid-soluble chloride titration method includes both background chlorides and free chlorides, it can be used to provide higher precision in the results (Berkeley, K. and Pathmanaban, S. 1990). The amount of acid-soluble chloride in a hydraulic-cement system is equal to the total amount of chloride in the system, except some initially insoluble organic matter (ASTM C 1152/C 1152M 2004).

Chloride concentration of the powdered sample from each depth is determined by using potentiometric titration. According to ASTM C 1152/C 1152M-04, a 10-gram powdered concrete sample is dissolved in 1:1 nitric acid solution and then brought to a rapid boil for not more than a few seconds. Then it is cooled and filtered using a coarse-textured filter paper. Finally, 2 ml of standard 0.05N NaCl solution is added to the filtered solution. The filtrate is titrated against 0.05N $AgNO_3$. The percent of chloride by mass of the concrete is found as follows.

$$Cl, \% = \frac{3.545\,[(V1 - V2) * N]}{W} \qquad \text{Eqn. 11)}$$

Where, V1 = milliliters of 0.05 N $AgNO_3$ solution used for sample titration (equivalence point)

V2 = milliliters of 0.05 N $AgNO_3$ solution used for blank titration (equivalence point)

N = exact normality of 0.05 N $AgNO_3$ solution

W = mass of sample, g

For calculating kilograms of chloride per cubic meter (or pounds of chloride per cubic yard) of concrete, multiply percent chloride by D1/100 or D2/100 to the nearest 0.1 kg/m^3 (lb/yd^3).

Where, D1 = oven dry density of concrete

D2 = saturated-surface-dry density of concrete

It is important to prevent any cross-contamination among the samples. Interpretation of the chloride concentration required to initiate corrosion can be conservatively taken as 0.7 kg/m^3 (1.2 lb/yd^3), though the actual interpretation is a range of values. The criteria for corrosion risk due to chloride contents in Europe are given in Table 10 (Broomfield, J.P 2007).

Table 10 – Corrosion Risk at given Chloride Contents

% Chloride by mass of cement	% Chloride by mass of sample (concrete)	Risk
< 0.20	< 0.03	Negligible
0.2 – 0.4	0.03 – 0.06	Low
0.4 – 1.0	0.06 – 0.14	Moderate
> 1.0	> 0.14	High

Diffusion Coefficients

Diffusion coefficient or diffusion constant is a measure of the penetration rate of chloride into the concrete. Diffusion constant was used in Fick's Second Law (Eqn. 12) to relate the concentration change to the time. A one-dimensional flow solution of the Fick's Second Law (Eqn. 13) may be used in the determination of the apparent diffusion coefficient.

$$\frac{\partial \varphi}{\partial t} = D_c \frac{\partial^2 \varphi}{\partial x^2} \qquad \text{Eqn. 12)}$$

Where, φ = concentration (amount/volume)

t = time

x = position

D_c = Diffusion Coefficient

$$C_{(x,t)} = C_0 \left(1 - erf \frac{x}{2\sqrt{D_c t}}\right) \qquad \text{Eqn. 13)}$$

Where, $C_{(x,t)}$ = concentration at depth x at time t

C_0 = surface chloride concentration

x = distance over which chloride has diffused

t = time for diffusion

erf = statistical error function

SERVICE LIFE MODELS

Service life models have been developed in order to predict the deterioration rate of bridge components. Also, it enables planned maintenance activities such as repairs and rehabilitation. Service life models can be generally divided into two types; deterministic and probabilistic.

Deterministic Models

Deterministic approach involves the usage of data averages collected from the structure, which also includes historical data. The deterministic models will require a large amount of data, which can satisfyingly be representative of the whole structure, prior to applying them in the analytical equations. These models do not take into account of the probabilistic nature of the individual data, while corrosion is probabilistic nature since it depends on a variety of factors. When the average values of data are used in a model that defines a whole structure, then the data is considered to be the same on the whole structure irrespective of the exposure condition differences. And such an assumption will lead to less reproducibility in the results. Deterministic models were developed earlier, due to the lack of field input data, since probabilistic models involved repetitive and numerous iterations.

Probabilistic Models

Probabilistic approach involves either the data collected from the structure or historical distributions of data or both. These models incorporate the stochastic nature of the variables required in the model. Generally, the structure is divided into many smaller parts where the concerned data is calculated independent of other locations, however in agreement with the corresponding probability distributions (Kirkpatrick, T.J. 2001). Since probabilistic models involve huge amount of calculations, these are better executed using computer programs. Usually, the deterministic models of analysis can be converted into probabilistic models by introducing variability into the variables, through methods such as Monte Carlo simulation. The input data used in these models are generally random sampled using two methods; simple bootstrapping and parametric bootstrapping.

Monte Carlo Simulation

Monte Carlo simulations are stochastic procedures that can generate random numbers leading to a probability distribution, which can replace experimental data in a probabilistic model. This method takes into consideration the stochastic nature of the input data for the model. The Monte Carlo simulation can be applied to a deterministic model by repeatedly generating random numbers within a range leading to a particular probability distribution, which introduces the probabilistic nature of the input variable into the model.

Simple Bootstrapping

Simple bootstrapping involves random sampling from a given set of data collected from the field. This method is used for structures where an incorporation of the properties, exclusive to the structure, in the model is required. A large amount of data from the actual structure is essential for the model to be representative. If only a scarce amount of data is available, the model cannot confidently stand for the actual condition of the structure.

Parametric Bootstrapping

Parametric bootstrapping, on the other hand, will make assumptions regarding the range of values for a particular data and a fitting distribution. This method requires extensive research for selecting a range and a fitting distribution of data, since the range and distribution must represent the actual conditions in the bridge with inconsequential errors. For instance, cover depths on a bridge deck are shown to be normally distributed. Thus, the range can be defined by using the mean and standard deviation of the collected data set (Williamson, G. 2007).

Chloride Diffusion Models

Bridge deck corrosion initiation occurs through the destruction of the protective layer over the reinforcement steel, coated and uncoated. For uncoated bar, the methods through which the passive (protective) layer can be neutralized are carbonation and chlorination. Since chlorination is the most extensive mode of corrosion initiation, the corrosion models discussed are chloride diffusion models.

Chloride diffusion into the concrete reinforcement can be modeled using the Fick's Second Law of diffusion. A solution assuming one-dimensional flow of the Fick's Second Law (Equation 14) describes the relationship between surface chloride contents, chloride contents at different depths, time for diffusion, and diffusion coefficients. However, the solution assumes a slab of infinite depth, constant surface concentration, and constant diffusion coefficient (Crack, J. 1975).

$$C_{xt} = C_0\left(1 - erf\,\frac{x}{2\sqrt{D_c\,t}}\right) \qquad \text{Eqn. 14)}$$

Where, C_{xt} = chloride concentration at depth x at time t,
C_0 = surface chloride concentration,
erf = statistical error function,
x = depth,
D_c = diffusion coefficient,
t = time.

Cady and Weyers Model (1983)

Cady and Weyers developed a service life model for reinforced concrete bridge decks based on the chloride diffusion (Cady, P.D. and Weyers, R.E. 1983). The service life was divided into four successive time periods such as time of initial damage at construction, time for diffusion of chlorides to reinforcement depth to cause corrosion initiation, time for corrosion cracking of the concrete surrounding the reinforcement, and the time for end of functional service life (EFSL) deterioration percentage. The model considers the chloride diffusion into the concrete as a result of Fickian diffusion and the moisture differential flow through subsidence cracking. Subsidence cracking of concrete primarily depends on the concrete clear cover and cement type, and not on the reinforcement type (Kyle N.L. 2001).

The first time period for the model was studied using cover depth data obtained from previous study and an assumed 2 inch (51 mm) slump. This model is deterministic in nature, thus empirical data for the variables C_{xt}, Co, D_c, and x were used as input in determining the service life. The model assumes that subsidence cracking occurs in all bridge decks to a certain extent irrespective of the concrete resistance to diffusion.

Mangat and Molloy Model (1994)

Diffusion coefficients for any concrete mixture will be high for a new structure, while it decreases rapidly to reach a steady value in 5 to 10 years (Williamson, G. 2007). A chloride diffusion model was developed by taking into consideration of time-dependant diffusion coefficients. A relationship was formed between the apparent diffusion coefficients and time as follows.

$$D_c = D_i t^{-m} \qquad \text{Eqn. 15)}$$

Where, D_c = effective diffusion coefficient at time t,
D_i = effective diffusion coefficient at time t equal to 1 second,
t = time,
m = empirical coefficient that depends on concrete mixture proportions.

D_i and m are the unknown factors required to calculate the diffusion coefficient including the time-dependant decaying effect. It is to be noted that the model assumes the commencement of chloride diffusion from time t = 1 second, which is the time of erection. The diffusion coefficient at time t = 1 second is estimated through regression analysis on the empirical chloride data fitted to a log-log plot. The value of m is equal to the slope of the regression fit, which is an indication of the concrete quality. The Equation 15 substituted in Equation 1 becomes the closed form solution equation of this model (Equation 16).

$$C_{xt} = C_0\left[1 - erf\left(\frac{x}{2\sqrt{\frac{D_i}{1-m}\,t^{1-m}}}\right)\right] \qquad \text{Eqn. 16)}$$

The slope m can also be calculated from the following relationship, if the water-cement ratio ($^{W}/_{C}$ ratio) of concrete is known.

$$m = 2.5(^{W}/_{C}) - 0.6 \qquad \text{Eqn. 17)}$$

It seems, the model is valid only for the assumption that the chloride diffusion starts at time t = 1 second from the erection. Apparently, the assumption of diffusion at t = 1 second will lead to

overestimation of the service life. Also, the estimation of the diffusion coefficient at time t = 1 second requires either multiple D_c measurements, which is not feasible, or back calculate from the slope m with the known $^{w}/_{c}$ ratio, which adds more variability to the model.

Bamforth Model (1999)

Bamforth model can be considered an improvement on Mangat and Molloy model, though not a serious one. In this model, the time of first chloride application is assumed at one year from the time of erection. One year time may be closer to the actual time of application than one second, since the deicing salt application is conducted only during winter every year. The diffusion coefficient including the decay effect can be estimated from the following equation (Equation 18).

$$D_{ca} = at^{n} \qquad \text{Eqn. 18)}$$

Where, D_{ca} = diffusion coefficient,
a = diffusion coefficient at time t = 1 year,
n = empirical constant

The Equation 18 is substituted in Equation 14 to form the closed form solution of this model, see Equation 19.

$$C_{xt} = C_0\left[1 - erf\left(\frac{x}{2\sqrt{\left[D_{ca(t_m)}\left(\frac{t}{t_m}\right)^{n} t\right]}}\right)\right] \qquad \text{Eqn. 19)}$$

Where, $D_{ca(t_m)}$ = diffusion coefficient at time t_m.

Apparently, this model is the same as Mangat and Molloy model with the exception of assuming the chloride application at one year time from the time of erection. This model cannot be considered to be an actual improvement on Mangat and Molloy model since it still uses the empirical constant similar to m. It has been verified numerically that the empirical constant n is a function of time and the prediction is not reliable (Maheshwaran and Sanjayan 2004).

Maheshwaran and Sanjayan Model (2004)

Maheshwaran and Sanjayan model can be considered as an improvement on Mangat and Molloy model of chloride diffusion. This model generalizes the Mangat and Molloy model. Customization of the initial time of chloride application over the bridge deck is allowed, giving the model more freedom.

$$D_t = D_{ref}\left(\frac{t_{ref}}{t}\right)^m \qquad \text{Eqn. 20)}$$

Where, D_t = diffusion coefficient at time t,

D_{ref} = diffusion coefficient at time t_{ref},

The first time of chloride application or the first winter, t_i, can be used in the diffusion coefficient expression including the decay effect. The solution equation of this model by substituting Equation 20 in Equation 14 is presented in Equation 21.

$$C_{xt} = C_0\left[1 - erf\left(\frac{x}{2\sqrt{\frac{D_{ref}\left(t_{ref}\right)^m}{1-m}\left[t^{1-m} - t_i^{1-m}\right]}}\right)\right] \qquad \text{Eqn. 21)}$$

Where, t_i = time at first application of chloride.

To be able to include the first time of chloride application solves a number of issues with the Mangat and Molloy model. But the model still involves the slope m, for which an estimation of appropriate value remains undependable.

Williamson Model (2007)

From the service life models that utilize the time-dependant diffusion coefficients, it can be noted that the concrete mixture properties heavily influence the chloride diffusion. The inherent variability associated with the concrete mixture leads to unreliable estimations of diffusion

coefficients. Thus, Williamson decided to use the Fick's Second Law with a constant apparent diffusion coefficient, D_c, measured from the field.

The model estimates the service life of a bridge deck by dividing the whole time period into three segments; time to corrosion initiation, time from initiation to cracking, and time for corrosion damage to propagate to end of service life (EFSL).

The time to corrosion initiation is taken as the time needed for the chlorides to diffuse and initiate corrosion and result in a constant 2% deterioration of any bridge deck. A deterioration value of 2% was selected because, modeling using Fick's law of diffusion could be misleading due to the multitude of factors affecting the rate of corrosion damage in a bridge deck. Following initiation, corrosion advances till the surrounding concrete cracks, where the time to cracking was modeled using corrosion cracking models.

The final time period in the model is the corrosion propagation time until EFSL of bridge deck is reached. In a survey participated by bridge engineers of state departments of transportation, it was determined that the EFSL is reached when 9.3 to 13.6 percent of the worst span lane of a deck has deteriorated (Fitch, M.G. et al 1995). This model utilizes a value of 12 percent deterioration for EFSL.

This model is a probabilistic model, which uses Monte Carlo simulation to introduce the variability in the parameters. A computer program was developed in VBA programming language by Liang et al. at Virginia Tech to be used for estimating service life (Liang et. al. 2001). One of the objectives of the current project is to reproduce the computer program in a sophisticated, more customizable and a hassle free stand-alone application. Cover depths, apparent diffusion constants, and surface chlorides are supplied to the model by simple bootstrapping, where at least 15 data points each were recommended. The chloride initiation rates (C_{xt}) are supplied by parametric bootstrapping, since the chloride contents at bar depth causing corrosion initiation may be limited to a range and a probabilistic distribution for a reinforcement bar type. Number of iterations required for the estimations of service life values to converge to a near constant value was calculated to be at least 64,000, which has a 95% confidence interval of 1.6 years. The time from corrosion cracking to EFSL may be calculated by using the Equation 22, which was formulated by regression analysis of data obtained from Virginia bridges.

$$Time\ To\ Deterioration = 8.61\left(\sqrt{\%Deterioration + 1.38} - 1.45\right) - 3.34 \qquad \text{Eqn. 22)}$$

A sensitivity analysis was performed on the parameters that are obtained by simple bootstrapping. It was found that the diffusion coefficients are the most sensitive of all parameters, especially values between 1 and 40 mm^2/year (0.0015 to 0.060 $inch^2$/year). It is essential to use higher number of diffusion coefficient values in the model to decrease the variability associated with it, since diffusion coefficients from a single bridge deck can be highly variable. Surface chlorides and cover depths also influence results, with the cover depths being the least sensitive.

Finite Element Modeling of Chloride Diffusion

Finite element method (FEM) is a numerical analysis method, which is used to approximate solutions to a set of partial differential equations. Solutions are usually extracted by reducing the partial differential equations to set of ordinary differential equations and then are integrated using the boundary conditions. Modeling the diffusion of chlorides into the concrete is possible through FEM, while being highly difficult. The additional factors considered in FE modeling while modeling the chloride diffusion process from that of the Fickian diffusion models are the influences of ionic fluxes of different ionic species in the concrete pore water, differential moisture, heat transfer, and other chemical reactions. The presence of different species of ions and differential moisture in the concrete system may attract or repel the diffusion of chlorides in a significant manner, which are not considered in the simple Fickian model.

Finite difference methods (FDM) approximate the solutions of the differential equations by using approximate difference quotients. In order to approximate a solution, the problem's domain must be divided. Thus, the FDM produces numerical approximations to the derivative in a time-stepping manner. Due to the approximation, finite difference methods are not capable of handling complex problems with high accuracies. FDM is generally used for modeling chloride diffusion into the concrete because of its simplicity and the ability to model time dependent parameters.

With the number of advantages the FEM has over the simple Fickian modeling, reliability of input variables still remain problematic especially with the increase in the number of factors considered in the FE models. Probabilistic nature of the parameters has been incorporated in the FE models in

the recent years. However, introducing the stochastic nature of parameters in a FE model also has increased the resources, time and thus cost involved by multiple folds.

Saetta, Scotta, and Vitaliani Model (1993)

A numerical model of the chloride diffusion in the coastal structures, subjected to tidal splashes, was developed by Saetta et al. using FE method. This model takes into account of the effects of the time-dependent diffusion coefficients, differential temperature, differential humidity, degree of cement hydration, and the presence of differential moisture. The model was validated by using laboratory experiments conducted by Collepardi and Biagini (1989) with concrete subjected to tidal splashes. It was found that the incorporation of the differential moisture in the model was significant, especially for a coastal structure. The applicability of this model to bridge decks are validated.

Boddy, Bentz, Thomas, and Hooton Model (1999)

A model was developed that included the effects of initial chloride profile, initial diffusion coefficient, time-dependent diffusion coefficients, time-dependent surface chlorides, varying temperature along the course of one year, nonlinear chloride binding isotherms, superposition of a hydraulic head in a coastal environment, and chloride build up due to wicking. The diffusion was modeled using the following partial differential equation. The model includes the effects of chloride diffusion, convective flow, and chloride binding.

The input parameters required by the model are presented as follows.

1. m, constant depending on the concrete mix proportions,
2. T, absolute temperature of exposure,
3. C_{crit}, critical concentration of chlorides to corrosion initiation,
4. D_{ref}, diffusion coefficient at time t_{ref} and temperature T_{ref},
5. K_{ref}, permeability coefficient at time t_{ref},
6. C_0, surface chloride,
7. Cover depth.

It can be noted that the model uses input parameters on concrete mix proportions, which are difficult to obtain and validate. The model uses Fick's Law for calculating diffusion coefficients, thus does not include the influence of ionic fluxes. A sensitivity analysis conducted on the model shows that the estimated service lives can vary up to 550% with only moderate changes in *m*.

Martin-Pérez, Pantazopoulou, and Thomas Model (2001)

A model was developed by Martin-Pérez et al. by introducing some improvements to Boddy et al. model. This model includes the influence of differential moisture contents and the diffusion of oxygen as a supplementary controlling factor after corrosion initiation. But, the effect of the ionic fluxes was not incorporated into the chloride diffusion. Even though this model addresses a number of issues with Boddy et al. model, this model being deterministic in nature is a disadvantage compared to the Fickian probabilistic models.

Ali Model (2010)

A model was proposed by Ali for the diffusion of chlorides into the concrete. This model includes the saturation condition of the concrete, and thus humidity and moisture transport within the system, as they affect the transport of chlorides as well as the diffusion. The mechanism of binding of diffused chloride was included in the model. A FE based computer program was developed as a part of this project called CPICS (Chloride Profile In Concrete Structures). Close agreement between results found using the program and a software called ANSYS was observed.

Conclusions formed in the simulation conducted as a part of validating the model are presented as follows.

1. The total chlorides diffusivity is near three times the free chloride diffusivity. Thus, the bound chlorides content is about two times the free chloride content.
2. The lower the water-cement ratio, the lower the diffusion rate of chlorides.
3. Higher the cement content, lower if the chloride diffusion.
4. Chloride transport predictions with no binding or constant diffusion are misleading.

Corrosion Cracking of Adjacent Concrete

After corrosion initiates in a bridge deck, it propagates and results in continuous deposition of corrosion byproducts. As corrosion products increase, the volumetric expansion causes internal tensile stresses in the concrete. Concrete, being weak in tension, cracks and forms into spalls or delaminations in the bridge deck. The corrosion service life models must include the time taken for the corrosion to crack the surrounding concrete from being initiated. Some of the existing corrosion cracking models is discussed as follows.

Bažant Model (1979)

A physical-mathematical model was developed for the concrete exposed to sea water. As a part of this model, a set of simplified equations was formulated to estimate the time to concrete corrosion cracking. According to Bažant, the time between the chloride inducted corrosion initiation and the concrete cracking can be estimated by using the Equation 23.

$$t_{cor} = \rho_{cor} \frac{D\Delta D}{sj_r} \qquad \text{Eqn. 23)}$$

Where,

t_{cor} = duration of steady-state corrosion,

ρ_{cor} = a function of densities of steel and rust ≈ 3.6 g/cm^2,

D = original bar diameter,

ΔD = change in bar diameter,

s = spacing between bars,

j_r = rate of rust production per unit area.

Corrosion cracking can occur either through inclined cracks or delaminations. It is assumed that for structures with s < 6D the primary cracking mode is inclined cracks and for structures with s > 6D the primary cracking mode is delamination. The critical value for the ΔD can be approximated by Equation 24 for inclined cracking.

$$\Delta D = 2f_t' \frac{L}{D} \delta_{pp} \qquad \text{Eqn. 24)}$$

Where, f_t' = tensile strength of concrete,

L = concrete cover depth,

δ_{pp} = bar hole flexibility.

The bar hole flexibility is the average of the calculated flexibility for a bar either in a thick wall cylinder or in infinite space. The flexibility for thick wall cylinder is presented in Equation 12 and the equation for infinite space is shown in Equation 25.

$$\delta_{pp}^{0} = \frac{D}{E_{ef}}(1 + v) + \frac{2D^3}{s^2 E_{ef}} \qquad \text{Eqn. 25)}$$

Where, v = Poisson's ratio,

E_{ef} = effective elastic modulus $\left(\frac{E_c}{1+\varphi_{cr}}\right)$,

φ_{cr} = creep coefficient of concrete.

$$\delta_{pp}^{1} = \frac{D}{E_{ef}}\left[1 + v + \frac{D^2}{2L(L+D)}\right] + \frac{2D^3}{s^2 E_{ef}} \qquad \text{Eqn. 26)}$$

The equation for delamination failure mode is presented in Equation 27.

$$\Delta D = f_t'\left(\frac{s}{D} - 1\right)\delta_{pp} \qquad \text{Eqn. 27)}$$

The model can be used to understand the various factors that influence the corrosion cracking of concrete, but have not been validated through experiments successfully. This physical-mathematical model was developed by making a few assumptions, which are presented below.

1. Oxygen and chloride transport through the concrete is one-dimensional in nature and is quasi-stationary.
2. Corrosion reactions proceed in a steady-state.
3. $Fe(OH)_3$ (red rust) results in volumetric expansion , not $Fe(OH)_2$.

Morinaga Model (1989)

Morinaga suggested some empirical equations for estimating the time to corrosion cracking in concrete, supported by field and laboratory data. The model assumes that the concrete cracking happens when a critical quantity of corrosion products have formed around the steel reinforcement. The critical amount of corrosion products can be found by using Equation 28.

$$Q_{cr} = 0.602\, d \left(1 + \frac{2c}{d}\right)^{0.85} \qquad \text{Eqn. 28)}$$

Where, Q_{cr} = critical mass of corrosion products,
c = concrete cover depth,
d = diameter of reinforcement.

The time for concrete cracking to occur can be estimated by utilizing Equation 29.

$$t_{cr} = \frac{Q_{cr}}{i_{cor}} \qquad \text{Eqn. 29)}$$

Where, t_{cr} = time to concrete cracking,
i_{cor} = corrosion current density.

Corrosion current density is a form of measuring the rate of corrosion. The corrosion rate data can be obtained either from field measurements or from statistical distributions from historical data. The model is relatively simple involving only the corrosion rate, concrete cover depth, and size of reinforcement.

A study was conducted to compare the actual cracking data to the estimated time for cracking (Peterson, J.E. 1993). The data collected from the experiment showed that the corrosion cracking occurred at 671 days, while the time for cracking estimated from the Morinaga model was 88 days, which is a highly underestimated value.

Liu and Weyers Model (1998)

Modeling the time to concrete corrosion cracking requires the understanding of the corrosion initiation process, propagation, and the factors affecting them. Generally, the time to concrete cracking will depend on the amount of corrosion products formed and their rate of production. Moreover, the rust production depends on the corrosion rate, reinforcement bar size, bar spacing, concrete cover depth, and the material properties of concrete. In this model, the entire process of corrosion cracking was divided into four processes; corrosion initiation, free expansion, stress initiation, and concrete cracking.

A small porous zone is present at the interface of the concrete and the steel reinforcement, the volume of which depends on the surface area of the reinforcement, $^{w}/_{c}$ ratio, degree of hydration, and the degree of compaction. Following the initiation of the corrosion, the rust forms and begins filling the volume of porous zone. As corrosion propagates, the porous zone gets filled with corrosion products and internal tensile stresses are formed in the concrete. When the tensile stresses reach a critical stress level or when the critical amount of corrosion products deposit around the reinforcement, the concrete will crack.

The critical amount of corrosion products required for the concrete to crack can be estimated using Equation 30.

$$W_{crit} = \rho_{rust} \left(\pi \left[\frac{C f_t'}{E_{ef}} \left(\frac{a^2 + b^2}{b^2 - a^2} + v_c \right) + d_0 \right] D + \frac{W_{st}}{\rho_{st}} \right) \quad \text{Eqn. 30)}$$

Where,

W_{crit} = critical amount of corrosion products,

ρ_{rust} = density of corrosion products,

C = concrete cover depth,

f_t' = tensile strength of concrete,

E_{ef} = effective elastic modulus of concrete = $\frac{E}{1+\varphi_{cr}}$,

v_c = Poisson's ratio of concrete,

d_0 = thickness of pore zone around the concrete-steel interface,

D = diameter of steel reinforcement,

W_{st} = mass of corroded steel = $\propto W_{crit}$,

ρ_{st} = density of steel,

The time to cracking (Equation 31) can be estimated by using the relation presented in the Equation 17 and the rate of corrosion.

$$t_{cr} = \frac{W_{crit}^2}{2\ k_p} \qquad \text{Eqn. 31)}$$

Where, t_{cr} = time to concrete cracking,

k_p = rate of rust production.

The rate of rust production (Equation 32) can be estimated by using its relation with the rate of corrosion.

$$k_p = 0.098 \left(\frac{1}{\alpha}\right) \pi D i_{cor} \qquad \text{Eqn. 32)}$$

Where, i_{cor} = annual mean corrosion rate.

The Liu and Weyers model was validated through experiments, where the time to cracking of the observed specimens was compared to the estimated time to cracking from the model.

Alonso et al. Model (1998)

Different parameters were studied to identify those that have the most influence on concrete corrosion cracking. Parameters studied are cover depth/reinforcement diameter ratio, cement proportions, $^{w}/_{c}$ ratio, cast position of the bar, and the rate of corrosion. An empirical model was developed by Alonso et al. based on Faraday's Law that relates the depth of corrosion penetration and the rate of corrosion.

$$x = 0.0116\ i_{cor}\ t \qquad \text{Eqn. 33)}$$

Where, x = depth of corrosion penetration,

i_{cor} = corrosion current density,

t = time.

A relationship between the depth of corrosion penetration required to induce concrete cracking and the cover/reinforcement diameter ratio was found (Equation 34).

$$x_0 = a + b\,\frac{C}{\varphi} \qquad \text{Eqn. 34)}$$

Where, x_0 = depth of corrosion penetration,

a = corrosion constant = 7.53,

b = corrosion constant = 9.32,

C = concrete cover depth,

φ = diameter of the reinforcement steel.

From the model, it was observed that a corrosion penetration depth of 50 μm (0.0002 inch) was needed to produce a crack in the concrete cover of width 0.05 mm (0.0002 inch), when C/φ ratio ≥ 2. If the C/φ ratio < 2, then a penetration depth of 15 to 30 (0.0006 to 0.0012 inch) was sufficient to produce the crack of same width. For C/φ ≥ 2, a corrosion penetration of 100 to 200 μm (0.0039 to 0.0079) will result in a crack of width 0.3 mm (0.012 inch). Observations from the experiments conducted to validate the model are presented below.

1. Higher corrosion rates will require greater penetration depths to result in cracks than the lower corrosion rates. It means that accelerated laboratory testing will require greater penetration depth to form cracks.
2. Concrete with higher $^{w}/_{c}$ ratios will allow slower crack propagation than the concrete with lower $^{w}/_{c}$. Since high strength concrete with lower $^{w}/_{c}$ ratios will have lower air content, the corrosion products will cause internal tensile stresses earlier than the low strength concrete with higher $^{w}/_{c}$ ratios.
3. Top reinforcement bars cause slower crack propagation than the bottom reinforcement bars.

Torres-Acosta and Sagüés Model (2004)

Corrosion cracking models generally take the formation of corrosion products as a uniform process over the whole length of the reinforcement. But, the presence of pitting corrosion, i.e. micro anodes, which have higher rate of corrosion may cause variable concrete cracking mechanism over the length of the reinforcement. Torres-Acosta and Sagüés included the effect of pitting corrosion on the uniformity of concrete cracking in their model. The model investigates the influence of the size of the anodes on the corrosion penetration depths required to crack the adjacent concrete. This model presents an empirical equation from the experimental data to estimate the amount of corrosion penetration required to cause concrete cracking (Equation 35).

$$x_{crit} \approx 0.011 \left(\frac{C}{\varphi}\right) \left(\frac{C}{L} + 1\right)^2 \qquad \text{Eqn. 35)}$$

Where, x_{crit} = critical corrosion penetration,
C = concrete cover depth,
φ = reinforcement bar diameter,
L = length of the anodic region.

Through experiments conducted to validate the model, it was observed that corrosion penetration depth range of 0.03 to 0.272 mm (0.0012 to 0.011 inch) was required to cause concrete cracking for the localized corrosion, while a corrosion penetration depth range of 0.003 to 0.074 mm (0.00012 to 0.0029 inch) was sufficient for a uniform corrosion process.

Vu, Stewart, and Mullard Model (2005)

Previous corrosion cracking models aimed at estimating the time to concrete cracking initiation. The time to concrete cracking initiation will not be equal to the actual time when the concrete cracking is detectable, because the time taken for the cracks to propagate in the concrete is neglected. Vu, Stewart, and Mullard model can be considered an improvement on the existing corrosion concrete cracking models, since it includes the time taken for excessive cracking.

This model incorporates the Liu and Weyers model for calculating the time to concrete cracking initiation. Factors affecting the time to excessive cracking are corrosion rate, concrete cover depth, $^{w}/_{c}$ ratio, and the maximum acceptable crack width.

$$t_{sp} \approx t_{1st} + k_R \times 0.0114\, i_{cor} \left[A \left(\frac{C}{wc} \right)^{B} \right] \quad \text{Eqn. 36)}$$

Where, t_{sp} =time to excessive cracking,

t_{1st} = time to concrete crack initiation,

k_R = rate of loading correction factor,

i_{cor} = corrosion current density,

C = concrete cover depth,

wc = water-cement ratio,

A and B are to limit crack widths

$$k_R \approx 0.95 \left[exp\left(-\frac{0.3 i_{corr(exp)}}{i_{corr(\text{real})}} \right) - \frac{i_{corr(exp)}}{2500 i_{corr(real)}} + 0.3 \right] \quad \text{Eqn. 37)}$$

Where, $i_{corr(exp)}$ = applied corrosion rate used in the experiment,

$i_{corr(\text{real})}$ = corrosion rate observed in the structure.

The model was fitted to experimental data for crack width limits such as 0.3 mm (0.012 inch), 0.5 mm (0.02 inch), and 1.0 mm (0.039 inch). It can also be able to estimate time to excessive cracking in the laboratory specimens subjected to accelerated corrosion rates by applying a rate of loading factors.

The values of A and B for the corresponding crack width limits are shown below.

Limit Crack Width	A	B
0.3 mm	65	0.45
0.5 mm	225	0.29
1.0 mm	700	0.23

In the Equations 36 and 37, the corrosion rates of the concerned systems are considered to be constant over time. The corrosion products formed in the corrosion process may result in the slowdown of the rate of corrosion. So, the model can be adjusted in order to incorporate the varying corrosion rates over time. The modified equation for estimating the time for excessive cracking is presented in Equation 38.

$$T_{sp} = \left[\frac{\beta+1}{\alpha} \times \left(t_{sp} - 1 + \frac{\alpha}{\beta+1}\right)\right]^{\frac{1}{\beta+1}} \quad \text{Eqn. 38)}$$

Where, T_{sp} = time to excessive cracking considering variable corrosion rate,

t_{sp} = time to excessive cracking from the constant corrosion rate model,

α, β = corrosion rate constants, recommended as 0.85 and -0.3 respectively.

Critical Metal Loss for Concrete Cracking

Most existing models depend on the amount of corrosion products formed around the reinforcement in order to estimate the time to corrosion cracking of concrete. Corrosion penetration values in the reinforcement at which the cracking of the adjacent concrete initiates is called the critical corrosion penetration or critical metal loss. Fixing a constant penetration level or a range of penetration values can result in simpler calculations to estimate the time to cracking. A collection of critical metal loss values suggested by different researchers are summarized in the Table 11.

Table 11 – Critical metal Loss Values from Different Studies

Researcher	Source	Metal loss mils (μm)
Spellman and Stratfull (1968)	Laboratory Experiment	0.1 (2.54)
Spellman and Stratfull (1968)	Field Measurement	Up to 29 (734)
Zdenek Bažant (1979)	Interpretation of Equations	0.3 (7.87)
Kenneth Clear (1989)	Interpretation of Results	3.7 (94)
Hladky et al. (1989)	Interpretation of Results	0.63 (16) to 1.26 (32)
Clemena et al. (Unpublished)	Interpretation of Results	600 (15240) to 1200 (30480)

The heterogeneous nature of concrete, in both macro-structure and micro-structure, and the fact that corrosion of steel in concrete is not uniform leads to a wide range of critical amount of metal loss to induce cracking of concrete (Liu and Weyers 1998).The time to concrete cracking due to corrosion of reinforcement is a difficult number to calculate, because of the variability associated with the concrete properties, composition of corrosion products, and geometry of the structure.

COMPUTER PROGRAMS

BRIDGE ANALYSIS PROGRAM

The bridge analysis program was written in VB .NET (2010) language. The program consists of modules for two operations; estimation of service life of bridges and calculation of diffusion coefficients (Dc).

Service Life Estimation

The corrosion prediction service life estimation of the bridge components is carried out by utilizing a probabilistic model, which incorporates the stochastic nature of the parameters. Only the chloride diffusion-induced corrosion, not the carbonation-induced corrosion, is taken into consideration. There are two ways to model chloride diffusion into concrete; Fickian diffusion model and finite element model. The current program uses the Fickian diffusion model, which depends on the Fick's second law of diffusion, see Equation 39.

$$\frac{\partial \varphi}{\partial t} = D \frac{\partial^2 \varphi}{\partial x^2} \qquad \text{Eqn. 39)}$$

Where, φ = concentration of substance, in lb/mm^3 or lb/inch^3

D = diffusion coefficient, in mm^2/s or inch^2/s

x = depth, in mm or inch

Using the Fickian equation of diffusion, a relation for the chloride diffusion in concrete has been derived for the conditions of a slab of infinite depth, constant chloride surface concentration and constant diffusion coefficient. The reduced form is presented as Equation 40.

$$C_{x,t} = C_o \cdot \left[1 - erf\left(\frac{x}{2\sqrt{D_c \cdot t}}\right)\right] \qquad \text{Eqn. 40)}$$

Where, $C_{x,t}$ = chloride content at depth 'x' in a time 't', in lb/cy or kg/m^3

C_o = surface chloride content, in lb/cy or kg/m^3

erf = standard error function

x = depth from top surface, in inch or mm

D_c = diffusion coefficients, in inch^2/year or mm^2/year

t = time, in years

The service life estimation module requires the following inputs. Input may be made in either US customary units or metric system of units.

- Cover depths
- Diffusion coefficients
- Surface chlorides
- Reinforcing type and associated corrosion initiation concentrations
- Deterioration percentage at EFSL

The probabilistic estimation process makes use of both simple bootstrapping and parametric bootstrapping for particular variables. Simple bootstrapping involves random sampling from the provided data set. Thus, simple bootstrapping will completely depend on the given data set and not on any historical data or assumptions of distributions of the data. Parametric bootstrapping on the contrary will random sample from a range or known distribution of data. It is useful when the available data set has small number of replications but know distribution parameters.

Input values from cover depths, diffusion coefficients, and surface chlorides are randomly selected using simple bootstrapping, so as to represent the actual conditions of the bridge deck. Six reinforcement types are given for selection and in addition, a customizable reinforcement type is given for other reinforcements. The chloride initiation rates may be input using three different methods, all of which utilize parametric bootstrapping for calculation. The program provides default initiation rates for all reinforcement types, which consists of a minimum, maximum, and a mode value that constitute a triangular distribution. Second choice will ask for a minimum, maximum, and a mode value for the triangular distribution. Third choice accepts mean and standard deviation for normal distribution of initiation rates.

With the input values of cover depths, diffusion coefficients, surface chlorides, and chloride initiation rates, time is calculated. The calculation is repeated for a recommended minimum iteration of 64000 times to establish the rate of damage as a function of time. For 64000 iterations the 95% confidence interval was found to be ±0.8 years by running the model five times

successively, which is acceptable for a bridge structure (Williamson, G. 2007). The confidence intervals improve as the number of iterations increase.

The program calculates and displays results according to two methods; method of corrosion propagation and method of pure diffusion. The first method is for black bar and calculates service life in three segments; time to corrosion initiation, time for crack propagation, and time to reach EFSL from corrosion initiation in a bridge. Once the corrosion damage has occurred at 2% deterioration for black bar, then the corrosion damage greater than 2% is no longer a function of Fick's diffusion mechanism. The time for crack propagation depends on the type of reinforcement used. It has been determined to be approximately 6 years for black bar. And, literature shows that the epoxy coated reinforcement (ECR) will extend the time for crack propagation by an additional 5 years, thus equal to 11 years. For other reinforcement types the crack propagation time is not known, thus the program allows customization of propagation time for all the reinforcement types. A deterioration of 12% was taken as the time for EFSL because it is the deterioration level in the worst span-lane at which the bridge decks are typically rehabilitated. An equation for calculating the time to deterioration, depending on the deterioration percentage is given in Equation 42.

$$\begin{aligned} Time\ to\ reach\ EFSL \\ &= Time\ for\ corrosion\ initiation\ (0\ to\ 2\%) \\ &+\ Time\ for\ crack\ propagation + Time\ to\ reach\ EFSL\ (2\%\ to\ 12\%) \end{aligned} \quad \text{Eqn. 41)}$$

$$Time\ to\ deterioration = 8.61\left(\sqrt{\%\ Deterioration + 1.38} - 1.45\right) - 3.34 \quad \text{Eqn. 42)}$$

The propagation method might not apply for other reinforcement types, so the pure diffusion curve may be used. Diffusion curve consists of the time taken for the chlorides to diffuse up to a deterioration of 12% plus the crack propagation time, which is estimated at 11 years for ECR. The flowchart of the program is presented in Figure 11.

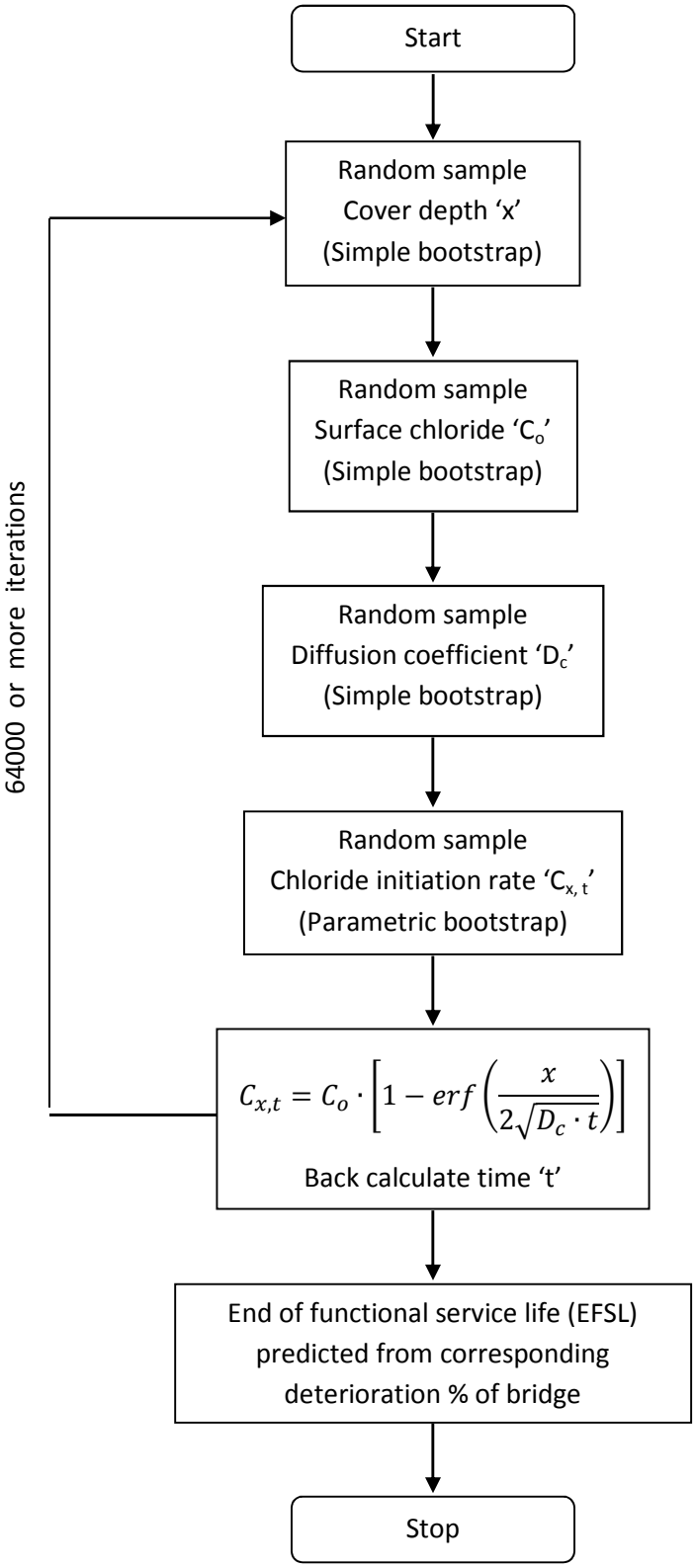

Figure 11 – Flow Chart of Operations in Bridge Analysis Program

Diffusion Coefficients

The program includes a module for calculating the diffusion coefficients of a given bridge. The diffusion coefficients are calculated from Fick's second law of diffusion. The module back-calculates diffusion coefficients using measured chloride contents at corresponding depths at a known age. The method followed in the calculation is the least sum of squared error curve fitting analysis. Generally the surface chlorides at a depth of 0.50 inch (13 mm) from the top surface, has the greatest influence on the diffusion coefficients for bridge decks. The inputs required are the chloride concentrations and the corresponding depth from top surface. For other exposure conditions, such as piles and other components with constant exposure to chloride laden water, surface chloride concentrations would be used.

Installation

For installation of the Bridge Analysis Program, the following prerequisites are necessary.

- Windows Installer 3.1
- .NET Framework 3.5 or later version

The steps to be followed are presented below with accompanying screenshots.

1. Open the "setup.msi" file. A setup dialog box appears, see Figure 12.

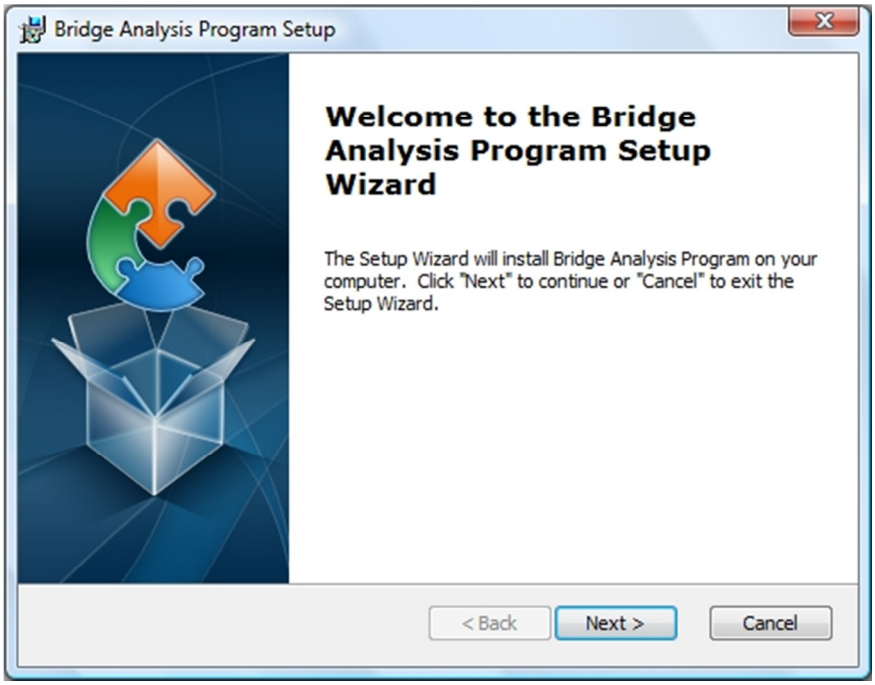

Figure 12 – Bridge Analysis Program Setup Dialog Box

2. Click “Next”. Enter or browse and select the folder in which the program to be installed, see Figure 13.

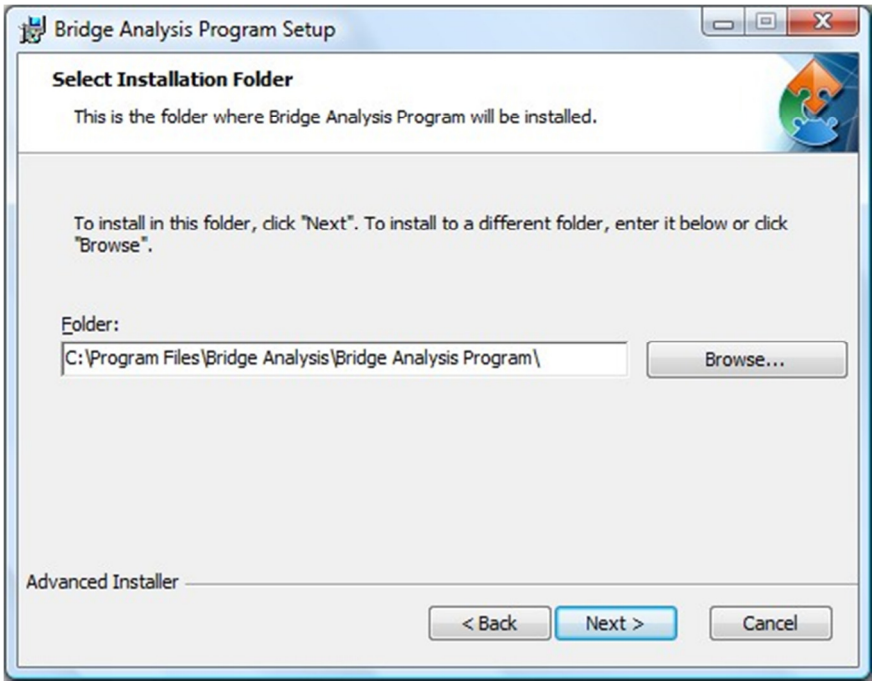

Figure 13 – Install Folder Selection

3. Click “Install”. The installation begins and it may ask for an administrative password.

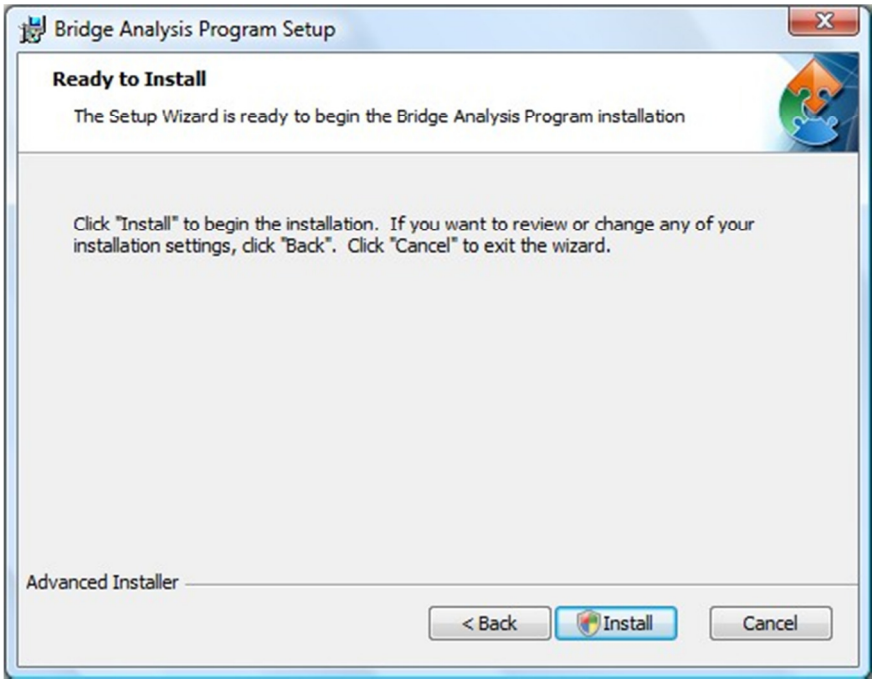

Figure 14 – Confirmation prior to Installation

Usage – Service Life Estimate

The interface of the program consists of three tabs; service life estimation, SLE results, and diffusion coefficients. The first tab will be used to input values for the service life estimation, see Figure 15. The second tab displays a summary of results from the service life estimation. Third tab is for the calculation of diffusion coefficients. The step-by-step procedure for using the Bridge Analysis Program to estimate service life model is presented below.

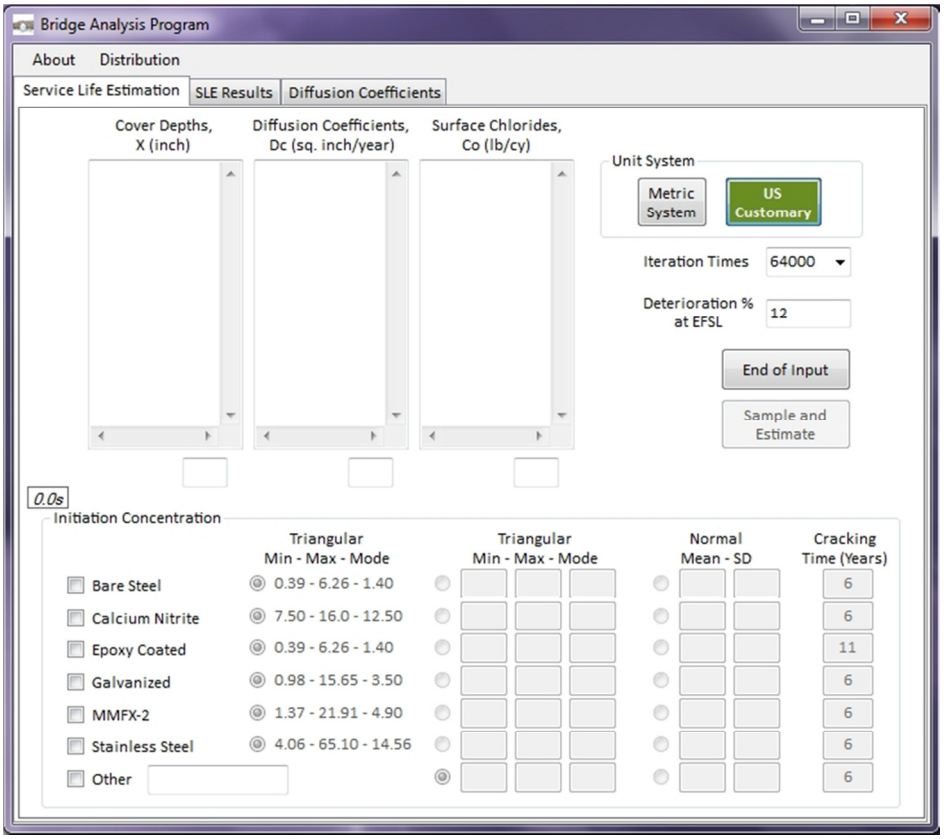

Figure 15 – Interface of Bridge Analysis Program

To change the unit system, the corresponding buttons can be clicked under the 'Unit System' panel. The selected unit system is shown in green color. Cover depths, diffusion coefficients, and surface chlorides must be entered in the corresponding text boxes either through simple or parametric bootstrapping. The reinforcement type and the chloride initiation concentration are to be selected from the 'Initiation Concentration' panel below. The initiation concentration can be entered in three ways, which can be chosen by selected the radio button in front of the method desired. The default time for crack propagation is given in the corresponding text boxes, which are editable. A default value of 64000 is displayed in the 'Iteration Times' text box, which can be changed to a desired

value but in no case is to be less than 10000 in order to limit calculation error. Also, the deterioration percentage of the structure, for which the service life is expected, can be entered in the 'Deterioration % at EFSL' text box.

Following the completion of all the necessary input requirements, the 'End of Input' button must be pressed. Then, the program checks for errors and possible mistakes in the input data and presents them in a message box. After correcting the errors, the 'End of Input' button must be clicked. A green tick mark appears on the right side of the 'End of Input' button, and the 'Sample and Estimate' button gets unlocked. The program is ready for analysis. The 'Sample and Estimate' button must be clicked and a progress bar appears above the 'Initiation Concentration' panel and shows the progress of the process. Once the estimation is complete, the program automatically takes the focus to the second tab 'SLE Results', to display the summary of results, see Figure 16. The results consists of two tables; table on left side contains results, which are calculated by using the concept in Equation 3, and the table on right side displays results from the diffusion method.

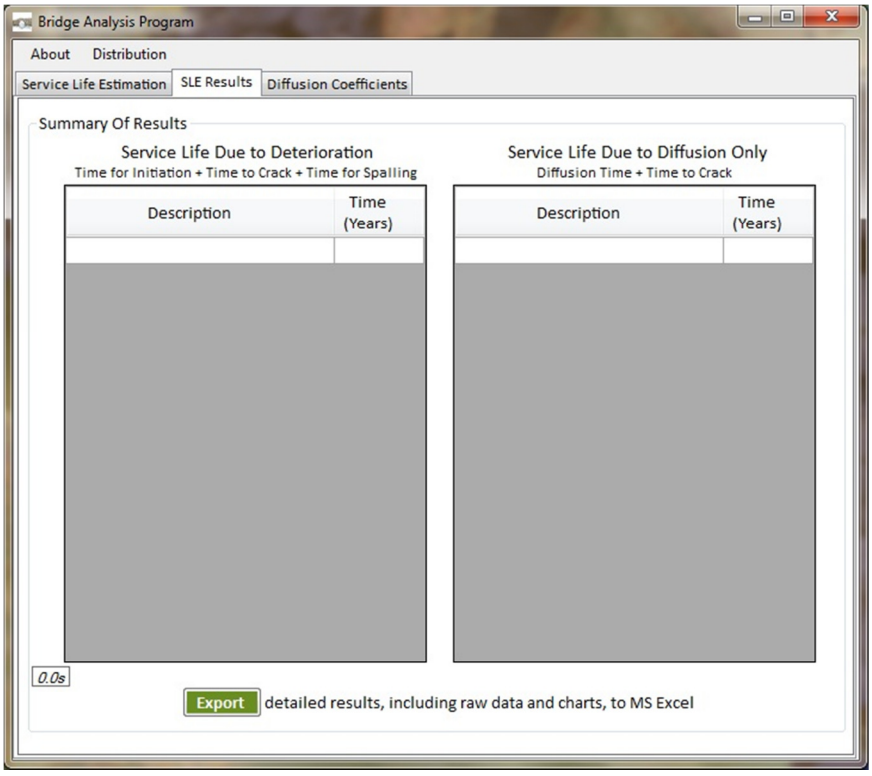

Figure 16 – Service Life Estimation - Summary of Results

To view the detailed results including the curves obtained from the analysis, the 'Export' button at the bottom of the 'SLE Results' tab can be pressed. A progress bar appears below the two tables and displays the process of data being transferred from the program to MS Excel.

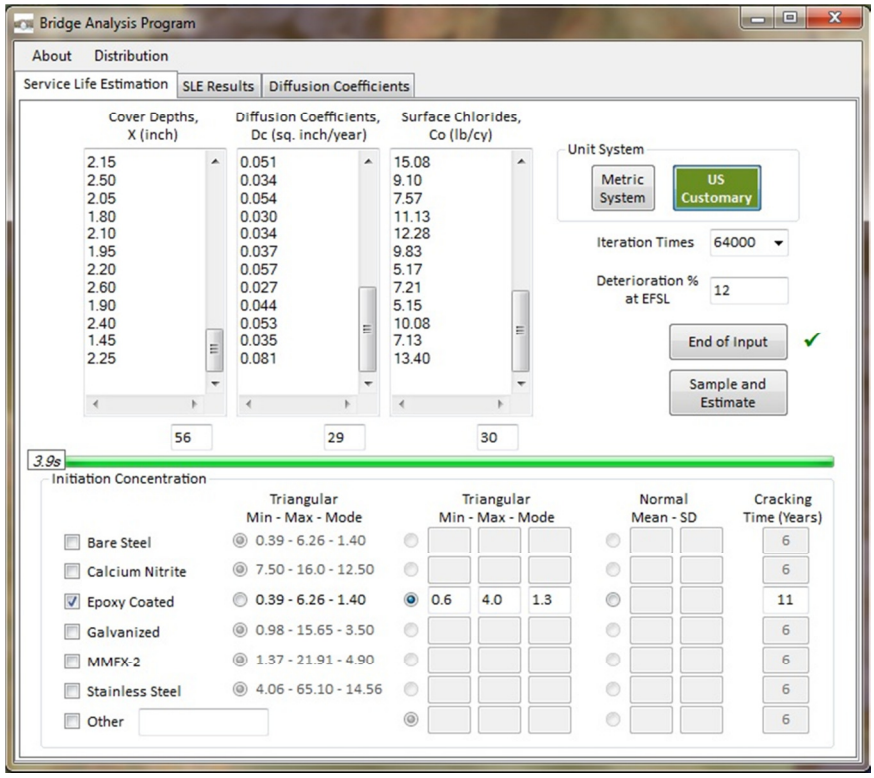

Figure 17 – Sample Inputs from a Bridge Deck

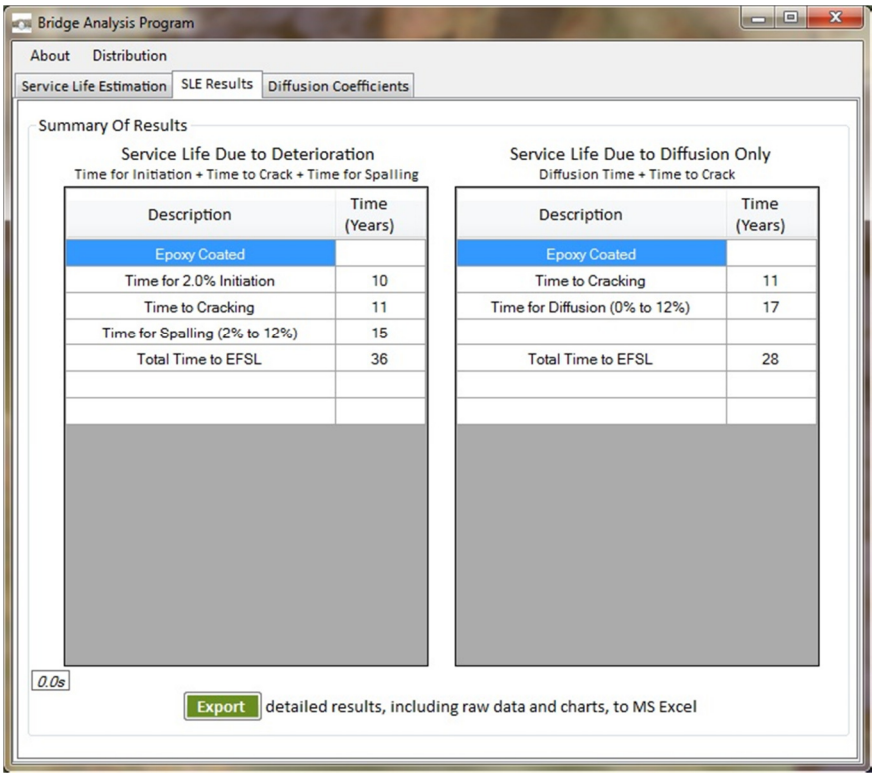

Figure 18 – Summary of Results from the Sample Inputs

The spreadsheet displays the deterioration at different service life stages and curves for both the methods of estimation. The raw data is contained in a separate spreadsheet and is hidden. It can be opened by right-clicking the spreadsheets tab and click 'unhide' and select the sheet. A sample calculation is displayed in Figures 17, 18, and 19. Figure 17 displays the first tab with all the inputs from a bridge structure. After the calculations are completed, the second tab with the summary of results is shown in Figure 18. The tables present the division of the results and the total service life in years. In order to obtain the raw data and the service life curves of the analysis, click "Export" button at the bottom of the "SLE Results" tab. Figure 19 displays part of the spreadsheet that presents detailed results from the service life estimation of the structure. The raw data can be accessed by clicking the 'unhide' option from the right-click menu of the spreadsheets tab (located at the bottom with tab names such as "Results", "Sheet2", and so on). Two curves are displayed in the spreadsheet,

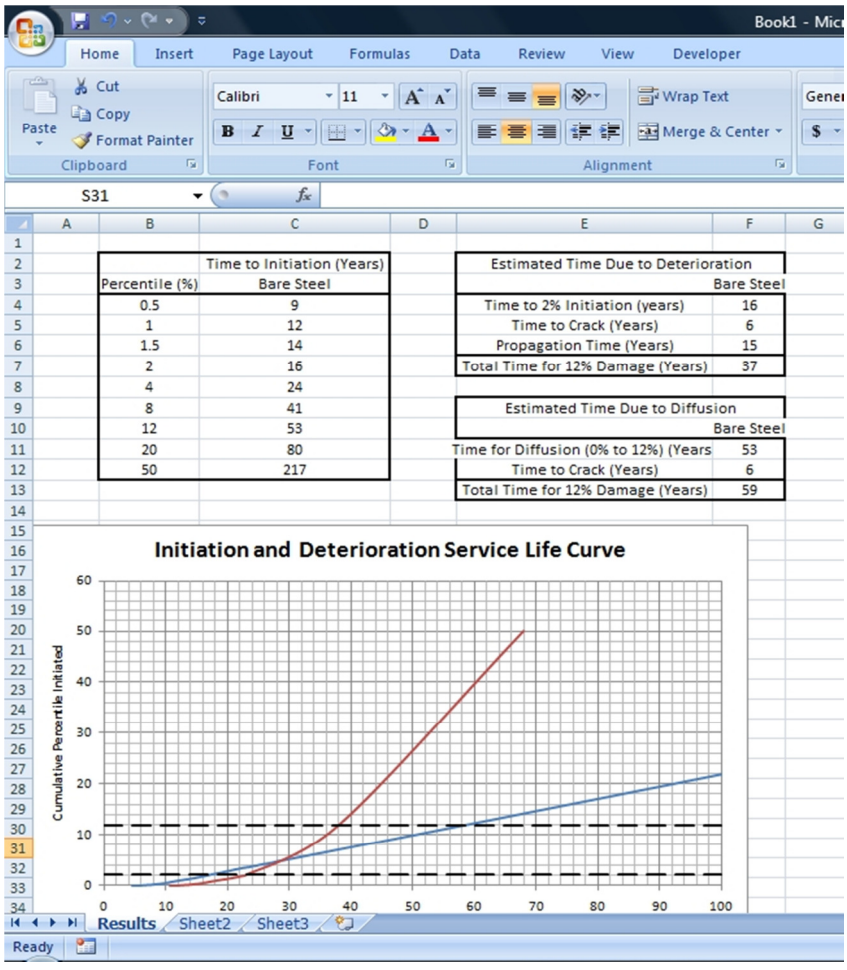

Figure 19 – Detailed Results in a Spreadsheet

Usage – Diffusion Coefficients

Calculating the diffusion coefficients can be performed by utilizing the module presented in the third tab of the program, see Figure 20. The program accepts the depths and corresponding chloride contents for each sample location on a bridge deck. Values of more than one location can be queued in the text boxes. The age of the structure must be entered in the 'Age' text box. The number of depths-chlorides from a single location is to be selected from the input box named 'Number of Depths in ONE Chloride Location' and a minimum of three depths is needed. After the input, the button with an arrow to the right side must be clicked once for each chloride sample location. The calculation is performed and the results are displayed in the table on the right. A sample calculation is presented in Figure 21. The 'Save as Excel File' button will transfer the contents of results table to a spreadsheet, enabling it to be saved.

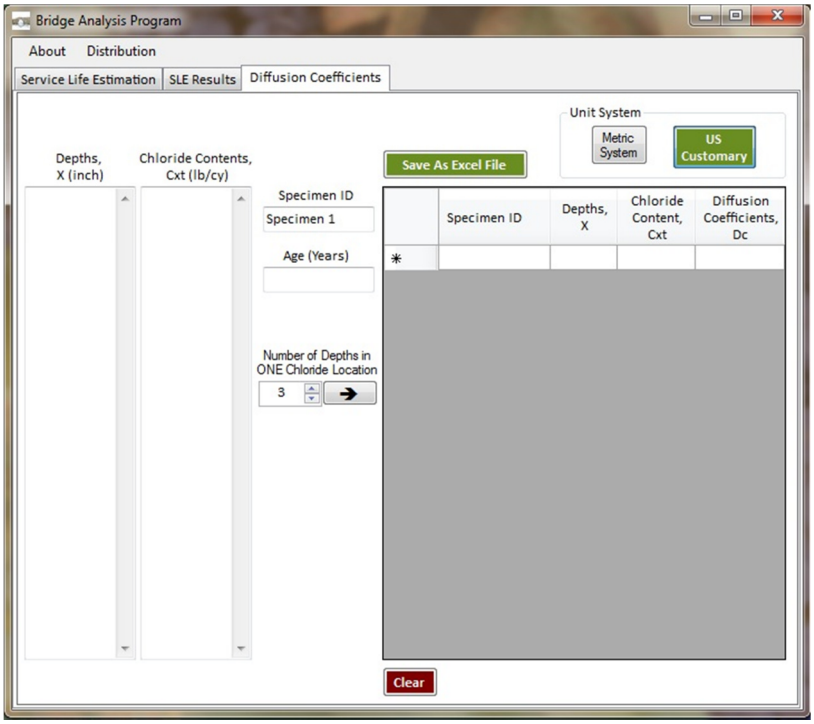

Figure 20 – Diffusion Coefficients Calculation Interface

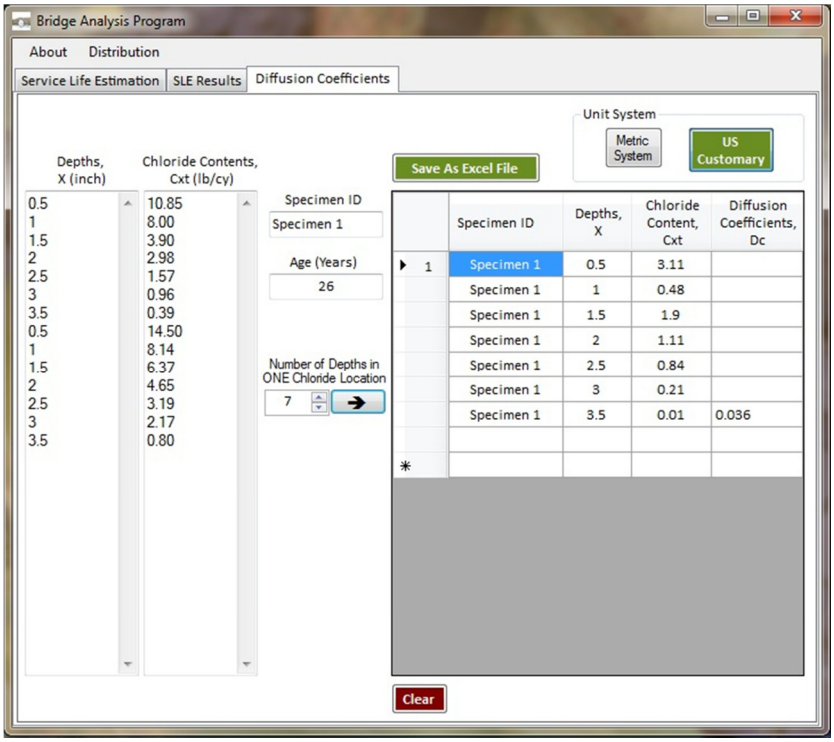

Figure 21 – Sample Diffusion Coefficients Calculation

3LP CALCULATOR

3LP Calc is a tool for calculating the corrosion current density (i_{corr}), polar resistance, MDD, and MPY for the potential and current values obtained from the 3LP instrument. Corrosion current is estimated by using the slope of the plot between the applied currents and potentials. The corrosion rate or the corrosion current density is calculated by using the corrosion current and the polarized steel area. It is assumed that during the test the polarized bar surface area is the whole circumference of the steel reinforcement times the length of the counter electrode probe. The following sections describe the installation process and the working of the program.

Installation

Prerequisites for the installation and working of the 3LP calculator are presented below.

- Windows Installer 3.1
- .NET Framework 3.5 or later version

Steps for installation of the program are presented as follows.

1. Open the “setup.msi” file. A setup dialog box appears, see Figure 22.

Figure 22 – Run 3LP Calc Program Installation Dialog Box

2. Click “Next”. Enter or browse and select the folder in which the program to be installed, see Figure 23.

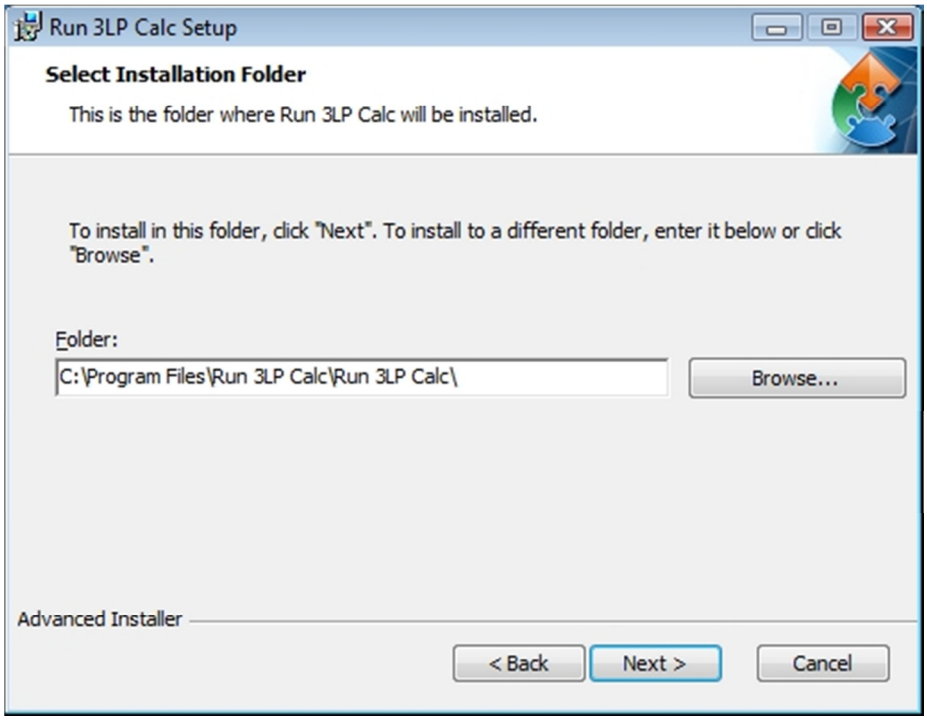

Figure 23 – Installation Folder Selection

3. Click “Install”. Installation begins and may ask for an administrative password.

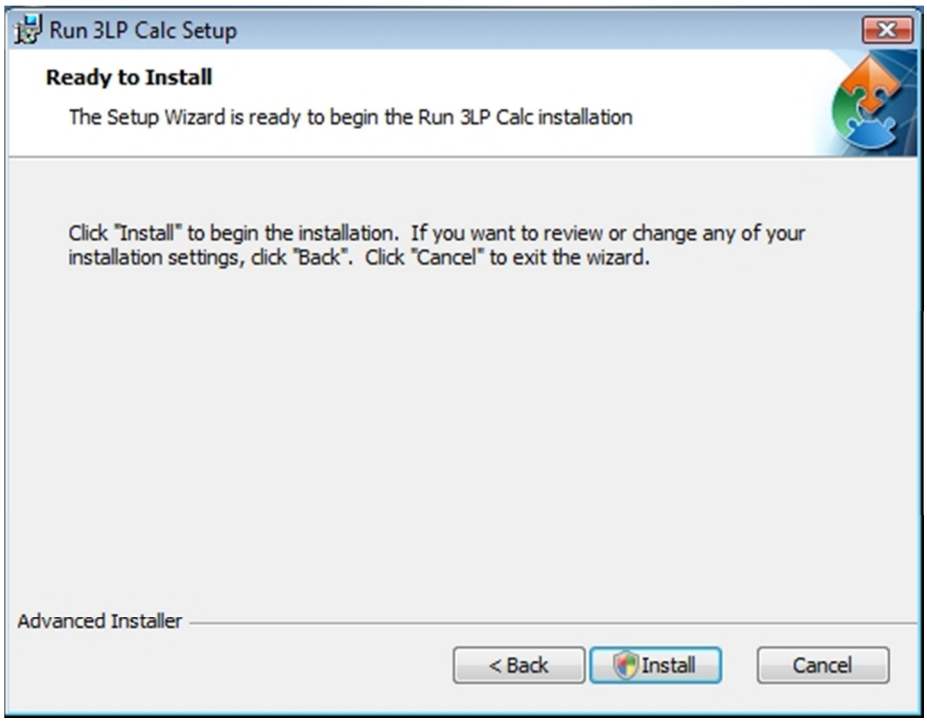

Figure 24 – Confirmation prior to Installation

Usage

Interface consists of two tabs, standard and custom. Input values needed for calculation are the polarized steel area, potentials and corresponding currents, and static potential. The polarized steel area can be entered either directly or by using the bar size and length of the counter electrode.

Figure 25 presents the interface of the standard tab of the program. The standard tab contains the four standard potentials, 0, 4, 8, and 12 mV, pre-entered and the input boxes for corresponding current values. The current values can either be entered in 10^{-3} Amps or 10^{-7} Amps for ease of use. After entering the input values, click “Calculate” button. The results such as corrosion current density, polar resistance, MDD, MPY, and the polarized steel area are displayed to the right side of the interface.

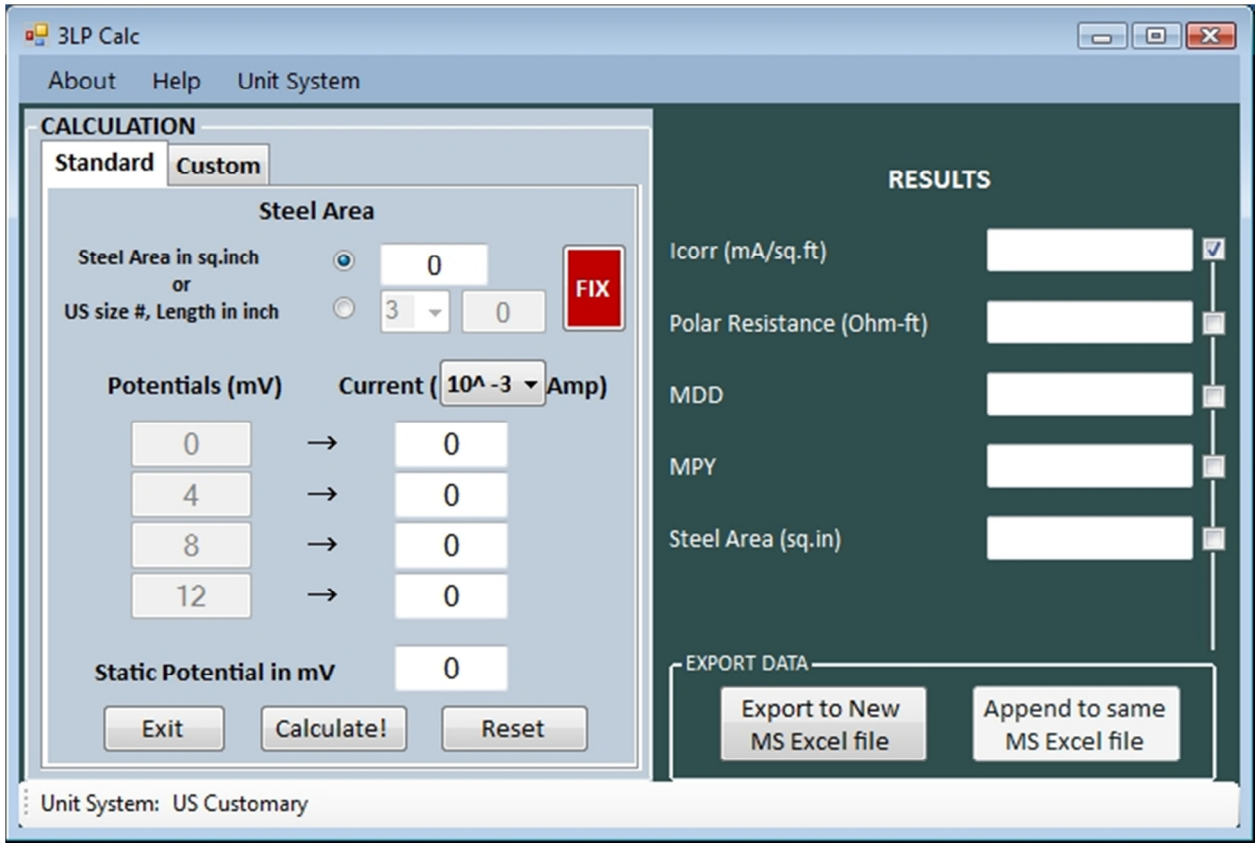

Figure 25 – Interface of "Run 3LP Calc" Program – Standard Tab

The results can be exported to MS Excel Spreadsheet by clicking on the "Export to New MS Excel file" button. It opens a new spreadsheet and transfers the required results, which can be selected by using the checkboxes to the right of the results text boxes. Subsequent calculations can be carried on and by using "Append to same MS excel file" button the results can be transferred to the same spreadsheet and stored row wise.

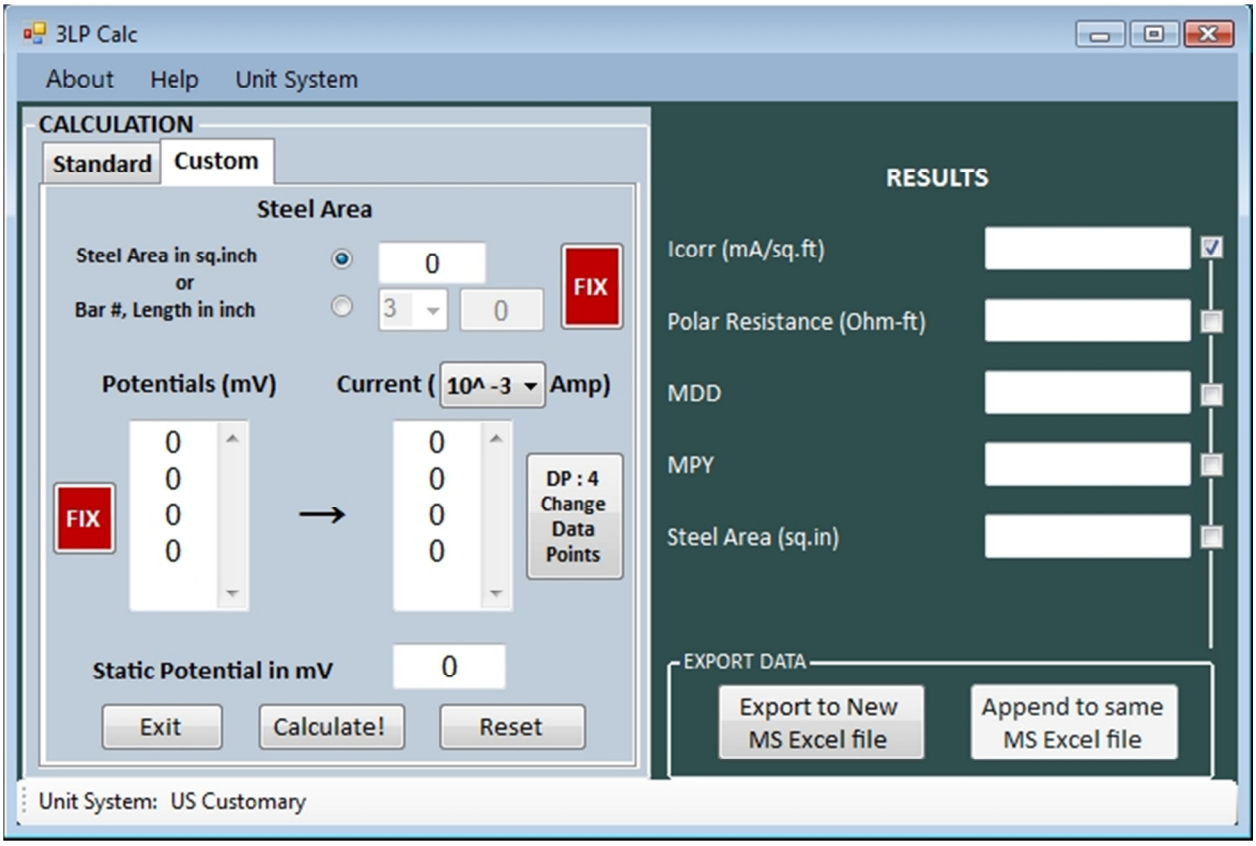

Figure 26 - Interface of "Run 3LP Calc" Program – Custom Tab

Figure 26 presents the custom tab of the program. The custom tab can be used for the same calculations but with more flexibility. If there is different number of data points than the standard 4 data points, the custom interface can be used. The "DP: 4 Change Data Points" button can be used to change the number of data points. The help menu can be used for accessing any information on the usage. This program can be run in both US customary unit system and the metric system, which can be changed by clicking on the "Unit System" menu.

RESULTS AND DISCUSSION

CORROSION ASSESSMENT OF PILOT BRIDGES

Bridge decks were selected for testing as a part of Federal Highway Administration's Long Term Bridge Performance (LTBP) project pilot phase.

VIRGINIA PILOT BRIDGE

BACKGROUND

The Virginia pilot bridge is located at the junction of United States (US) Route 15 and Interstate (I) 66, south of Gainesville. The bridge was built in 1979 and carries James Madison Highway (U.S. 15) southbound traffic over I 66. The bridge is 276 ft. (84.1 m) long and 39 ft. (11.8 m) wide, see Figures 27 and 28.

Figure 27 – U.S.-15 Bridge over I-66

The bridge is a two-span continuous structure, with a cast-in-place composite concrete deck of approximately 8.5 in. depth. The reinforced concrete deck was built with removable formwork. Six built-up steel girders support the deck. The bridge deck consists of two 12 ft. (3.66 m) travelling lanes, a 9 ft (2.74 m) break down lane and a 6 ft. (1.83 m) shoulder.

Figure 28 – U.S. Route 15 Southbound Deck

Annual Average Daily traffic (AADT) on the bridge in 2009 was 16,500 vehicles with approximately 6% being truck traffic. The Virginia Department of Transportation (VDOT) is directly responsible for inspection and maintenance of the structure.

VDOT inspection records for the structure (National Bridge Inventory (NBI) Number 14178) show that the deck had rating of 6 in 2007. A general condition rating of 6 is interpreted as "Satisfactory condition – structural elements show some minor deterioration" (FHWA 1995), see Figure 28. The inspection report cites delaminations in the top surface of the deck, map cracking, transverse cracks, and delaminations in the bottom surface of the deck. The original deck has been patched and cracks sealed a number of times over the maintenance years.

The deck was built with epoxy-coated reinforcement (ECR) as the top reinforcement mat, while the bottom reinforcement mat is black bars. Alternating transverse top mat ECR bars are truss bars. In the positive moment regions, the truss bars turn down into the bottom mat. Thus, alternating bottom reinforcing bars in positive moment regions are ECR. The original concrete mixture proportions and construction test reports are not available. However, the deck was built in a era where the deck concrete water to cement ratio (w/c) was specified as a maximum of 0.45 and a minimum 2 in. (51 mm) cover depth was required.

FIELD PERFORMANCE ASSESSMENT

The initial field condition assessment was conducted from September 17-20, 2009, with team members from Parsons-Brinckerhoff (PB), the Virginia Transportation Research Council (VTRC), Virginia Tech (VT), Rutgers University (RU), and Utah State University (USU).

The PB team conducted the visual inspection, noting the locations of patches, spalls, delaminations, and cracks on the deck top and bottom surfaces, footings, and abutments, and steel girder condition. The RU team conducted the non-destructive testing (NDT) of the deck riding surface, including ultra sonic waves, impact echo, ground penetration radar, concrete resistivity, and corrosion half-cell potentials.

The deck corrosion performance assessment team consisted of members from VTRC, VT, and USU. The concrete deck condition assessment team conducted on-site testing and extracted laboratory test samples. The following suite of assessment activities were conducted within 30 sound concrete areas of the deck riding surface:

- Top and bottom mat electrical continuity tests,
- Magnetic induction reinforcing steel cover depths,
- Copper – copper sulfate half-cell (CSE) corrosion potentials
- Unguarded linear polarization corrosion current density measurements (3LP corrosion rates)
- Four-point and single point concrete resistivity measurements
- Drilled concrete powder samples segmented as a function of depth for chloride content.

In addition, concrete cores were taken for compressive strength and modulus and electrical indication of resistance for chloride penetration.

TESTING METHODOLOGIES

Visual Inspection and Sounding

The visual inspection consisted of locating and sizing existing visible defects, patches, spalls, and cracks. To locate and quantify the delaminations, the entire deck was sounded by chain-dragged, see Figure 29. The compiled data was input into a bridge inspection program. The program uses CAD interface to store defect information in a two-dimensional geometric space. It is capable of generating information about the defects and also allows the user to input the location of the defect directly on a CAD drawing. The results of the damage survey, patches, spalls, cracks, and delamination were used to identify locations of sound concrete for the corrosion survey work, which included cover depth, corrosion potential, resistivities, corrosion current density, and powder concrete samples for chloride testing.

Along with the inspection of the top of deck, the underside was also visually inspected. The overall visual condition of the girders, bearings, and abutments was observed and recorded. These results were used by VT team members to aid in the assessment of the structural performance of the structure.

Figure 29 – Deck Chain Dragging

Cover depths

Concrete resistance to chloride penetration and clear concrete cover act in concert to delay the time to corrosion initiation. Thus, cover depth variability is essential to modeling and estimate corrosion service life performance. Figure 30 illustrates the measuring of clear cover depths using magnetic flux cover meter (pachometer). A relatively large statistical sample size, 30 total, 15 on each span, were selected as shown in Figure 31 and 32.

Figure 30 – Cover Depth Measurements Being Taken

All cover measurements were performed using a pachometer. Two measurements were taken at each location, one on a straight transverse top bar and one on the top truss bar.

Continuity

The bridge deck was built using ECR as the top reinforcement and black bars for the bottom reinforcement. Straight and truss bars alternate such that every other transverse bar in top reinforcement is a truss bar. The top truss bars are bent towards the bottom reinforcement mat in the positive moment regions.

Prior to conducting corrosion potential and rates, electrical continuity of the reinforcing bar must be confirmed. Eight locations were selected, six on the top ECR mat and two on bottom bars. Figure 33 illustrates the continuity testing. Positive connection to the ECR at the eight locations was established through exposing the ECR by concrete core drilling, drilling and tapping the ECR and

installing a section of stainless steel all thread. Continuity between locations was measured with a multimeter and low resistance copper wire.

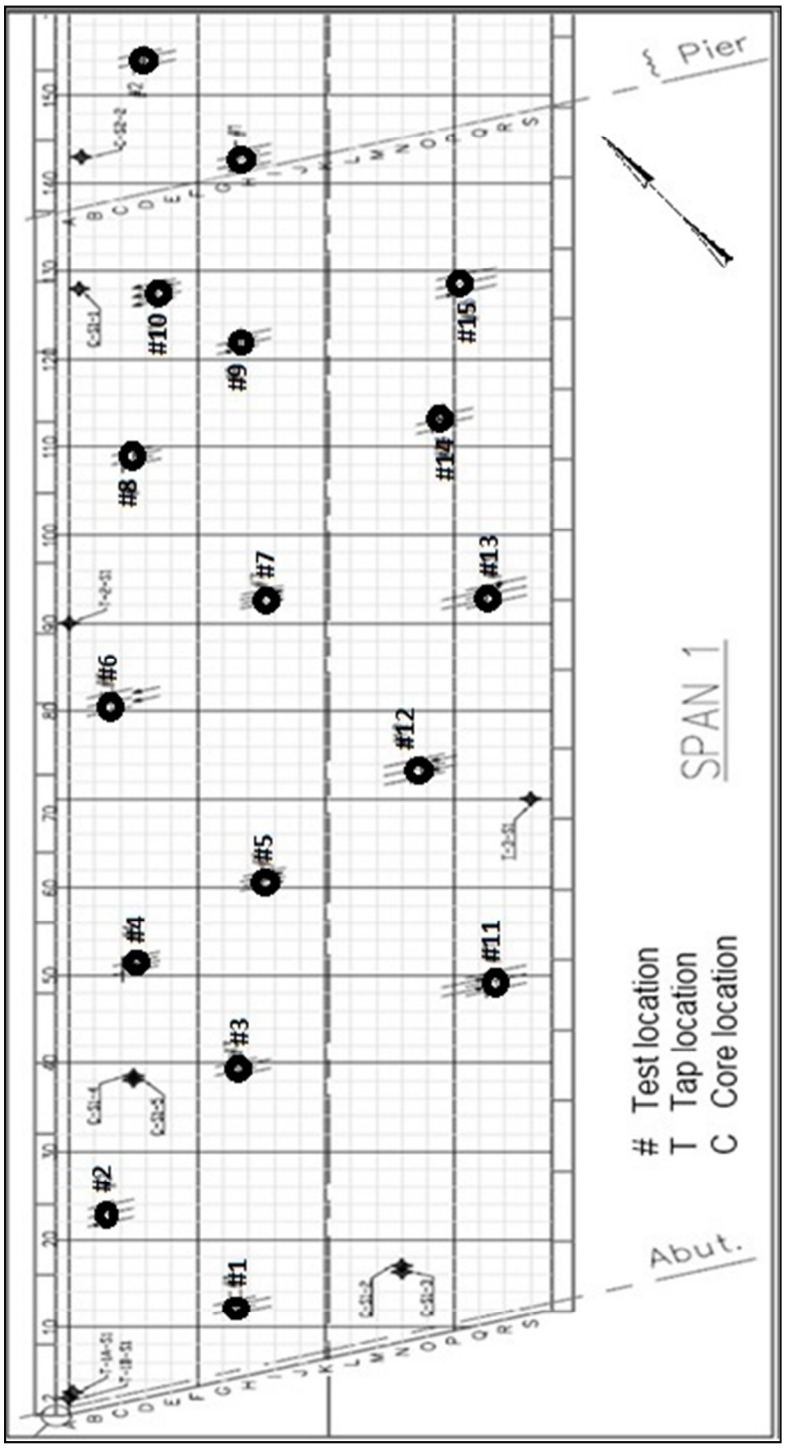

Figure 31 – Deck Testing Locations – Span 1

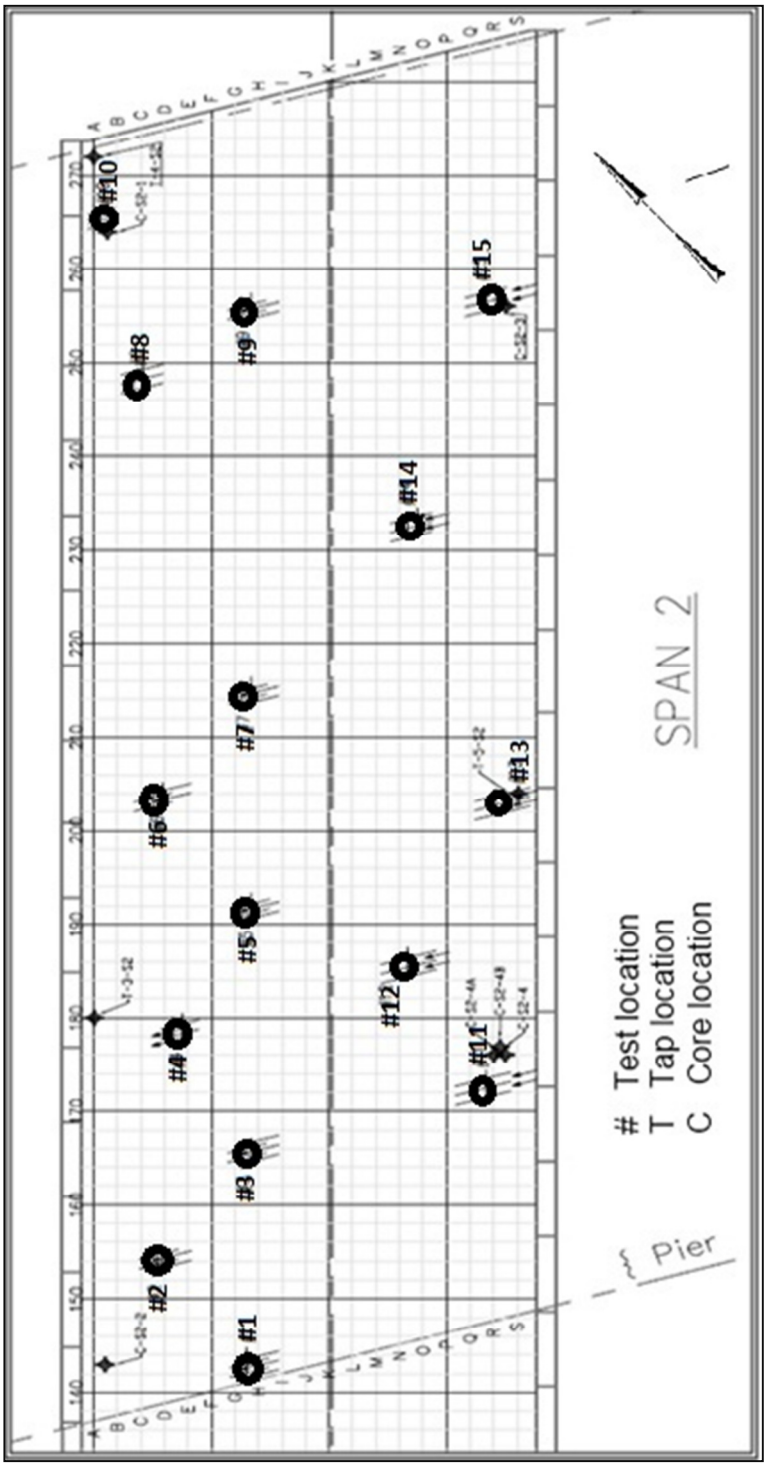

Figure 32 – Deck Testing Locations – Span 2

Figure 33 – Continuity Test on Bridge Deck

Corrosion Potentials

Corrosion potentials were taken according to the procedure presented in ASTM C 876-09, "Standard Test Method for Half-Cell Potentials of Uncoated Reinforcing Steel in Concrete".

Figure 34 shows the CSE half-cell test apparatus.

It is important to note that ASTM C 876-09 test procedure specifically states that it is applicable to uncoated steel (UCS) and thus not ECR. However, Ramniceanu (2004) has shown that half-cell potential readings on aged ECR are stable and normally distributed. However, no guidelines were presented for interpretation of results on ECR.

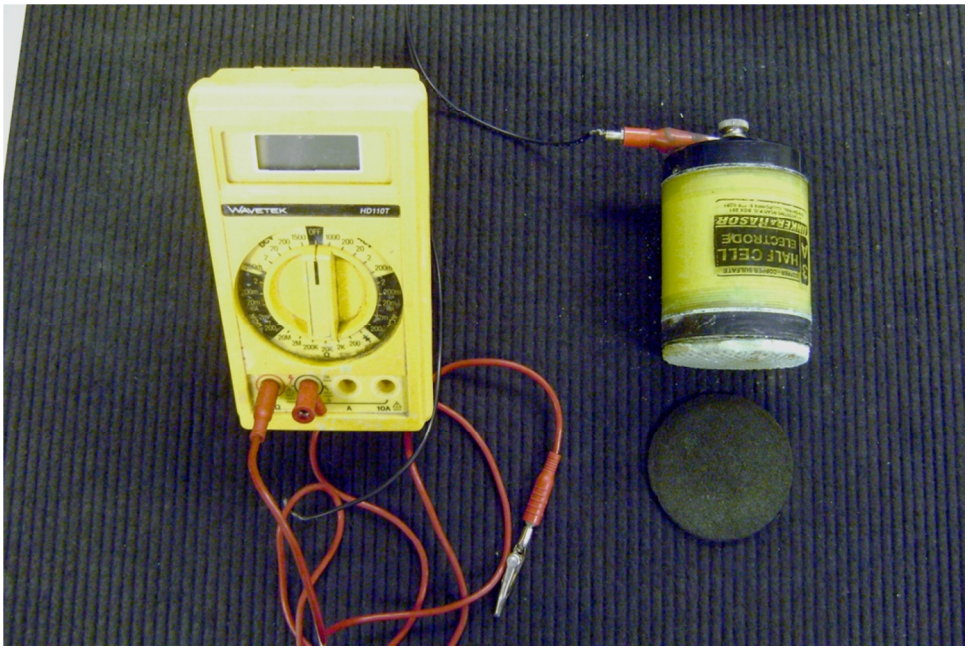

Figure 34 – Half-Cell Potential Apparatus

Corrosion Rates (CCD)

Corrosion rates were measured using three-electrode linear polarization (3LP) device, which measures the corrosion current density (CCD) of the reinforcing steel at a test location, see Fig 35. The three electrodes are:

1. A reference half-cell electrode
2. A working electrode (the reinforcing steel, in this case)
3. A counter electrode

An electrical connection is first made to the reinforcing steel (Clear 1989). The polarized surface area (PSA) of the reinforcing steel is assumed to be circumference of the reinforcing bar multiplied by the length of the bar below the counter electrode. The basic procedure of this test is:

1. Measure the static potential (CSE half-cell potential),
2. Measure the current between the counter and working electrodes required to produce a small change in the potential of the working electrode of 4 mV.
3. Repeat the previous step for 8 and 12 mV.
4. Determine the best-fit linear line for current versus potential.

Figure 35 – Corrosion Rate Testing with 3LP Device

The slope of the best fit line on the potential vs. current represents the polarization resistance (1/R). Then, corrosion current can be calculated using the Stern-Geary equation, in the form below (Clear 1989).

$$I_{corr} = \frac{\Delta I_{appl}(\beta_a \beta_c)}{2.3\Delta\varphi(\beta_a + \beta_c)} \quad \text{Eqn. 43)}$$

$$i_{corr} = \frac{40.76 * I_{corr}}{A_{bar}} \quad \text{Eqn. 44)}$$

Where I_{corr} = corrosion current in mA

I_{appl} = DC current required to cathodically polarize the bar from its natural electrical half-cell potential to 4, 8, and 12 mV.

$\Delta\varphi$ = Absolute value of cathodic polarization potential minus the natural electrical half-cell potential

β_a = Anodic Tafel constant = 150 mV/decade

β_c = Cathodic Tafel constant = 250 mV/decade

i_{corr} = corrosion current density (CCD) in mA/sf.

A_{bar} = area of polarized steel in ft²

Note that this unguarded 3LP test was developed for UCS. The epoxy coating used on reinforcing steel may be dielectric with holidays and other imperfections, so the area of polarization is highly uncertain.

However, Ramniceanu (2004) noted that based on the limited data, a possibility exists for the 3LP test to be used on ECR.

Concrete resistivity

Whereas the CSE and 3LP tests provide information regarding the corroding state of the reinforcing steel, they provide no direct evidence of the moisture content of the concrete. Concrete moisture content and connectivity not only influence the reinforcing steel corrosion and rate of chloride ingress, but almost every other reinforced concrete deterioration mechanism. Since concrete resistivity varies across a deck, a distribution of values is needed for performance assessment purposes. Resistivity readings were taken at the same previously shown 30 test locations. Two type of resistivity tests were used, four-point (Bungey, 1989) and single point tests. The four-point Wenner probe (FPWP), resistivity test is illustrated in Fig. 36. The four-point resistivity is calculated as follows (Carino, 1999).

$$\rho = \frac{2\pi aV}{I} = 2\pi aR \qquad \text{Eqn. 45)}$$

Where ρ = resistivity of the concrete

a = spacing between the probes

V = voltage potential between probes, volts

I = input AC square wave of 10 Hz

R = measured resistance, ohms

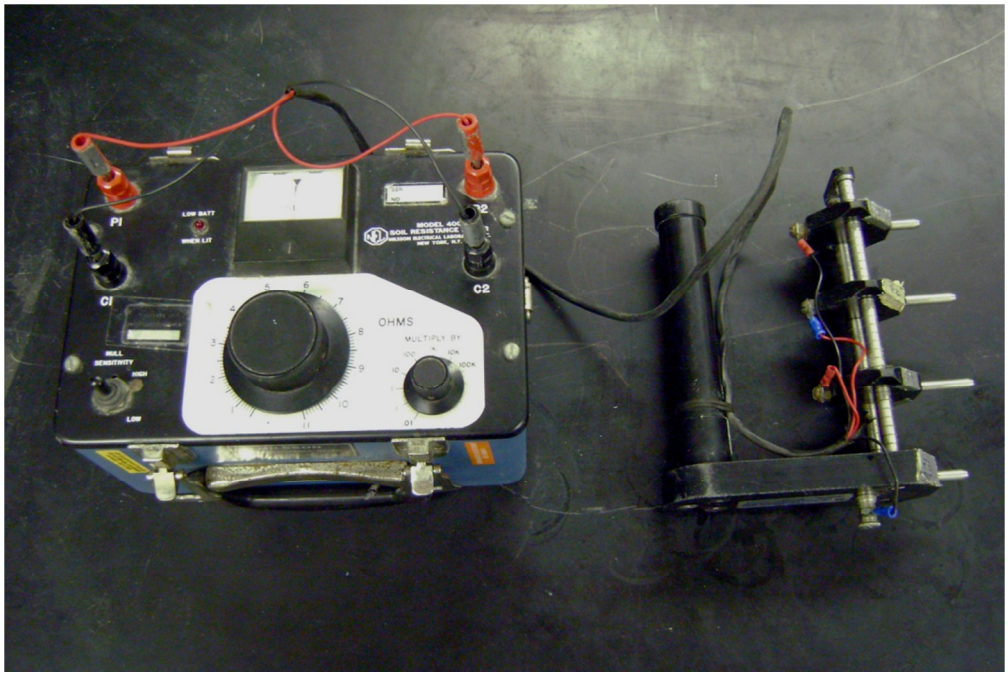

Figure 36 – Four Point Wenner Probe Apparatus

Thus, the FPWP is to measure the resistivity of the concrete to depth of the spacing of the probes, which was set at 2.0 in. (51 mm). It is highly influenced by the concrete moisture content and concrete pore water connectivity. The single point resistivity uses the same meter as the FPWP, but a single probe of size 3 in. diameter is placed directly over a located reinforcing bar. The clear concrete cover depth is measured. Fig. 37 shows the single point resistivity. The resistivity is calculated as:

$$\rho = \frac{\pi {d_e}^2}{4 * (D_c + \frac{1}{2} d_b)} \qquad \text{Eqn. 46)}$$

Where, ρ = resistivity, ohm-m

d_e = diameter of electrode, m

D_c = cover depth, m

d_b = diameter of steel bar, m

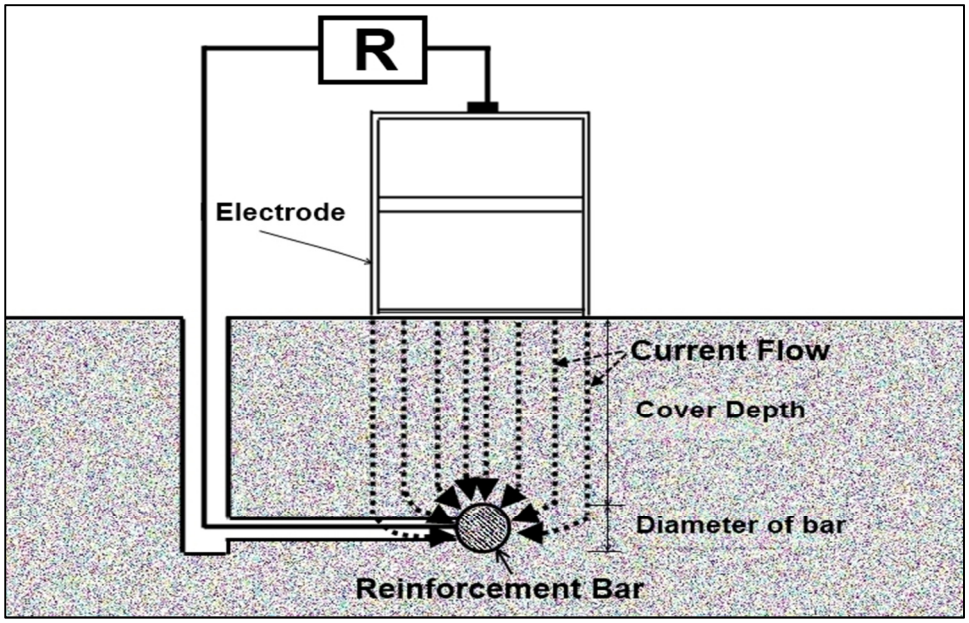

Figure 37 – One Point Resistivity Measurement

Chloride Content

Chloride content of the concrete is perhaps the most important measure in determining the overall corrosion state of the deck. Determining the chloride content at various depths is used to assess the corrosion state of the reinforcing bar and the determination of the chloride ingress rate need to model the corrosion resistance performance of reinforced concrete structural components. Test locations are the same 30 locations as the other corrosion survey locations. Powdered samples were drilled dry using a rotator impact hammer drill. The bit diameter was 1.25 in., slightly greater than 1.5 times the maximum aggregate size of 0.75 in. (19 mm) and in 0.5 in. (13 mm) depths in order to provide a representative concrete sample and quantity for chloride testing. Powder samples were collected by vacuum and deposited in a filter chamber. Between each depth sampling, the powdered sample and filter were removed and placed in marked sample bags. The collection unit, drill bit, and drill hole were cleaned to prevent cross contamination. The drill bit was inserted in the hole to the bottom of the hole before drilling was again started. Powdered samples were collected for the following depth ranges and average:

Range, in. (mm)	Average, in. (mm)
0.25 (6.3 mm) to 0.75 (19 mm)	0.50 (13 mm)
0.75 (19 mm) to 1.25 (32 mm)	1.00 (25.4 mm)
1.25 (32 mm) to 1.75 (44 mm)	1.50 (38 mm)
1.75 (44 mm) to 2.25 (57 mm)	2.00 (51 mm)
2.25 (57 mm) to 2.75 (70 mm)	2.50 (63.5 mm)
2.75 (70 mm) to 3.25 (83 mm)	3.00 (76 mm)
3.25 (83 mm) to 3.75 (95 mm)	3.50 (89 mm)

The top 0.25 in. of deck concrete was discarded due to the large concentration changes which take place during winter salting months and the remaining precipitation periods. The chloride content was determined in accordance with ASTM C 1152/C 1152M-04 –Test Method for Acid-Soluble Chloride in Mortar and Concrete. The chloride titration results are based on the weight of the concrete test sample and are then used to develop a chloride concentration profile from the near surface to the sample depth.

Concrete Cores

A total of 20 cores were removed from the deck, locations are also shown in Figures 31 and 32. Table 12 presents the grid locations and dimensions of the cores. All the cores but one were free of reinforcing steel, see Fig. 38. The cores were drilled using a water-cooled diamond drill bit. Surface water was allowed to dry before the cores were wrapped in plastic sheet and then aluminum foil and duct tape to preserve the in situ moisture conditions. The concrete cores were then tested to measure compressive strength, static modulus, moisture content, unit weight, permeability, and electrical charge passed. The core containing a piece of reinforcing steel was also subjected to corrosion rate and corrosion potential testing.

Figure 38 - Core Showing Cracking Over Corroded ECR

The compressive strength was conducted in accordance with ASTM C 39/C 39M-09a – Standard Test Method for Compressive Strength of Cylindrical Concrete Specimens, and static modulus in accordance with ASTM C 469-02 – Standard Test Method for Static Modulus of Elasticity and Poisson's Ratio of Concrete in Compression. These properties will be used for characterizing and evaluating structural behavior and refining the Finite Element Model of the bridge.

Table 12 – Table of Core Grid Locations and Dimensions

CORE	LOCATION		DEPTH (in)	DIAMETER (in)
	L (ft)	T (ft)		
C-S1-1	128	A.5	2.00	4.00
C-S1-2	17	N	8.00	4.00
C-S1-3	16.5	N	5.50	4.00
C-S1-4	38.5	C.5	6.25	4.00
C-S1-5	38	C.5	8.25	4.00
C-S2-1	264	A.5	6.00	4.00
C-S2-2	143	A.5	6.75	4.00
C-S2-3	256	R.5	5.75	4.00
C-S2-4	176	R.5	3.75	4.00
C-S2-4A	176	R	3.00	3.63
C-S2-4B	176	R.5	4.00	4.00

T-SOUTH-ABUT.	4	J	1.00	2.00
T-NORTH-ABUT.	270	J	1.25	2.00
T-1A-S1	1	A	7.00	4.00
T-1B-S1	1	A	2.75	4.00
T-2-S1	90	A	1.50	4.00
T-3-S1	70	S	2.25	4.00
T-3-S2	180	A	2.25	4.00
T-4-S2	270	A	2.50	4.00
T-5-S2	204	S	2.75	4.00

The electrical charge passed was measured using ASTM C 1202-10 – Standard Test Method for Electrical Indication of Concrete's Ability to Resist Chloride Ion Penetration. Based on the charge passed, the concrete resistance to chloride penetration can be characterized using criteria set forth in ASTM C 1202-10.

ANALYSIS AND DISCUSSION

Damage Survey:

Table 13 presents the percent damaged surface area.

Table 13 – Percent Deck Surface Damages on Virginia Pilot Bridge

Delaminations	Passing Lane Shoulder	Passing Lane	Travel Lane	Break Down Lane	Total
Span 1	16.6	3.5	12.0	23.2	13.1
Span 2	9.7	11.0	11.1	26.8	14.8
Total	13.1	7.2	11.5	25.0	13.9

Although the percent total damaged area on spans 1 and 2 are about equal, 13.1% and 14.8% respectively, there is difference between areas. Span 1 passing lane shoulder is significantly greater than span 2, 16.6% and 9.7% respectively. The reverse is true for the passing lane of spans 1 and 2, 3.5% and 11.0% respectively. Whereas, the travel lane and break down lane in spans 1 and 2 are somewhat similar, see Table 13. The combined span 1 and 2 travel and break down lanes contained 71% of the total damaged area. Of interest is the deck surface water drainage which drains transversely across the deck to the drains in the break down lane. Also, during winter months, snow and melt water would pond in the break down lane area.

Cover Depths

Bridge deck cover depth specifications are configured to result in a low percentage of reinforcing steel with a cover depth of 2.0 in. Bridge deck cover depths are typically normally distributed with a standard deviation of less than 0.38 in. Figure 39 presents the cover depth distribution along with the descriptive statistical terms. As shown, the distribution is approximately normal and the mean and median are equal considering the practicalities of construction methods, 2.25 and 2.27 in., respectively. Considering normal distribution characteristics with a mean of 2.25 in. and a standard deviation of 0.27 in., 95 percent of the reinforcing steel has a cover depth between 1.72 and 2.78 in. And 17.6 percent of the reinforcing steel has a cover depth of less than 2.0 in.

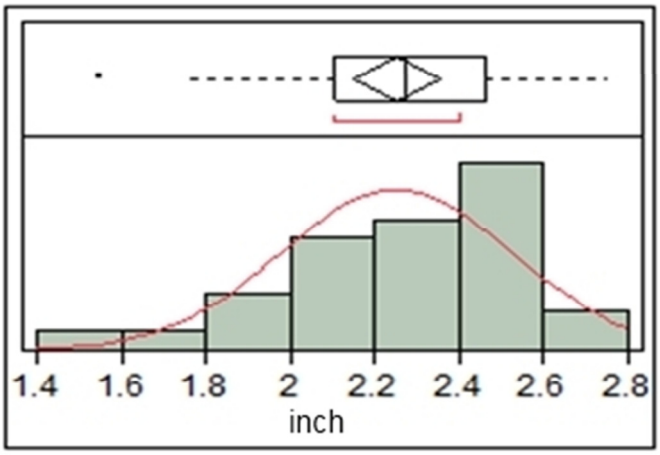

Figure 39 – Distribution of Transverse Cover Depths taken from 30 Test Locations

The cover depth distribution is used in the service life corrosion performance model. As such, cover depths can be an indicator of the possibility of early corrosion activity. With 17.6 percent of reinforcing steel having a concrete cover of less than 2.0 in. would in general, indicate a less than desirable corrosion protection provided by the concrete. The relatively low concrete cover would have had an influence on the 14 percent delaminated area occurring within the 30 year service life.

Continuity

Figure 40 presents the location plan for the continuity testing. Table 14 presents the grid locations as longitudinal and transverse distances and the measured ohmic resistance between the numbered locations.

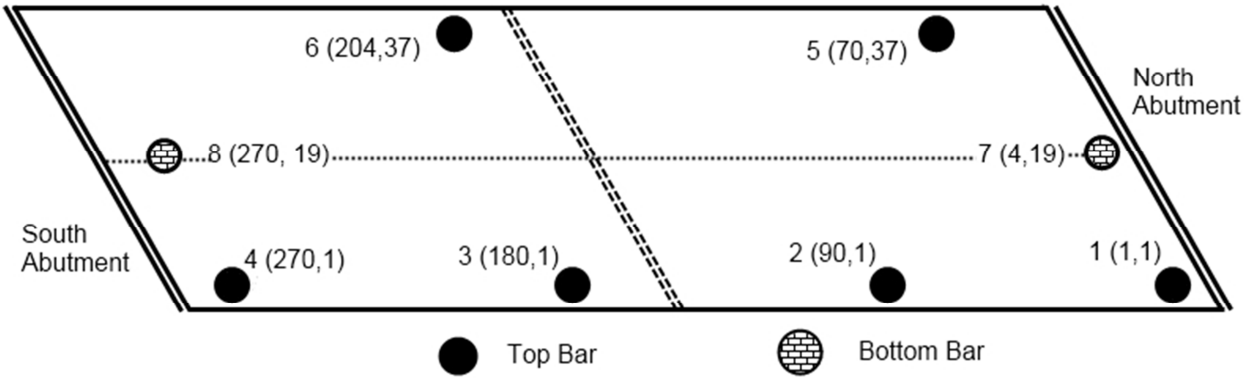

Figure 40 – Plan Locations of Continuity Locations

As shown, ohmic resistance is relatively constant with a range of 1.9 to 2.8 ohms and an average of 2.5 and a standard deviation of 0.3 ohms. The measured ohmic resistance of the spooled wire is 2.1

ohms. One connectivity resistance value (1.9 ohm) was found to be less than the resistance of spooled wire, which may be related to contact error. Thus, the top ECR mat is electrically continuous, the bottom uncoated mat is electrically continuous, and the top and bottom mats are electrically continuous with each other. The continuity condition allowed for the conduction of electrical corrosion tests, potentials, corrosion rates, and single point resistivity, using the various top mat tap locations.

Table 14 – Continuity Connection Locations and Ohmic Resistance between Locations

Connection Locations				Measured Resistance		
No.	Longitudinal (ft)	Transverse (ft)	Rebar Mat	Location A	Resistance (Ohm)	Location B
1	1	1	top	1	2.5	2
2	90	1	top	2	2.6	3
3	180	1	top	3	1.9	4
4	270	1	top	1	2.6	3
5	70	37	top	1	2.8	4
6	204	37	top	2	2.8	4
7	4	19	bottom	3	2.5	8
8	270	19	Bottom	7	2.5	8
				5	2.7	6

Corrosion Potentials

Corrosion potentials are considered to be normal distributions. Figure 36 presents the distribution of corrosion potentials with associated descriptive statistic parameters for a normal distribution. As shown in Figure 41, the potential distribution appears somewhat of a normal distribution. However, the difference between the mean and median is somewhat large, 32 mV. Ninety five percent of the potentials are between 110 and 493 mV, considering the potentials as normally distributed.

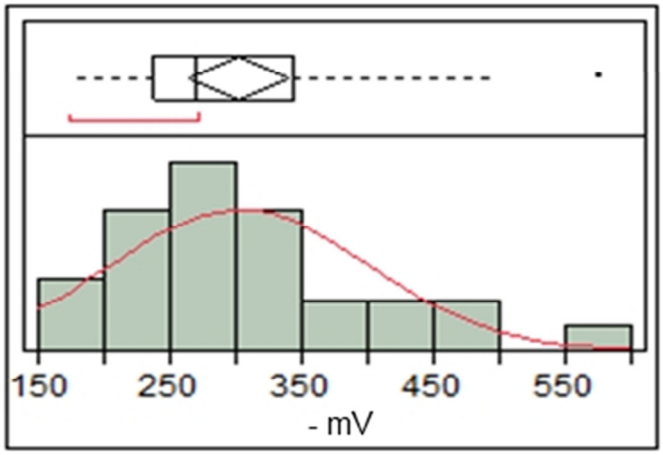

Mean	302
Std. Dev.	97.7
Median	270
Upper 95%	493
Lower 95%	110
n	30

Figure 41 – Distribution of Corrosion Potentials taken from 30 Test Locations

As previously stated, the ASTM standard test method for corrosion potentials of reinforcing steel in concrete is for uncoated bar. However, Ramniceanu (2004) has shown that corrosion potentials of ECR can be measured for field structures and the measurements are normally distributed. Brown (2002) conducted a chloride corrosion resistance study of ECR in concrete cores taken from Virginia bridge decks. The cores were ponded with a chloride solution and corrosion initiation was measured over time using electrochemical impedance spectroscopy (EIS). Of the 256 ECR cores, corrosion initiation was identified in 93 cores. Analysis of the EIS measurements of the 93 cores using the change in CSE corrosion potential along with the associated change in impedance and phase angle was conducted to identify the risk of corrosion for ECR using CSE potentials measurements. Table 15 presents the results of the analysis for corrosion risk and CSE potentials for ECR.

Table 15 – Interpretation of Corrosion Risk of ECR in Concrete from CSE Potential Measurements

Corrosion Risk	Potential (mV)
High	< -300
Moderate	-200 to -300
Low	> -200

The interpretations of the CSE for ECR presented in Table 12 are in general agreement with ASTM C 876-09 and with a study conducted by Balakumaran (2010) for uncoated bar. The percentages of corrosion risk based on the ranges in Table 15 are presented in Table 16.

Table 16 – ECR Corrosion Risk of Virginia Pilot Bridge Deck

Corrosion Risk	Percent CSE Values
High	50
Moderate	35
Low	15

As shown in Table 16, only 15 percent of the measured ECR shows a low risk of active corrosion.

Three-Electrode Linear Polarization

Figure 42 presents the distribution of the 30 3LP CCD measurements along with the descriptive statistic parameters. As shown, the CCD values are highly variable, coefficient of variation (C.V.) of 86 percent and the distribution is not normal, skewed to the lower values.

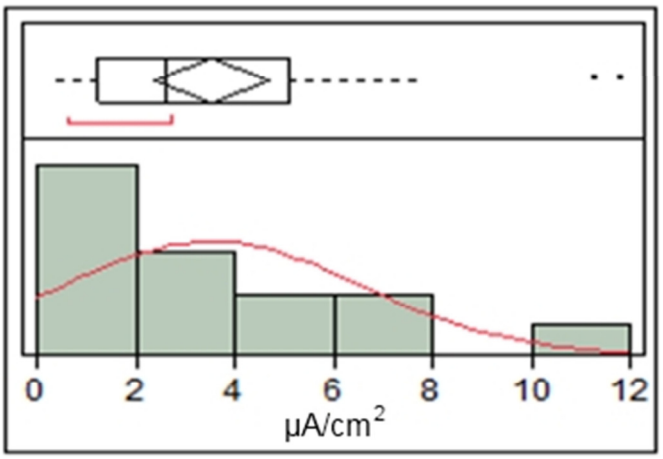

Figure 42 – Distribution of Corrosion Current Densities

Table 14 shows an interpretation of 3LP measurements conducted by Balakumaran (2010) on uncoated bar (UCR) and percentage of CCD values with the corrosion risk categories.

Table 17 – Interpretation of 3LP Measurements on Uncoated Reinforcing Steel and Percentage of ECR Measurements

Corrosion Risk	3LP/CCD (μA/cm²)	VA Pilot Bridge Deck (%)
High	> 3.0	40
Moderate	1.0 to 3.0	37
Low	< 1.0	23

As shown in Table 13 and 14, the relative risk of corrosion of the ECR as indicated by the CSE and CCD measurements are in general agreement with 50 vs. 40, 35 vs. 37, and 15 vs. 23 percent high, moderate, and low, respectively for the percentages of CSE vs. CCD.

One-Point Resistivities

The one-point resistivities values represent the combined resistivity as a cylindrical volume of concrete directly above the ECR and the resistivity of the epoxy coating. Figure 43 presents the distribution of OPR values. As shown by the descriptive statistical parameters, the distribution is not normally distributed, skewed to the lower value and extremely variable, C.V. = 103%.

The OPR test is a relatively new method on UCR and ECR, thus there is presently no interpretation of measured values and corrosion risk. However, there should be an interaction between CSE, CCD, and OPR. An assessment of this interaction is presented in the following section.

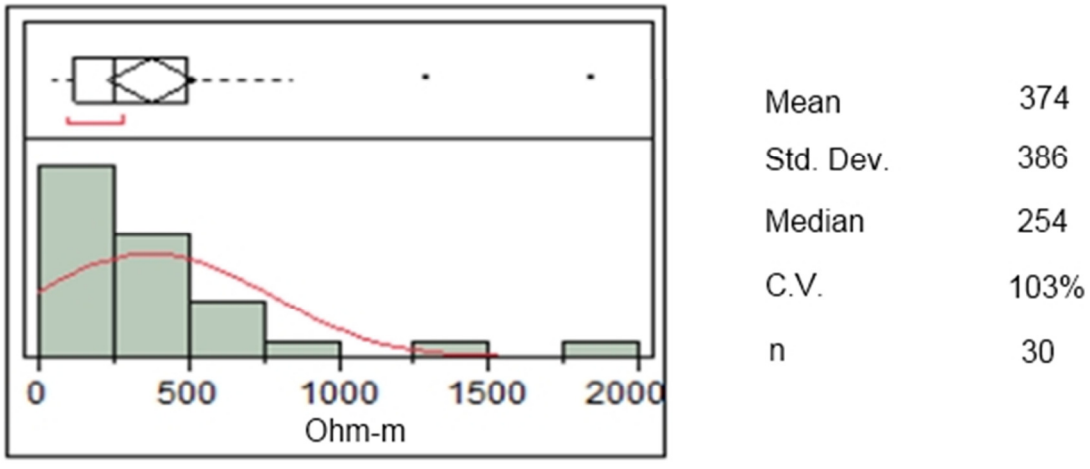

Figure 43 – Distribution of One-Probe Resistivities

CSE/CCD/OPR

Simply considering Ohm's law:

$$E = IR \qquad \text{Eqn. 47)}$$

Where, E = potential, volts

I = current, amps

R = resistance, ohms

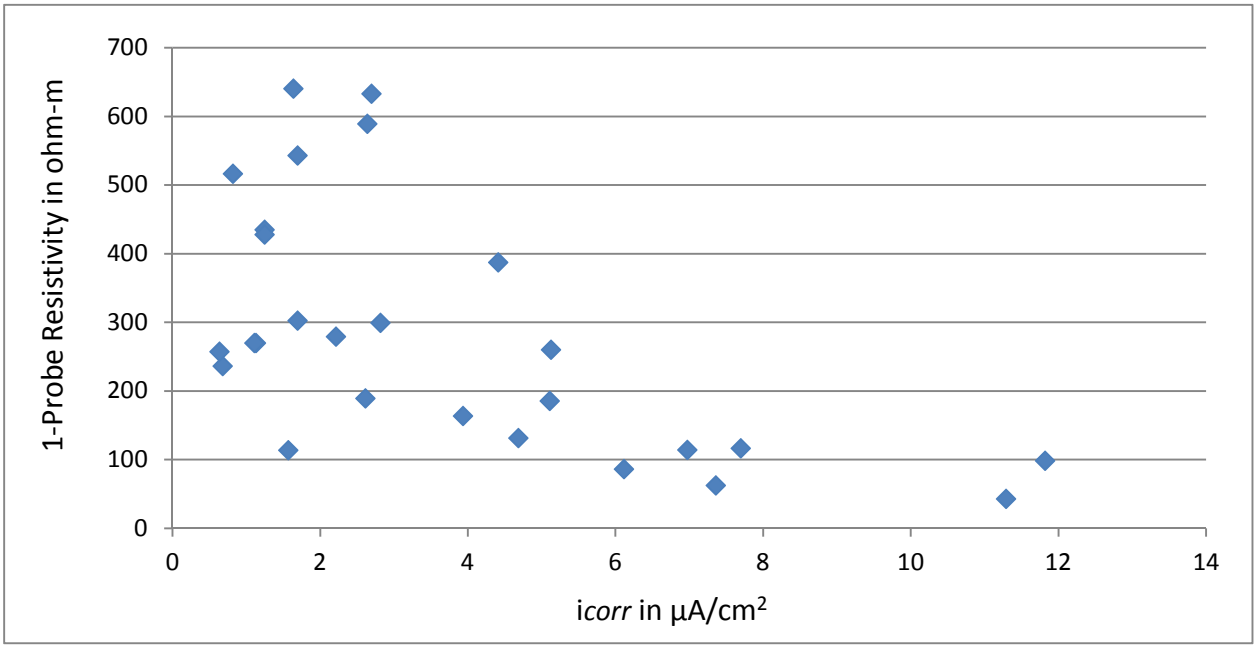

Figure 44 – One-Point Resistivity Versus Corrosion Current Density

CCD should have the form of 1/OPR. As shown in Figure 44, the general form of the relationship is met, lower resistivity results in high corrosion current density and higher resistivity results in lower corrosion current density.

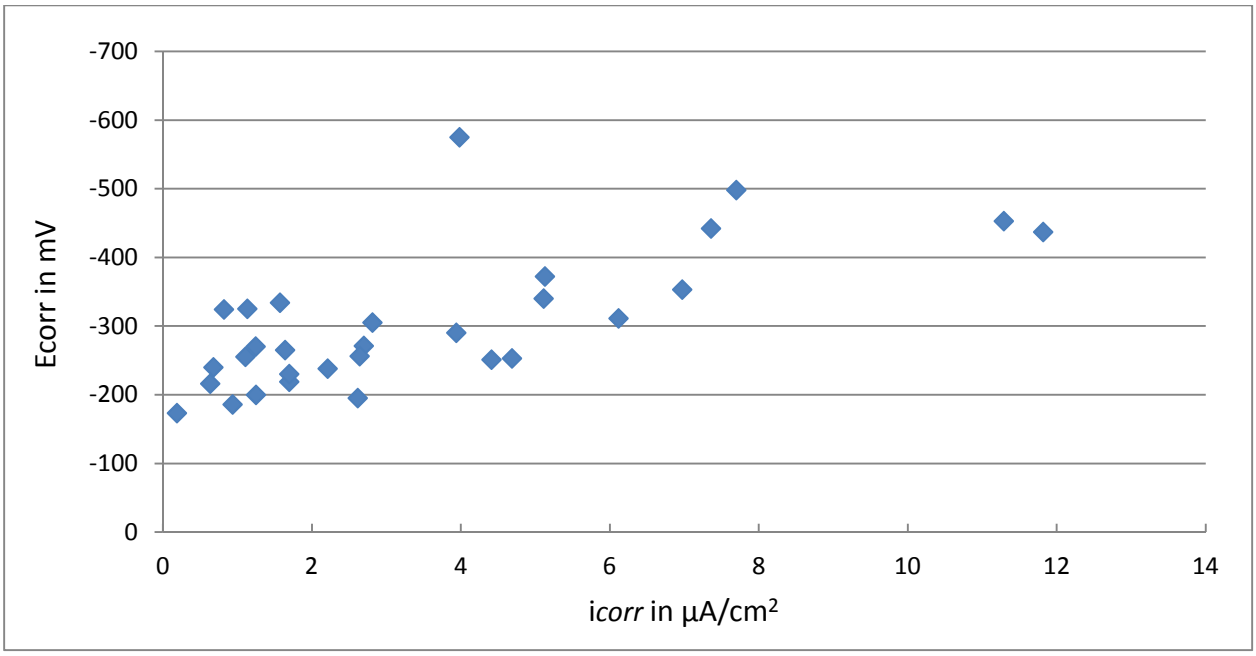

Figure 45 – CSE Potentials Versus Corrosion Current Densities

Likewise, as the CSE potential increases, the CCD should also increase. Figure 40 demonstrates this general form, the more negative the CSE potential the greater the CCR. Also illustrated in Figure 45, for CSE > -200 mV, the CCD is less than 1 µA/cm², between -200 and -300 mV the CCD ranged between 1 and 3 µA/cm² and less than -300 mV the CCD was generally greater than 3 µA/cm². Thus, the result of the 3LP measurements on this structure built with ECR is similar to the interpretation of uncoated reinforcing steel.

Four-Point Wenner Probe Resistivities

Figure 46 presents the distribution for FPWR, as shown the data is approximately normally distributed with a relatively high variability, CV = 49%. However, OPR variability is larger than the FRWP as illustrated the CV's of 49 and 103% respectively. The larger variability of the OPR may be related to the resistivity variability of the epoxy coating. As the FPWR is a measured concrete property, whereas, the OPR measurements consist of cover concrete and coated bar state.

Figure 47 present the relationship between the OPR and FPWR. As shown, as the FPWR increases with increasing OPR but the relationship is very poorly defined, $R^2 = 0.1031$. Lack of correlation is most likely the result of the high variability of the results of both the OPR and FPWR.

Whereas the high variability of the OPR may be related to the resistivity of the epoxy coating, the high variability of the FPWR is related to the contact resistance of the four points, Ramniceanu (2004).

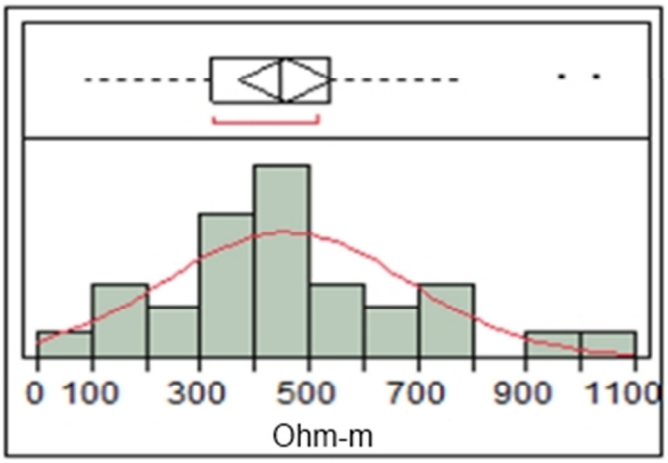

Figure 46 – Distribution of Four-Point Resistivities

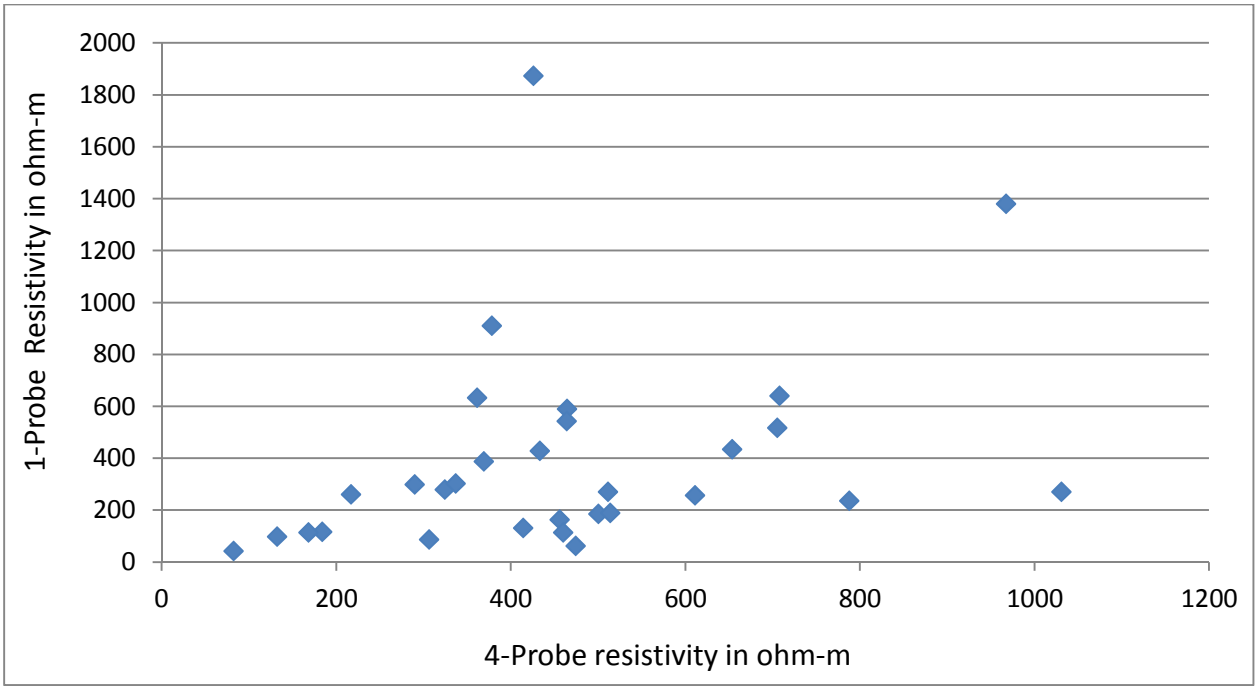

Figure 47 – One-Point Versus Four-Point Resistivities

Chloride Contents

Figure 48 present the distribution of the chloride content at an average depth of 0.5 in. The near surface chloride contents are the measured minus background. The distribution is normally distributed and relatively uniform for near surface chloride concentrations with a C.V. of 36%. The 95% limits are 14.6 and 2.62 lb/yd^3 with a mean of 8.64 lb/yd^3. The near surface chloride concentrations are typical for the Northern Virginia area where the average roadway chloride exposure is 4370 kg-Cl/lane-km (Kirkpatrick (2001), Brown (2002), Ramniceanu (2004), and Williamson (2007)).

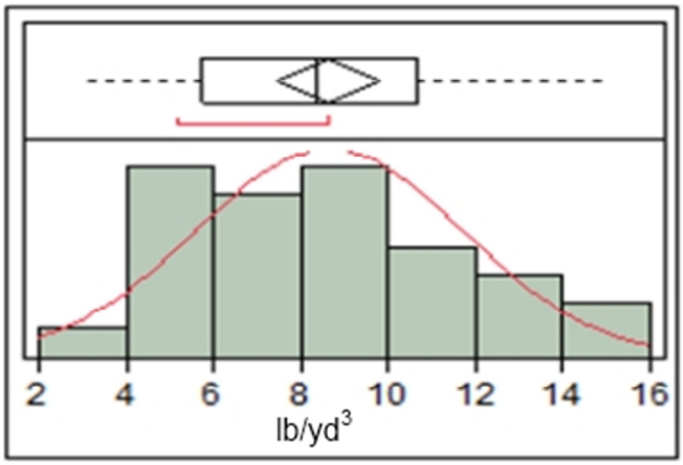

Mean	8.64
Std. Dev.	3.07
Median	8.33
C.V.	36%
Upper 95%	14.6
Lower 95%	2.62
n	30

Figure 48 – Distribution of Near Surface Chloride Contents at 0.25 – 0.75 in. depth

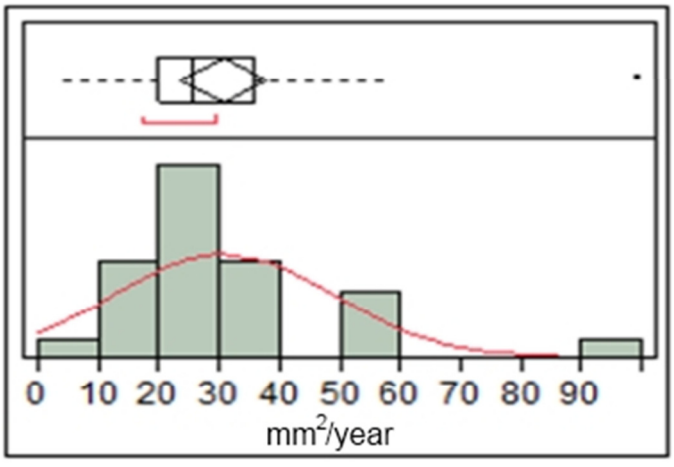

Mean	31
Std. Dev.	18
Median	26
C.V.	51%
n	30

Figure 49 – Distribution of Apparent Diffusion Coefficients

Figure 49 presents the distribution of apparent chloride diffusion constants. The apparent chloride diffusion constants were calculated using a unique solution to Fick's Second Law of diffusion as follows:

$$C_{(x,t)} = C_0 \cdot \left[1 - \text{erf}\left(\frac{x}{2\sqrt{D_c t}}\right)\right] \qquad \text{Eqn. 48)}$$

Where, $C_{(x,t)}$ = chloride concentration at depth x and time t

C_0 = near surface chloride concentration

D_c = apparent chloride diffusion concentration

Background chloride was subtracted from the seven measured depth values in determining the 30 apparent chloride diffusion constants. As shown in Figure 50, the values ranged from about 10 to 100 mm²/year. The distribution which is not normally distributed and variability of the apparent chloride diffusion constants are also typical for Virginia bridge decks (Kirkpatrick (2001), Brown (2002), Ramniceanu (2004), and Williamson (2007)).

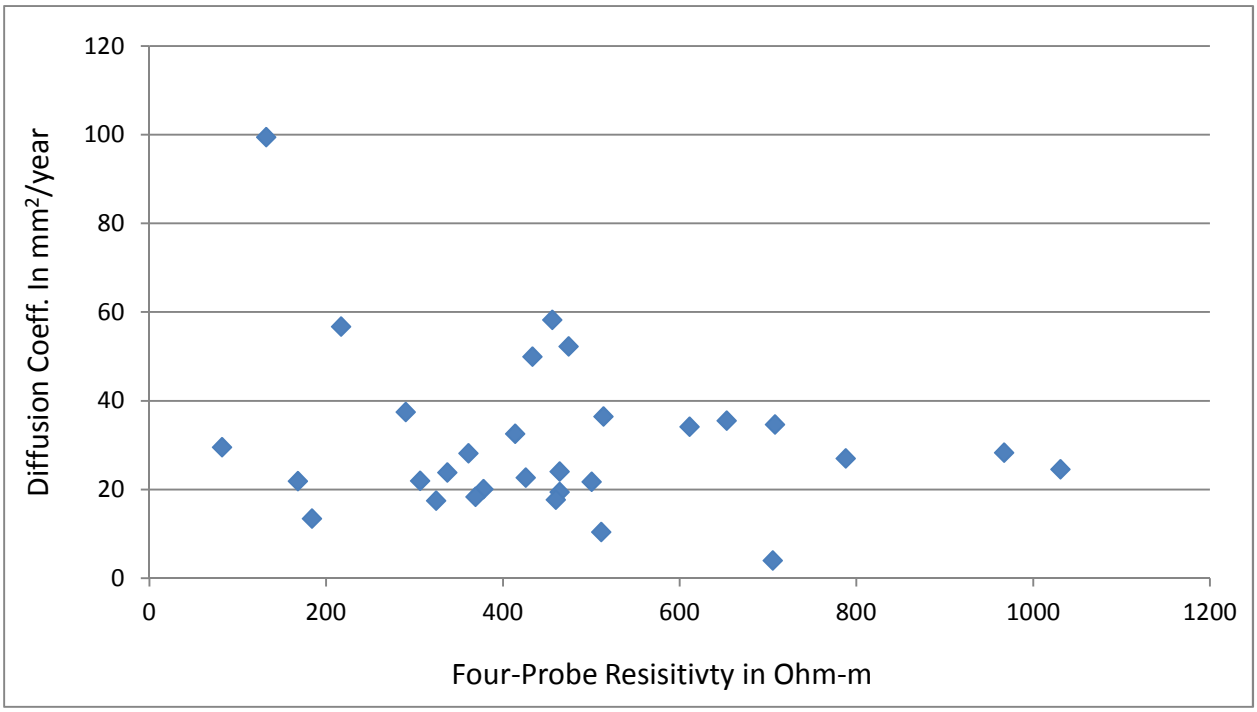

Figure 50 – Relationship between Diffusion Coefficients and Four-Point Resistivities

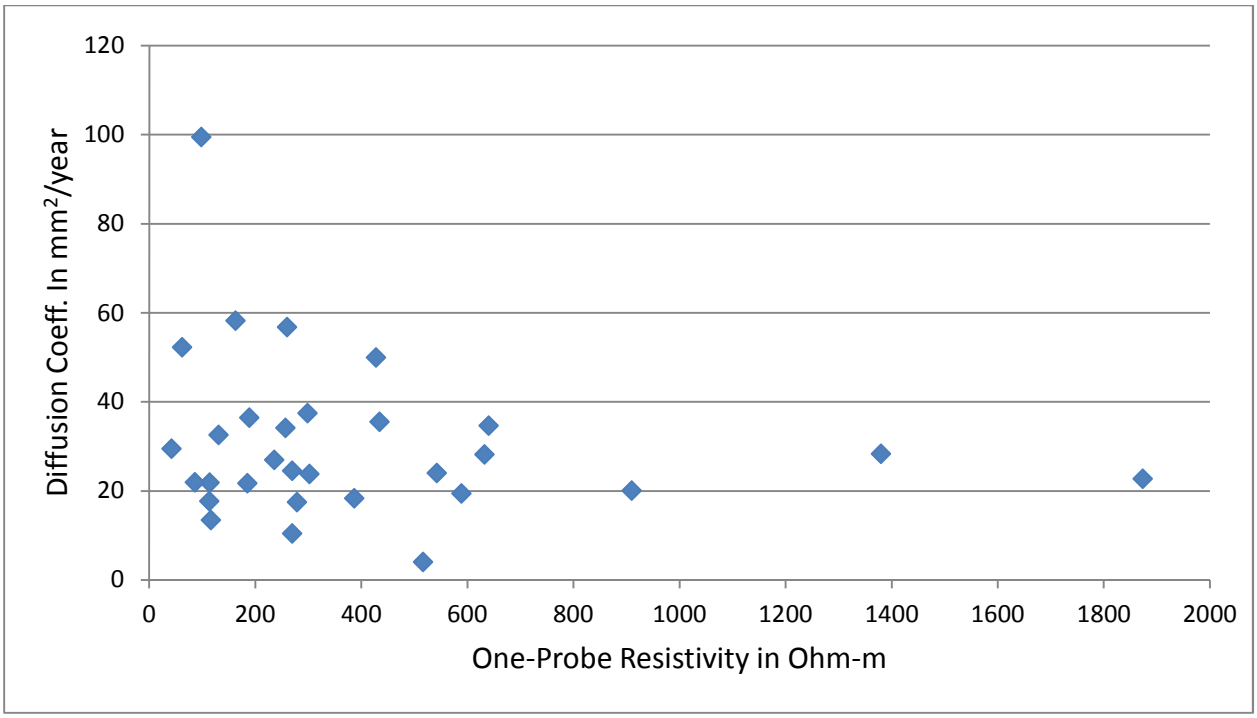

Figure 51 – Relationship between Diffusion Coefficients and One-Point Resistivities

As the FPWR and the OPR measurements, to somewhat of a less degree, are measured concrete properties influenced by the moisture content of the concrete and its ion contents, these measurements may be related to the apparent chloride diffusion constant.

Figure 50 and 51 present the apparent diffusion constant versus the FPWR and OPR, respectively. As shown, no correlation was found for these relationships.

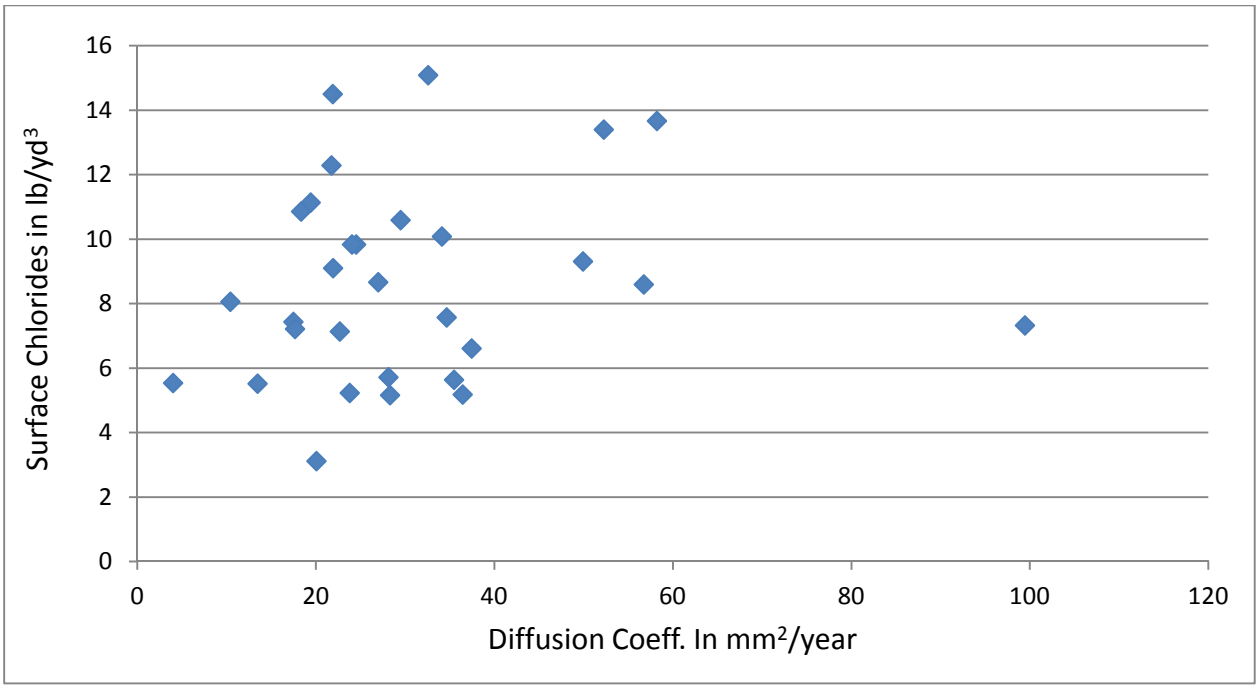

Figure 52 – Relationship between Surface Chlorides and Diffusion Coefficients

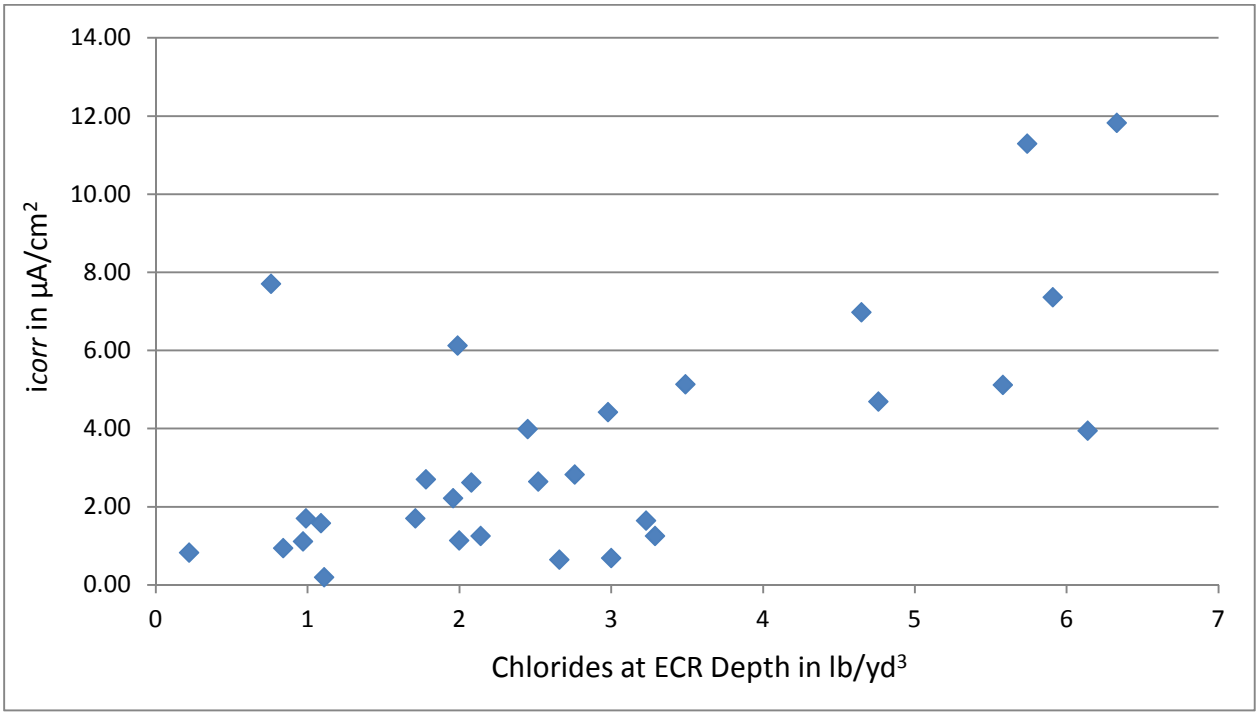

Figure 53 – Relationship between Corrosion Rates and Chlorides at ECR Depth

Figure 52 present the relationship between the near surface chloride content and the apparent chloride diffusion constant. As shown, there is no interrelationship between these parameters; they are independent as demonstrated by Fick's Second Law.

Figure 53 presents the relationship between corrosion rate and chloride content at the ECR depth. As shown, the relationship is weak, $R^2 = 0.44$, but rate of corrosion of the ECR increases within increasing chloride content.

Of interest is the observation that the measured CCD of 1.0 $\mu A/cm^2$ corresponds to a chloride concentration of 1 to 3 lb/yd^3, between 1 and 3 $\mu A/cm^2$ the chloride range is also between 1 and 3 lb/yd^3, and greater than 3 $\mu A/cm^2$ the chloride content is between 2 and 6 lb/yd^3. There are also slight variations in these observations, where corrosion rates were less than 1 $\mu A/cm^2$ and chloride content is about 3.2 lb/yd^3 and a measured corrosion rate of about 7 $\mu A/cm^2$ occurred at a chloride content of less than 1 lb/yd^3. Brown (2002) observed that cracking of 0.5 in. cover occurred at some chloride concentrations less than and some greater than that of uncoated bars. Brown (2002) also showed that some of the chloride corrosion initiation concentrations for ECR occurred at values less than and some greater than that of uncoated bars and the distribution appeared bimodal. The distribution of chloride concentration at bar depth is compared with Brown's (2002) chloride concentration at initiation, see Figure 54. Range of chlorides from this study appears to be a subset of Brown's (2002) range of values.

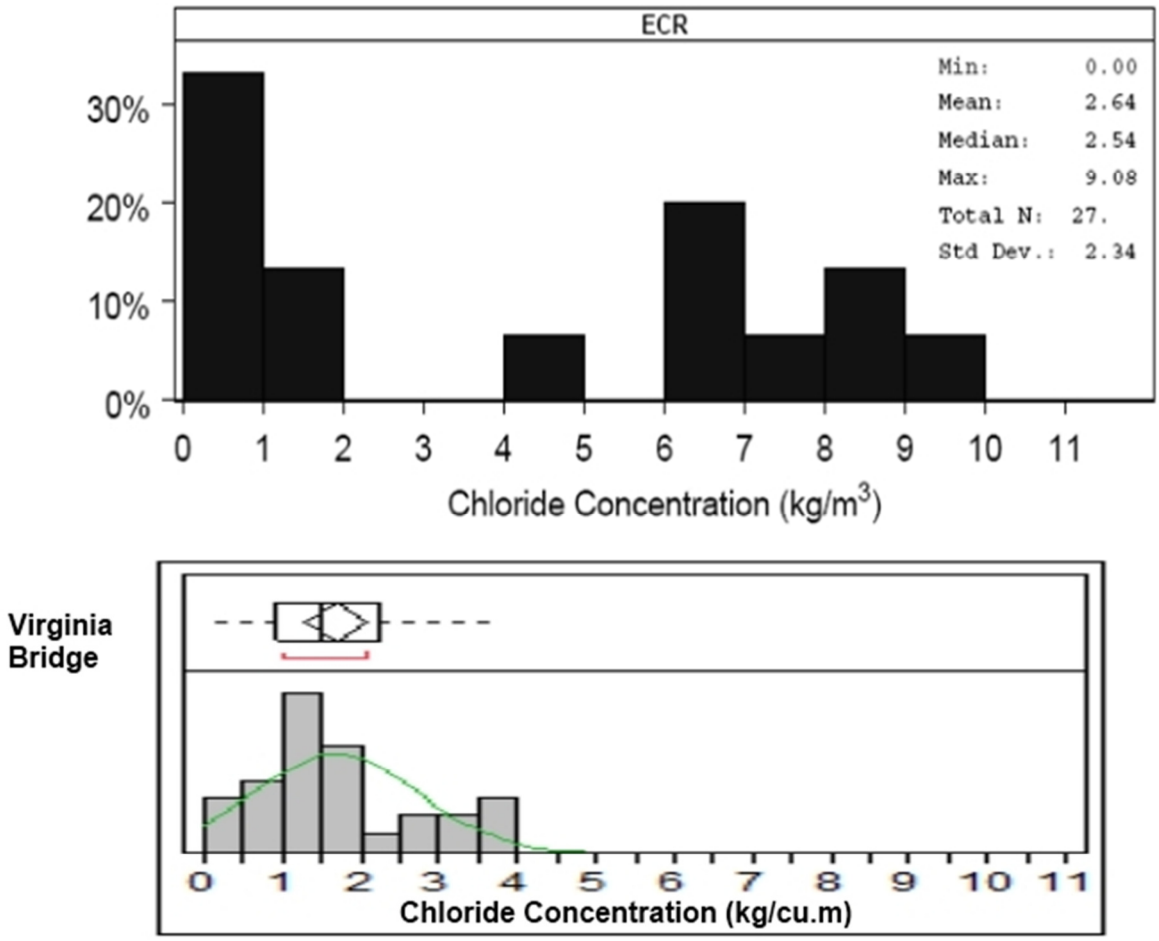

Figure 54 – Distributions of Chloride Concentration at Initiation by Brown and VA Bridge

FPWR/CCD/Chloride Concentration at ECR Depth

As shown in Figure 53, chloride concentration at ECR depth is directly related to corrosion current density. With the increasing corrosion rates, the chloride contents at ECR depth increased. The FPWR represents the electrical resistance property of concrete. It is expected to form an inverse relationship with the corrosion rates, according to the Ohm's law. Consequently, the FPWR values must also form an inverse relationship with the chloride concentration at initiation, since with higher concrete resistivities the chloride diffusion to the ECR surface will be slowed. A three-way relationship between chloride concentration at ECR depth, CCD, and FPWR, when met, may indicate the interaction of the three parameters on the corrosion of steel in concrete.

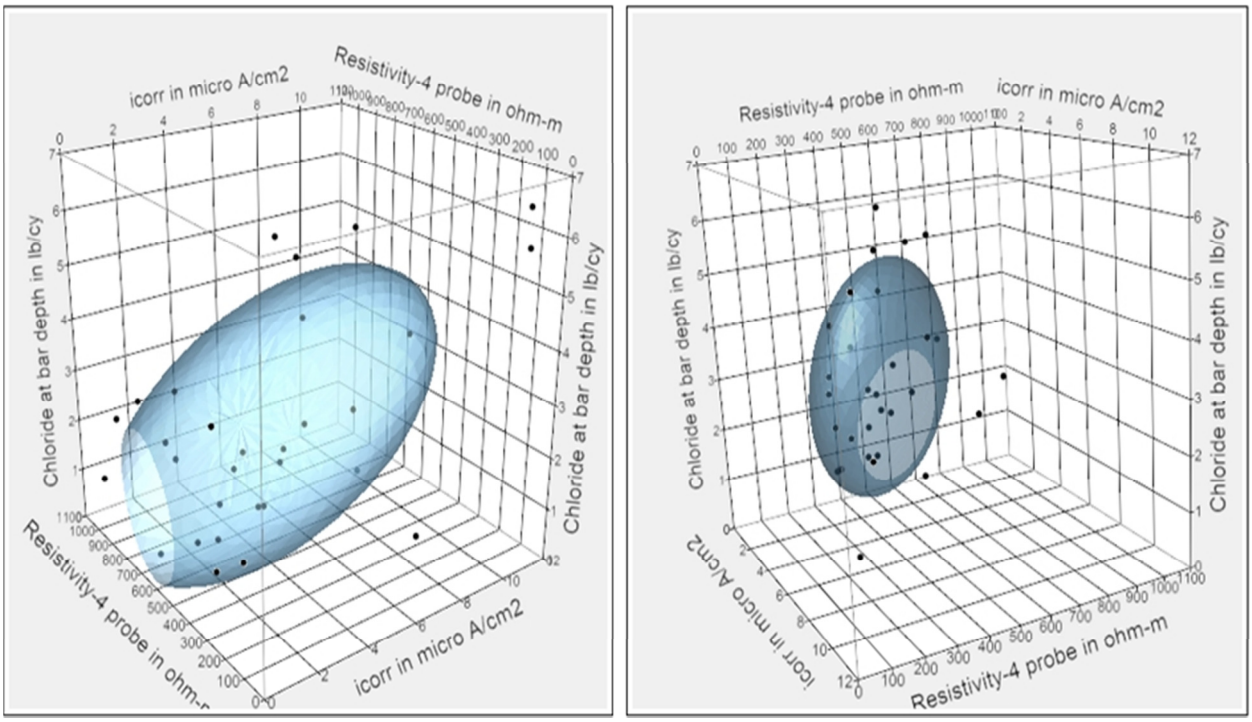

Figure 55 – Relationship between FPWR, CCD, and Chloride Concentration at ECR Depth

Figure 55 presents the two facets of the 3D scatter plot between FPWR, CCD, and chloride concentration at ECR depth. A normal contour ellipsoid was drawn over the plotted points in order to identify any patterns in the relationship, with the condition that the ellipsoid must cover at least 50% of the data points. When drawing an ellipsoid with a higher coverage, the ellipsoid became too large to be able to show a pattern.

From Figure 55, the orientation of the ellipsoid in the 3D space represents the observed data pattern. With increasing FPWR, the corrosion rates, i*corr*, and chloride concentration at ECR depth increase. The approximate orientation of the ellipsoid follows the diagonal of the 3D cube with the lower leg at the point where FPWR is maximum and, CCD and chloride concentration are minimum, and the higher leg is at the point where FPWR is minimum and, CCD and chlorides are minimum. The data points not encompassed by the ellipsoid are the result of the inherent variability in the associated corrosion measurements and the corrosion mechanisms.

Sample Size and Power

Number of tests required to obtain results which will include representative variations, similar to the whole system, to form definite conclusions about the condition of the entire structure can be estimated using a statistical term called power. Power denotes the strength of the data collected

and with increased power, the probability of type-II error decreases. The minimum sample size necessary to obtain a power of 0.9 was calculated for cover depths, diffusion coefficients, and surface chlorides.

Table 18 – Sample Size and Power Calculation

Data	Confidence	Difference to detect (Units)	Power	Sample size
Surface Chloride C_o *(lb./cy)*	95%	2	0.9	23
Diffusion Coeff. D_c *(mm^2/year)*	95%	8	0.9	29
Cover Depth X_i *(in.)*	95%	0.18	0.9	30

Table 18 presents the calculation and results of the sample size calculation. To find a difference of 2 lb/cy in the surface chlorides, we need a minimum sample size of 23. Cover depth measurements are to be performed at a minimum of 30 locations to obtain a difference of 0.18 in the resulting data, which can be obtained easily. To determine a difference of 8 mm^2/year, we need a sample of size of at least 29 for diffusion coefficients.

Service Life Estimation

Service life estimation of the Virginia pilot bridge was conducted using the chloride diffusion model based on Fick's Second Law of diffusion. The data needed to run the service life estimation are cover depths, diffusion coefficients, surface chlorides, and chloride initiation values. Cover depths, diffusion coefficients, and surface chlorides are sampled using simple bootstrapping, which involves random sampling from the given dataset. The chloride initiation values are sampled using parametric bootstrapping, either by a triangular or normal distribution.

For parametric bootstrapping of chloride initiation values, the minimum, maximum, and mode of the triangular distribution must be supplied. The chloride initiation concentrations for ECR bars were taken from the range presented in Brown's study (2002) and several iterations of minimum, maximum, and mode were selected from the cumulative distribution plot of the chloride

concentration at bar depth, see Figure 56. The slopes may indicate the accumulation of the chloride near the bar depth, while the flat zones may indicate the saturation of chloride at a particular location causing corrosion initiation.

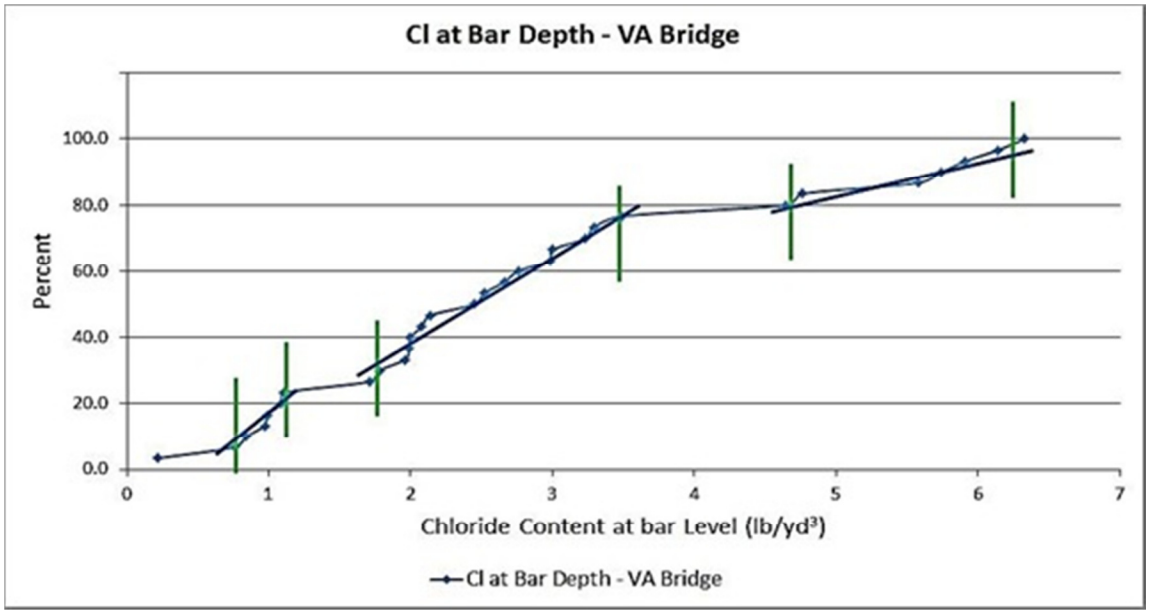

Figure 56 – Cumulative Distribution Plot for Chloride at Bar Depth of VA Bridge

Table 19 – Chloride Initiation Rates and Corresponding Service Lives for ECR

Trials	C_{xt} (lb/yd³)			14% Initiation (year)	Cracking time (year)	Total (year)
	Min	Max	Mode			
1	0.66	10.6	2.37	38	11	49
2	0.6	4.8	1.2	20	11	31
3	0.6	3.6	1.2	18	11	29
4	0.6	3.0	1.5	18	11	29
5	0.6	4.0	1.0	18	11	29
6	0.6	4.0	1.3	19	11	30
7	0.6	4.0	1.5	20	11	31
8	0.6	5.0	1.3	20	11	31

The iterations were used in the service life estimation program to determine the service lives at 14% deterioration level, which was the deterioration level of Virginia pilot bridge at 30 years. Table 19 presents the different combinations of chloride initiation values, and the corresponding estimated service life for ECR bars. As shown by trial 1, using the full range presented in Brown's work for first mode, the model overestimated the time required to reach 14% damage by 19 years (49 minus 30).

Seven chloride corrosion initiation triangular distributions were identified to be within plus/minus of one year of the 30 year damage level of 14%. Whereas trial 6 estimated 30 years to reach 14% was in agreement with the measured deck damage. Trial 6 minimum, maximum, and mode of 0.6, 4.0 ,and 1.3 lb/yd^3 (0.36, 2.4, and 0.77 kg/m^3) are in general agreement with the lower bimodal area presented in Brown's work, see Figure 54.

Trial 2 and 3, show that with a minimum and mode of 0.6 and 1.2 lb/yd^3, an increase in the maximum of 33%, from 3.6 to 4.8 lb/yd^3 resulted in only a decrease of 2 years. Likewise, keeping the minimum and maximum constant at 0.6 and 4.0 lb/yd^3 and increasing the mode from 1.0 to 1.3 and 1.5 lb/yd^3, also only resulted in a 2 year increase, see Trials 5, 6, and 7. Also, increasing the maximum by 1.0 lb/yd^3 increased the time estimate by one year, trials 6 and 8.

For service life estimation of Virginia pilot bridge, chloride initiation values were taken from the trial #6. Figure 57 represents the corrosion deterioration curve due to diffusion plus 11 year time to cracking period as the best estimate of service life performance. Accordingly, the bridge will be expected to undergo accelerated deterioration in a short time.

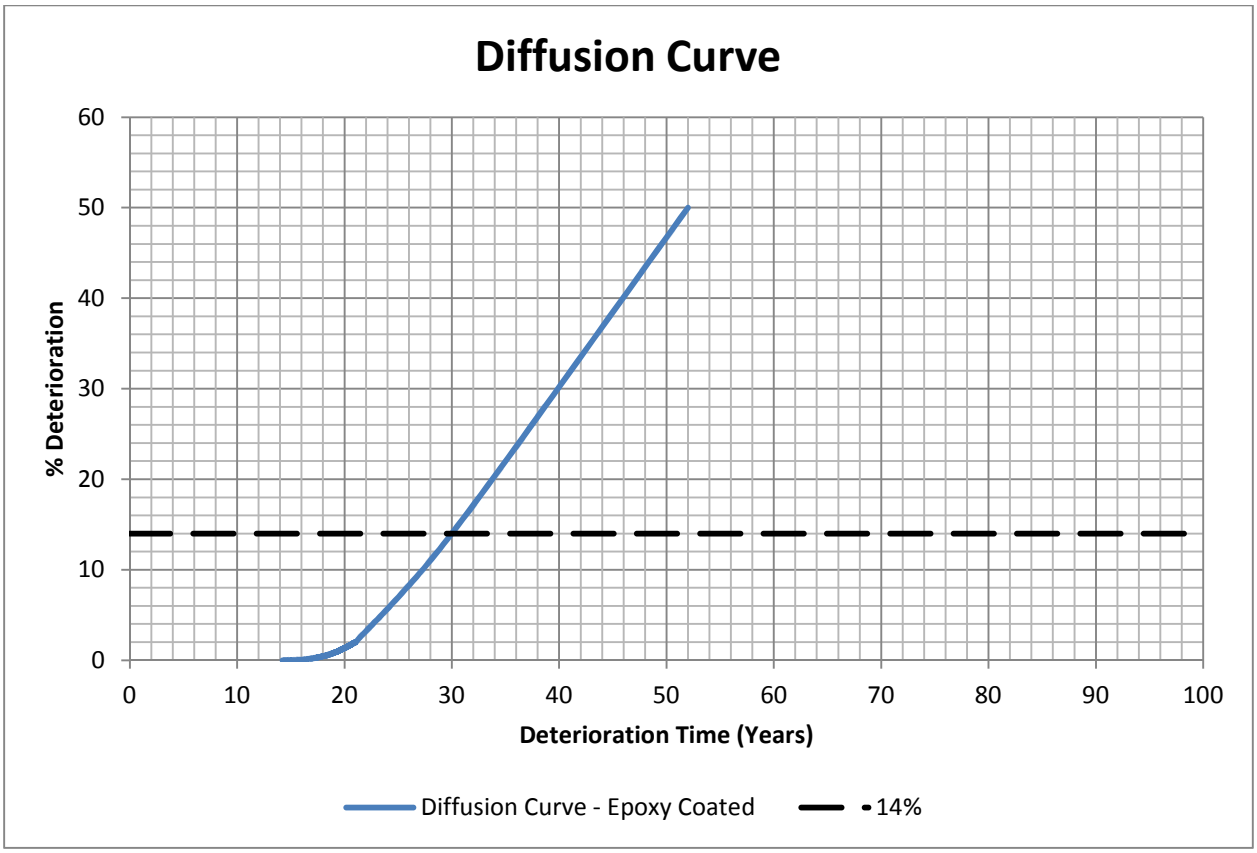

Figure 57 – Diffusion Curve for Virginia Pilot Bridge

FLORIDA PILOT BRIDGE

BACKGROUND

The Florida pilot bridge is located at the intersection of State Route 430 and Halifax River in Daytona Beach, in Volusia County, see Figure 58. The bridge was built in 1997 and carries SR 430 West bound over the Halifax River. The total length of the bridge is 2320 ft. (707.1 m) and the width of the deck including the sidewalk, barriers, and parapet is 48 ft. (14.6 m).

Figure 58 – Seabreeze Bridge over Halifax River

The bridge is a prestressed concrete continuous structure with segmental box girder design. The top flange of the box girder serves as the riding surface of the bridge. The bridge deck has variable depth along the transverse direction with 9 in. (0.23 m) as the minimum depth and 19 in. (0.48 m) as the maximum depth at the intersection of box webs and top flange, while there is a transition zone of linearly variable depth from 9 in. to 19 in. for 4.42 feet (1.35 m) from the inner edge of box web towards box centerline. The bridge deck roadway consists of a 5 ft. (1.52 m) left shoulder, two travel lanes each of 12 ft. (3.66 m) width, and a 10 ft. (3.05 m) right shoulder, of which the widths

adds to 40 ft. (12.2 m). The left barrier is 1.54 ft. (0.47 m) wide and the right barrier between the right shoulder and the sidewalk is 1.5 ft. (0.46 m) wide, while the sidewalk is of width 10 ft. (3.05 m) and rightmost parapet is 1 ft. (0.305 m) wide.

Inspection records for the pilot bridge show that the deck and superstructure were given a condition rating of 7, which stands for "Good Condition". Lateral, longitudinal, and diagonal cracks were observed with a maximum width of 1/64th of an inch throughout the deck surface. Patched areas cast during the construction can be observed on the deck surface. Cracks up to 1/32th of an inch width and spalls were observed in the top surface of deck overhang. Efflorescence appears in the cracks of deck underside and deck overhangs. Figure 59 shows the side view of a pier and bottom of box beam.

Figure 59 – Side View of Pier and Prestressed Box Beam

Apart from the transverse and longitudinal post tensioning bars, the top flange of the box girder has bare steel reinforcements of US #4 size (0.5 in.es diameter).

FIELD PERFORMANCE ASSESSMENT

Initial field assessment was conducted with teams from Parsons-Brinckerhoff (PB), the Virginia Transportation Research Council (VTRC), Virginia Tech (VT), and Rutgers University (RU).

PB team performed the visual inspection noting the locations of patches, spalls, delaminations, and cracks on the deck top and bottom surfaces, and abutments. The RU team conducted the non-destructive testing (NDT) of the deck riding surface including, ultra sonic waves, impact echo, ground penetration radar, concrete resistivity, and corrosion half-cell potentials.

The deck corrosion performance assessment team consisted of members from VTRC, and VT. The concrete deck condition assessment team conducted on-site testing and extracted laboratory test samples. The following suite of assessment activities were conducted within the selected areas of the deck riding surface.

- Top and bottom mat electrical continuity tests,
- Magnetic induction reinforcing steel cover depths,
- Corrosion copper – copper sulfate half-cell (CSE) potentials
- Unguarded linear polarization corrosion current density measurements (3LP corrosion rates)
- Four and single point concrete resistivity measurements
- Drilled concrete powder samples as a function of depth for chloride content.

In addition, concrete cores were taken for compressive strength and modulus and electrical indication of chloride penetration resistance.

TESTING METHODOLOGIES

Visual Inspection

In order to quantify the damages experienced by the bridge deck, visual inspection and sounding was conducted. Visual inspection involved the identification and sizing of the spalls, cracks, and patches. Sounding was performed by chain dragging the entire bridge deck to identify the delaminations. The collected data regarding the location and size of the damages were stored in a computer program in the form of a CAD two dimensional geometry. In addition to the surveying of the top of the bridge deck, the underside was also visually inspected. Figure 60 shows the map cracking observed on the surface of the bridge deck.

Figure 60 – Visual Inspection – Map Cracking

Cover Depths

Concrete cover over the reinforcements is the basic protection against environmental deterioration and chloride diffusion. A total number of 18 cover depth measurements, six on each of three spans, were taken at selected test locations. A pachometer was used in measuring the concrete cover depths.

Continuity

In order to conduct the corrosion tests, half-cell potentials, corrosion rates, and single probe resistivities, electrical connection to the reinforcement is necessary. To make an electrical connection to the steel reinforcement, the cover concrete is removed by utilizing coring and drilling a metallic fastener into the reinforcement for easier connection. It is not feasible to core and drill the steel reinforcements corresponding to all the testing locations, because of the number of testing locations. Thus, a few tap locations were selected and then the electrical continuity between the tapped reinforcements checked using a low resistance wire. Care was used to certify continuity throughout test locations as the reinforcing steel is not continuous across segments within spans. Figure 61 presents the picture of the connection made between two tap locations using a low resistance wire.

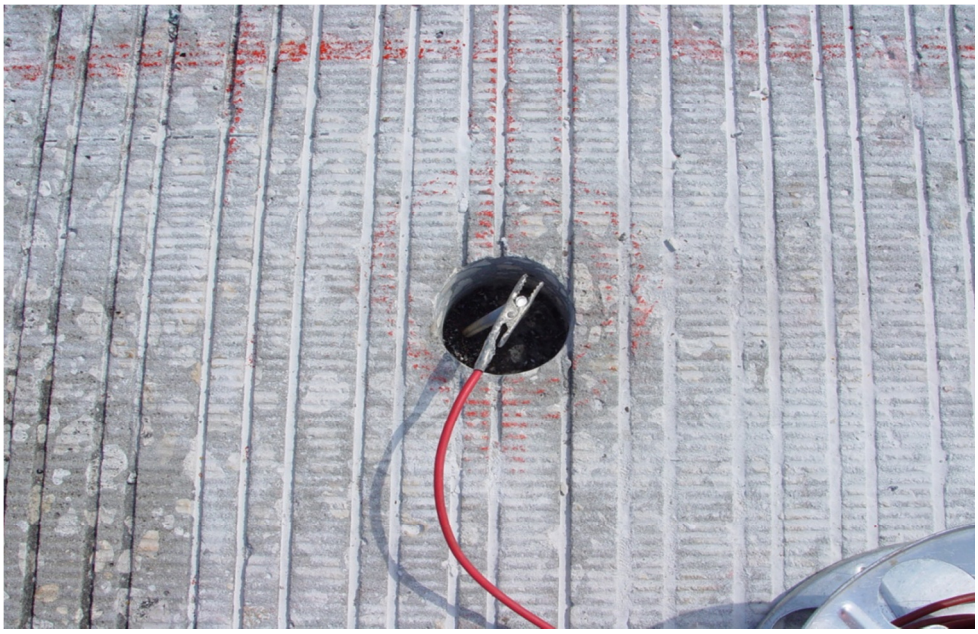

Figure 61 – Continuity Test – Low Resistance Wire Connection

Test Locations

Test locations for the corrosion tests were selected based on the schedule of the reinforcement bars and lack of any post-tensioned bars. A total number of 18 test locations were selected on the bridge deck, 6 locations on each span. Tested segments are shaded and the test locations are marked in figures 62, 63, and 64.

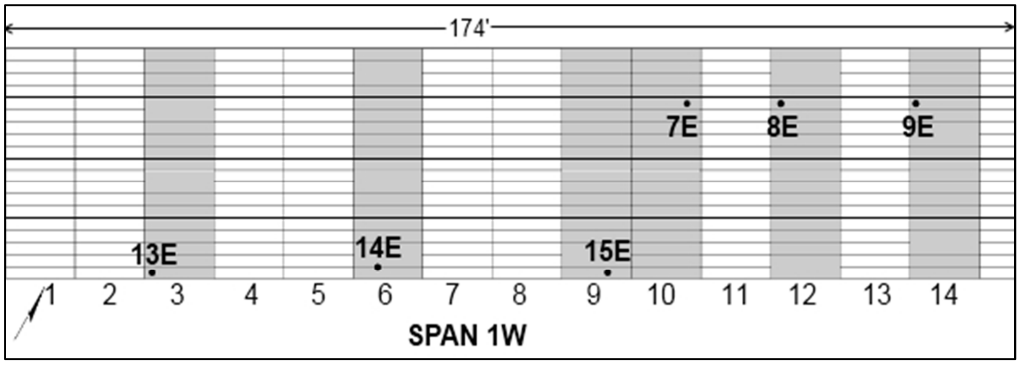

Figure 62 – Test Locations on Span 1 of FL Bridge

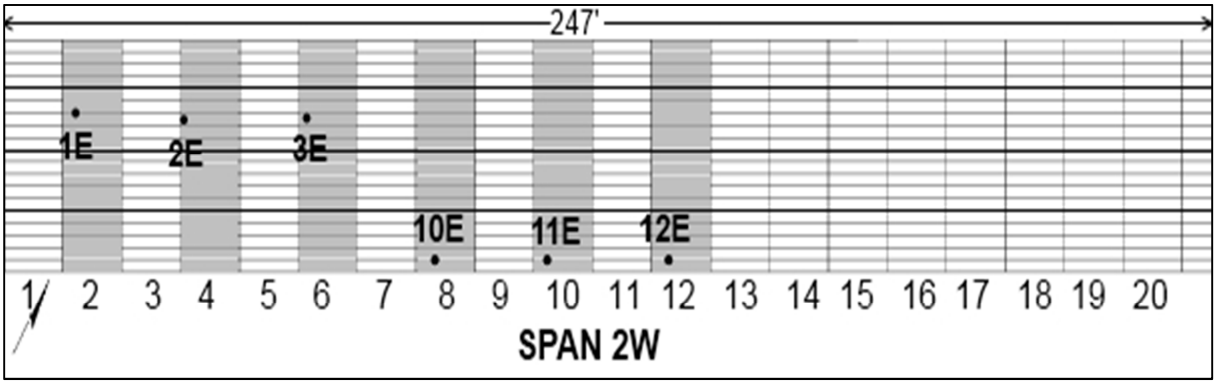

Figure 63 – Test Locations on Span 2 of FL Bridge

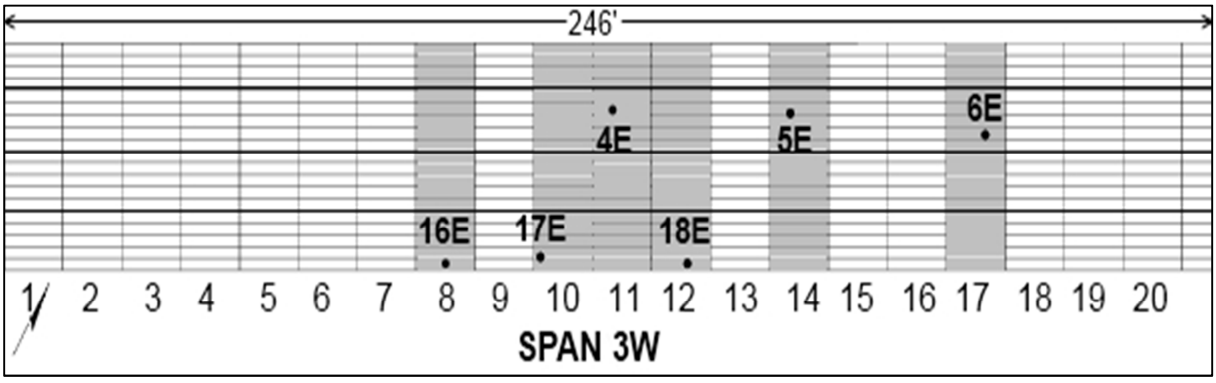

Figure 64 – Test Locations on Span 3 of FL Bridge

Corrosion Potentials

Corrosion potentials were taken according to the procedure presented in ASTM C 876-09, "Standard Test Method for Half-Cell Potentials of Uncoated Reinforcing Steel in Concrete". the half-cell potential measurements were conducted at 18 test locations on 3 spans. It is to note that ASTM

C 876-09 test procedure specifically states that is applicable to uncoated steel (UCS), and thus applicable to the FL bridge deck.

Corrosion Rates

The 3LP device was used for measuring the corrosion currents at the selected test locations. Then the corrosion current density or the corrosion rate can be calculated from the corrosion current and the area of polarized steel. Corrosion rate measurements were performed at the selected 18 test locations. It is to be noted that the 3LP device was built for measuring corrosion rates of uncoated steel bars, which applies to the FL bridge deck. Figure 65 shows the measurement of 3LP corrosion current on the FL deck.

Figure 65 – Three-Electrode Linear Polarization Measurement

Corrosion Resistivity

Resistivity of concrete may represent the quality of concrete and is inversely related to the moisture content and amount of voids. One-point resistivity and four-point resistivity tests were employed on the bridge deck concrete. Both resistivities were conducted on a total of 18 locations on 3 spans of the deck.

Four-point resistivity was conducted by using a Nilsson resistivity meter connected to four points. Moist wooden plugs were used at the end of four points to enable contact with the concrete surface. One-point resistivity test was conducted by using a 3 in. diameter single point. Both resistivity tests were conducted at each test location.

Chloride Content

Chloride content at various depths of deck concrete can be used to understand the extent of chloride contamination of the bridge deck. Diffusion coefficients can be estimated by using the chloride contents at several depths. It was not expected to find significant amounts of chlorides in the Florida deck concrete, since deicing salt usage is not required in the warmer weather zones. Thus, a total number of 12 chloride sampling locations were selected from the selected 18 corrosion test locations. Surface concrete up to a depth of 0.25 in. (6.3 mm) was neglected, because of the inconsistency. The chloride sampling depths are presented below.

Range, in. (mm)	Average, in. (mm)
0.25 (6.3 mm) to 0.75 (19 mm)	0.50 (13 mm)
0.75 (19 mm) to 1.25 (32 mm)	1.00 (25.4 mm)
1.25 (32 mm) to 1.75 (44 mm)	1.50 (38 mm)
1.75 (44 mm) to 2.25 (57 mm)	2.00 (51 mm)
2.25 (57 mm) to 2.75 (70 mm)	2.50 (63.5 mm)

The chloride content was determined in accordance with ASTM C 1152/C 1152M-04 –Test Method for Acid-Soluble Chloride in Mortar and Concrete.

Concrete Cores

Figure 66 presents the picture of the concrete coring procedure using handheld coring equipment. A total of 19 cores were taken, where 14 were from the tap locations. The handheld coring equipment could drill a core of 2 in. diameter. Core pH was tested using a color indicator (Rainbow Test), see Figure 67. From Figure 67, it can be noted that the cement paste shows purple/black, which indicate strong basic behavior (pH = 11 to 14). And the coarse aggregates show yellow/red, which indicates acidic behavior (pH = 3 to 6). This result was typical for all the pH color tests. Cores were wrapped in plastic sheet and then aluminum foil and duct tape to prevent any loss of

moisture. Table 20 presents the location information and the cover depths at corresponding location for each core.

Figure 66 – Concrete Coring using Handheld Equipment

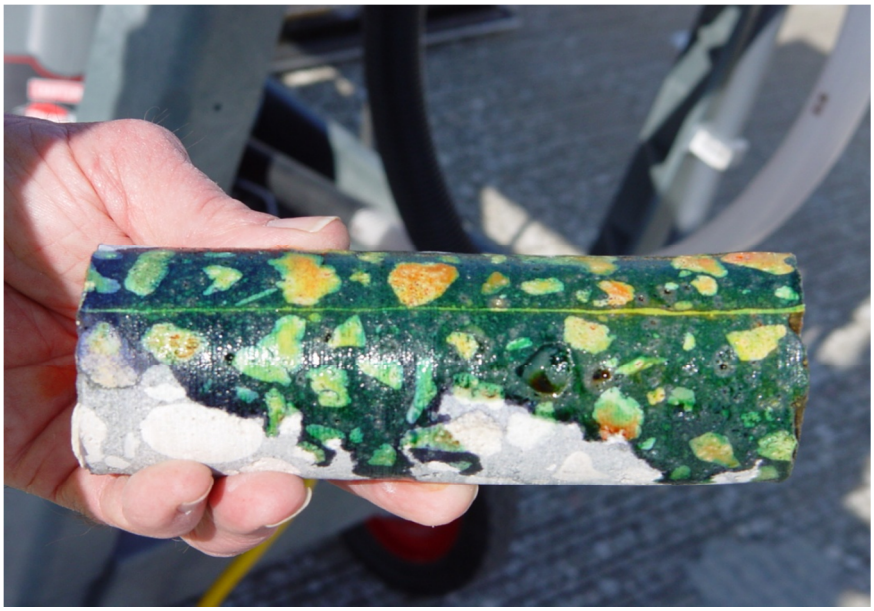

Figure 67 – pH Color Indicator Test on Concrete Cores

Table 20 – Table of Core Grid Locations and Dimensions

ID	Coordinates		Cover Depth
	Longitudinal (ft.)	Transverse (ft.)	
T8	2296	27	2
T7	2256	27	1.65
T6	2222.5	27	1.75
T3	1770	29	2.1
T4	1740	23.5	2.1
T5	1700	20	2.25
T11	2290	2	2.4
T12	2257	1	2.05
T13	2217	1	2.25
T9	2258	1	2.05
T10	2211	1.2	2.2
T14	1811.2	2	1.6
T15	1791	2	1.95
T16	1760	2	2.35
C3	1768.5	26.5	2.1
C11	2290	1.8	2.4
C13	2217	1.5	2.25
C9	2257	1.3	2.05
C10	2210	1.3	2.2

ANALYSIS AND DISCUSSION

Cover Depths

Figure 68 presents the distribution of the transverse reinforcement cover depths of the Florida pilot bridge deck. It appears that the mean and median are the same and the distribution normal. Standard deviation of the cover depth values is 0.22 inch. Usually, the bridge deck cover depths are normally distributed and the standard deviation is below 0.38 in., where a high percentage of the reinforcements are configured to have a cover depth of at least 2 inch. Florida pilot bridge data shows that about 28% of the reinforcements have concrete covers less than 2 in.

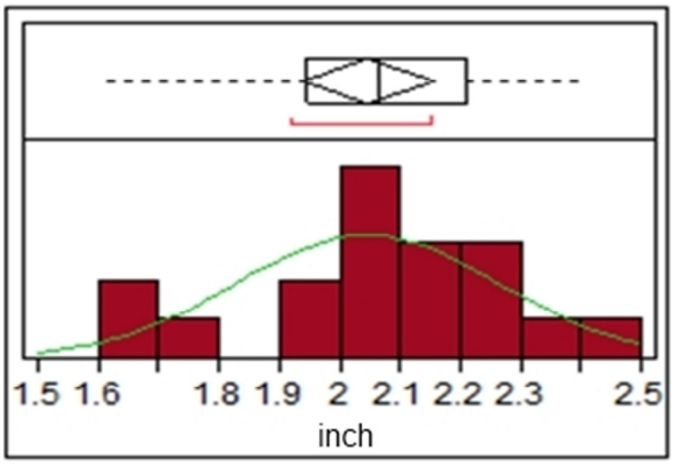

Mean	2.05
Std. Dev.	0.22
Median	2.06
Std. Err. Mean	0.05
Upper 95%	2.48
Lower 95%	1.62
n	18

Figure 68 – Distribution of Transverse Cover Depths taken from 18 Test Locations

Cover depth values are entered into the deterioration model to estimate the EFSL of the bridge deck. With 28% of the cover depths under 2 in. in severe chloride environmental regions, it is expected that bridge decks will rapidly deteriorate. However, the chloride concentration at the near-surface of the deck and the chloride diffusion rates into the concrete determine the rate with which the deterioration of the bridge deck will occur.

Continuity

Span 1 of the bridge deck is 147 ft. in length, while both spans 2 and 3 are 247 ft. long. Segmental construction requires immediately placed tap locations for connecting the testing equipment with the reinforcement steel because of the general condition of lack of continuity between segments. Table 21 presents the locations of the taps and the corresponding resistance measured between

them. From the table, it can be seen that the resistance between the reinforcements are low and thus electrical continuity exist. The continuity between different segments exists probably because of the continuous parapet construction over the deck and the metallic post tensioning ducts. The variability of resistant values between the five values may be related to probe contact resistances. However, the resistance for the FL bridge is to be considered very low and are in general agreement with the VA bridge.

Table 21 – Continuity Connection Locations and Ohmic Resistance between Locations

Span & Segment A	Span & Segment B	Resistance (Ohm)		
		Straight	Reversed	Average
3, 11	3, 14	2.14	2.13	2.14
3, 11	3, 17	0.06	0.46	0.26
3, 14	3, 17	2.19	2.25	2.22
2, 10	2, 8	0.90	1.01	0.96
2, 10	2, 12	0.90	0.92	0.91

Corrosion Potentials

The data collection was conducted over a period of three days. It was noted on the first day that the bridge deck was very dry on the surface and consequently, the electrical measurements were difficult to obtain because of the time taken for stabilization. Thus, the deck was wetted with water a few hours before the measurements were taken on days 2 and 3. The wetting of the deck surface allowed for measurements to stabilize relatively quickly.

Corrosion potential distribution for the Florida pilot bridge is presented in Figure 69. Distribution appears to be approximately normal. Mean and median of the corrosion potential dataset are about the same, -47 mV and -54 mV respectively, with a relatively higher standard deviation of 26 mV. Though there is higher variation in the data, the range of the whole set of data is limited within 0 mV and -90 mV.

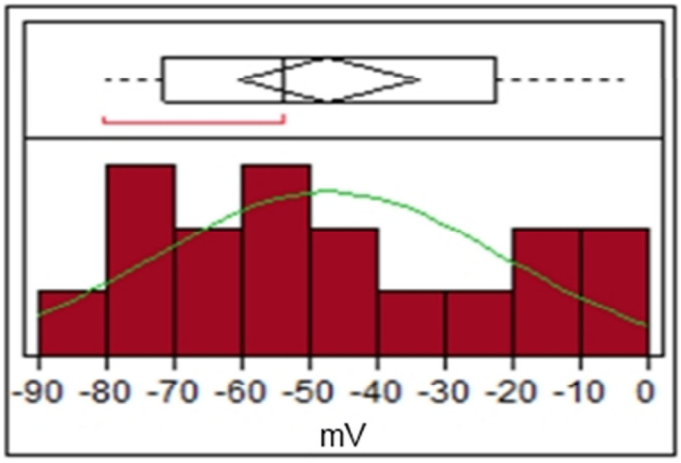

Figure 69 - Distribution of Corrosion Potentials taken from 17 Locations

Table 22 presents the interpretation range for uncoated steel bars and the corresponding percentage of data in each interpretation range. Clearly, the whole dataset lies in the lower corrosion risk interpretation zone, thus, indicating a low probability of corrosion activity.

Table 22 – Uncoated Steel Corrosion Risk Interpretation and Percent CSE Values of Florida Pilot Bridge Deck

Corrosion Risk	Potential (mV)	Percent CSE Values
High	< -300	0
Moderate	-200 to -300	0
Low	> -200	100

Three-Electrode Linear Polarization

Distribution of the corrosion current density measured from the Florida pilot bridge is presented in Figure 70. Mean and median of the distribution are approximately the same, 0.44 and 0.42 $\mu A/cm^2$ respectively, and the standard deviation is fairly large, 0.16 $\mu A/cm^2$. The distribution appears to be left skewed, similar to the VA pilot bridge.

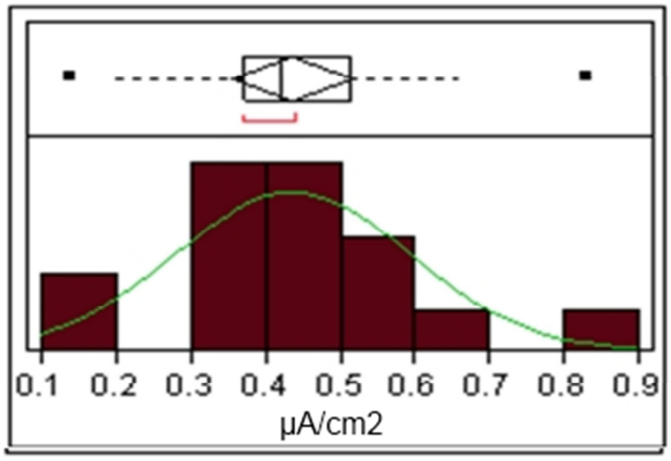

Figure 70 – Distribution of Corrosion Current Densities

Table 23 – Interpretation of 3LP Measurements on Uncoated Steel and Corresponding Percentage of Measurements

Corrosion Risk	3LP/CCD (µA/cm²)	NJ Pilot Bridge Deck (%)
High	> 3.0	0
Moderate	1.0 to 3.0	0
Low	< 1.0	100

Table 23 presents the interpretation ranges of 3LP CCD measurements on uncoated steel reinforcement and percentage of measurements in each interpretation zone. Similar to the corrosion potentials, the 3LP CCD values are all in the lower corrosion risk interpretation zone.

One-Point Resistivities

One-point resistivities distribution and associated statistic parameters are presented in the Figure 71. Mean and median of the distribution are approximately the same in magnitude, but the standard deviation is fairly large, 340 ohm-m, causing the coefficient of variation to increase to 50%. The distribution appears to be skewed to the left similar to the data obtained from VA pilot bridge.

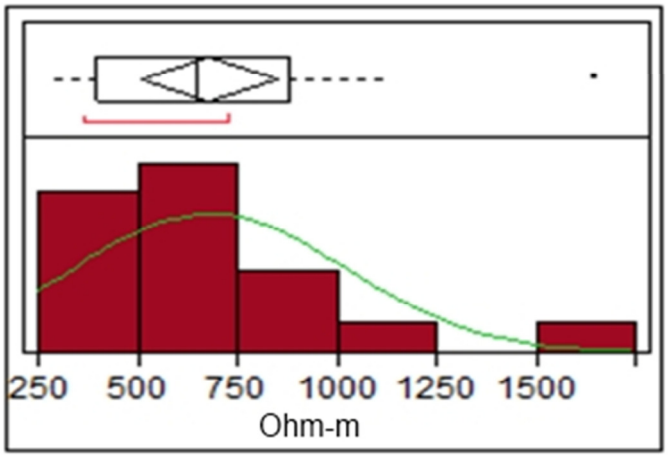

Figure 71 – Distribution of One-Point Resistivities from Florida Bridge Deck

CSE/CCD/OPR

Rephrasing Ohm's Law, electric current is directly related to the electrical potentials and inversely related to the resistance. Thus, the electrical measurements taken from the bridge deck should be similar in response to Ohm's Law. Figure 72 shows the relationship between 1-point resistivity values and CCD values.

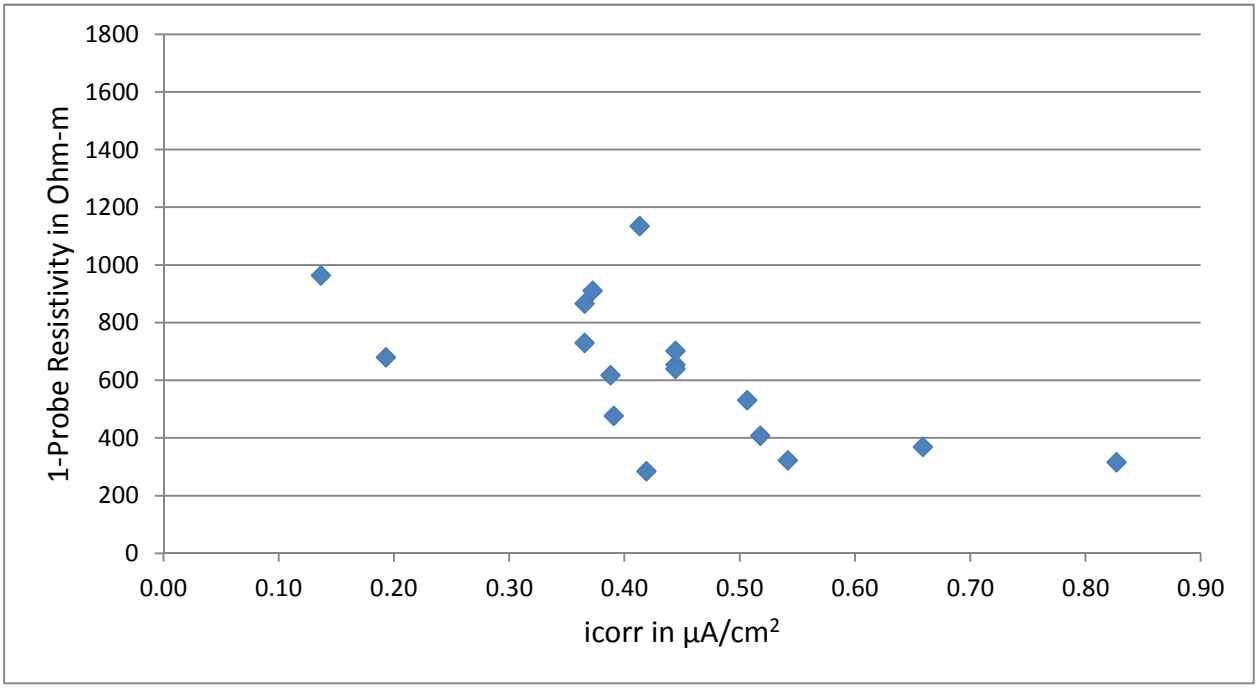

Figure 72 – One-Point Resistivity vs. Corrosion Current Density

Though there are only 18 number of data points, there is definite relationship between the two factors. With increasing CCD the resistivity decreases and with decreasing CCD the resistivity increases. Relationship between corrosion potentials and the CCD values is presented in Figure 73. The correlation is not bold, but it might be due to the lack of sufficient number of readings.

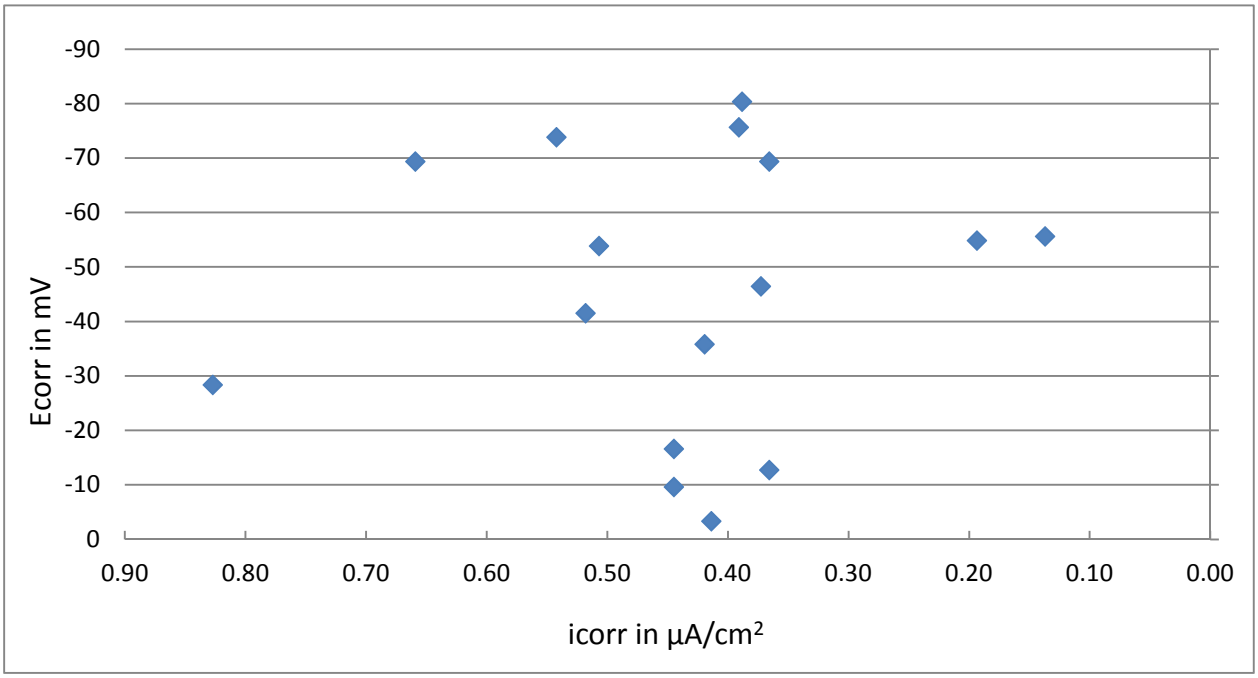

Figure 73 – CSE Potentials vs. Corrosion Current Densities

Four-Point Resistivities

Figure 74 presents the distribution of the four-point resistivities. It does not appear to be normally distributed. Mean and median are different, 1618 ohm-m and 1392 ohm-m, respectively, and the standard deviation is very high, 827 ohm-m.

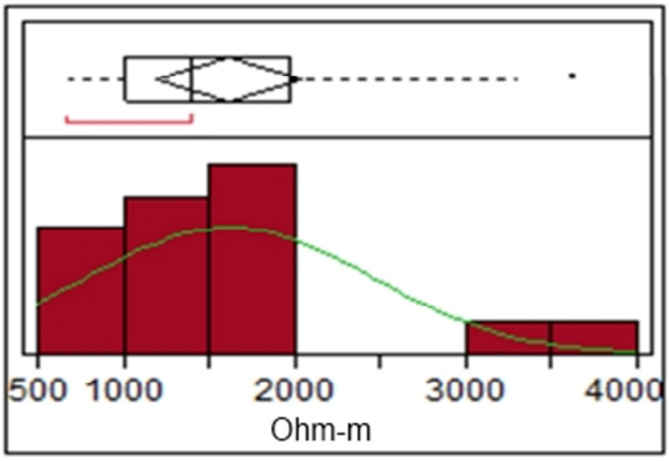

Figure 74 – Distribution of Four-Point Resistivities from FL Bridge Deck

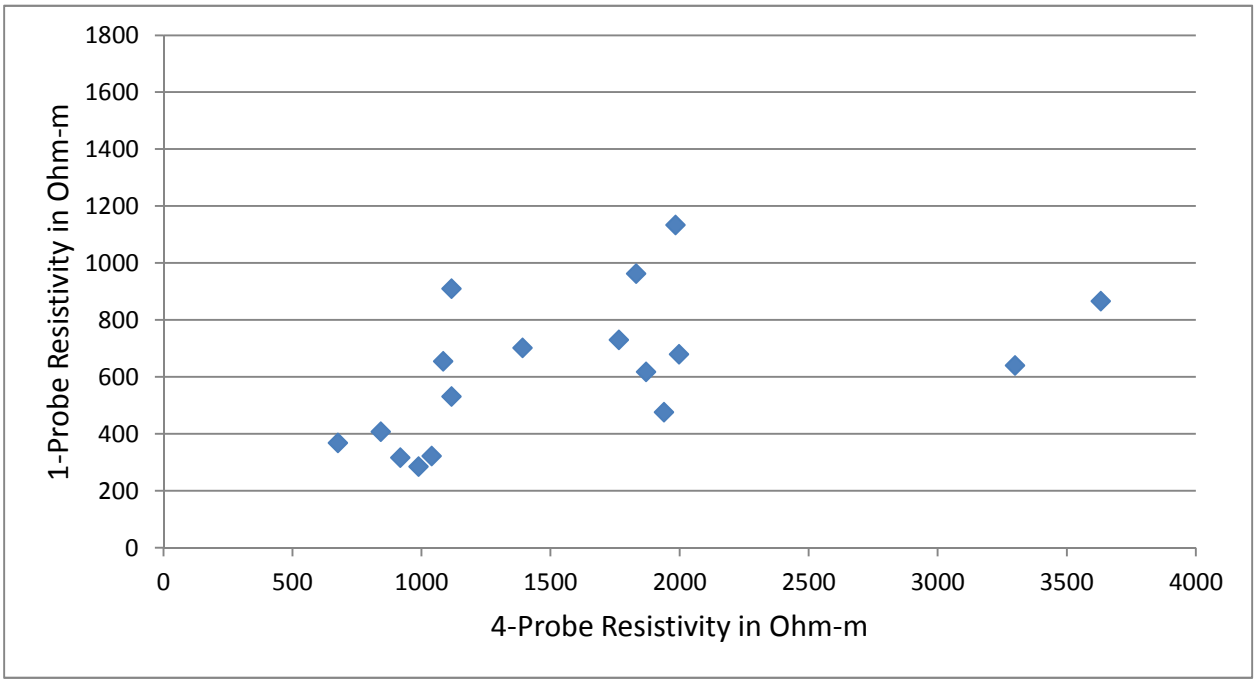

Figure 75 - One-Point Resistivity vs. Four-Point Resistivity

Figure 75 presents the relationship between 1-point and 4-point resistivities. There is only a weak correlation between the two factors, which may be related to the surface dryness of the bridge deck.

Chloride Contents

Chloride content data are essential for the service life estimation model. Since the Florida pilot bridge did not receive any deicing salt treatments previously, significant chloride content values were not expected. Thus, only 12 locations were selected to gather chloride content data. Figure 76 presents the distribution of the near-surface chloride concentrations of FL bridge deck.

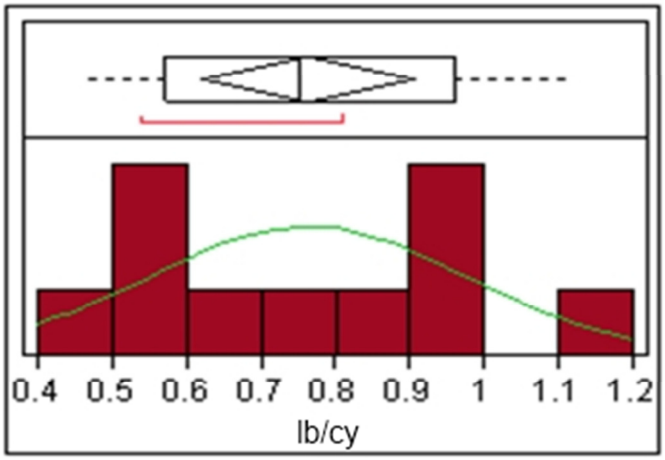

Mean	0.76
Std. Dev.	0.21
Median	0.75
Std. Err. Mean	0.06
Upper 95%	1.17
Lower 95%	0.35
n	11

Figure 76 – Distribution of Near Surface Chloride Contents at 0.25 – 0.75 in. depth

Mean and median of the distribution are the same, 0.76 and 0.75 lb/yd^3 respectively, while the standard deviation is fairly higher, 0.21 lb/yd^3. The 95% confidence limits for the distribution are 0.35 and 1.17 lb/yd^3. Chlorides at five consecutive depths were found at each location and the diffusion coefficients were estimated. The background chloride content was approximately taken as 0.15 lb/yd^3 from the chlorides at lower depths. Mean chloride concentration at bar depth was 0.20 lb/yd^3, which includes the background. Thus, lower chloride concentration agrees with the lower potentials, lower corrosion rates, and higher resistivities indicating no corrosion activity in the bridge deck.

Figure 77 presents the distribution of the apparent diffusion coefficients. The mean and median are 4.75 and 3.5 mm^2/year respectively, while the standard deviation is 2.86 mm^2/year. It can be noted that the diffusion coefficients are extremely low compared to VA bridge deck data which is most likely related to difference in the quality of concrete. From the construction plans of the Florida pilot bridge, it was observed that the cast-in-place concrete consisted of microsilica. The presence of pozzolon in the concrete mix may be the reason behind the lower diffusion constants.

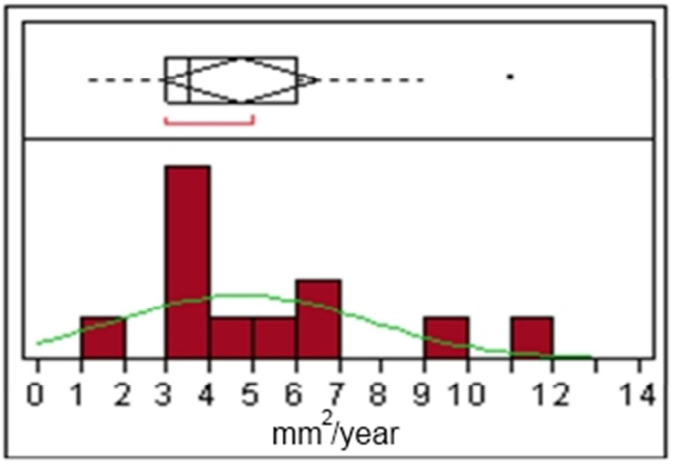

Figure 77 – Distribution of Apparent Diffusion Coefficients

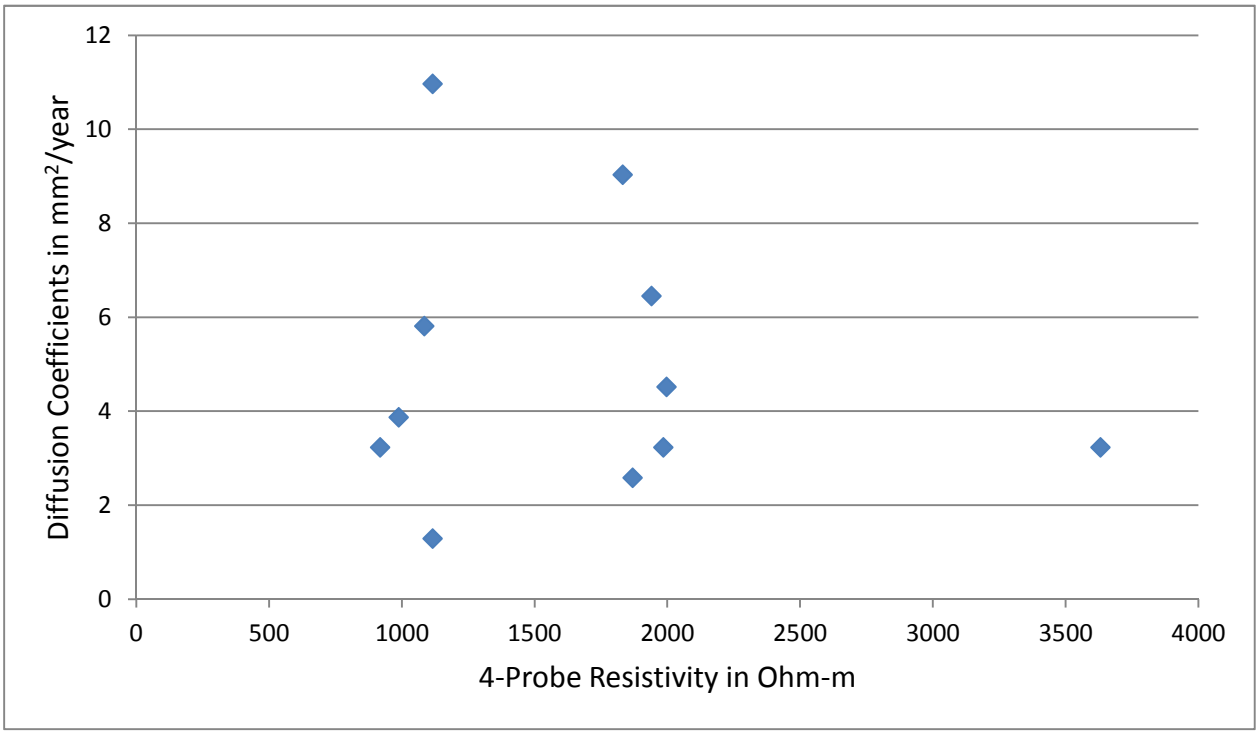

Figure 78 - Relationship between Diffusion Coefficients and Four-Point Resistivities

Figure 78 presents the relationship between the diffusion coefficients and four-point resistivities. It is desired to find a relationship between the resistivities and diffusion coefficients for the reason that resistivities are easier to obtain while diffusion coefficients are not. But the scatter plot appears to show no correlation between the two factors. Figure 79 presents the scatter diagram for diffusion coefficients and one-point resistivities, which also shows no correlation.

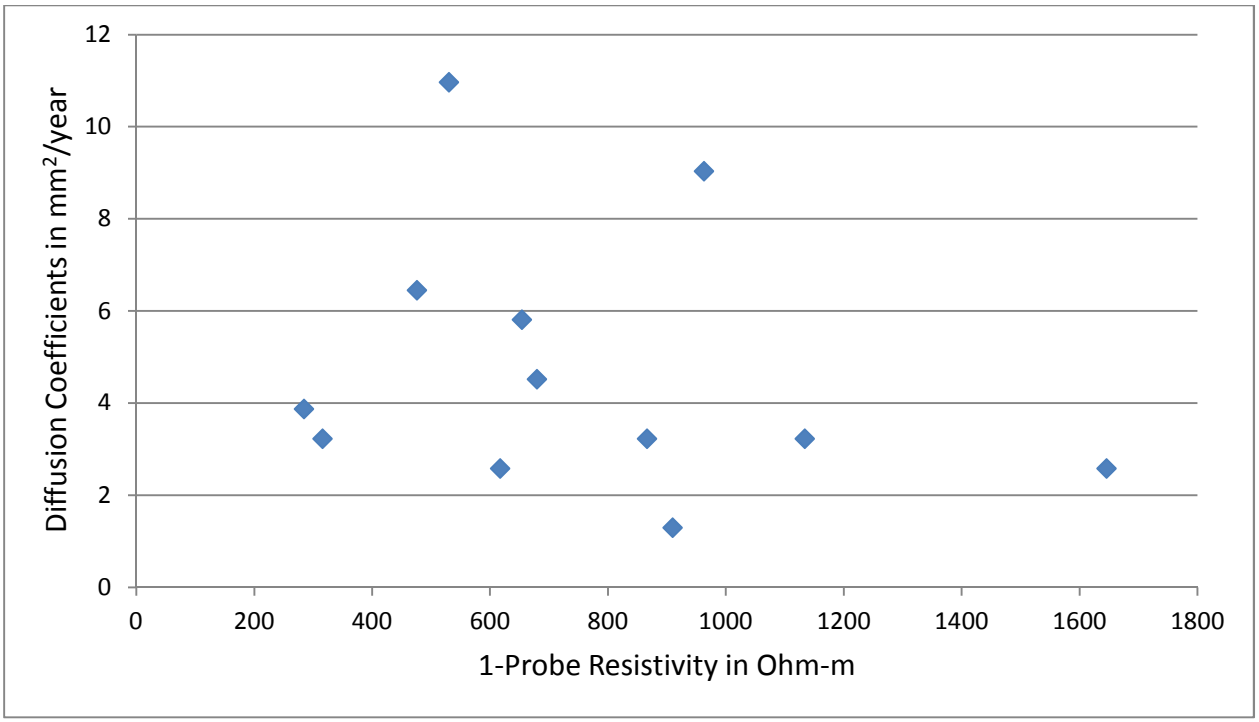

Figure 79 – Relationship between Diffusion Coefficients and One-Point Resistivities

Since diffusion coefficients depend upon the concrete density, permeability, and moisture content, surface chlorides are not expected to correlate with the coefficients. Figure 80 presents the relationship between the diffusion coefficients and surface chloride concentration. No correlation can be observed from the scatter plot as expected, particularly as they are independent variables in Fick's Second Law.

Figure 81 shows the relationship between the CCD values and the chloride concentration at the bar depth. At the depth of the reinforcement, the chloride concentrations found were generally considered background values. Thus, no relationship was observed between the two factors which is in agreement with the interpretation of corrosion risk.

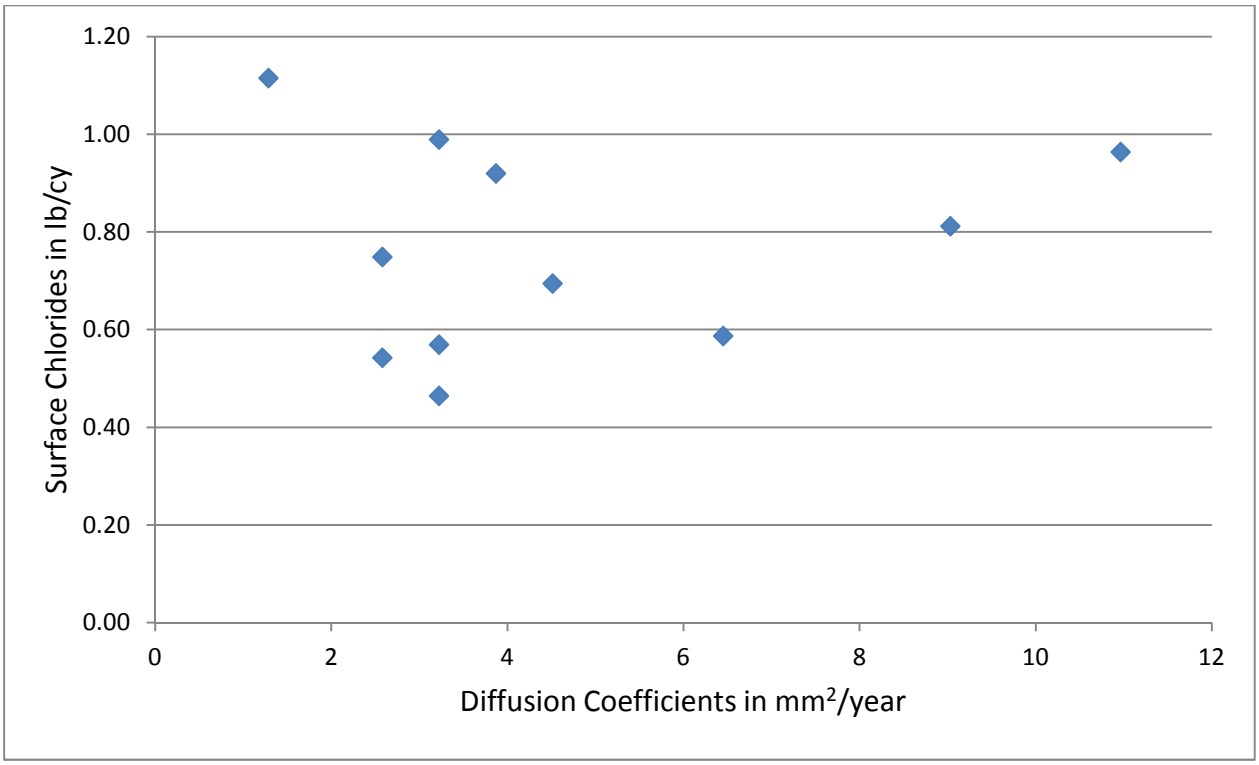

Figure 80 – Relationship between Surface Chlorides and Diffusion Coefficients

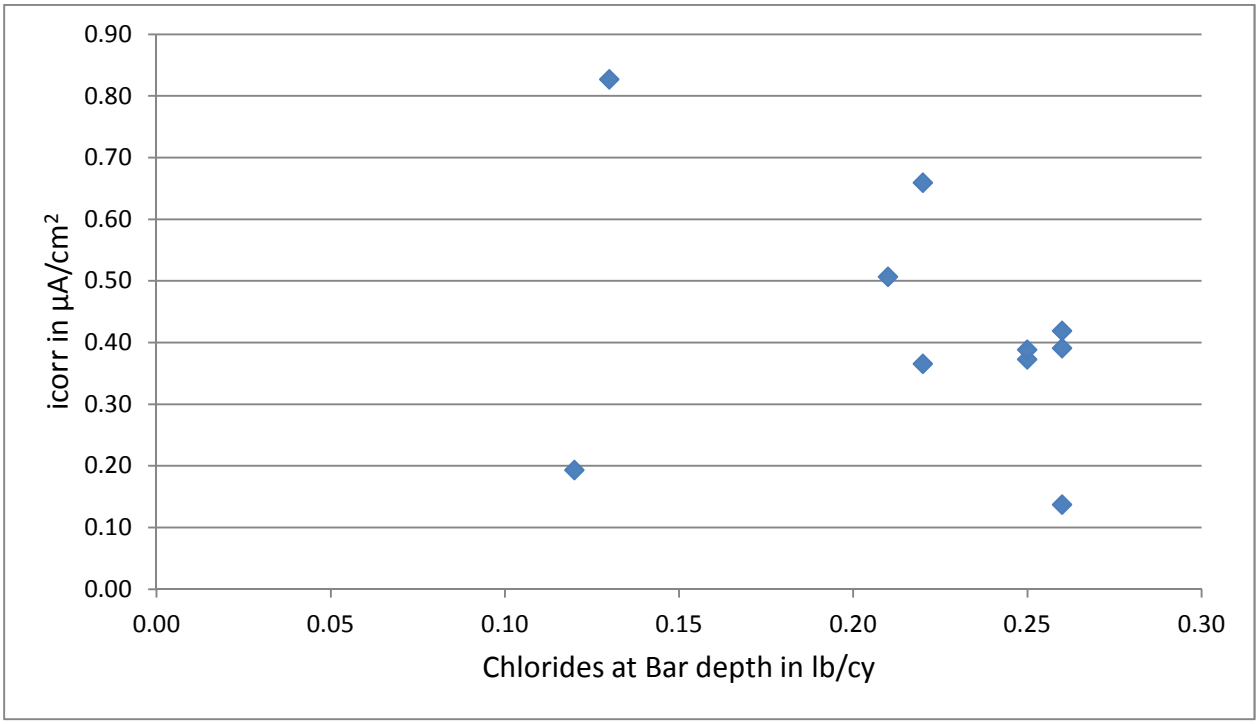

Figure 81 - Relationship between Corrosion Rates and Chlorides at Bar Depth

Service Life Estimation

Service life estimation of Florida pilot bridge was performed using the chloride diffusion model based on Fick's Second Law of diffusion. Cover depths, diffusion coefficients and surface chlorides were entered through simple bootstrapping for the model. Chloride initiation values are entered using parametric bootstrapping.

With an insignificant amount of surface chloride concentration and very slow diffusion rate, it is not expected for the bridge deck to deteriorate to a large extent. Also, the electrical tests such as resistivities, half-cell potentials, and corrosion current densities indicate no active corrosion in the system. To check the prediction of the chloride diffusion deterioration model on the service life of the bridge deck, the model was run using the data collected from deck, cover depths, surface chlorides, and diffusion coefficients, and chloride initiation rates selected for the Virginia pilot bridge. From the model results, it appears that the time taken for 0.5 % deterioration due to chloride diffusion was found to be 4245 years and time taken for 1 % and further deterioration percentages was found to be 9999 years, which is the upper limit set on the deterioration model. Thus, according to the deterioration model, the Florida pilot bridge will not suffer severe deterioration because of the chloride diffusion in the future. Thus, model prediction is in agreement with experience, Florida pilot bridge does not have a deck deterioration problem.

NEW JERSEY BRIDGE

BACKGROUND

The New Jersey pilot bridge is located 1.6 miles east of the county route 539, Monmouth County, New Jersey. The bridge structure was built in 1969 and consists of two simple span structures, the eastbound and westbound deck spans. The bridge carries Interstate (I) 195 over Sharon Station Road, see Figure 82.

Figure 82 – I-165 Bridge over Sharon Station Road

The eastbound bridge structure (National Bridge Inventory (NBI) Structure Number 1330151) was selected as the pilot structure for the LTBP project, owing to its accessibility to utilities. The span of the bridge is 89 ft. (27.1 m) long and approximately 39 ft. (11.9 m) wide, which excludes the width of the parapets. Deck comprises two traffic lanes of 12 ft. (3.66 m) width, a break down lane of 12 ft. (3.66 m) width, which is to the right of the traffic lanes, and a shoulder of 3 ft. (0.91 m) width on the other side of the deck. The reinforced concrete deck was cast-in-place as a composite section over six rolled steel, wide flange girders, by using shear connectors. Concrete deck was built with a low skew of approximately 3° and has stay-in-place forms. Six steel girders were laterally braced with diaphragms, see Figure 83. The annual average daily traffic (AADT) on the pilot bridge is 22,899 vehicles with approximately 14% being truck traffic. The higher truck traffic ratio was one of the reasons for the selection of this bridge for testing.

Figure 83 - View of Steel Girders and Stay-in-Place Forms

NJDOT inspection records for the bridge structure show that the deck had a rating of 7. A condition rating of 7 stands for "Good Condition – some minor problems". Superstructure of the bridge was given a rating of 8 and the substructure was given a condition rating of 7. Condition rating of 8 represents "Very good condition – no problems noted". In addition, a latex modified concrete (LMC) overlay was cast at an average depth of 1.75 in. (44.4 mm) over the existing base concrete in 1997. The LMC overlay might be the rationale for the good deck condition rating. It is reasonable, as typically done, that at least 0.25 in. (6 mm) of base concrete was removed during the overlay operation to enhance bonding.

The concrete deck was built with black bars as the top and bottom reinforcement. Every other bar in the top reinforcement mat is a truss bar.

FIELD PERFORMANCE ASSESSMENT

Based on the bridge selection criteria, researchers from Virginia Tech (VT), Virginia Transportation Research Council (VTRC), and Utah State University (USU) selected the pilot bridge from the three visited bridges. Then, the initial condition assessment was conducted with team members from Parsons-Brinckerhoff (PB), VTRC, and Virginia Tech.

Team members from PB conducted the visual damage survey, which involves the identification of patches, cracks, spalls, and delaminations on the top and bottom surfaces of deck. The damages were quantified by using non-destructive testing methods, which follows criteria established through LTBP program.

The deck corrosion performance evaluation was performed by team members from Virginia Tech, and VTRC. The list of tests and type of samples collected are as follows:

1. Deck reinforcement mat continuity test
2. Reinforcement cover depth determination
3. Resistivity tests – one and four points
4. Half-cell potential tests
5. Three linear polarization measurements
6. Collection of powdered concrete samples for chloride contents
7. Extraction of concrete cores for various laboratory tests, such as compressive strength, modulus, electrical resistance, permeability, and absorption.

TESTING METHODOLOGIES

Visual Inspection

Visual inspection of the bridge deck involved the identification and quantification of the damages such as cracks, spalls, and patches. It also involves identification of delaminated areas by using sounding technique, namely chain dragging, over the entire deck. All the collected data about damages were fed into a bridge inspection computer program. The program stores the data about the location and size of damages by using a CAD two-dimensional geometry. It can generate required information about the input data. The location information of the damages was used to select testing locations for corrosion test and sample collections, so that predetermined numbers of test locations were selected on undamaged and damaged areas. Figure 84 shows the inspection grid layout and the chain dragging equipment.

Figure 84 – Visual Survey of Cracks and Chain Dragging Equipment

Visual inspection also involved the assessment of the bottom of deck. Other superstructure elements such as the girders, diaphragms, joints, connections, and abutments were thoroughly

observed. The damage survey performed on the bridge can be used to estimate service life of the bridge.

Cover Depths

Cover depths of the reinforcement bar mat are essential in making diagnostics on the state of the bridge deck, and also are used in various corrosion calculations. A total number of 32 cover depth measurements were conducted at selected locations on the bridge deck. Figure 85 shows the measurement of cover depth using a pachometer.

Figure 85 – Cover Depth Measurement using Pachometer

Two measurements were taken, one on a transverse bar and other on a truss bar, if identified.

Continuity

Before conducting corrosion tests, it is essential to check the electrical continuity of the reinforcement mats. The bridge deck consists of black bars for the top and the bottom reinforcements.

Six locations were selected for continuity test, four on top of deck and two on bottom of the deck, at tap locations presented in Figure 86. Positive connection to the steel bars at the eight locations was established by drilling and exposing the reinforcement. The connection was made to the stainless steel screw, which was threaded into the exposed reinforcement bars. Then, the electrical continuity was measured by connecting a multimeter to the low resistance copper wire, which was used to connect all the test locations.

Figure 86 – Continuity Test on Bridge Deck

Test Locations

Testing locations for resistivities, potentials, corrosion rates, and chloride contents were selected and are presented in Figures 87 and 88. A total number of 32 corrosion testing locations were selected. Out of 32 locations, two were positioned over delaminated areas, 31 and 32. For concrete coring, 8 locations were selected and are also presented in Figures 87 and 88.

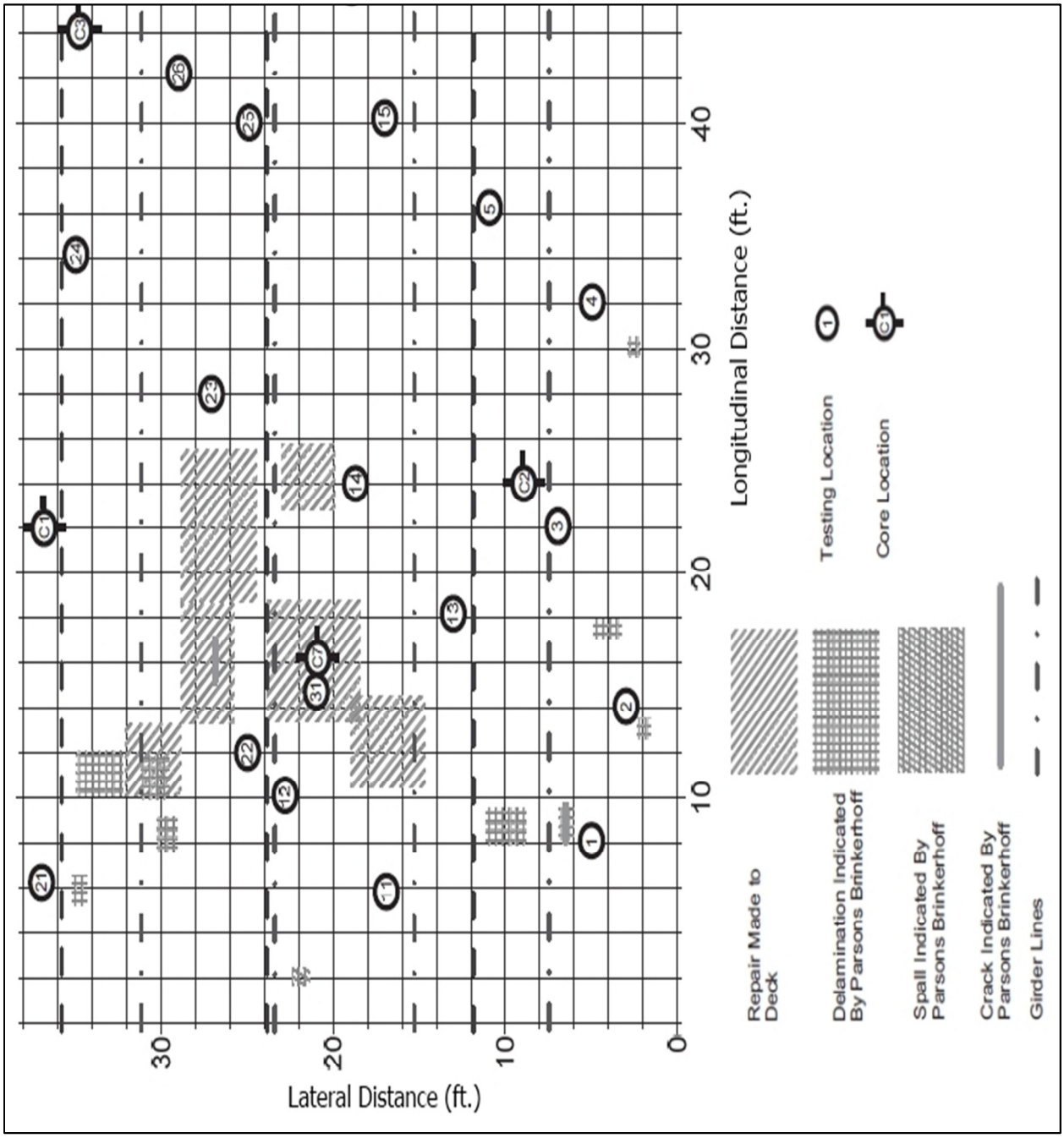

Figure 87 – Testing Locations of First Half of Deck

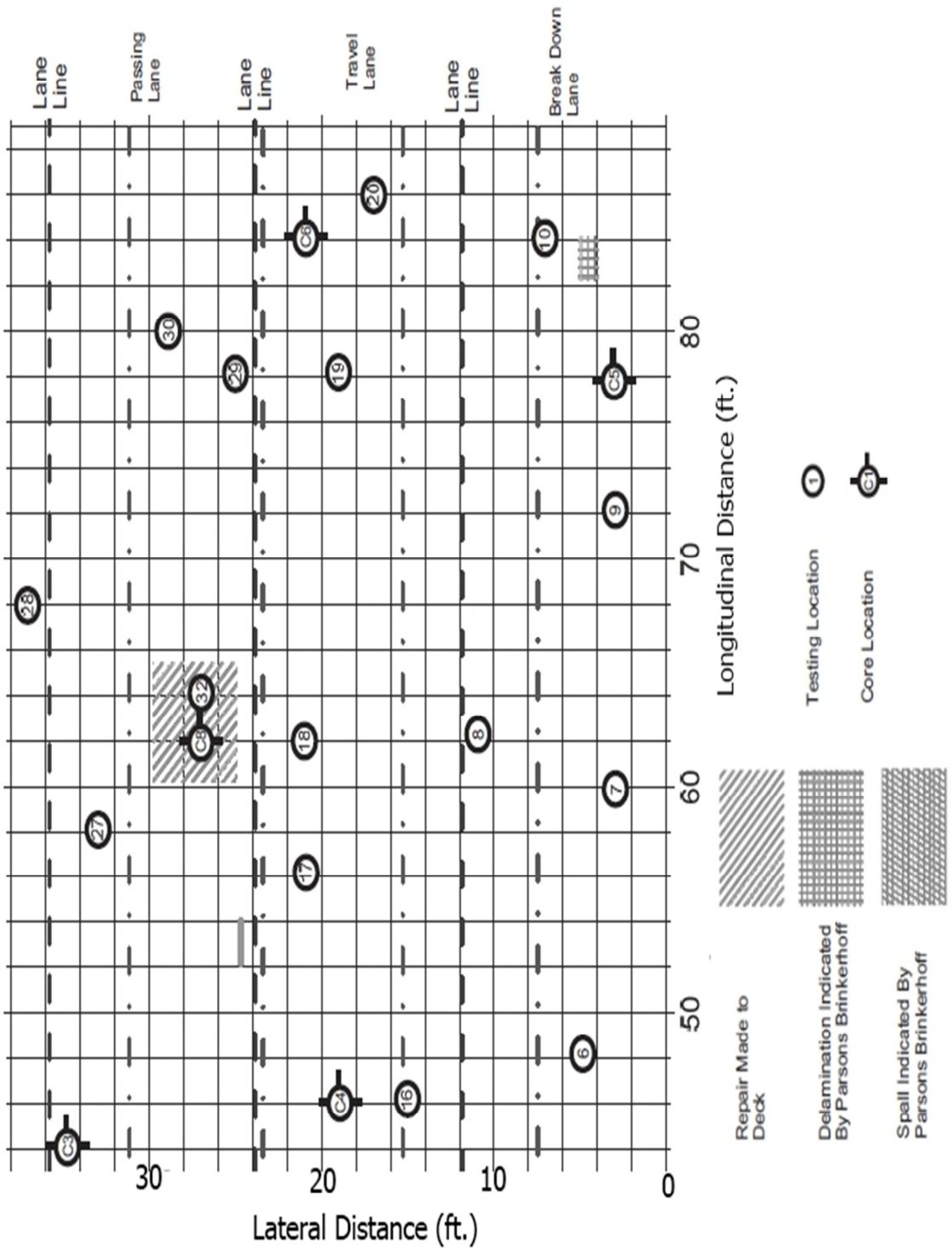

Figure 88 – Testing Locations of Second Half of Deck

Corrosion Potentials

A total number of 32 corrosion potentials were measured on the entire bridge deck. Corrosion potentials were measured according to the procedure presented in ASTM C 876-09, "Standard Test Method for Half-Cell Potentials of Uncoated Reinforcing Steel in Concrete". The same 3LP device used for corrosion current measurement was used for corrosion potentials. It is to note that ASTM C 876-09 test procedure specifically states that it is applicable to uncoated steel (UCS), thus it was conveniently used in NJ bridge.

Corrosion Rates

The 3LP device was used to measure the corrosion currents at the designated test locations. Corrosion current density or the corrosion rate was calculated from the corrosion current and the area of polarized steel. Also, the rate of metal loss can be calculated from the corrosion current density in MPY (mils per year). Corrosion rate measurements were performed at the selected 32 test locations. It is to be noted that the 3LP device was built for measuring corrosion rates of uncoated steel bars.

Corrosion Resistivity

Resistivity is a material property of the concrete, which indicates the ability of concrete to resist the reactions associated with the corrosion. The resistivity of concrete is inversely related to its moisture content. Two ways to measure resistivity were used on the bridge deck, namely one-point resistivity and four-point resistivity.

Four-point resistance was measured by utilizing the Wenner four-point resistivity meter, see Figure 89. One-point resistance was measured using the same meter, but with a single probe of 3 in. diameter. Then, the resistivity was calculated. Both resistivity measurements were conducted at each testing location.

Figure 89 – Measurement using Four-Point resistivity Meter

Chloride Content

Chloride content at consecutive depths is an important factor in estimating the condition of the bridge deck. The diffusion coefficients can be calculated using the chlorides at consecutive depths, which indicate the rate of chloride diffusion into the concrete. Powdered samples were collected by using a 1.25 in. diameter drill bit, at 8 consecutive depths. Concrete up to a depth of 0.25 in. (6.3 mm) was neglected, because of the impurities and inconsistency. The depths at which the chloride samples were taken are presented below. Drilling process is shown in Figure 90.

Range, in. (mm)	Average, in. (mm)
0.25 (6.3 mm) to 0.75 (19 mm)	0.50 (13 mm)
0.75 (19 mm) to 1.25 (32 mm)	1.00 (25.4 mm)
1.25 (32 mm) to 1.75 (44 mm)	1.50 (38 mm)

1.75 (44 mm) to 2.25 (57 mm)	2.00 (51 mm)
2.25 (57 mm) to 2.75 (70 mm)	2.50 (63.5 mm)
2.75 (70 mm) to 3.25 (83 mm)	3.00 (76 mm)
3.25 (83 mm) to 3.75 (95 mm)	3.50 (89 mm)

Figure 90 – Drilling to Collect Chloride Samples

The chloride content was determined in accordance with ASTM C 1152/C 1152M-04 –Test Method for Acid-Soluble Chloride in Mortar and Concrete. The titration results of chlorides in the concrete were then used to generate a chloride concentration profile from the near surface to the depth of the top layer of reinforcing steel.

Concrete Cores

Concrete cores are essential in understanding the actual state of concrete in the bridge deck. A total number of eight cores were collected on the top surface of deck, where two of them are on delaminated areas. Also, six concrete cores were collected from the bottom of deck. Table 24 presents the locations, depths, and diameters of the corresponding cores.

Table 24 – Core Locations and Dimensions

Core ID	Location		Depth (in)	Diam. (in)
	L (ft.)	T (ft.)		
C1	22	37	9.00	4
C2	24	9	8.00	4
C3	44	35	7.50	4
C4	46	19	7.50	4
C5	78	3	8.50	4
C6	84	21	8.00	4
C7-A	16	21	3.00	4
C7-B	16	21	3.50	4
C8	62	27	7.75	4
T1	x	x	1.75	2
T2-A	3.25	1.25	1.75	2
T2-B	3.25	1.25	3.25	2
T3	85.8	1.3	3.25	2
T4	x	x	1.00	2
T5	5.40	37.1	2.50	2
T6	88	37.5	2.25	2

Tap T1 was located closer to T5 but on the upper surface of the deck, while T4 was located closer to T3 but on the bottom surface of the deck. The cores were extracted by using a water cooled diamond drill bit. The concrete cores were then tested to measure compressive strength, static modulus, moisture content, unit weight, permeability, and electrical charge passed.

ANALYSIS AND DISCUSSION

Damage Survey

After being in service for 28 years, the bridge deck was overlaid with LMC. Thus, the damages accrued in the form of delaminations, spalls, cracks, and patches were reset. With the LMC overlay in place for 13 years, the damage percentile of the bridge deck was found to be less than 1.0 percent. As expected, the presence of a low permeability overlay significantly influence the damage accumulating rate.

For the estimation of the service life of the deck, the damage percentile from the bridge deck plan before overlaying was calculated to be approximately 5%. Deterioration percentage was calculated from the repaired surface area of concrete displayed in the resurfacing plans before the LMC overlay was laid in 1997. This data was used to run the service life estimation model to predict the future damages and time for EFSL.

Cover Depths

Figure 91 presents the distribution of the transverse reinforcement cover depths of the New Jersey pilot bridge deck. The mean and median are not different and the distribution is approximately normal. The standard deviation of the dataset is 0.26 in. In general, bridge deck cover depths are normally distributed and the standard deviation is below 0.38 in., where a high percentage of the reinforcements are configured to have a cover depth of at least 2 in. From the NJ pilot bridge cover depth data, it can be noted that about 95% of the cover depths are greater than 2.06 in.

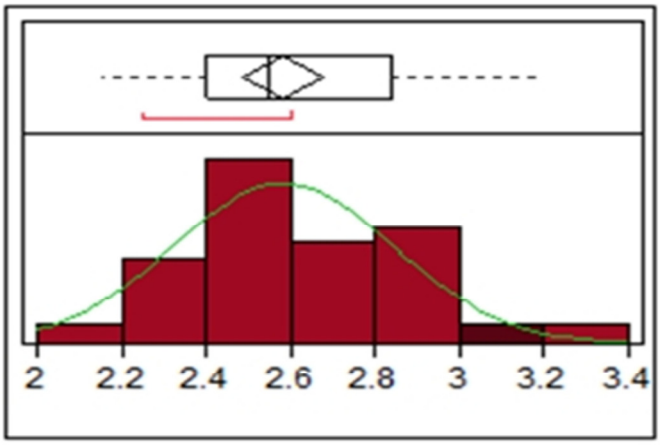

Mean	2.583
Std. Dev.	0.262
Median	2.550
Std. Err. Mean	0.046
Upper 95%	3.107
Lower 95%	2.059
n	32

Figure 91 – Distribution of Transverse Cover Depths taken from 32 Test Locations

As shown on the concrete cores that the average overlay depth was 1.75 in. With a mean present cover depth of about 2.5 in., 2.5 – 1.75 = 0.75 in. is very low cover, thus a considerable depth of base concrete was removed before the overlay was placed. It is reasonable that at least 1.25 in. of base concrete was removed to remove the higher existing chloride concentrations from the top depths. If 1.25 in. was removed, then the average cover depth at original construction was about 2.0 in. (0.75 + 1.25), which appears reasonable, considering the age at overlay and environmental exposure location.

Cover depths are utilized in the estimation of the service life of the structure. With all the cover depths greater than 2 in., the corrosion protection offered by the concrete cover is significant. The bridge deck being overlaid with latex modified concrete (LMC) overlay at an age of 28 years explains the relatively higher present cover depths.

Continuity

Figure 92 shows the tap locations on a generalized bridge deck plan view. Table 25 presents the measured resistance between different combinations of tap locations. With a mean resistance of 2.2 ohms and a standard deviation of 0.6 ohms, the resistances between the tap locations are relatively constant and are in general agreement with the VA and FL decks. Low resistances indicate electrical continuity among top bare reinforcement mat, among bottom bare reinforcement mat, and between the top and bottom reinforcement mats. Continuity in the tap locations allows for conduction of various corrosion tests by utilizing any of the taps.

Figure 92 – Plan Locations of Continuity Locations

Table 25 – Continuity Connection Locations and Ohmic Resistance between Locations

Measured Resistance		
Location A	**Resistance (Ohm)**	**Location B**
T1	1.7	T2
T1	3.0	T3
T1	3.0	T4
T1	1.0	T5
T1	1.0	T6
T2	2.1	T3
T2	2.1	T4
T2	2.3	T5
T2	2.3	T6
T3	2.2	T4
T3	2.3	T5
T3	2.4	T6
T4	2.0	T5
T4	2.0	T6
T5	3.1	T6

Corrosion Potentials

Distributions of corrosion potentials are regarded to be normal. Figure 93 presents the distribution of corrosion potentials with the statistic parameters for a normal distribution. The corrosion potentials appear to be normally distributed with some higher values. The mean and median are very close and the standard deviation is fairly large, 55.3 mV. Regarding the distribution as normal, the upper and lower 95% of the potentials are -272 mV and -56 mV respectively.

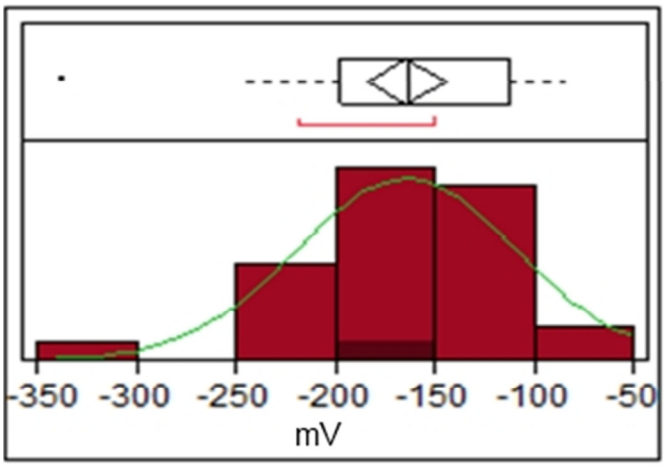

Figure 93 – Distribution of Corrosion Potentials taken from 32 Test Locations

NJ bridge deck contains uncoated steel bars for reinforcement which satisfies the ASTM standard test method for uncoated steel bars. The interpretations of the corrosion potentials vs. CSE for uncoated bars are formed based on a previous study conducted (Balakumaran 2010) on uncoated reinforcement, see Table 26.

Table 26 – Interpretation of Corrosion Risk of Uncoated Bars from CSE Potentials Measurements

Corrosion Risk	Potential (mV)
High	< -300
Moderate	-200 to -300
Low	> -200

Table 27 – Uncoated Bar Corrosion Risk of New Jersey Pilot Bridge Deck

Corrosion Risk	Percent CSE Values
High	3
Moderate	22
Low	75

Percentages of corrosion potentials in each of the interpretation ranges are presented in Table 27. From Table 24, only 3 percent of measured potentials show high risk of corrosion, while 75 percent of potential values indicate low corrosion risk. The deck overlay placed at age of 28 years and the

removal of the highly chloride contaminated concrete in the upper 1.5 in. would account for lower corrosion risk in NJ bridge deck compared to VA bridge deck. The high and moderate corrosion risk components are most likely related to higher chloride contents left-in-place.

Three-Electrode Linear Polarization

Figure 94 presents the distribution of 32 corrosion current density measurements from NJ bridge deck and the basic statistic parameters. There is difference between the mean and median, 0.21 μA/cm², and the standard deviation is relatively large, 1.05 μA/cm², which gives a large coefficient of variation of 66 percent. The distribution appears to be skewed to the left, and not normal.

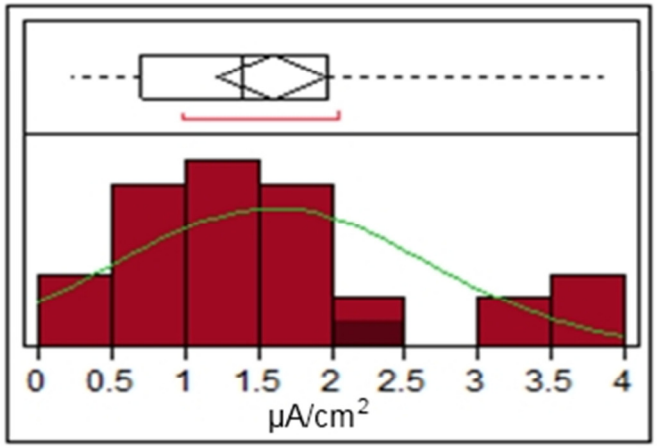

Mean	1.60
Std. Dev.	1.05
Median	1.39
Std. Err. Mean	0.18
Upper 95%	3.66
Lower 95%	0.46
n	32

Figure 94 – Distribution of Corrosion Current Densities

Interpretation formed from the study conducted on uncoated reinforcement (Balakumaran 2010) and the percentage of CCD values in each of the ranges is shown in Table 28.

Table 28 – Interpretation of 3LP Measurements on Uncoated Steel and Corresponding Percentage of Measurements

Corrosion Risk	3LP/CCD (μA/cm²)	NJ Pilot Bridge Deck (%)
High	> 3.0	16
Moderate	1.0 to 3.0	56
Low	< 1.0	28

As shown in Table 28, high, moderate, and low corrosion risk of 16, 56, and 28 % are higher than the potential risk values of 3, 22, and 75 %. During the half-cell and CCD measurements, the probes

are placed over the concrete above the reinforcement. The reinforcement cover depths appear to be deeper than the overlay depths. Thus, the current passed in the above mentioned corrosion tests pass through two different layers of concrete with varying density and moisture content. Also, the LMC overlay appeared to have smaller coarse aggregates, which have higher resistance to the flow of current compared to the mortar, that were exposed on the surface. Thus, the flow route of the current in the concrete might be different in every successive measurement, which may explain the higher variability in the corrosion rates. Thus, the disagreement between the corrosion potentials and corrosion rates in terms of the interpretation may be related to the presence of LMC overlay and higher variability in the CCD values.

One-Point Resistivities

One-point resistivities represent the resistivity of cylindrical volume of concrete below the single probe up to the reinforcement bar and the resistivity of reinforcement bar surface characteristics, such as surface rust. The concrete cylinder in this case is a composite of varying percents of portland cement concrete and LMC. The distribution of one-point resistivities is presented in the Figure 95 along with the statistic parameters.

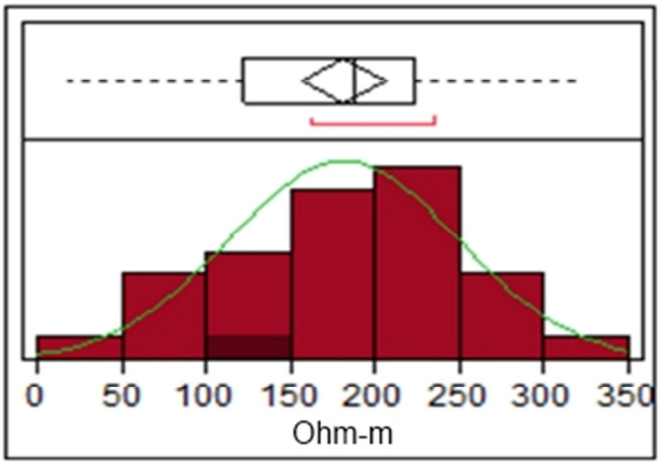

Mean	181
Std. Dev.	67
Median	188
Std. Err. Mean	12
Upper 95%	312
Lower 95%	50
n	32

Figure 95 – Distribution of One-Point Resistivities from NJ Bridge Deck

From Figure 95, the distribution of one-point resistivities appear to be normal, which was not observed for VA pilot bridge deck. The distribution is normal maybe because of the absence of any coatings on the reinforcement. The mean and median are somewhat close and the standard

deviation is comparatively smaller to the VA bridge values, 67 ohm-m, which results in a relatively smaller coefficient of variation, 37 percent.

Since the one-point resistivity (OPR) test is not a standard method, there is no accepted interpretation of the measured values and the corresponding corrosion risk.

CSE/CCD/OPR

According to the Ohm's law, current is directly related to the potential, and the inversely related to the resistance. Figure 96 presents a scatter plot between resistivity and corrosion current density values. An inverse trend can be plainly identified from the plot, which states that lower concrete resistivity results in higher corrosion rates and higher resistivity results in lower corrosion rates.

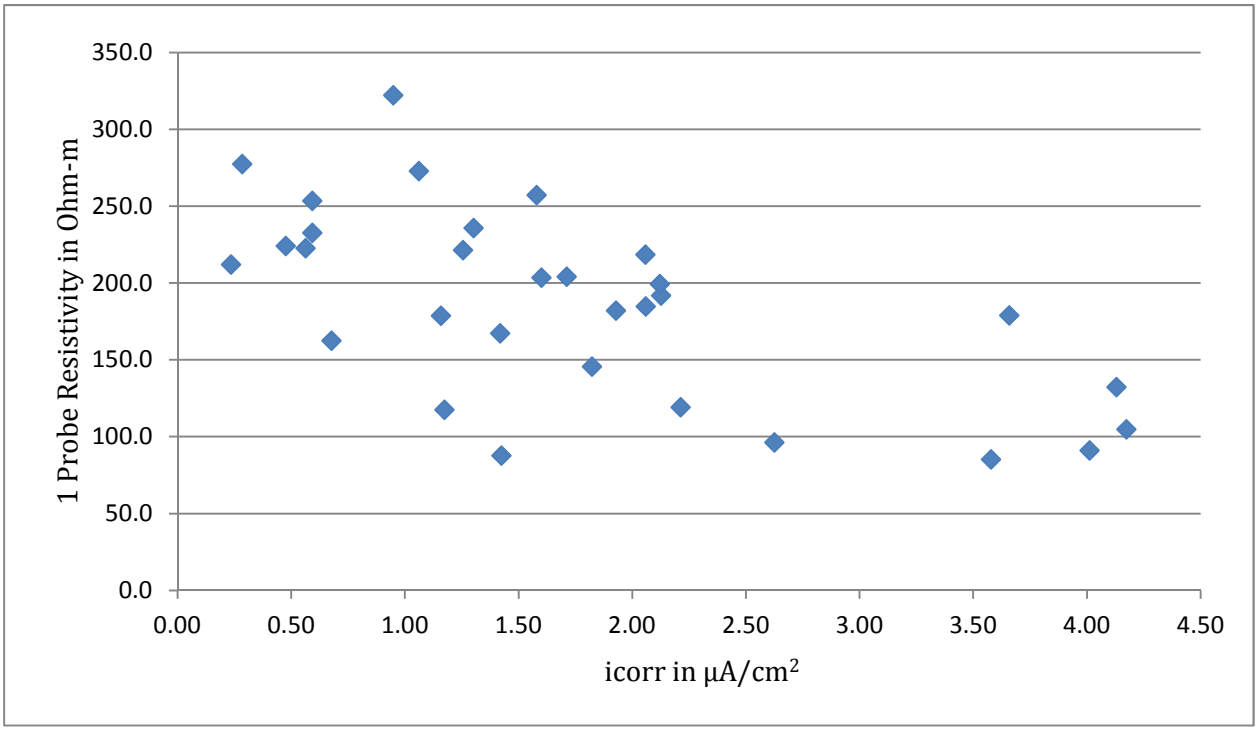

Figure 96 – One-Point Resistivity vs. Corrosion Current Density

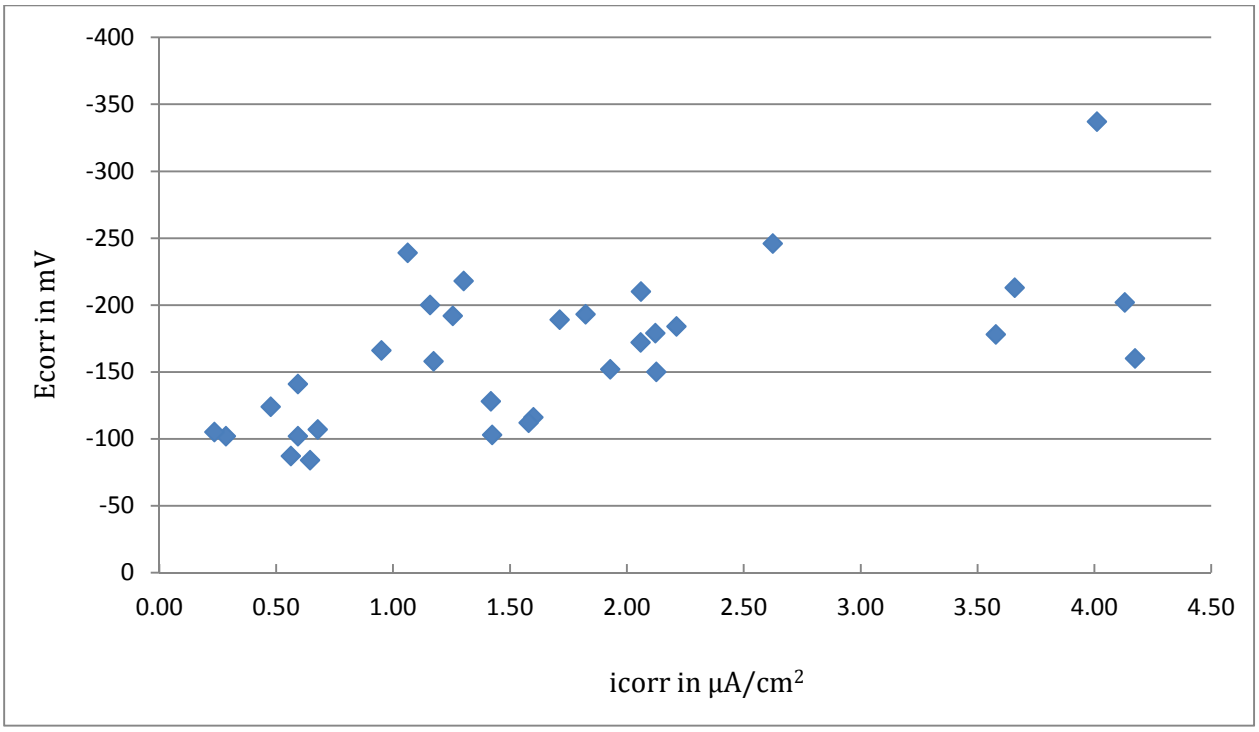

Figure 97 – CSE Potentials vs. Corrosion Current Densities

Figure 97 represents a scatter plot between the corrosion potentials and the corrosion current densities. A positive trend can be identified from the plot, which agrees with the Ohm's Law relationship. Higher potentials yields higher corrosion rates and lower potential difference yields lower corrosion rates.

Four-Point Wenner Resistivities

Figure 98 presents the distribution of four-point Wenner resistivities, which appears to be normally distributed with a few higher values. The variation is relatively high with 59% CV. In the of NJ pilot bridge deck, the four-point resistivities are extremely higher than the one-point resistivities. This might be related to the presence of the LMC overlay. The overlay appeared to have relatively smaller coarse aggregates that were found to be exposed on the surface. Since the coarse aggregates have higher resistivity than concrete mortar and since the interference could not be completely avoided, the higher resistivity might be attributed to the LMC overlay.

Figure 99 presents the scatter diagrams for the one-point and four-point resistivities. Though there is a significant difference between the magnitudes of resistivities, there is an observed relationship between them, higher values correspond with higher values and versus.

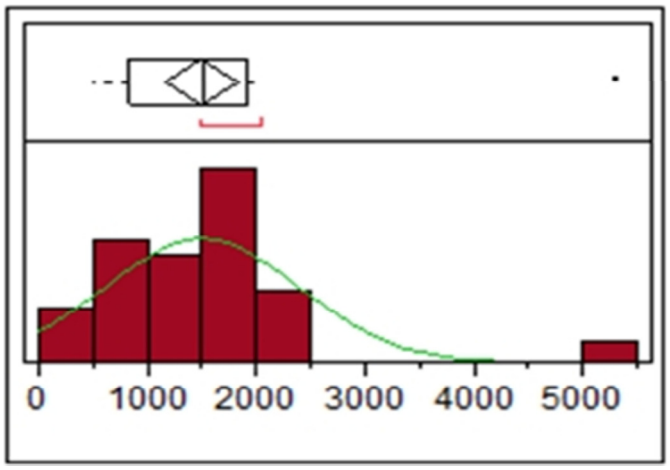

Mean	1501
Std. Dev.	892
Median	1526
C.V.	59%
n	32

Figure 98 – Distribution of Four-Point Resistivities from NJ Bridge Deck

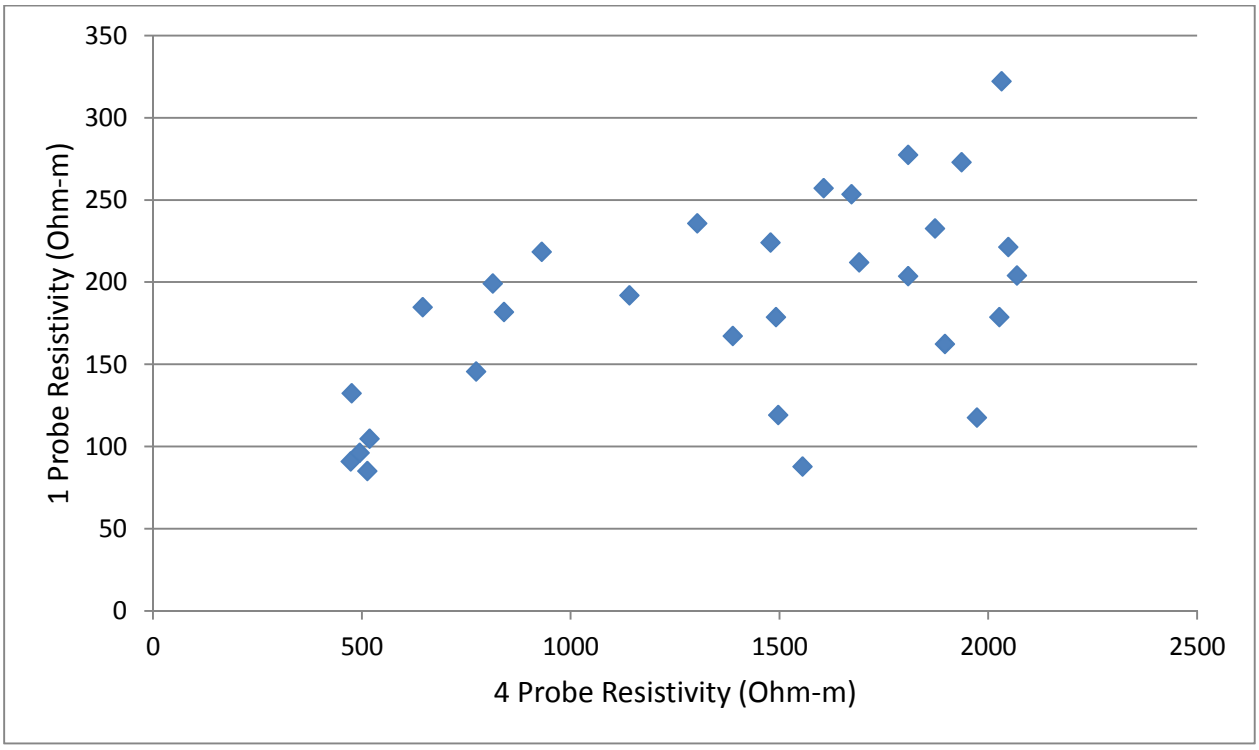

Figure 99 - One-Point Resistivity vs. Four-Point Resistivity

Chloride Contents

Distribution of the chloride content at an average depth of 0.5 in. (surface chloride) is presented in Figure 100. It appears that the distribution is normally distributed and has a relatively low C.V. of 22%. Mean surface chloride concentration is 5.95 lb/yd^3, while the 95% confidence limits are 8.43 and 3.47 lb/yd^3.

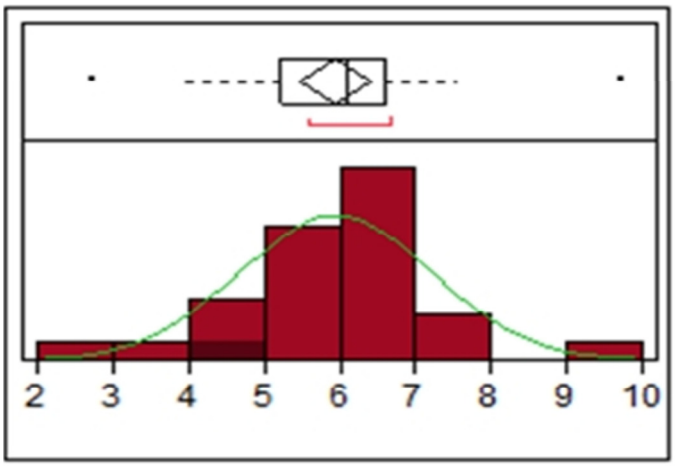

Mean	5.95
Std. Dev.	1.28
Median	6.09
C.V.	22%
Upper 95%	8.43
Lower 95%	3.47
n	32

Figure 100 – Distribution of Near Surface Chloride Contents at 0.25 – 0.75 in. depth

The chloride content across the depth for each test location was plotted to understand the profile. It was found that the chloride profiles were parabolic in shape, similar to the decks with no overlays. The influence of the LMC overlay on the chloride diffusion profile was not observed in the plotting of the chloride values as a function of depth. However, it is reasonable that over the course of exposure period while the chloride is diffusing from the top surface, the chloride from substrate concrete may move into the base of the LMC overlay concrete. This would have resulted in the parabolic profile after 13 years of service (Weyers et. al. SHRP 668, 1994). Figure 101 shows a possible diffusion behavior in the deck concrete.

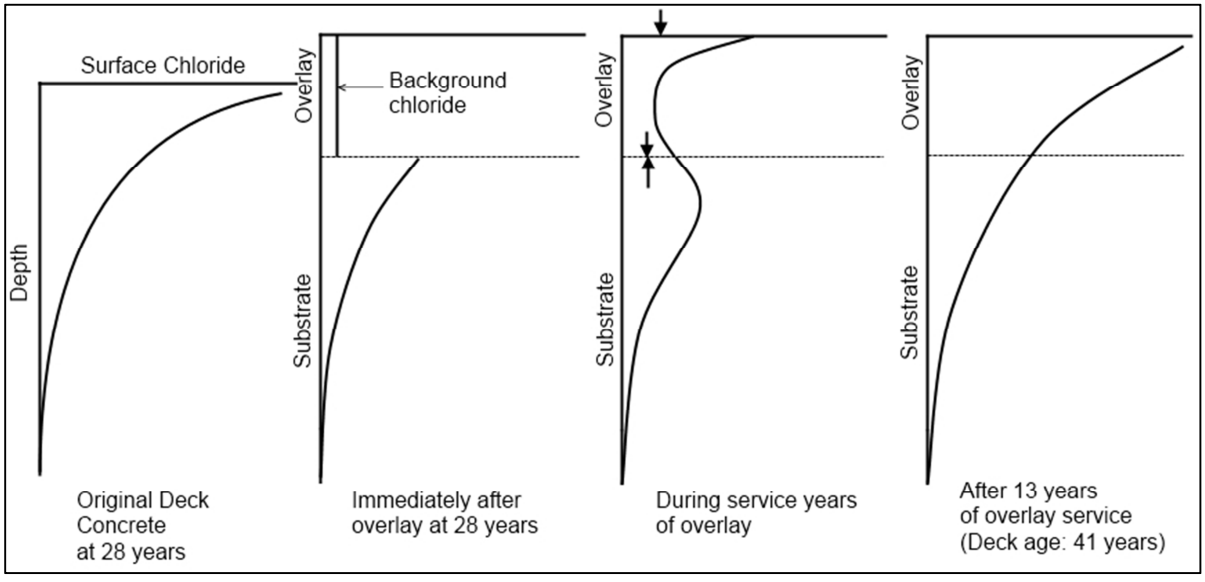

Figure 101 – Chloride Diffusion through Service Life of Overlaid Deck

However it has been shown that the chloride does not or at least very small amount of chloride would move upward into the lower permeable LMC concrete (Weyers et. al. SHRP 668, 1994). The rationale behind the stabilized diffusion through the two layers of concrete may be related to the higher moisture content in the low permeable overlay.

Diffusion Coefficients

Since the bridge deck was overlaid at 28 years of service, the influence of the overlay on the diffusion coefficients must be analyzed. Five different cases were assumed and the diffusion coefficients were estimated. First case was run with all the eight chloride depths, which includes the top three LMC overlay depths and bottom five base concrete depths, with 41 years of service life. Second case ignores the presence of LMC overlay and estimates diffusion coefficients for base concrete only with 41 years of service life. Whereas, the third case estimates diffusion coefficients for the LMC overlay separately that had 13 years of service life.

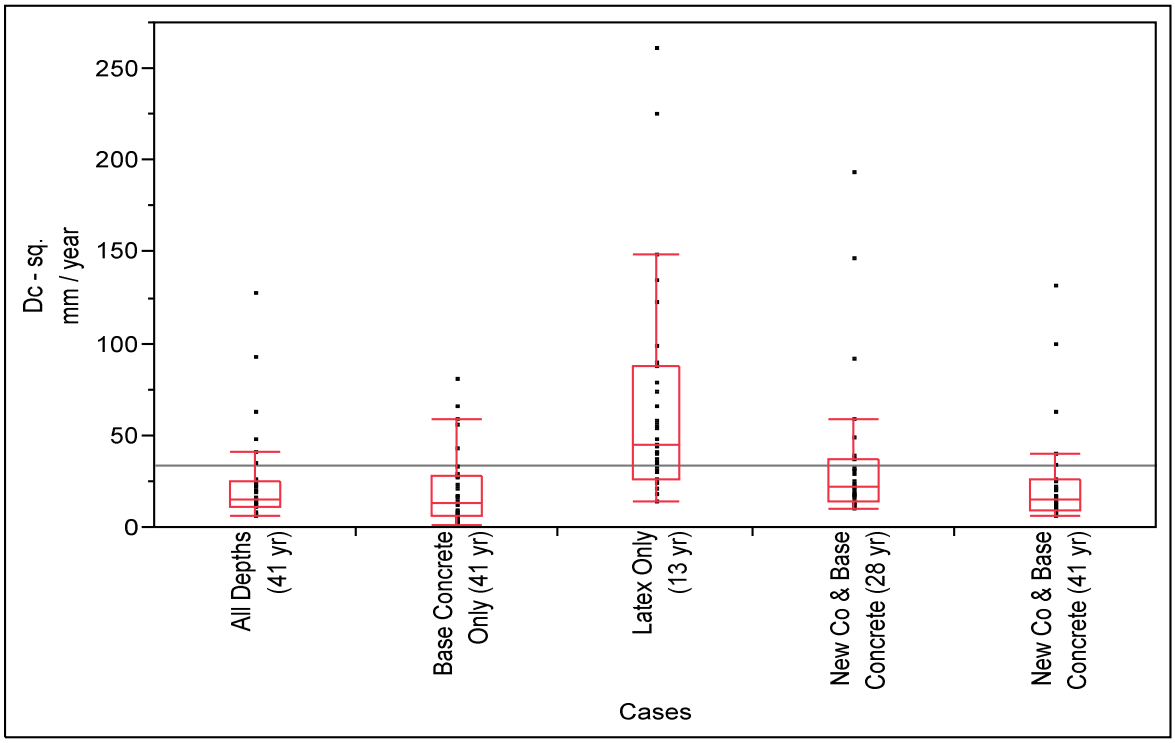

Figure 102 – Different Cases in Estimation of Diffusion Coefficients

With the fourth case, the effect of the current surface chloride values on the diffusion coefficients was analyzed by using the top depth (0.25" to 0.75") and the base concrete depths. Since the diffusion coefficient for a location can be taken as constant after being in service for a certain years,

the estimation for the fourth case was performed with 28 years as service life at which the overlay was laid. In order to estimate the diffusion coefficients from the current surface chloride values and chlorides in the base concrete only, assuming the overlay was not placed, the fifth case was run using the chlorides from the top depth and the base concrete depths with 41 years of service life.

Figure 102 presents the comparison of the diffusion coefficients estimated from the five cases. It can be noted that the LMC overlay alone has allowed higher diffusion rates than expected. Otherwise, the diffusion coefficients estimated from the cases 1, 2, 4, and 5 are not different from each other. Thus, it was decided to utilize the diffusion coefficients from case 1, which includes chlorides from all the depths, for the service life estimation. The diffusion coefficients of LMC overlay and base concrete are not very different even with the difference in the permeability of concrete mixtures, which may be related to the moisture content of the concrete.

Figure 103 presents the distribution of the apparent diffusion coefficients from case 1. The values ranged from 6 to 128 mm^2/year, which is the same range as that of Virginia pilot bridge (10 to 100 mm^2/year). The distribution appears to be skewed to the left and has a higher C.V. of 107%.

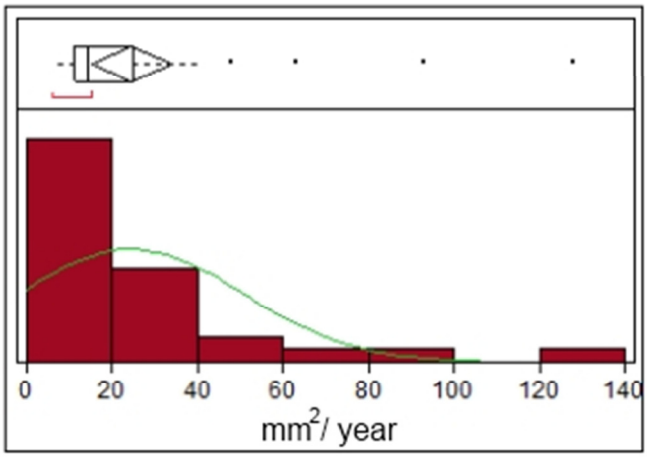

Mean	24.5
Std. Dev.	26.27
Median	14.5
Std. Err. Mean	4.64
n	32

Figure 103 – Distribution of Apparent Diffusion Coefficients from Case 1

Diffusion rate in a concrete medium depends upon the moisture content and its quality, as is resistivity. Thus, scatter diagrams of diffusion coefficients and FPWR, and OPR measurements are shown in Figures 104 and 105 respectively. It appears that there is no correlation between these factors similar to the data from Virginia pilot bridge.

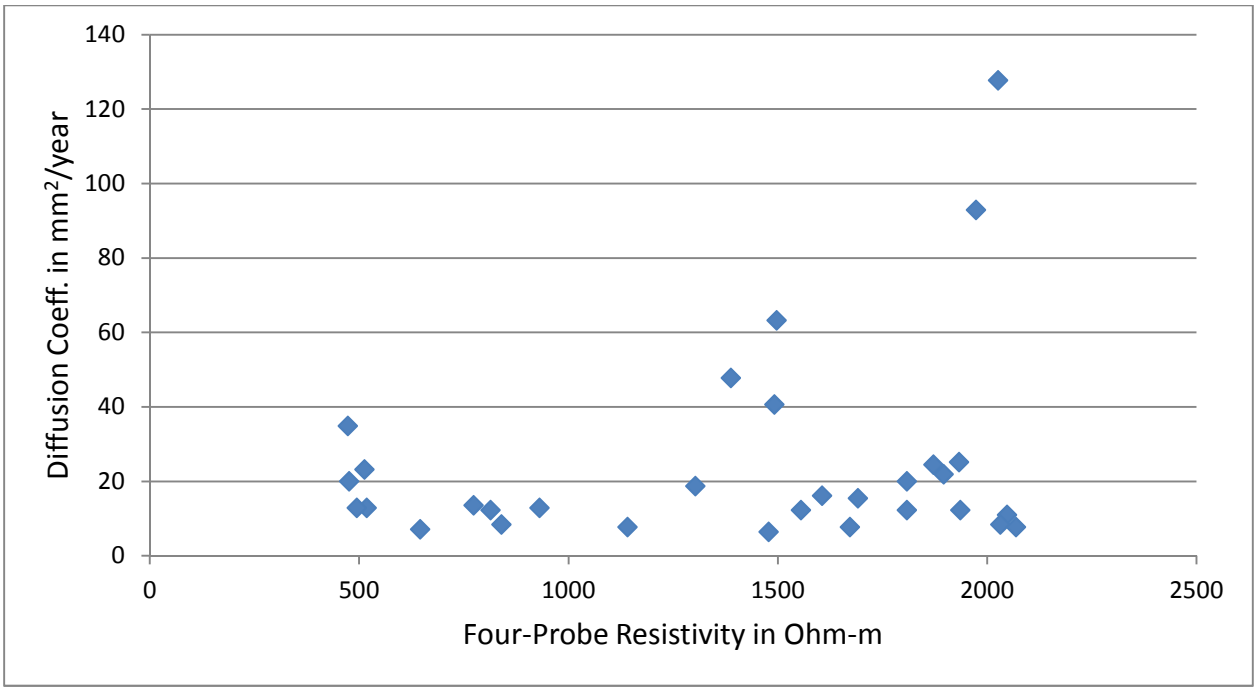

Figure 104 - Relationship between Diffusion Coefficients and Four-Point Resistivities

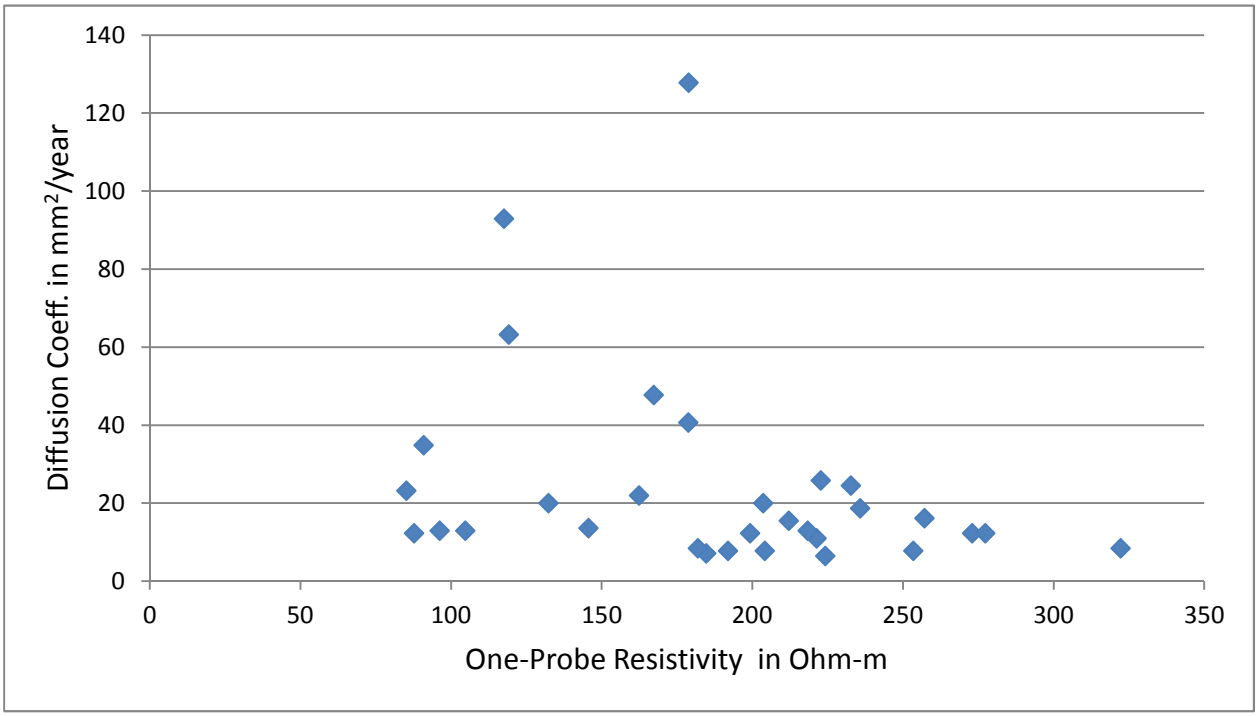

Figure 105 – Relationship between Diffusion Coefficients and One-Point Resistivities

Scatter diagrams for the surface chlorides and diffusion coefficients are shown in Figure 106. As shown, the two factors are independent of each other, which agree with Fick's Second Law.

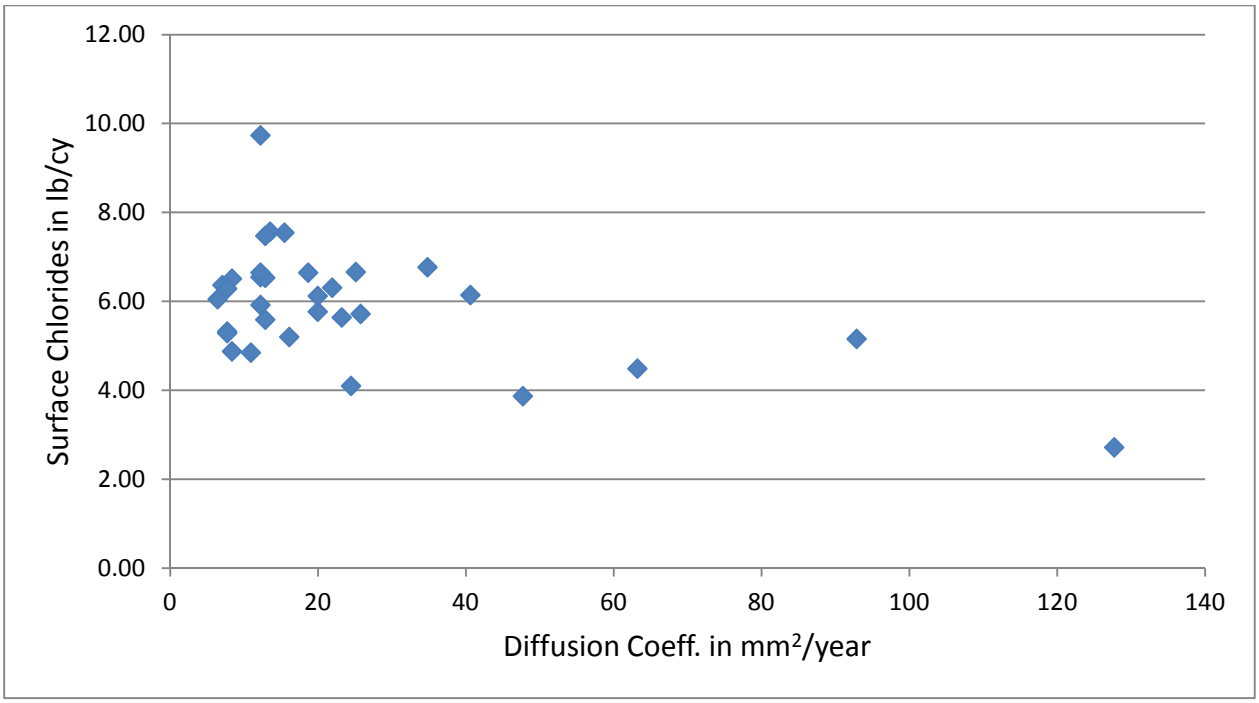

Figure 106 – Relationship between Surface Chlorides and Diffusion Coefficients

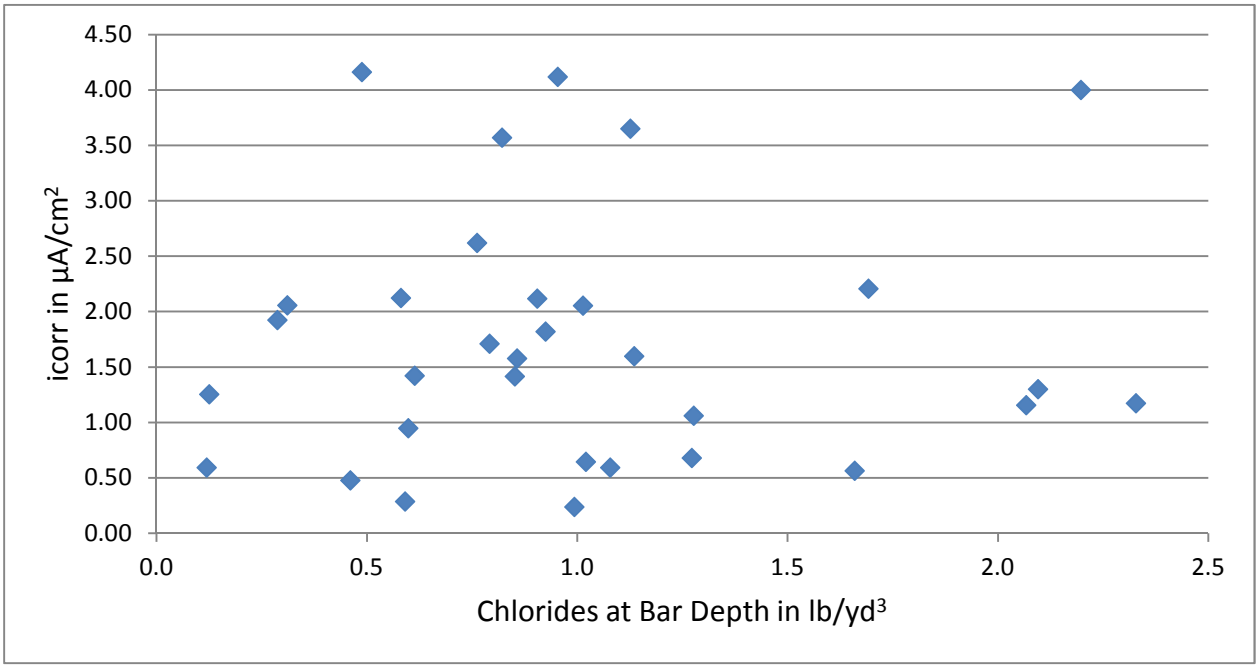

Figure 107 - Relationship between Corrosion Rates and Chlorides at Bar Depth

Figure 107 presents the scatter diagrams for the 3LP corrosion rates and the chlorides at bar depth. It appears that there is no relationship between the two factors. The absence of a relationship may

be related to the LMC overlay and moisture content of the concrete surrounding the reinforcing bars, which could have effectively restricted the diffusion of chlorides into the concrete.

Resistivity/CCD/Chloride Concentration at Bar Depth

Unlike the data from Virginia pilot bridge, there is no relationship between the corrosion current density and chloride concentration at steel bar depths (Figure 107). However from Figure 96, it appears that there is a relationship between OPR and CCD according to Ohm's Law. Thus, a 3-dimensional scatter plot was plotted in order to see if any relationship exists between the three factors.

Figure 108 presents the 3D scatter plot between FPWR, CCD, and chloride concentration at bar depth. The normal contour ellipsoid drawn over the points shows that CCD is directly related to the chloride concentration at bar depth and inversely related to the FPWR. Nevertheless, the major axis of the ellipsoid is not coinciding with the diagonal plane of the 3D space. The presence of the LMC overlay might be the explanation for the poorly observed relationship between the factors.

To determine whether OPR, instead of FPWR, can form the expected relationship in a 3D scatter plot another plot is shown in Figure 109.

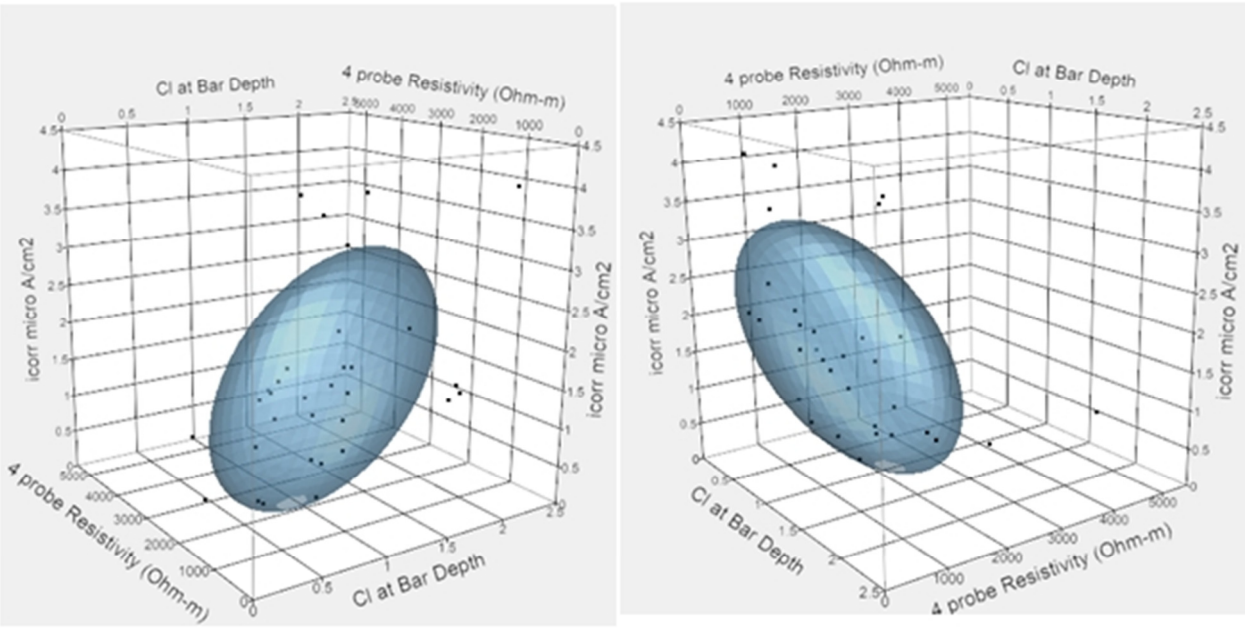

Figure 108 – Relationship between FPWR, CCD, and Chloride Concentration at Bar Depth

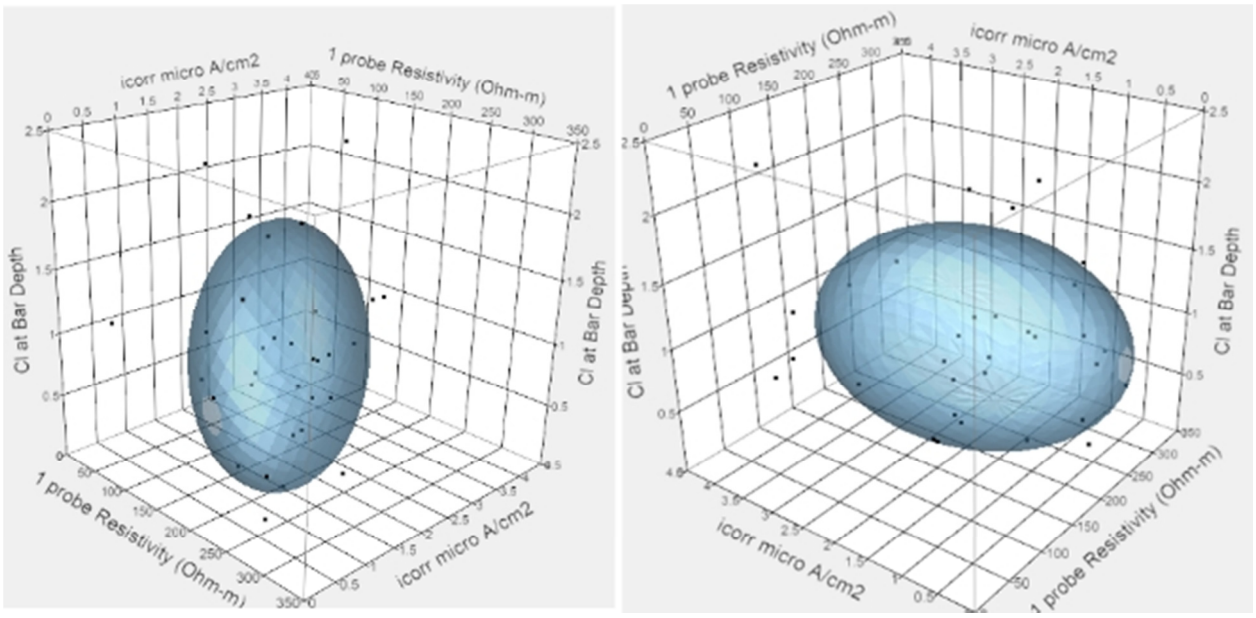

Figure 109 – Relationship between OPR, CCD, and Chloride Concentration at Bar Depth

From Figure 109, it appears that the normal contour ellipsoid coincides with the diagonal plane of the 3D space. Since the measurement of OPR involves directing of current to flow towards the reinforcement, the OPR values were not affected as much as the presence of the overlay as the FPWR, for which the flow of the current could be easily affected. The higher FPWR values might represent the resistivity of the top LMC overlay layer only.

Service Life Estimation

Service life estimation of New Jersey pilot bridge was conducted using the chloride diffusion model based on Fick's Second Law of diffusion, similar to the Virginia pilot bridge. Cover depths, diffusion coefficients and surface chlorides were entered as simple bootstrapping for the model. The chloride initiation values are to be entered using parametric bootstrapping. Figure 110 presents the estimated chloride concentration at the reinforcement level during corrosion initiation for the bare steel bars (Brown 2002). The range of chloride concentration values is not different from the distribution of chloride concentrations at reinforcement depth (Figure 54).

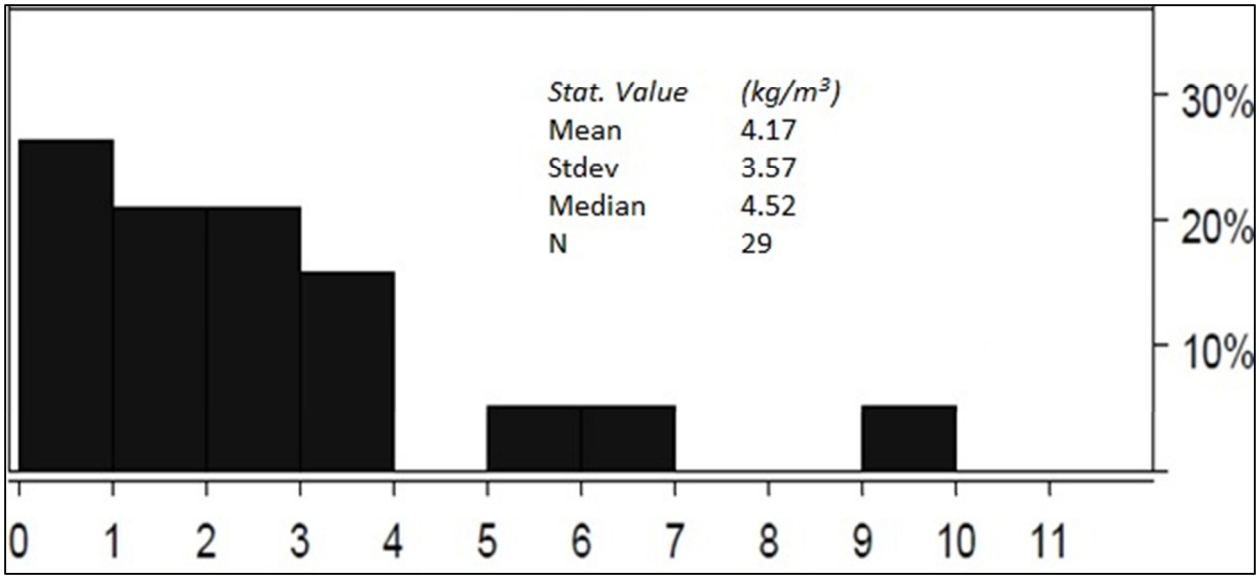

Figure 110 – Estimation of Chloride Concentration at Reinforcement Depth at Corrosion Initiation

Table 29 – Chloride Initiation Rates and Corresponding Service Lives for Bare Steel

Trials	Min	Max	Mode	5% Initiation + Crack Time (6) (year)	EFSL (12% Det.) (year)
1	0.66	10.6	2.37	69	127
2	0.6	3	1.3	26	38
3	0.6	3.5	1.3	28	47
4	0.6	4	1.3	30	50

Table 29 presents the trials conducted by entering different sets of chloride initiation values for the model. The first trial uses the whole range of chloride concentration values suggested by first mode of distribution from Brown's work (Brown, MC 2002). But, the service life is overestimated at 5% damage and consequently at 12% EFSL, 69 and 127 years respectively. Trials 2, 3, and 4 are the similar chloride values used for VA bridge service life estimation model. It appears that the trial #3 with minimum, maximum, and mode of 0.6, 3.5, and 1.3 lb/yd^3 respectively predicts 5% damage at 28 years, which is the time of LMC overlay. Thus, the prediction of 47 years as the EFSL can be taken as the service life of the New Jersey pilot bridge, if the bridge deck was not overlaid. The effect of overlay on the extension of service life of a bridge deck depends upon several factors such

as type of overlay, overlay thickness, uniformity across the deck and the amount and degree of chloride contaminated concrete left-in-place. Extensive data from overlaid bridge decks are necessary to integrate the additional service life offered by the overlay. Figure 111 presents the percent deterioration versus estimated time for deterioration for NJ pilot bridge.

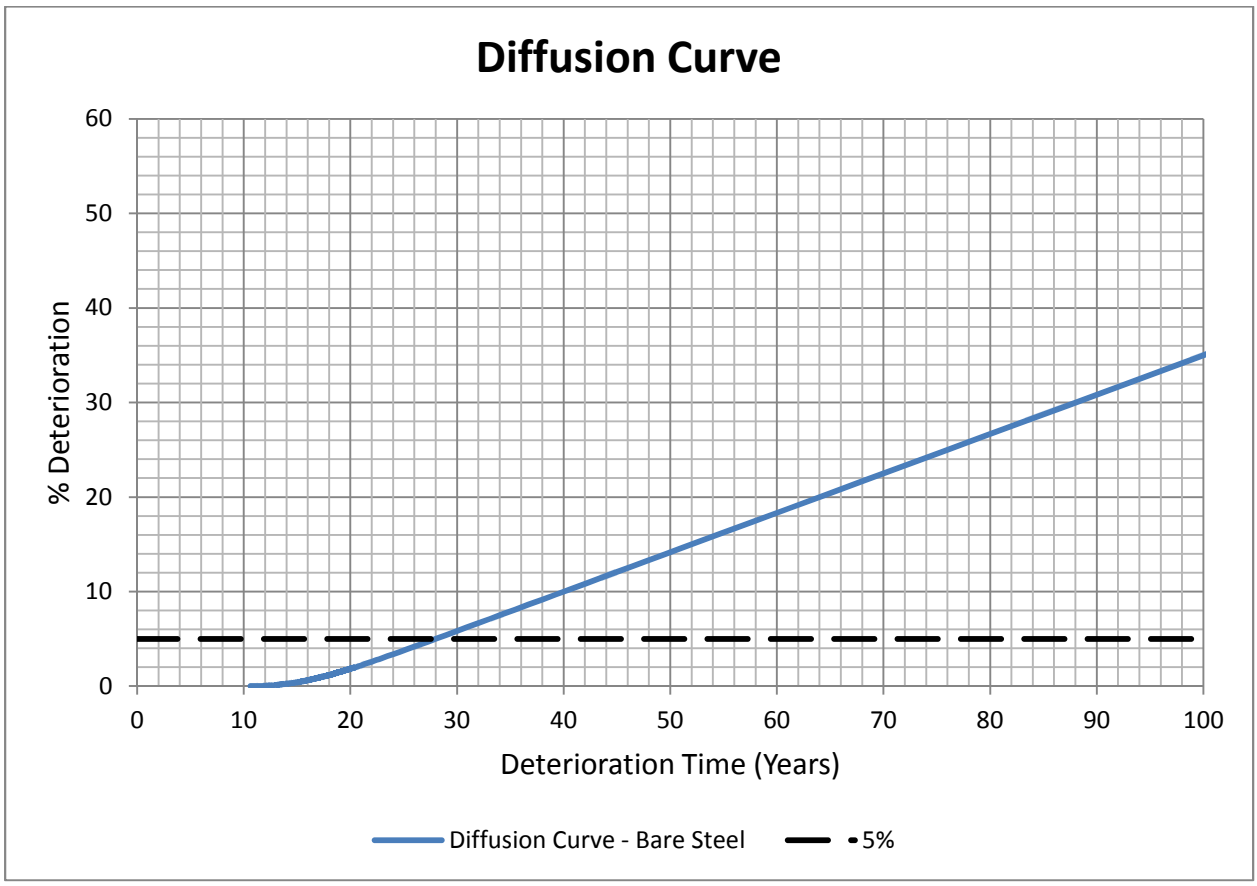

Figure 111 – Diffusion Curve for New Jersey Pilot Bridge

NEW YORK PILOT BRIDGE

BACKGROUND

The New York pilot bridge is located about 120 miles west of Binghamton in Almond, New York. The bridge (NBI Structure Number: 1016310) was built in 1990 and it is a prestressed concrete adjacent box beam structure. Condition surveys were conducted in 2011 at an age of about 21 years. This structure carries State Route 21 over Karr Valley Creek, as shown in Figure 112.

Figure 112 – Route 21 Bridge over Karr Valley Creek

The NY pilot bridge consists of two simple spans, which are made continuous for the live load by using a continuity diaphragm over the center pier. The location of the bridge is representative of wet-freeze regions of United States. The span of the bridge structure is approximately 174 ft. (53 m) long and is 28 ft. (8.5 m) wide excluding the sidewalks, and with a 24 degree skew (right ahead). Bridge includes sidewalks on either side of approximately 6.25 ft (1.9 m) width each. The superstructure includes a deck of 6 in. (0.15 m) thickness and sidewalks of 7.5 in. (0.19 m) thickness on top of the deck. Karr Valley Creek runs below the bridge resulting in a humid environment. The deck riding surface rests on ten prestressed concrete box beams, which have rectangular hollow cores. The deck was tied to the adjacent box beams using hairpins. No overlay was present on the deck surface. The annual average daily traffic (AADT) on the pilot bridge is approximately 9000 vehicles.

Figure 113 – View of Deck Surface

In the bridge condition rating scale, the primary members of the superstructure were rated 4 by the inspectors. A rating of 4 is “poor condition”, also described by “Advanced section loss, deterioration, spalling, or scour”. The outside fascia box beams had shear cracks at all the eight corners. Leakage of water was detected throughout the deck in the longitudinal direction, especially at the center of the deck, which is an evidence of shear key failure. NYDOT inspection reports show that the deck was awarded a rating of 7, which is “good condition”. Also, the substructure was given a rating of 8, which stands for “very good condition”. A view of the deck span is presented in Figure 113.

The entire deck was reinforced by using a steel fabric reinforcement of size No. 4 uncoated bars. Longitudinal epoxy coated top reinforcement bars were provided at 4.25 in. (0.108 m) spacing in the middle region of the deck, on top of pier, for continuity and resisting negative moments.

FIELD PERFORMANCE ASSESSMENT

The field performance assessment involves the visual damage survey and the corrosion assessment of the deck. Teams from Virginia Tech (VT), Virginia Transportation Research Council (VTRC), Rutgers University (RU), and Parsons-Brinckerhoff (PB) conducted various tests on the deck.

The damage survey involved the identifying and quantifying the damage indicators of cracks, spalls, delaminations, and patches. Team members from PB utilized non-destructive methods to conduct the damage survey at the top and bottom of the deck.

Deck corrosion assessment was performed by team members from Virginia Tech, and VTRC. The assessment included corrosion electrical testing, chloride sampling, and concrete core sampling. The tests conducted on the deck are listed below.

1. Deck reinforcement continuity test
2. Cover depth determination
3. Resistivity tests – one-point and four-point
4. Half-cell potential testing
5. Corrosion rate determination
6. Chloride sampling
7. Concrete core extraction for various laboratory tests.

TESTING METHODOLOGIES

Visual Inspection and Sounding

Visual inspection was conducted on the bridge deck to identify, locate, and quantify the damages as spalls, cracks, and patches. Sounding was employed to identify the delaminations present in the bridge deck. The data collected were supplied to a computer program as input and which stores the data in the two dimensional geometry of the deck. These data were used in selecting the test locations for various corrosion tests, and core collections. The quantified damages of spalls, delaminations, and patches are used in the estimation of the service life of the bridge. The visual inspection was performed thoroughly on different bridge components girders, joints, and abutments.

Figure 114 – Marking of Delamination Locations Using Sounding Techniques

Figure 114 displays the markings of delaminations on the deck surface, using a red chalk marker, found by utilizing sounding techniques. Also shown are longitudinal cracks between box beams which have been sealed with a black material.

Cover Depths

Prior to taking any electrical measurements, it is essential to locate the position of reinforcement bars and determine the cover depth in a non-destructive manner. The cover depths measurements were carried out using a pachometer. Measurements were taken by dividing the whole deck into spans 1 and 2, and lanes north bound, and south bound. A total of 22 measurements were taken on the span 1 and 23 measurements were obtained from span 2, including the north bound and south bound lanes. Most locations of the readings were centered near the length-wise middle of the deck, since the longitudinal reinforcements are present only in this region. Figure 115 illustrates the measuring of cover depths.

Figure 115 – Cover Depth Measurement Using Pachometer

Continuity

The bridge deck consists of ECR for longitudinal reinforcements and the uncoated mesh. Before performing any electrical corrosion tests, the continuity of the reinforcement mat must be tested, so that the number and position of taps required for the electrical tests can be determined. Two locations were selected in spans 1 and 2 each. After concrete core drilling, and tapping the reinforcement, threaded stainless steel metal pieces were installed.

Figure 116 – Drilling and Tapping for Continuity Test

The resistance was measured by utilizing a multimeter, after the corresponding taps were connected by a low resistance copper wire. Figure 116 shows the drilling of the reinforcing steel prior to tapping and installation of a stainless steel rod for continuity testing.

Test Locations

For performing electrical corrosion tests such as resistivities, half-cell potentials, corrosion rates, and chloride sampling, test locations were selected on the deck. For one-point resistivity test, nine locations were selected on north bound lane and 13 locations on south bound lane. Similarly, nine locations were selected on north bound and 14 locations on south bound for four-point resistivity test. Test locations for corrosion rates and potentials were located at 16 positions on north bound lane and 17 on south bound lane.

Corrosion Potentials

Corrosion potentials were measured by using the three-linear polarization (3LP) device, which was also used for corrosion rate tests. A total number of 33 measurements were acquired from the deck. The test was conducted in accordance with ASTM C 876-09, since a study by Ramniceanu (2004) has shown that the test can be applied to epoxy coated steel bars (ECR). It is to be noted that there are no guidelines present for the interpretation of half-cell potentials of ECR.

Corrosion Rates

As stated above, the 3LP device was used to measure the corrosion currents at the designated test locations. Since the 3LP device was built to measure the rates of uncoated steel, the same guidelines applied for the interpretation of uncoated steel corrosion rates might not be applicable for the ECR. A total number of 33 corrosion current measurements were performed on the bridge deck.

Corrosion Resistivity

Corrosion resistivity is a material property of concrete, which will indicate the readiness with which the concrete will allow the corrosion reactions to occur. One-point and four-point resistivity tests were both conducted on the NY bridge deck.

Four-point resistance was measured by employing the Wenner's four-point resistivity meter over the concrete surface. This provides only the resistivity of the deck concrete. Resistivity can be calculated by assuming that the applied current flows through the concrete up to a depth equal to that of the probe spacing used. A total number of 23 tests were performed for four-point resistivity.

One-point resistance was measured by utilizing a disc electrode of 3 in. in diameter. Then, the resistivity can be calculated by estimating the applied current flow to the top reinforcement steel. The current flow depth in this case was equal to the sum of cover depth and half the depth of the steel bar. One-point resistivity includes the resistivity of concrete and the rebar coating, if any.

Chloride Content

Chloride content of the deck concrete at subsequent depths can be found only by drilling and collecting the concrete samples. It was decided to collect concrete samples from 8 subsequent depths from the deck surface, at an interval of ½ in., since it was intended to study the chloride diffusion at least up to the reinforcement depth. The top ¼ in. concrete was discarded because of the inconsistency of chloride content at the top surface. The chloride sampling locations were divided into three categories; no-crack regions, transverse crack regions, and longitudinal crack regions. Six locations were positioned in each of the above categories. Also, three chloride samples were collected from the middle of the deck, in between the two lanes, since the region contained severe deep wide cracks. The depths of concrete samples collected are listed below. Figure 117 illustrates chloride concrete powder sample extraction technique.

Range, in. (mm)	Average, in. (mm)
0.25 (6.3 mm) to 0.75 (19 mm)	0.50 (13 mm)
0.75 (19 mm) to 1.25 (32 mm)	1.00 (25.4 mm)
1.25 (32 mm) to 1.75 (44 mm)	1.50 (38 mm)
1.75 (44 mm) to 2.25 (57 mm)	2.00 (51 mm)
2.25 (57 mm) to 2.75 (70 mm)	2.50 (63.5 mm)
2.75 (70 mm) to 3.25 (83 mm)	3.00 (76 mm)
3.25 (83 mm) to 3.75 (95 mm)	3.50 (89 mm)

Figure 117 – Chloride Sampling Process

After the powdered concrete samples were collected, the chloride contents were found by titrating against 0.05N silver nitrate solution. The procedure followed was in accordance to the ASTM C 1152/C 1152 M-04, which is the potentiometric titration process of acid soluble chlorides.

Concrete Cores

To characterize the quality of the deck concrete it is necessary to collect and analyze concrete cores. The cores were collected by using water cooled diamond core drilling equipment on the top surface of the deck and the bottom of the prestressed box beams. Once the cores were cut, they were visually inspected and then photographically documented before being wrapped with layers polyethene sheeting, aluminum foil and duct tape to pressure the in-place moisture content . Then, the cores were tested for compressive strength, permeability, absorption, and other properties.

Figure 118 – Concrete Coring at Bottom of Bridge Deck

Figure 118 displays the process of concrete core extraction in the bottom of a prestressed box beam. A total number for 11 concrete cores were collected, where nine are from the deck surface and two from the bottom of prestressed box beam. The two box beam cores were taken in an area where significant leakage through the deck had occurred. One core was taken in the center of the box beam, the other near the edge of the box beam, see Figure 118. The cores had an average diameter of 3.89 in. Most cores contained the US No. 3 mesh, while a few cores intentionally contained the longitudinal ECR bars for corrosion tests. Note, it was not possible to detect the presence of the mesh in the deck concrete because of its small diameter and cover depth. Core lengths varied between 3.10 to 6.76 in. Core locations are presented in Table 30 as Cx and Txs reinforcing steel tap locations, respectively.

Table 30 – Concrete Core Locations

Span	ID	Coordinates	
		Longitudinal (ft)	Transverse (ft)
1	C1	19	3
1	C2	60	10
2	C3	117	10
2	C4	151	5
1	T1	68	10
2	T2	108	0.5
1	C5	10	22
1	C6	32	18
2	C9a	78	24
2	C9b	78	24
2	C10	90	19
2	C11	93	23
2	C7	130	25
2	C8	150	17
1	T4	51	27
2	T3	100	18.5

ANALYSIS AND DISCUSSION

Damage Survey

Figures 119 and 120 present the damage survey results of the span 1 and span 2 of New York pilot bridge. The delaminations were primarily confined to the ends and along a centerline crack. There are significant numbers of cracks running along the longitudinal length of the span, which are caused by the differential movement of the adjacent box beams, which is the result of failed shear keys. Delaminations and crack locations are typical for adjacent box beam / overlaid deck concrete construction. Also, note that the delaminated areas occur at edges, ends of the spans and between lanes of concrete topping placements. These are typically high bound stress areas for toppings. Thus the damage is most likely not corrosion related, considering there is no ECR at the end locations.

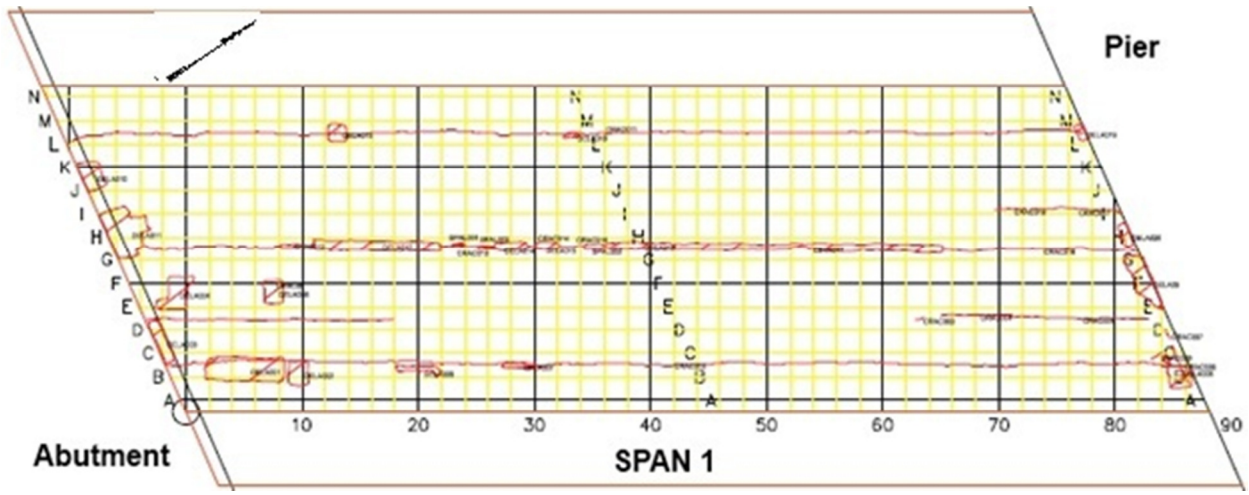

Figure 119 – Damage Survey Results from New York Bridge Span 1

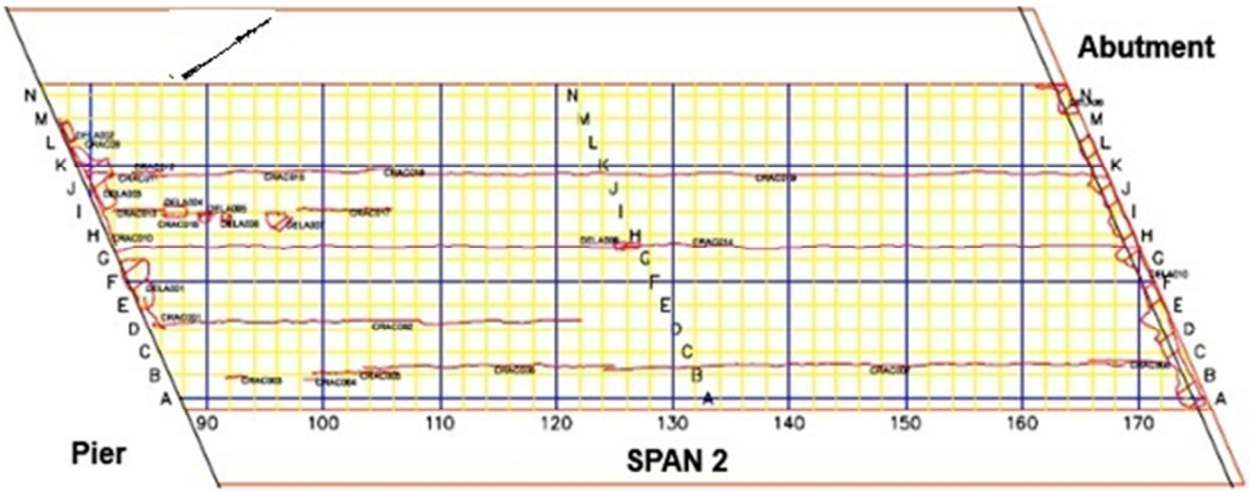

Figure 120 – Damage Survey Results from New York Bridge Span 2

The damaged areas of the deck are summed up approximately from Figures 119 and 120 to get a deterioration percentage of about 5 %. During the deterioration percentage calculation, the contribution of the cracks was not included.

Cover Depths

Figure 121 presents the distribution of the cover depths measured from 36 test locations on the deck. The standard deviation is somewhat greater at 0.34 in. Mean and median of the cover depth distribution are 2.21 and 2.22 in. respectively. Considering the distribution as normal, 95 percent of the reinforcements have a cover depth between 2.88 and 1.54 in. Based on a normal distribution, 25 percent of the reinforcements have a cover depth of less than 2.0 in. The larger percent steel cover depths less than 2.0 in. resulted from the larger standard deviation.

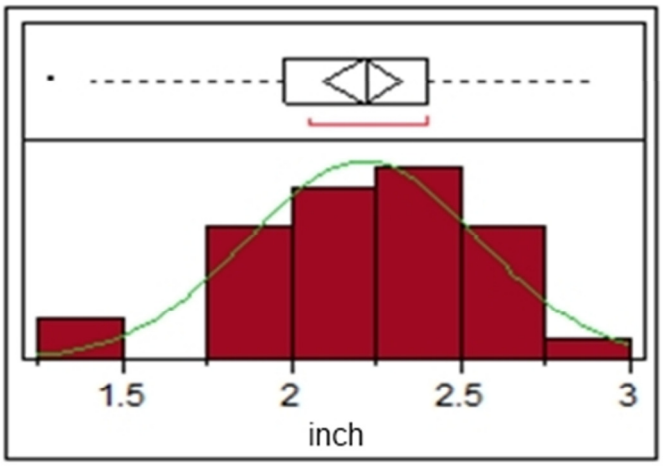

Mean	2.21
Std. Dev.	0.34
Median	2.22
Std. Err. Mean	0.06
Upper 95%	2.88
Lower 95%	1.54
n	36

Figure 121 – Distribution of Cover Depths taken from 36 Test Locations

With 25 percent of the reinforcement steel having a concrete cover of less than 2.0 in., the protection offered by the concrete cover against chloride diffusion will be less than desired.

Continuity

The bridge deck consists of two spans and the electrical continuity was checked between the two spans. Figure 122 presents the tap locations on a bridge plan view. Table 31 shows the measured resistance between the two tap locations. Negating the lead wire resistance from the measured resistance between the tap locations, it appears that the resistance is relatively high, thus limiting connectivity between the reinforcements of two spans. So the measurements taken in a span were conducted by connecting to the tap locations of the same span. Two more tap locations were located T3 and T4 in the southbound lane, one in each span for ease during measurements.

Although the resistance between tap points 1 and 2 is somewhat higher, it is not excessive. As previously stated, the ECR bars are in the center section of the bridge over the pier. The ECR should be in contact with the uncoated mesh. Thus, higher resistance should be related to the resistance of the epoxy coating. But the coating in concrete will increase in moisture making it more conductive.

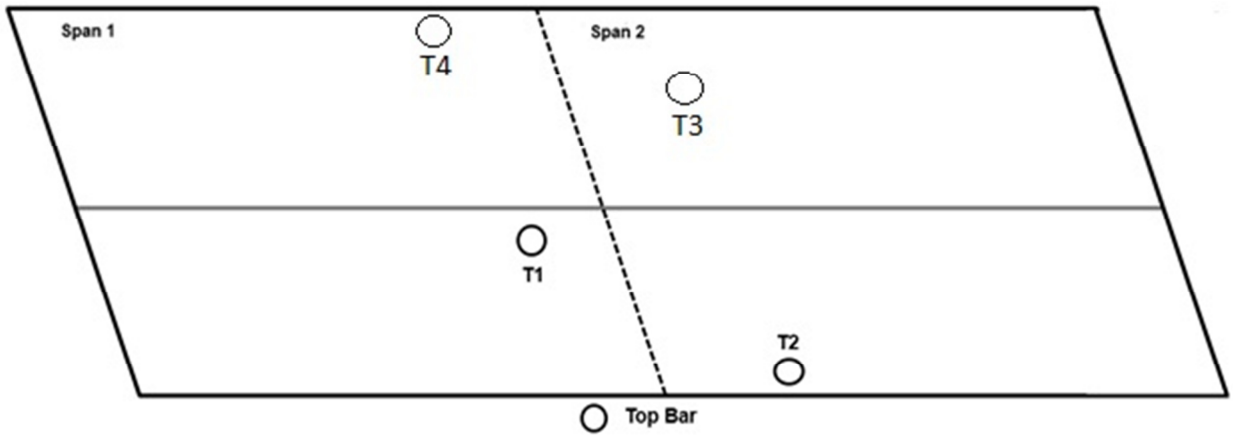

Figure 122 – Plan Locations of Continuity Locations

Table 31 - Continuity Connection Locations and Ohmic Resistance between Locations

Measured Resistance			Lead Wire Resistance (Ohm)	Adjusted Resistance (Ohm)
Location A	Resistance (Ohm)	Location B		
T1	55	T2	2.05	52.95

Corrosion Potentials

Figure 123 presents the distribution of the corrosion potentials with the statistic parameters for a normal distribution. Mean and median of the corrosion potentials are similar, -361 and -352 mV respectively, with a standard deviation of 79 mV. Considering the distribution as normal, the upper and lower 95% of the potentials are -516 and -206 mV respectively.

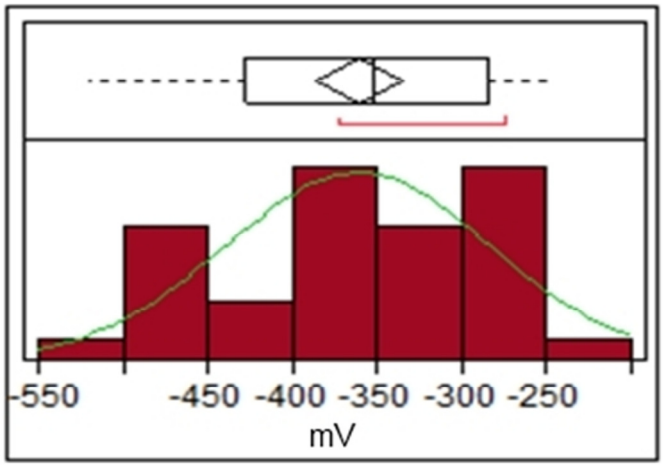

Mean	-361
Std. Dev.	79
Median	-352
Std. Err. Mean	13
Upper 95%	-516
Lower 95%	-206
n	39

Figure 123 - Distribution of Corrosion Potentials taken from 39 Locations

Table 32 – ECR Corrosion Risk Interpretation and Percent CSE Values of New York Pilot Bridge Deck

Corrosion Risk	Potential (mV)	Percent CSE Values
High	< -300	72
Moderate	-200 to -300	28
Low	> -200	0

Table 32 presents the interpretation of the measured potentials for ECR bars and the percentage of potential values in each interpretation range. It appears that a majority of potentials are in the higher corrosion risk zone, while the remaining values are in the moderate corrosion risk zone and no values in the lower corrosion risk zone. This might indicate that the bridge is undergoing active corrosion, which might be related to higher deicing salt usage in New York.

Three-Electrode Linear Polarization

Figure 124 presents the distribution of 38 corrosion current measurements from the NY pilot bridge deck. The distribution does not appear to be normal and there is difference between the mean and median, 0.34 µA/cm^2. The standard deviation is relatively large, 0.94 µA/cm^2, and the coefficient of variation is relatively high 45%. There are a larger number of smaller corrosion current densities causing a skew to the lower values.

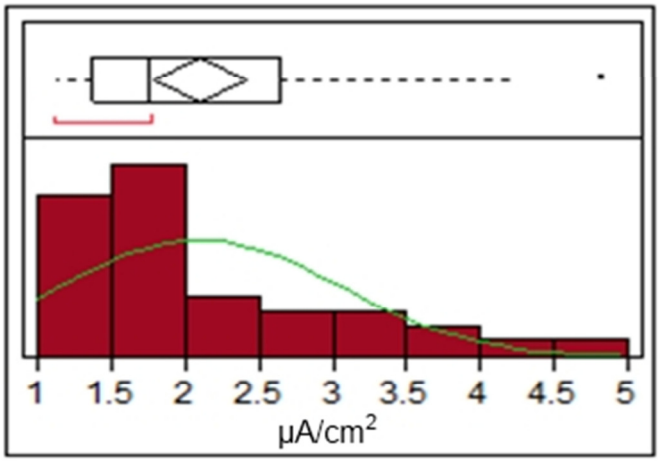

Figure 124 – Distribution of Corrosion Current Densities

From Table 33, it appears that a significant percentage of corrosion rate values are in the moderate corrosion risk interpretation zone, while the remaining values are in the higher corrosion risk zone and no values in the lower corrosion risk zone. This is similar to the measured potentials, except for the difference in the high and moderate corrosion risk zones, which indicates higher probability of corrosion.

Table 33 – Interpretation of 3LP Measurements on Uncoated Steel and Corresponding Percentage of Measurements

Corrosion Risk	3LP/CCD (μA/cm²)	NJ Pilot Bridge Deck (%)
High	> 3.0	18
Moderate	1.0 to 3.0	82
Low	< 1.0	0

One-Point Resistivities

Distribution of one-point resistivities and related statistic parameters are presented in the Figure 125. Mean and median of the distribution are similar, but the standard deviation is fairly large, 495 ohm-m, causing the coefficient of variation to increase to 56%. The distribution is similar to normal distribution with a little skew to the lower values similar to the data obtained from Virginia pilot bridge. However, due to the higher variance in both the cases it cannot be stated with confidence that the one-point resistivity values form a left-skewed distribution for ECR bars.

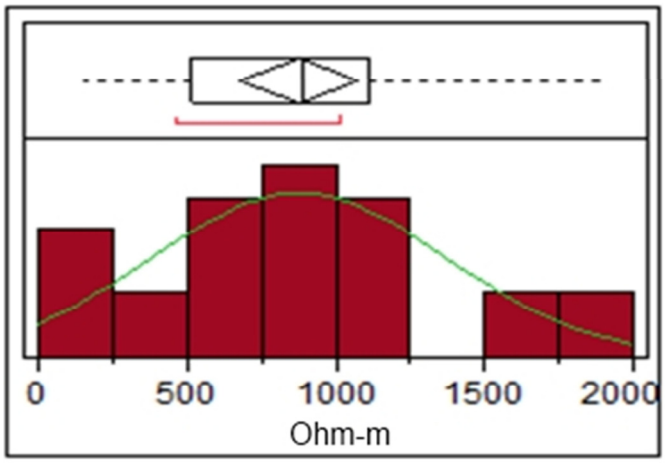

Figure 125 – Distribution of One-Point Resistivities from New York Bridge Deck

CSE/CCD/OPR

It is expected for the electrical readings measured on the bridge deck would be respective to Ohm's Law. Corrosion current density values are to be directly related to the corrosion potentials and inversely related to the resistivities. Figure 126 presents the relationship between the OPR and CCD values. It appears that there is an inverse relationship, though slight, between the two factors.

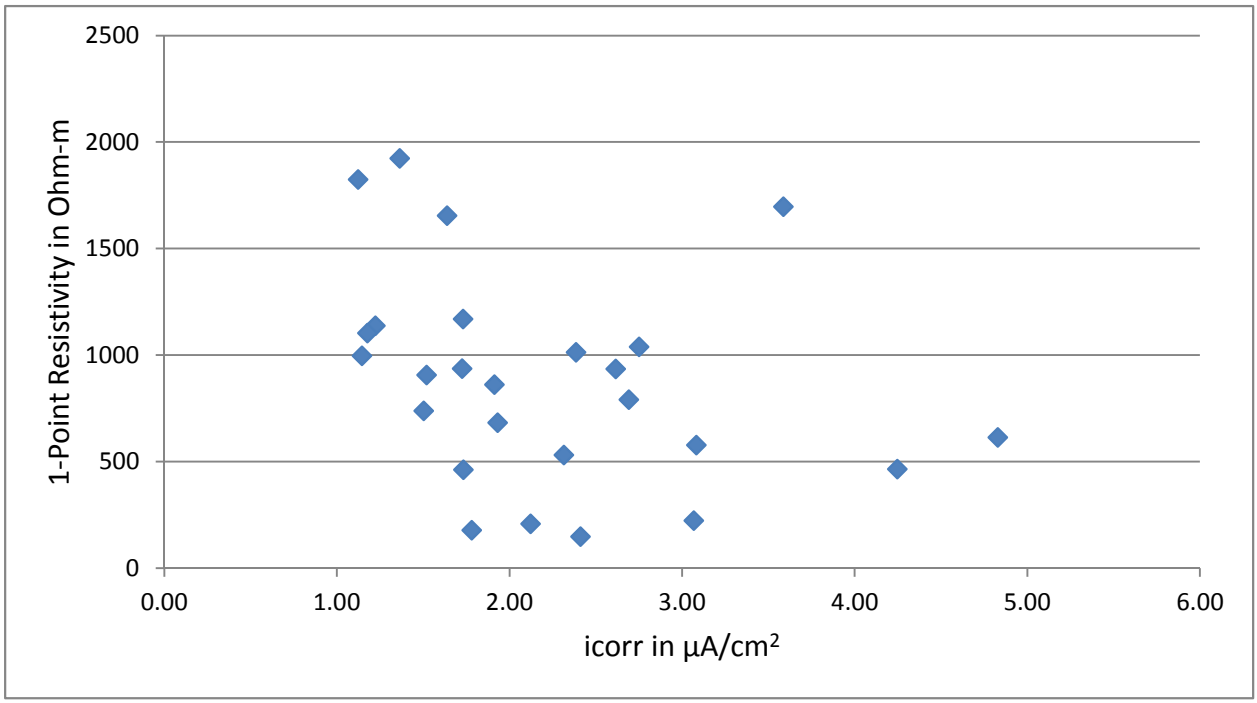

Figure 126 – One-Point Resistivity vs. Corrosion Current Density

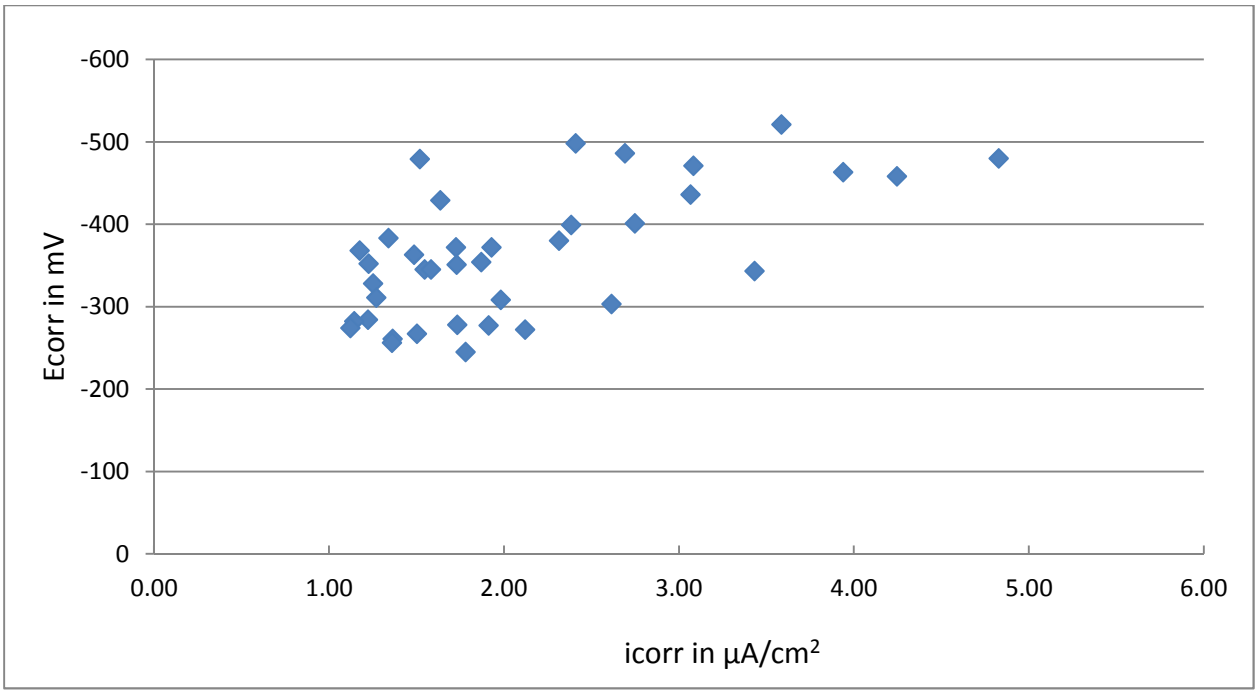

Figure 127 – CSE Potentials vs. Corrosion Current Densities

Figure 127 presents the relationship between the corrosion potentials and corrosion current densities. There is a definite positive relationship between the two factors. Thus, the data collected from the bridge deck agree with the Ohm's Law and consequent analysis may be meaningful.

Four-Point Resistivities

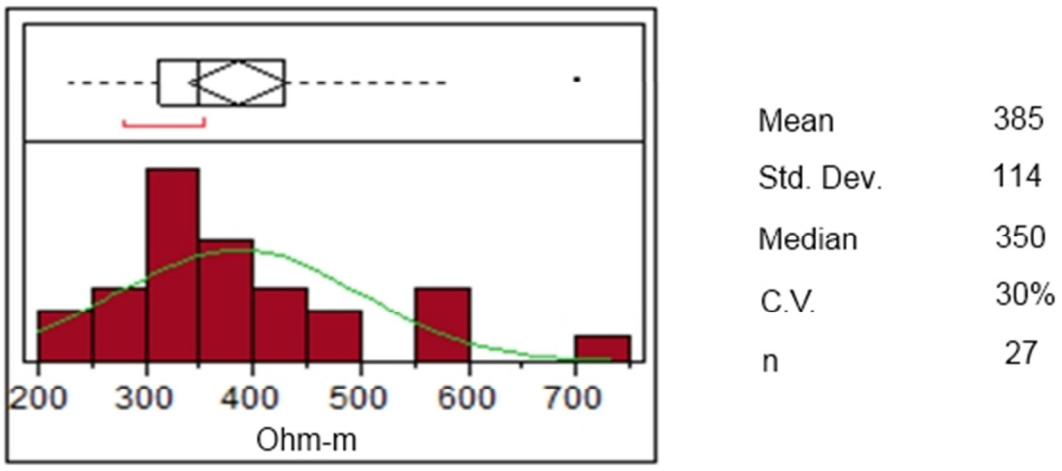

Figure 128 – Distribution of Four-Point Resistivities from NY Bridge Deck

Figure 128 shows the distribution of the four-point resistivities and the associated statistical parameters. Mean and median of the distribution are different, 385 ohm-m and 350 ohm-m respectively, and the standard deviation is large, 114 ohm-m.

Figure 129 presents the relationship between the one-point and four-point resistivity values. From the scatter diagram, it appears that there is no relationship between the two resistivities.

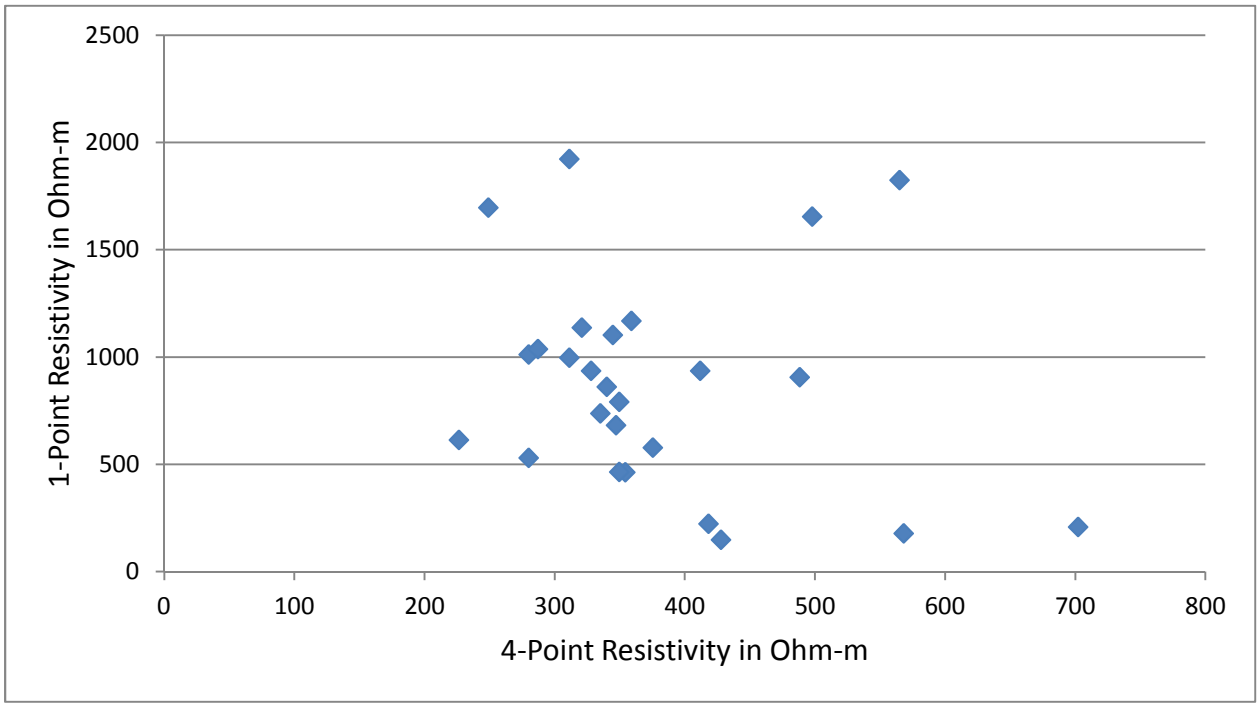

Figure 129 - One-Point Resistivity vs. Four-Point Resistivity

The one-point resistivities may have been influenced by the epoxy coating on the reinforcing steel. As the OPR measures the combined resistance of the concrete and the epoxy and FPWR measurement represents only the surface concrete resistance.

Chloride Contents

Chloride contents were extracted from six locations in non-cracked locations, six from transverse cracked locations, and six from longitudinal cracked locations. Distribution of the chloride content at an average depth of 0.5 in. (surface chloride) for both cracked and non-cracked locations is presented in Figure 130. It appears that the distribution is normally distributed and has a relatively low C.V. of 26%. Mean surface chloride concentration is 20.6 lb/yd^3, while the 95% confidence limits are 31.0 and 10.2 lb/yd^3. The near surface chloride concentration is vastly higher than the

Virginia and New Jersey pilot bridges, which is typical for the amount of snowfall received in the New York state region.

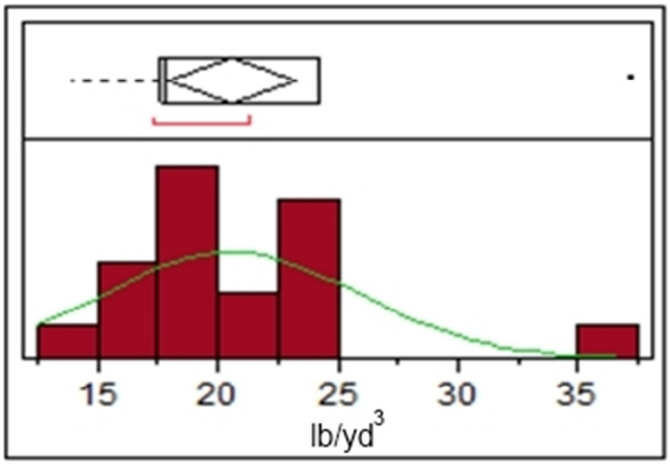

Mean	20.6
Std. Dev.	5.3
Median	17.8
Std. Err. Mean	1.3
Upper 95%	31
Lower 95%	10.2
n	18

Figure 130 – Distribution of Near Surface Chloride Contents at 0.25 – 0.75 in. Depth

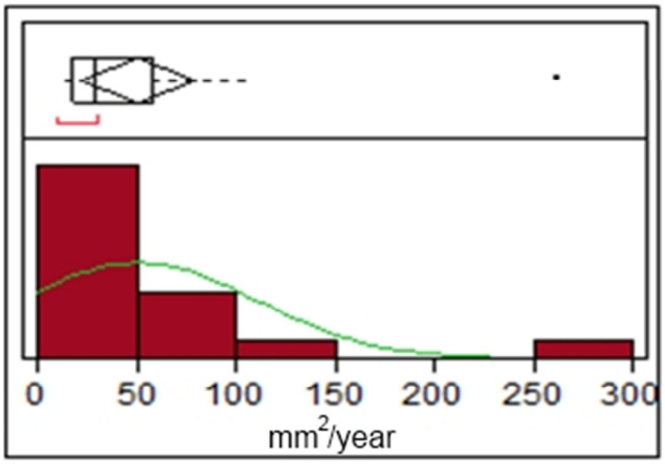

Mean	51
Std. Dev.	59
Median	29
C.V.	116%
n	18

Figure 131 – Distribution of Apparent Diffusion Coefficients

Figure 131 presents the distribution of the apparent diffusion coefficients calculated from the chloride concentrations at different depths for both cracked and non-cracked locations. The background chloride concentration of 0.6 lb/yd^3 was subtracted from the chloride values before the estimation of diffusion coefficients. The range of diffusion coefficients from New York pilot bridge is from 10 to 110 mm^2/year, when one outlier values was removed, and is the same as that of Virginia pilot bridge deck.

Figure 132 presents the scatter diagrams for the diffusion coefficients and four-point resistivities. There appears to be no relationship between the two factors. Figure 129 presents the relationship between the diffusion coefficients and one-point resistivities. Though somewhat better, there is no appreciable relationship between the factors.

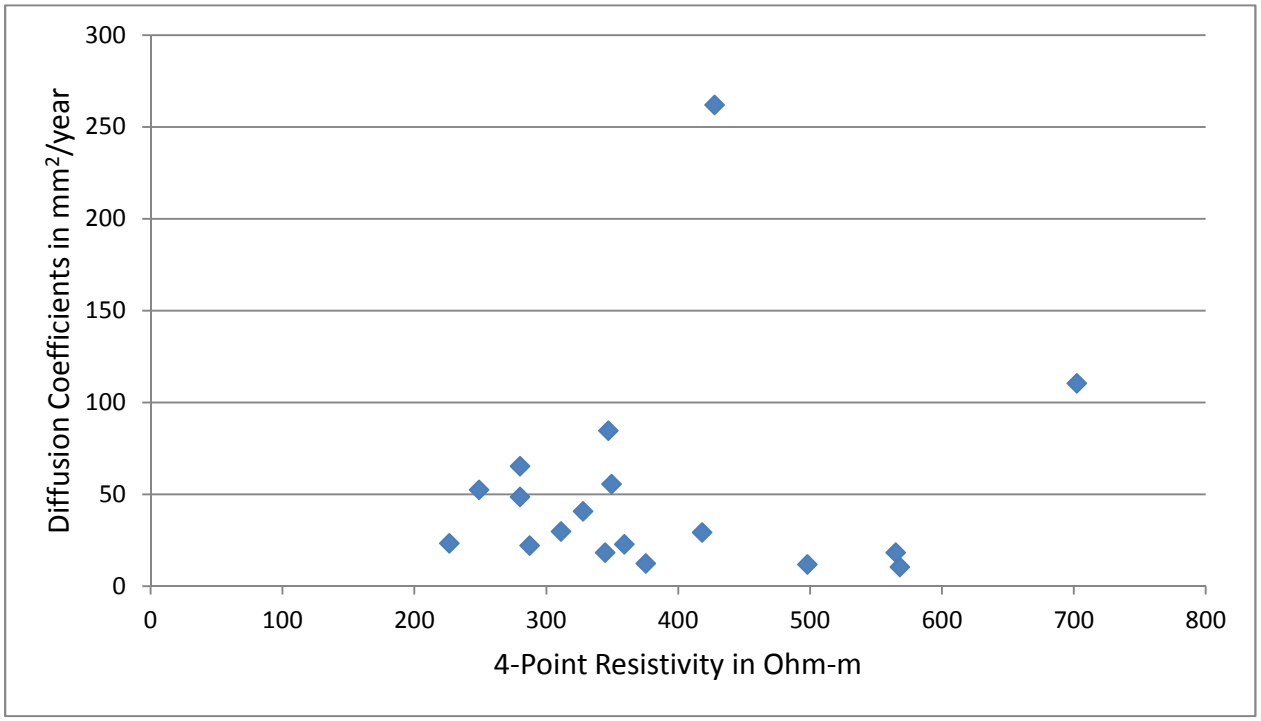

Figure 132 - Relationship between Diffusion Coefficients and Four-Point Resistivities

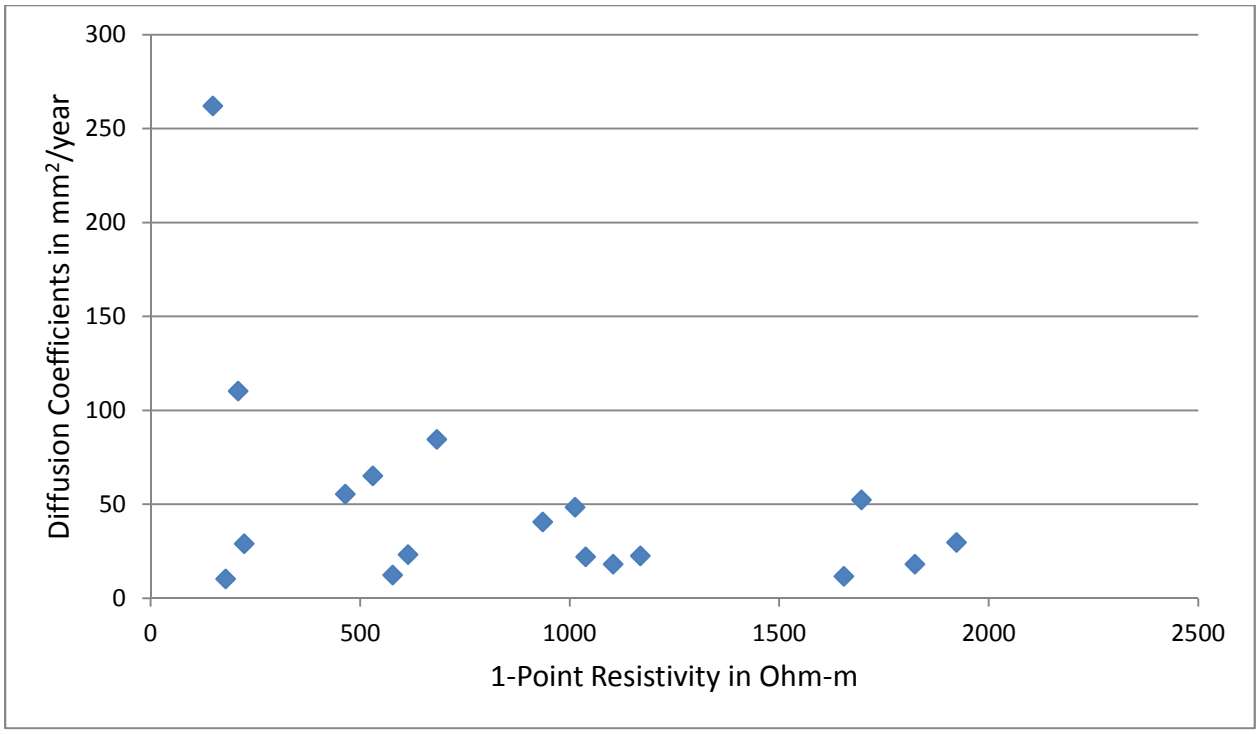

Figure 133 – Relationship between Diffusion Coefficients and One-Point Resistivities

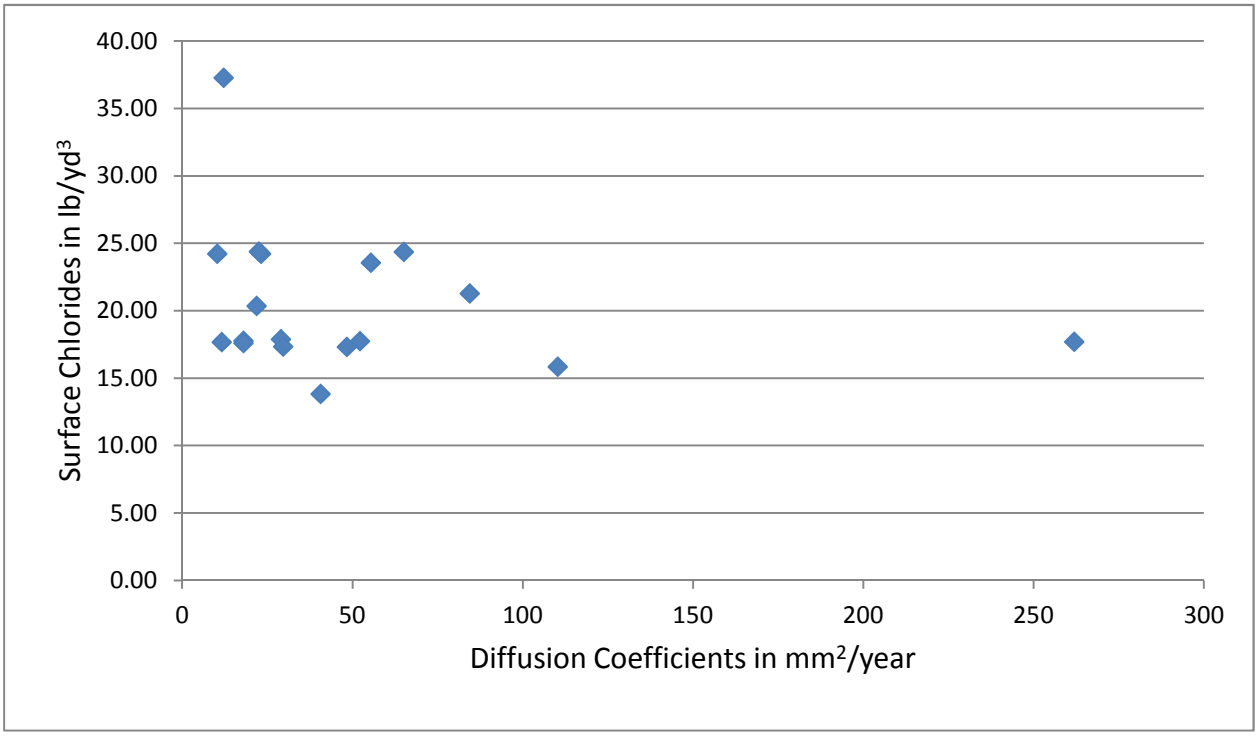

Figure 134 – Relationship between Surface Chlorides and Diffusion Coefficients

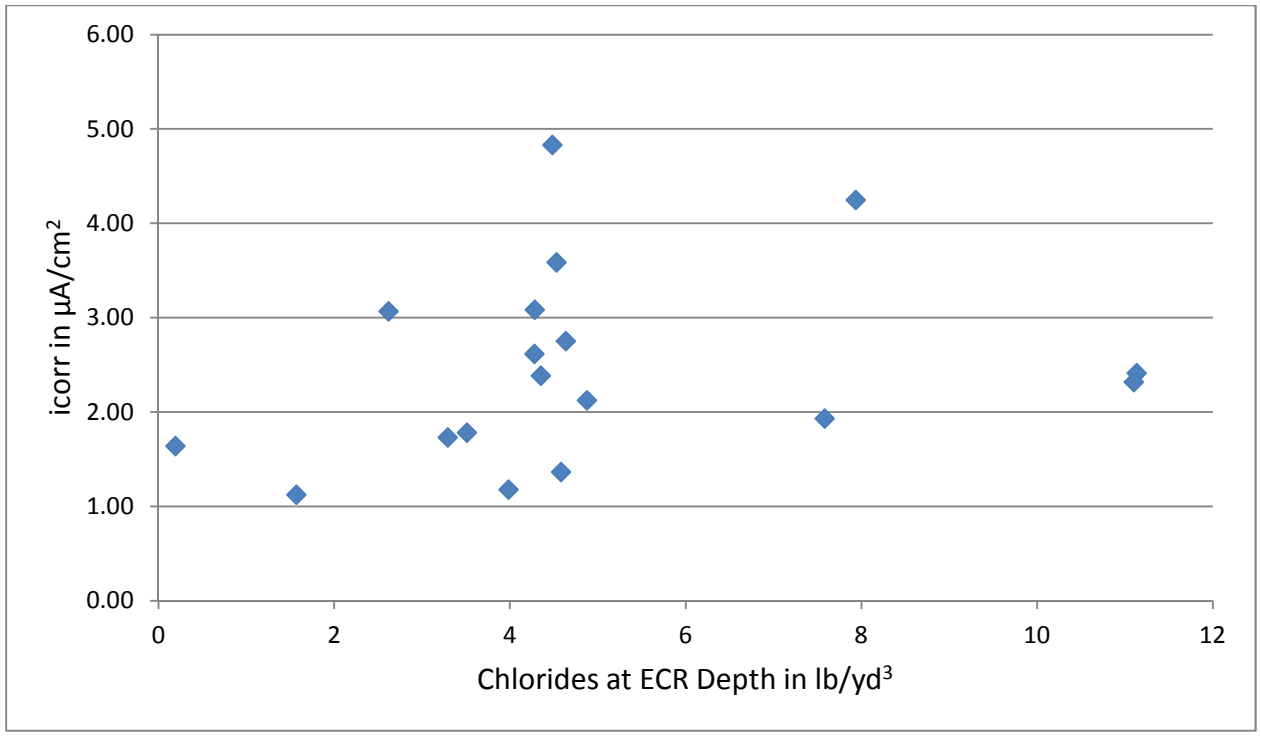

Figure 135 - Relationship between Corrosion Rates and Chlorides at ECR Depth

Figure 134 shows the scatter plot between surface chloride concentration and the diffusion coefficients. As expected according to the Fick's Second Law of diffusion, there is no relationship between the two factors. Figure135 presents the relationship between the corrosion current densities and chloride concentration at the ECR depth. This is in contrast to the VA deck where the corrosion current density increased with chloride concentration at the ECR depth. It illustrates the difference in performance of ECR that appears to be related to coating corrosion protection performance, as observed in Brown's work (2002).

Crack Influence

It is reasonable to expect the presence of cracks to have an influence on the rate of ingress of chloride into the concrete. Figure 136 presents a scatter diagram of cracks widths and diffusion coefficients for the 12 readings. No relationship is observed, which may be related to the limited amount of observations.

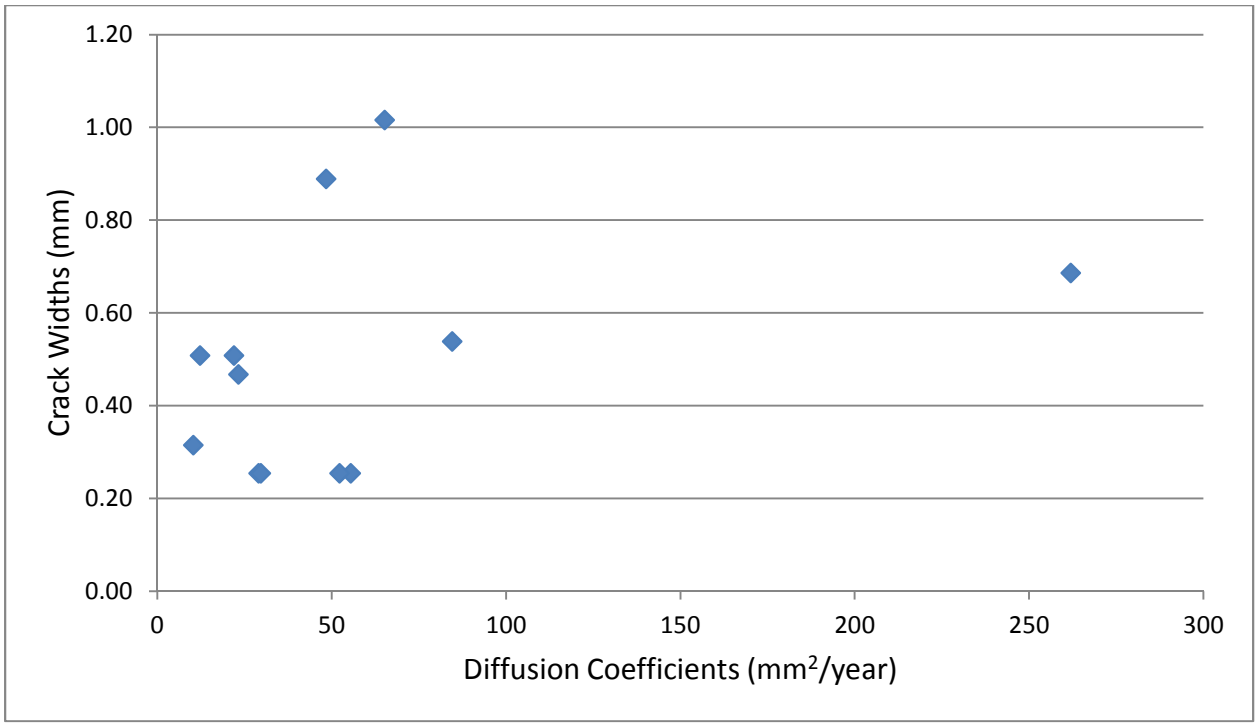

Figure 136 – Relationship between Crack Widths and Diffusion Coefficients

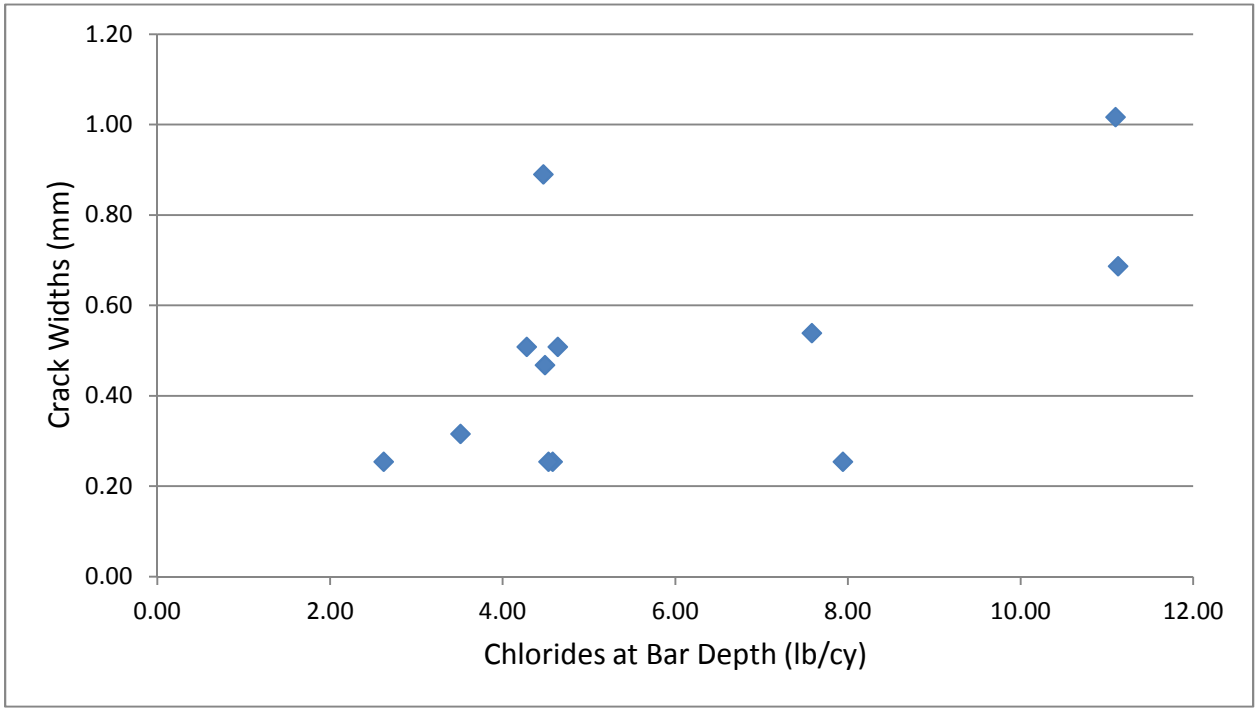

Figure 137 – Relationship between Crack Widths and Chlorides at Bar Depth

Figure 137 presents a scatter diagram between cracks widths and corresponding chloride contents at bar depths. A direct relationship can be observed from the scatter plot. It will be beneficial to check the influence of cracks on corrosion measurements as well.

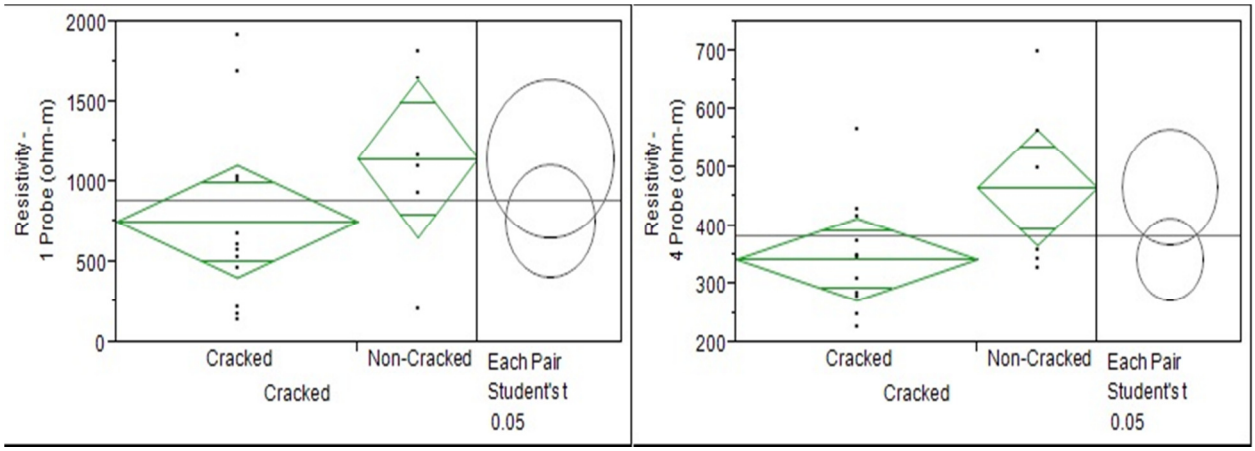

Figure 138 – ANOVA of One-Point and Four-Point Resistivities for Cracked and Non-Cracked Locations

Figure 138 presents the ANOVA statistical analysis performed between cracked and non-cracked locations for one-point and four-point resistivities. It can be noted that there are no significant differences between the cracked and non-cracked locations for OPR, which is not unexpected if the crack is not filled with water. There is a significant difference observed from the student's t-test for FPWR.

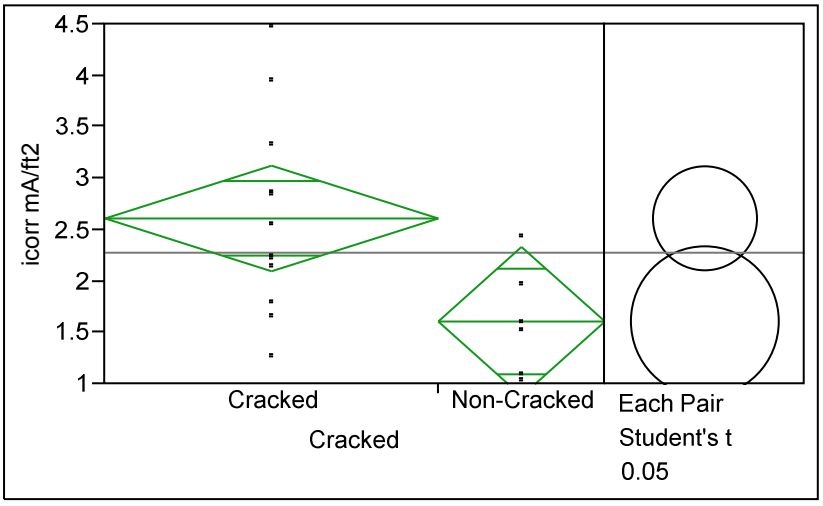

Figure 139 – ANOVA of Corrosion Current Densities for Cracked and Non-Cracked Locations

Figure 139 presents the ANOVA on 3LP corrosion rates for cracked and non-cracked locations. A significant difference may be noted from the student's t-test. The cracked locations exhibit higher corrosion rates compared to the non-cracked locations.

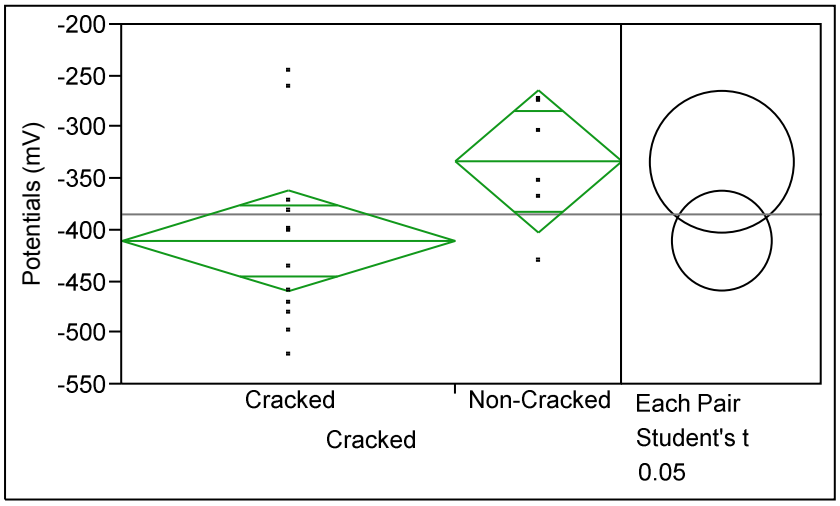

Figure 140 – ANOVA of Corrosion Potentials for Cracked and Non-Cracked Locations

Figure 140 presents the ANOVA on corrosion potentials for cracked and non-cracked locations. The non-cracked measurements show lower potentials for corrosion compared to the cracked locations. But, there is no significant difference between them.

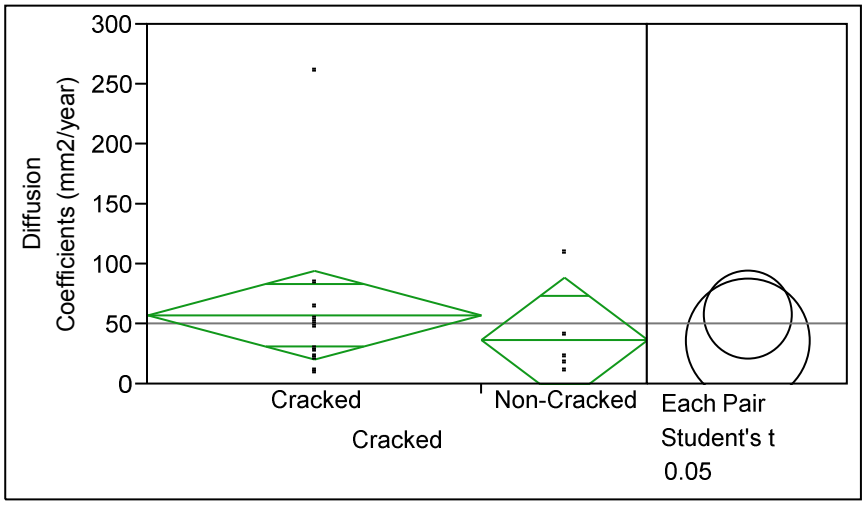

Figure 141 – ANOVA of Diffusion Coefficients for Cracked and Non-Cracked Locations

Figure 141 presents the ANOVA on diffusion coefficients for cracked and non-cracked locations. No significant difference can be observed from the analysis.

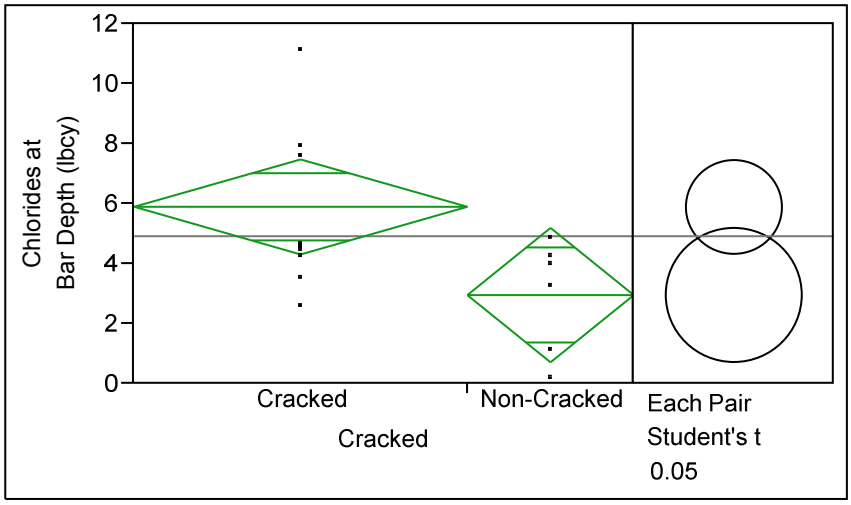

Figure 142 – ANOVA of Chlorides at Bar Depth for Cracked and Non-Cracked Locations

Figure 142 presents the ANOVA of Chlorides at Bar Depth for Cracked and Non-Cracked Locations. A significant difference can be observed from the analysis, which agrees with the relationship between crack widths and chlorides at bar depths. Thus, presence of cracks may have an influence on the diffusion of chlorides to the reinforcement bar depths.

The service life estimation was not performed on New York pilot bridge, since there are insufficient amount of values for diffusion coefficients and surface chloride concentrations.

MINNESOTA PILOT BRIDGE

BACKGROUND

Minnesota pilot bridge is located about 90 miles north of Minneapolis in Sandstone, Pine County, Minnesota. The bridge was built in 1948 and carries Trunk Highway 123 over Kettle River. It was rebuilt in 1984. The structure (NBI Structure Number: 5718) is designed as a steel continuous truss structure. The bridge was inspected in 2010 during when the deck had been in service for 26 years.

The bridge is a three span continuous structure with two lanes. Length of the whole bridge deck is 403 ft. (122.8 m), span1 and span3 being 101 ft. (30.78 m) long each and span 2 201 ft. (61.26 m) long, and the width is 32 ft. (9.75 m) excluding the sidewalk. The annual average daily traffic was 2050 in the year 2004. In the inspection report, the deck was reported with “Satisfactory Condition”, while superstructure with “Fair Condition” and substructure with “Good Condition”. The concrete deck was built with epoxy-coated reinforcement.

FIELD CONDITION ASSESSMENT

Visual inspection and damage survey was conducted on the pilot bridge by the personnel from Parsons-Brinckerhoff. The corrosion assessment of the bridge deck was conducted by the personnel from Utah State University and Birmingham Young University in 2010. The list of test and samples collected are as follows.

1. Deck reinforcement mat continuity test
2. Reinforcement cover depth determination
3. Resistivity tests – one and four points
4. Half-cell potential tests
5. Linear polarization measurements
6. Rebound hammer testing
7. Collection of powdered concrete samples for chloride contents
8. Extraction of concrete cores for various laboratory tests.

ANALYSIS AND DISCUSSION

To run the service life estimation model, damage percentile, reinforcement cover depth, surface chloride concentration, diffusion coefficients, and chloride initiation rates are necessary. For corrosion tests and chloride sampling, 20 locations were selected form the bridge deck, 5 from spans 1 and 3, and 10 from span 2.

Damage Survey

Damage survey was conducted to quantify the delaminations, spalls, and cracks in the bridge deck. Figures 143, 144, and 145 present the damage survey results mapped on the deck plan of span 1, span 2 and span 3, respectively.

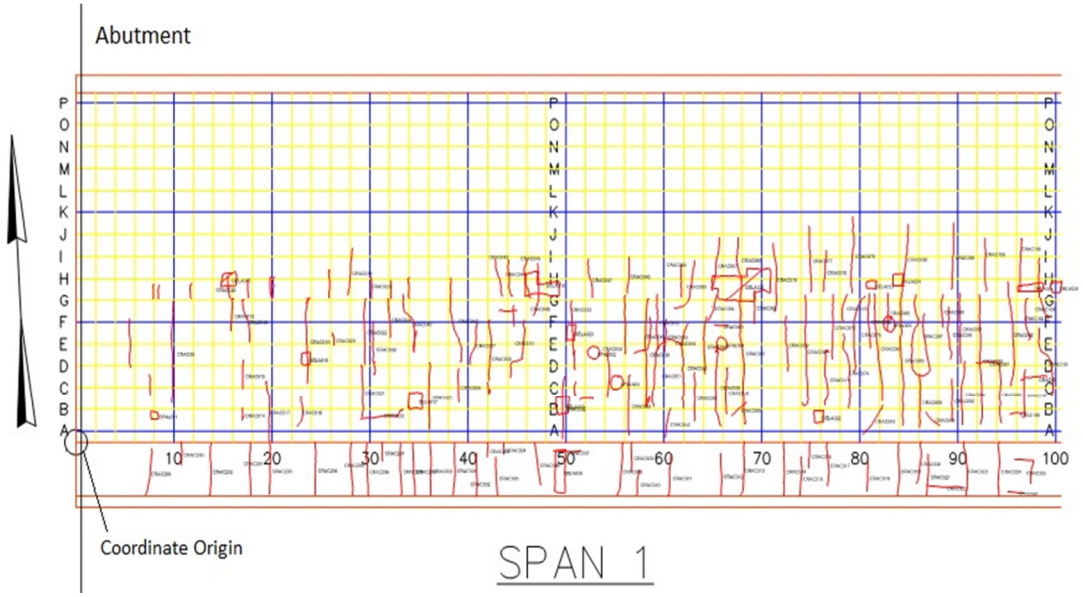

Figure 143 – Damage Survey of Span 1

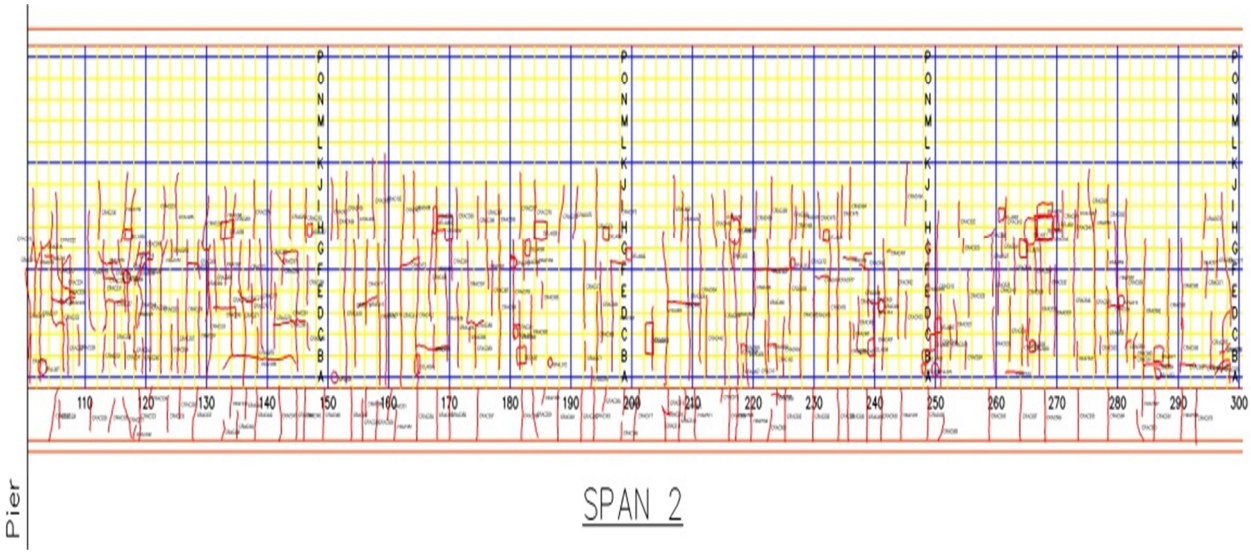

Figure 144 – Damage Survey of Span 2

It can be noted that there are a large number of cracks throughout the length of all three spans. Delaminations and spalls are distributed throughout the deck. The deterioration percentage of the whole bridge deck was visually calculated to be approximately 4 % at the time of inspection. Note that the damage survey results represent only the half of the bridge deck.

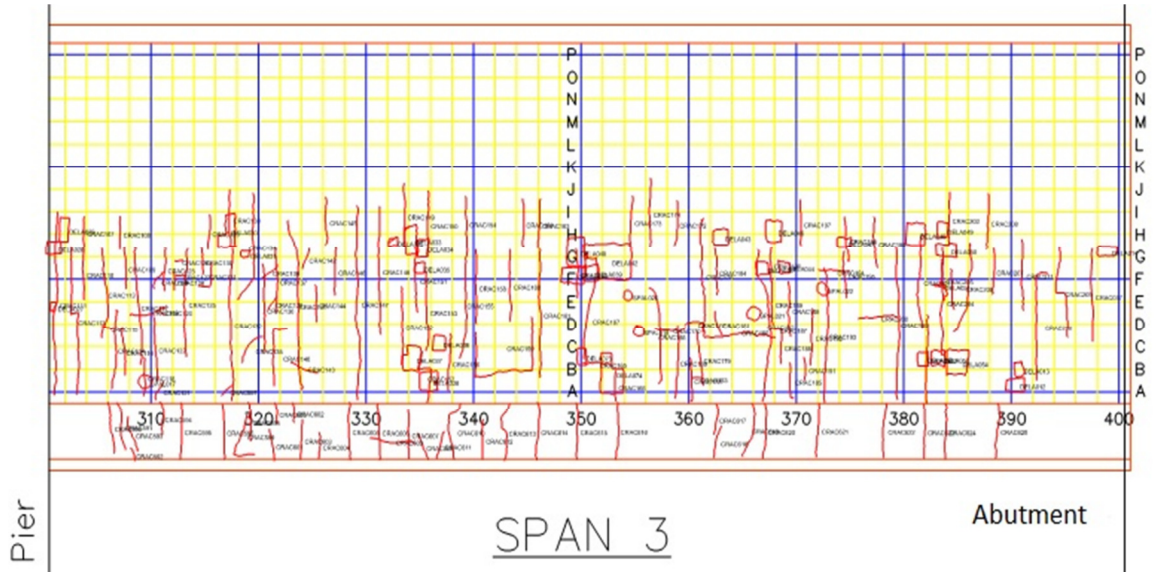

Figure 145 – Damage Survey of Span 3

Cover Depths

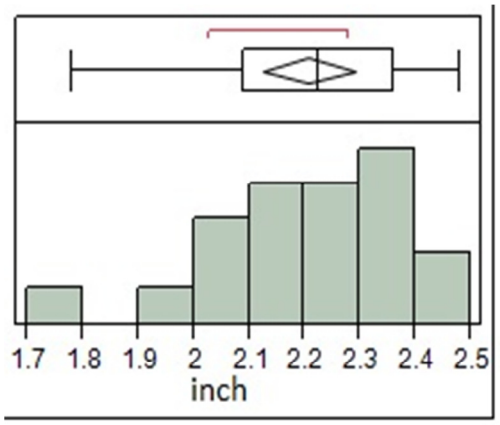

Mean	2.20
Median	2.22
Stdev	0.18
Upper 95%	2.56
Lower 95%	1.84

Figure 146 – Distribution of Cover Depths from 20 Locations

Figure 146 presents the distribution of the longitudinal cover depths taken from 20 test locations. Mean and median are not different at 2.2 in. (56 mm) and the standard deviation is 0.18 in. (4.6 mm). Based on a normal distribution, 10% of the ECR has a cover depth of less than 2 in. (51 mm).

Surface Chloride Concentration

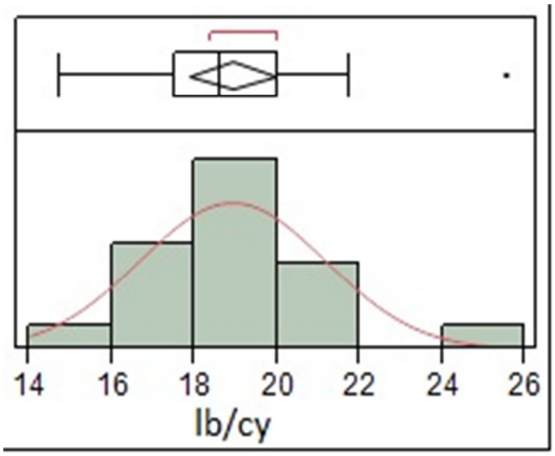

Mean	18.91
Median	18.64
Stdev	2.24
Upper 95%	23.39
Lower 95%	14.43
N	20

Figure 147 – Distribution of Surface Chloride Concentration from 20 Locations

Figure 147 presents the distribution of the surface chloride concentration from 20 locations. The distribution appears to be normal with the mean and median equal at 18.9, 18.6 lb/yd^3, respectively.

Diffusion Coefficients

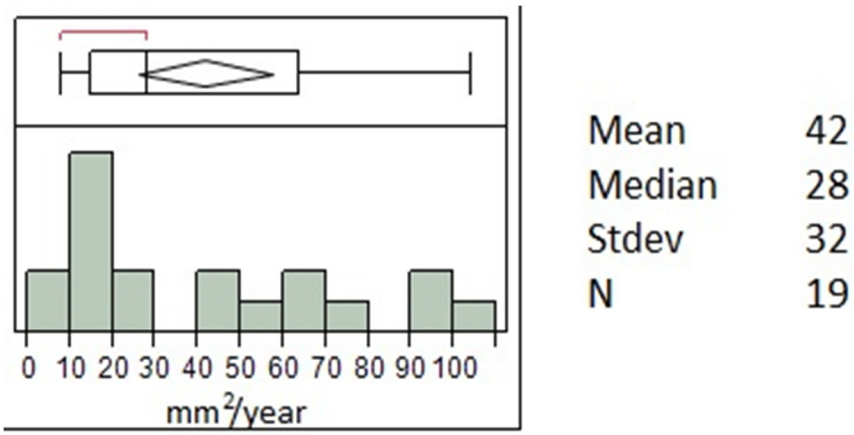

Figure 148 – Distribution of Apparent Diffusion Coefficients

Figure 148 presents the distribution of the apparent diffusion coefficients by discarding one very large value. The distribution appears similar to that of VA, NJ, NY, and FL pilot bridges, skewed towards the lower values. It is to be noted that the range of the diffusion coefficients are the same as that of VA, NJ, and NY pilot bridges, those without pozzolons.

Service Life Estimation

The service life estimation of the MN pilot bridge deck was run using the above data. The bridge deck was 26 years in service when the inspection was conducted. Table 34 presents the trials of chloride initiation rates used in the model.

Table 34 – Chloride Initiation Rates and Service Life Trials

Trials	C_{xt} (lb/yd³)			4% Initiation (year)	Cracking time (year)	Total (year)
	Min	Max	Mode			
1	0.66	10.6	2.37	6	11	17
2	0.66	10.6	6	13	11	24
3	0.66	12	7	14	11	25

It can be noted that when the whole range of chloride initiation rates are used, the prediction of service life is 9 years less than the actual life. When the chloride initiation mode and maximum are increased, this service life is closer to the actual life 26 years.

However, it is suspected that the actual deterioration rate at the time of inspection is much higher than the value used. The presence of large number of cracks over the entire length of the bridge deck was ignored in the calculation of the deterioration rate. It is reasonable to expect the cracks to have an influence on corrosion as illustrated in the NY pilot bridge. In addition, the smaller number of data points needed to provide a 95% confidence at a power 0.9 as illustrated in the VA pilot bridge results in uncertainty in the results. The diffusion curve for MN pilot bridge is presented in Figure 149.

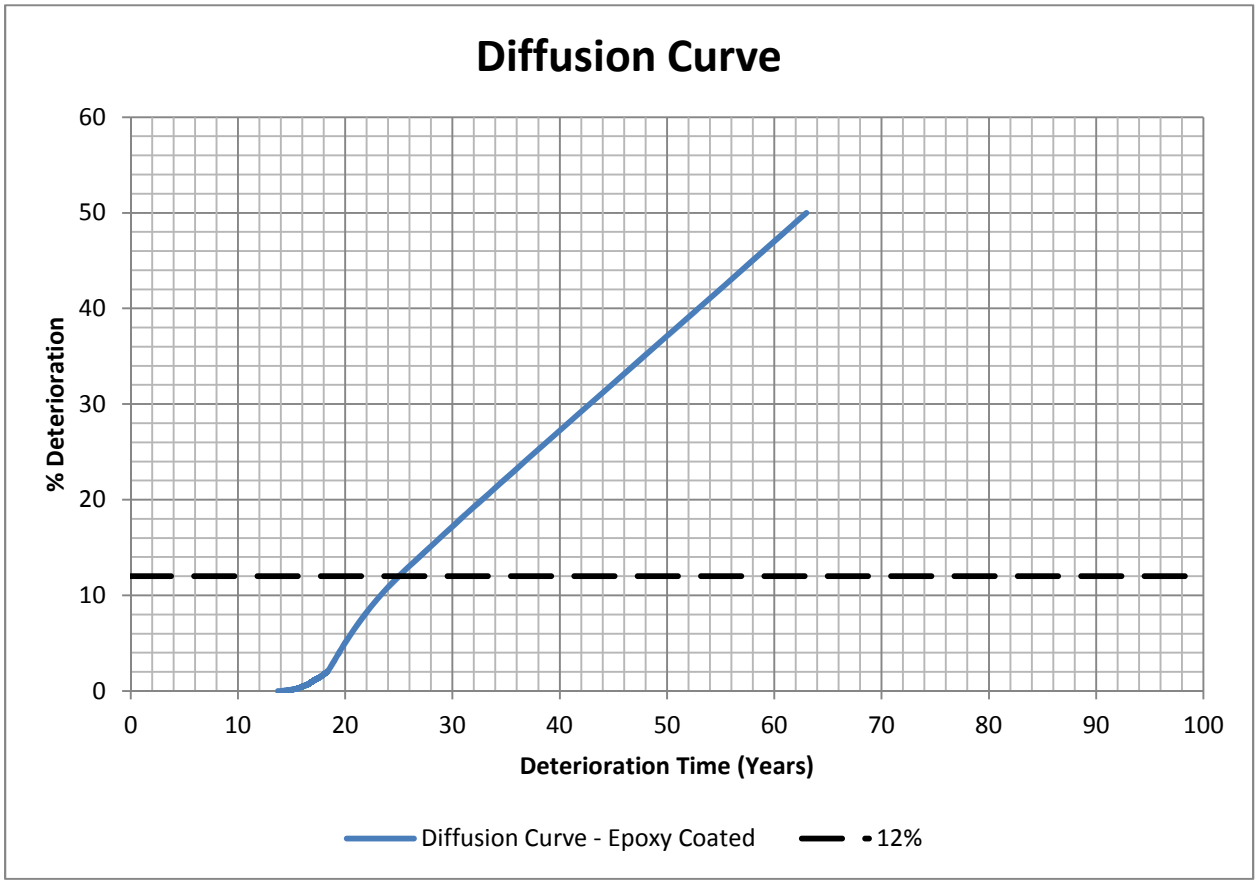

Figure 149 – Diffusion Curve of Minnesota Pilot Bridge

CONCLUSIONS

During the analysis of the data from LTBP eastern pilot bridges, conclusions and recommendations were formed in order to improve the process of data collection, to identify more precise testing methodologies, and improve the interpretation of the analyzed data.

1. Testing locations should be selected such that the data collected from the sample spaces are representative of the condition on the entire bridge deck. Collected from the Virginia Bridge, data obtained from the undamaged areas of the deck appear to be representative of the whole deck.

2. Interpretation of the various testing methodologies utilized needed to be refined. The following interpretations match the existing conditions of the Virginia pilot bridge which contains ECR. Majority of data from New Jersey pilot bridge, which contains bare steel, were in low to moderate corrosion risk interpretation range, which may be representative of the deck corrosion condition. Most of the data from New York pilot bridge, which contains ECR, were in moderate to high corrosion risk interpretation range that may be representative of the deck corrosion condition. Florida pilot bridge service life estimation showed that active corrosion has not initiated yet in the deck, which supports the electrical test data that are in low corrosion risk range.

Table 35 – Revised Interpretations for Tests

Corrosion Risk	Potentials (mV)	Corrosion Rate ($\mu A/cm^2$)	Four- Point Resistivity (ohm-m)
High	< -300	> 3.0	< 400
Moderate	-200 to -300	1.0 to 3.0	400 to 650
Low	> -200	< 1.0	> 650

3. Corrosion potentials may be sufficient to characterize the corrosion state of decks built either with bare steel or ECR, provided continuity of the top mat is established.

4. Single probe resistivity test may be useful in assessing the condition of the epoxy coating. However, further field investigations are needed to determine and verify the best interpretations.

5. Thirty test locations are needed to sufficiently determine the variability associated with the surface chlorides, diffusion coefficient and cover depth for use in the service life estimate model.

6. For the triangular chloride corrosion initiation function, a minimum of 0.6, mode of range 1.0 to 1.5, and maximum of range 3.0 to 5.0 lb/yd^3 may be used for ECR steel bars. In the service life model of VA pilot bridge, a minimum, maximum, and mode of 0.6, 4, 1.3 lb/yd^3 was found suitable. For NJ pilot bridge with bare steel, minimum, maximum, and mode of 0.6, 5, and 1.3 lb/yd^3 were suitable. In some cases the corresponding distribution may be needed. For Minnesota pilot bridge with ECR, a minimum, maximum, and mode of 0.66, 12, and 7 lb/yd^3 were found suitable. However, further field investigations are needed to better identify varying performance conditions.

7. Reinforced concrete bridges components are to be wetted a few hours before the electrical measurements are taken. The increase and uniformity of concrete moisture content aids to quickly stabilize the electrical readings and comparison of results between multiple bridges.

8. Presence of a low permeability overlay can significantly increase the service life, provided the existing top surface concrete that contained considerable chlorides has been removed completely. The service life estimation of the NJ pilot bridge using the deterioration model in Figure 107 presents that at 41 years of service, the bridge would have gone through approximately 7% of damages. But, the actual damage percentile recorded at 41 years of service was less than 1%.

9. It should be noted that the diffusion coefficients calculated for the VA, NJ, and MN pilot bridges are in similar ranges, 10 to 110 mm^2/year, 6 to 128 mm^2/year, 9 to 108 mm^2/year respectively. Diffusion coefficients for NY pilot bridge are in range 10 to 110 mm2/year, if one value, 262 mm^2/year, is ignored. It may be related to the similar concrete mix used in the VA, NJ, MN, and NY bridge decks. Whereas the diffusion coefficients calculated for FL

pilot bridge is in the range of 1 to 12 mm^2/year, which may be related to the microsilica pozzolon in the concrete mix.

Table 36 – Diffusion Coefficients of Bridge Decks

Bridge	Virginia	New Jersey	New York	Minnesota	Florida
Diff. Coeff. (mm^2/year)	10 to 110	6 to 128	10 to 110	9 to 108	1 to 12

10. Surface chlorides increase with the increasing usage of deicing salts. New York and Minnesota pilot bridges with very high deicing salt application had surface chloride ranges of 13.8 to 37.3 lb/yd^3, and 14.8 to 25.5 lb/yd^3, respectively. Virginia and New Jersey pilot bridges with moderate deicing salt application had surface chloride ranges of 3.1 to 15.1 lb/yd^3, and 2.7 to 9.7 lb/yd^3, respectively. Florida pilot bridge, where deicing salt is not applied, has a surface chloride range of 0.31 to 0.96 lb/yd^3. In none of the above cases, a relationship between surface chloride and diffusion coefficients was found. Thus, diffusion coefficients depend upon the concrete quality.

Table 37 – Surface Chloride Concentrations of Bridge Decks

Bridge	Virginia	New Jersey	New York	Minnesota	Florida
Surface Chloride (lb./$yd.^3$)	3.1 to 15.1	2.7 to 9.7	13.8 to 37.2	15.0 to 25.8	0.46 to 1.1

RECOMMENDATIONS

For future bridge deck chloride-induced corrosion modeling performance, the following is recommended.

1. Damage survey (Patches, spalls, and delaminations)

2. Thirty surface chloride contents

3. Thirty cover depths

4. Three cores to determine diffusion coefficients to indicate the range of values

5. Modeling diffusion coefficient beginning values minimum, maximum, and mode 8, 100, and 15 mm^2/year for concrete with no pozzolon.

6. One core for petrographic analysis to determine presence or absence of pozzolons.

RECOMMENDATIONS FOR FUTURE RESEARCH

A diffusion coefficient profiling must be conducted for various weather conditions across the country, since the diffusion rates are the hardest to obtain. This study only included five bridge decks, the results of which do not have enough confidence to form a profile.

Overlaying the bridge deck increases the service life of the structure. It is important to test a number of structures with overlays to be encapsulated and run using the service life program.

The crack prone structures such as the adjacent box beam structures must have their damage percentiles calculated by including the cracks with a suitable multiplier. More research is necessary on a number of such bridge decks to estimate the suitable multipliers needed. Data from a number of bridge decks must be analyzed to further verify the chloride initiation concentration for ECR and bare steel reinforcement.

REFERENCES

Ali H. Al-Gadhib, “Numerical Simulation of Chloride Diffusion in RC Structures and the Implications of Chloride Binding Capacities and Concrete Mix”, International Journal of Civil & Environmental Engineering IJCEE-IJENS Vol. 10 No. 5, 2010.

Alonso, C., Andrade, C., Rodriguez, J., and Diez, J.M., “Factors controlling cracking of concrete affected by reinforcement corrosion,” *Materials and Structures*, Vol. 31, pp.435-441, 1998.

ASTM C 39/C 39M-09a - Standard Test Method for Compressive Strength of Cylindrical Concrete Specimens. ASTM Annual Book of ASTM Standards, Vol. 04.02.

ASTM C 469-02 - Standard Test Method for Static Modulus of Elasticity and Poisson's Ratio of Concrete in Compression. ASTM Annual Book of ASTM Standards, Vol. 04.02.

ASTM C 876-09 - Standard Test Method for Half-Cell Potentials of Uncoated Reinforcing Steel in Concrete. ASTM Annual Book of ASTM Standards, Vol. 04.02.

ASTM C 1152/C 1152M-04 - Standard Test Method for Acid-Soluble Chloride in Mortar and Concrete. ASTM Annual Book of ASTM Standards, Vol. 04.02.

ASTM C 1202-10 - Standard Test Method for Electrical Indication of Concrete's Ability to Resist Chloride Ion Penetration. ASTM Annual Book of ASTM Standards, Vol. 04.02.

Balakumaran, S.S.G. (2010). Influence of Bridge Deck Concrete Parameters on the Reinforcing Steel Corrosion, Civil and Environmental Engineering. Blacksburg, VA, Virginia Polytechnic Institute and State University, MS, p188.

Bažant, Z. P., “Physical Model for Steel Corrosion in Concrete Sea Structures - Theory,” *Journal of the Structural Division*, Vol. 105, ST6, pp. 1137-1154, 1979.

Bažant, Z. P., “Physical Model for Steel Corrosion in Concrete Sea Structures - Application,” *Journal of the Structural Division*, Vol. 105, ST6, pp. 1155-1166, 1979.

Bamforth, P.B., “The derivation of input data for modeling chloride ingress from eight-year UK coastal exposure trials,” *Magazine of Concrete Research*, Vol. 51, No. 2, pp.87-96, 1999.

Berkeley, K.G.C., Pathmanaban, S., "Cathodic Protection of Reinforcement Steel in Concrete", Butterworth & Co. (Publishes) Ltd., 1990.

Boddy, A., E. Bentz, M.D.A. Thomas, and R.D. Hooton, “An overview and sensitivity study of a multimechanistic chloride transport model,” *Cement and Concrete Research*, Vol. 29, pp. 827-837, 1999.

Broomfield, J.P., “Corrosion of Steel in Concrete”, Taylor and Francis, 2007.

Brown, M.C., “Corrosion Protection Service Life of Epoxy Coated Reinforcing Steel in Virginia Bridge Decks”, Civil and Environmental Engineering, Virginia Polytechnic Institute and State University, Blacksburg, PhD Dissertation, 2002.

Buchanan, M.P., “Shrinkage of Latex-Modified and Micro Silica Concrete Overlay Mixtures”, Civil and Environmental Engineering, Virginia Polytechnic Institute and State University, Blacksburg, MS Thesis, 2002.

Bungey, J. (1989). "Testing of Concrete in Structures", 2nd Edition. New York, NY, Chapman & Hall.

Cady, P.D. and R.E. Weyers, “Chloride Penetration and the Deterioration of Concrete Bridge Decks,” *Cement, Concrete, and Aggregates*, CCAGDP, Vol. 5, No. 2, pp. 81-87, Winter 1983.

Cady, P.D. and R.E. Weyers, “Deterioration Rates of Concrete Bridge Decks,” *Journal of Transportation Engineering,* Vol. 110, No. 1, 1984.

Carino, J. (1999). "Nondestructive Techniques to Investigate Corrosion Status in Concrete Structures." "Journal of Performance of Constructed Facilities" 13(3): 11.

Clear, K. C., Measuring Rate of Corrosion of Steel in Field Concrete Structures. Sterling, VA, Kenneth C. Clear, Inc. Concrete Materials and Corrosion Specialists, 1989.

Clemena, G. G., Jackson D. R., and Crawford G. C. “Use of Rebar Corrosion Rates in Condition Surveys of Concrete Bridge Decks,” an unpublished paper.

Collepardi, M. and S. Biagini, “Effect of Water/Cement Ratio, Pozzolanic Addition and Curing Time of Chloride Penetration into Concrete,” ERMCO 89, 1989.

Crank, J., “The Mathematics of Diffusion, Second Edition,” Oxford University Press, USA, 1980.

Feliu, S., Andrade, C., Gonzalez, J.A., Alonso, C., “A New Method for In-situ Measurement of Electrical Resistivity of Reinforced Concrete”, Materials and Structures, Vol. 29, pp 362-365, 1996.

FHWA Report, “2008 Status of the Nation’s Highways, Bridges, and Transit: Conditions & Performance, Report to Congress”, 2008.

Fitch M.G., R.E. Weyers, and S.D. Johnson, "Determination of End of Functional Service Life for Concrete Bridge Decks," *Transportation Research Record*, No. 1490, pp. 60- 66, 1995.

Hladky, K. et al., “Development in Rate of Corrosion Measurements for Reinforced Concrete Structures,” Corrosion *89*, No. 169, NACE, Houston, TX, 1989.

Kirkpatrick, T., “Impact of Specification Changes on Chloride Induced Corrosion Service Life of Virginia Bridge Decks,” Civil and Environmental Engineering. Blacksburg, VA, Virginia Polytechnic Institute and State University. MS Thesis, 2001.

Kotnarowska, D. “Influence of Ultraviolet Radiation and Aggressive Media on Epoxy Coating Degradation”, Progress in Organic Coatings Vol. 37 pg. 149 – 159, 1999.

Kuhlmann, L.A., “Latex Modified Concrete for the Repair and Rehabilitation of Bridges”, The International Journal of Cement Composites and Lightweight Concrete, Vol. 7 Num. 4, November 1985.

Kyle, N.L., “Subsidence Cracking of Concrete Over Steel Reinforcement Bar in Bridge Decks”, Civil and Environmental Engineering. Blacksburg, VA, Virginia Polytechnic Institute and State University. MS Thesis, 2001.

Larsen, E. “Service Life Determination of Concrete Bridge Decks and Bridge Deck Overlay Systems”, Civil and Environmental Engineering, Virginia Polytechnic Institute and State University, Blacksburg, MS Thesis, 1993.

Liang, L., T. Kirkpatrick, C. Anderson-Cook and R.E. Weyers, “Bridge Corrosion Analysis,” Software developed at Virginia Tech, 2001.

Liu, Y. and Weyers, R.E., “Modeling the Time-to-Corrosion Cracking in Chloride Contaminated Reinforced Concrete Structures,” *ACI Materials Journal*, Vol. 95, No.6, November-December 1998.

Liu, Y., “Modeling the Time-to-Corrosion Cracking of the Cover Concrete in Chloride Contaminated Reinforced Concrete Structures”, Civil and Environmental Engineering, Virginia Polytechnic Institute and State University, Blacksburg, PhD Dissertation, 1996.

Maheshwaran, T. and J.G. Sanjayan, “A semi-closed-form solution for chloride diffusion in concrete with time-varying parameters,” *Magazine of Concrete Research*, Vol. 56, No. 6, pp. 359-366, 2004.

Mangat, P.S., and B.T. Molloy, “Prediction of long term chloride concentration in concrete,” *Materials and Structures*, Vol. 27, pp. 338-346, 1994.

Manning, D.G., "Corrosion Performance of Epoxy-Coated Reinforcing Steel: North American Experience", Construction and Building Materials v. 10n. (5), pg. 349-365, 1996.

Martín-Pérez, B., S.J. Pantazopoulou, and M.D.A. Thomas, “Numerical solution of mass transport equations in concrete structures,” *Computer and Structures*, Vol. 79, pp. 1251-1264, 2001.

Mehta, K.P. Concrete: Microstructure, Properties, and Materials. 3rd Edition, New York: The McGraw-Hill Companies, 2005.

Millard, S.G., Gowers, K.R., “Resistivity Assessment of In-situ Concrete: The Influence of Conductive and Resistive Surface Layers”, Proceedings of The Institution of Civil Engineers - Structures and Buildings, Vol. 94 issue 4 pp 389-396, 1992.

Morinaga, S., “Prediction of Service Lives of Reinforced Concrete Buildings Based on Rate of Corrosion of Reinforcing Steel,” Special Report of the Institute of Technology, Skimiza Corporation, Japan, 1989.

Peterson, J. E., “A Time to Cracking Model for Critically Contaminated Reinforced Concrete Structures, Masters of Science Thesis, Virginia Polytechnic Institute and State University, Blacksburg, December, VA, 1993.

Pyć, W.A., “Field Performance of Epoxy Coated Reinforcing Steel in Virginia”, Civil and Environmental Engineering, Virginia Polytechnic Institute and State University, Blacksburg, PhD Dissertation, 1998.

Ramniceanu, A., “Investigation of Parameters Governing the Corrosion Protection Efficacy of Fusion Bonded Epoxy Coatings”, Civil and Environmental Engineering, Virginia Polytechnic Institute and State University, Blacksburg, PhD Dissertation, 2007.

Ramniceanu, A., Correlation of Corrosion Measurements and Bridge Conditions with NBIS Deck Rating. Civil and Environmental Engineering. Blacksburg, VA, Virginia Polytechnic Institute and State University. MS, 2004.

Ramniceanu, A., Weyers, R.E., Mokarem, D.W., “Bridge Deck Concrete Volume Change”, Virginia Transportation Research Council VTRC 10-CR5, 2010.

Saetta, A.V., R.V. Scotta, and R.V. Vitaliani, “Analysis of Chloride Diffusion into Partially Saturated Concrete,” *ACI Materials Journal*, V. 90, No. 5, 1993.

Spellman, D.L., and Stratfull R.F. “Chlorides and Bridge Deck Deterioration,” State of California Department of Public Works, Division of Highways, Materials and Research Department, Paper Sponsored by Committee on Effect of Ice Control and Presented at 49th Annual Meeting.

Sprinkel, M.S., “Performance Specification for High Performance Concrete Overlays on Bridges”, Virginia Transportation Research Council VTRC 05-R2, 2004.

Sprinkel, M.S., Ozyildirim, C., “Evaluation of High Performance Concrete Overlays Placed on Route 60 over Lynnhaven Inlet in Virginia”, Virginia Transportation Research Council VTRC 01-R1, 2000.

Torres-Acosta, A. and Sagüés, A.A., “Concrete Cracking by Localized Steel Corrosion, Geometric Effects,” *ACI Materials Journal*, Vol. 101, No. 6, Nov.-Dec., 2004.

US Environmental Protection Agency, “Bisphenol Action Plan”, 29 March, 2010.

Vu, K., Stewart, M.G., and Mullard, J., “Corrosion-Induced Cracking: Experimental Data and Predictive Models,” *ACI Structural Journal*, Vol. 102, No. 5, September- October, 2005.

Wenner, F., “A Method of Measuring Earth Resistivity”, Bulletin of the Bureau of Standards, Washington, Government Printing Office, 1915.

Weyers et al., “Concrete bridge Protection, Repair, and Rehabilitation Relative to Reinforcement Corrosion: A Methods Application Manual”, Strategic Highway Research Program-S-360. 1994.

Weyers et al., “Concrete Bridge Protection and Rehabilitation: Chemical and Physical Techniques – Service Life Estimates”, Strategic Highway Research Program-S-668. 1994.

Williamson, G., “Service life Modeling of Virginia Bridge Decks,” Civil and Environmental Engineering. Blacksburg, VA, Virginia Polytechnic Institute and State University. PhD Dissertation, 2007.

Zimmerman, L., Elsener, B., BÖhni, “Critical Factors for the Initiation of Rebar Corrosion”, “Corrosion of Steel in Concrete” Session at EUROCORR ’99, Aachen, Germany.

APPENDICES

Appendix A
Electrical Measurements of Pilot Bridges

VIRGINIA PILOT BRIDGE

Table A1 – CCD and Corrosion Potentials of VA Bridge

Span	Location	Location ID	Icorr *(mA/ft2)*	Icorr *(µA/cm2)*	Static Potential *(mV)*
1	1	G12	0.87	0.94	-186
1	2	B22	4.10	4.41	-251
1	3	G38	7.15	7.70	-498
1	4	C52	6.48	6.97	-353
1	5	H60	2.51	2.70	-271
1	6	B80	10.49	11.29	-453
1	7	H92	2.62	2.82	-305
1	8	C108	10.98	11.82	-437
1	9	G120	2.06	2.22	-238
1	10	D126	4.77	5.13	-372
1	11	Q48	1.16	1.25	-270
1	12	N72	0.76	0.82	-324
1	13	Q92	1.05	1.13	-325
1	14	O112	1.03	1.11	-255
1	15	Q128	0.63	0.68	-240
2	1	G142	1.16	1.25	-200
2	2	C152	3.66	3.94	-290
2	3	G164	1.58	1.70	-219
2	4	D178	4.35	4.69	-253
2	5	G190	5.68	6.12	-311
2	6	C202	1.52	1.64	-265
2	7	G216	2.46	2.64	-256
2	8	C248	4.75	5.11	-340
2	9	G254	1.58	1.70	-230
2	10	A264	2.43	2.62	-195
2	11	Q172	1.46	1.57	-334
2	12	N184	0.18	0.19	-173
2	13	R202	0.59	0.64	-216
2	14	N232	3.70	3.99	-575
2	15	Q256	6.84	7.36	-442
Mean			3.29	3.54	-303
Std dev			2.83	3.05	98
CV			86%	86%	-32%

Table A2 –OPR and FPWR Values of VA Bridge

Span	Location	Location ID	1-Probe Resistivity *(Ohm-m)*	4-Probe Resistivity *(Ohm-m)*
1	1	G12	910	378
1	2	B22	387	369
1	3	G38	116	184
1	4	C52	114	168
1	5	H60	633	361
1	6	B80	42	83
1	7	H92	299	290
1	8	C108	98	132
1	9	G120	279	325
1	10	D126	260	217
1	11	Q48	434	654
1	12	N72	516	706
1	13	Q92	270	1031
1	14	O112	270	512
1	15	Q128	236	788
2	1	G142	428	434
2	2	C152	163	456
2	3	G164	302	337
2	4	D178	131	414
2	5	G190	86	307
2	6	C202	640	708
2	7	G216	589	465
2	8	C248	185	501
2	9	G254	543	464
2	10	A264	189	514
2	11	Q172	113	460
2	12	N184	1380	967
2	13	R202	257	611
2	14	N232	1873	426
2	15	Q256	62	474
Mean			393	458
Std dev			398	225
CV			101%	49%

Table A3 – Cover Depths of VA Bridge

Span	**Location**	**Location ID**	**Transverse Bar Depth** *(in)*	**Truss Bar Depth** *(in)*
1	1	G12	2.50	2.10
1	2	B22	2.10	
1	3	G38	1.75	1.45
1	4	C52	1.90	
1	5	H60	1.80	1.60
1	6	B80	2.50	
1	7	H92	2.10	2.00
1	8	C108	2.15	2.15
1	9	G120	2.50	2.15
1	10	D126	2.45	2.40
1	11	Q48	2.20	2.10
1	12	N72	2.15	2.00
1	13	Q92	2.25	2.10
1	14	O112	2.40	2.40
1	15	Q128	2.10	2.15
2	1	G142	2.35	2.10
2	2	C152	2.40	2.40
2	3	G164	2.55	2.15
2	4	D178	2.60	2.50
2	5	G190	2.35	2.05
2	6	C202	1.90	1.80
2	7	G216	2.30	2.10
2	8	C248	2.20	
2	9	G254	2.25	1.95
2	10	A264	2.50	2.20
2	11	Q172	2.75	2.60
2	12	N184	2.40	1.90
2	13	R202	2.45	2.40
2	14	N232	1.55	1.45
2	15	Q256	2.15	2.25
Mean			2.25	2.09
Std dev			0.27	0.29
CV			12%	14%

FLORIDA PILOT BRIDGE

Table A4 – CCD and Corrosion Potentials of FL Bridge

Span	**Location**	**ID**	**Segment**	**Coordinate**		**Potentials**	**i_{corr}**
			(From South)	*Long. (ft)*	*Trans. (ft)*	*mV*	*μA/cm²*
1	Right lane (North)	7E	10	2296	29	-16.6	0.44
1	Right lane (North)	8E	12	2256	29	-3.3	0.41
1	Right lane (North)	9E	14	2222.5	29	-12.7	0.37
2	Right lane (North)	1E	2	2130	26	-46.4	0.37
2	Right lane (North)	2E	4	2110	25	-55.6	0.14
2	Right lane (North)	3E	6	2082.5	25	-76	
3	Right lane (North)	4E	11	1770	27	-54.8	0.19
3	Right lane (North)	5E	14	1740	26.5	-69.3	0.37
3	Right lane (North)	6E	17	1700	23	-80.3	0.39
1	Left Shoulder (South)	13E	3	2290	1	-35.8	0.42
1	Left Shoulder (South)	14E	6	2256	2	-9.6	0.44
1	Left Shoulder (South)	15E	9	2216	1	-28.3	0.83
2	Left Shoulder (South)	10E	8	2058	2	-53.8	0.51
2	Left Shoulder (South)	11E	10	2035	2		0.44
2	Left Shoulder (South)	12E	12	2010	2	-75.6	0.39
3	Left Shoulder (South)	16E	8	1810	1	-69.3	0.66
3	Left Shoulder (South)	17E	10	1791	2	-73.8	0.54
3	Left Shoulder (South)	18E	12	1760	1	-41.5	0.52
	Mean					-47.2	0.44
	Std dev					25.7	0.16
	CV					54	36

Table A5 –OPR and FPWR Values of FL Bridge

Span	Location	ID	Segment	Coordinate		1-Probe Resistivity	4-Probe Resistivity
			(From South)	*Long. (ft)*	*Trans. (ft)*	*(Ohm-m)*	*(Ohm-m)*
1	Right lane (North)	7E	10	2296	29	654	1085
1	Right lane (North)	8E	12	2256	29	1134	1985
1	Right lane (North)	9E	14	2222.5	29	866	3632
2	Right lane (North)	1E	2	2130	26	910	1117
2	Right lane (North)	2E	4	2110	25	963	1832
2	Right lane (North)	3E	6	2082.5	25	1646	
3	Right lane (North)	4E	11	1770	27	680	1998
3	Right lane (North)	5E	14	1740	26.5	730	1765
3	Right lane (North)	6E	17	1700	23	618	1870
1	Left Shoulder (South)	13E	3	2290	1	285	989
1	Left Shoulder (South)	14E	6	2256	2	640	3300
1	Left Shoulder (South)	15E	9	2216	1	316	919
2	Left Shoulder (South)	10E	8	2058	2	531	1117
2	Left Shoulder (South)	11E	10	2035	2	702	1392
2	Left Shoulder (South)	12E	12	2010	2	476	1941
3	Left Shoulder (South)	16E	8	1810	1	369	677
3	Left Shoulder (South)	17E	10	1791	2	322	1041
3	Left Shoulder (South)	18E	12	1760	1	407	843
	Mean					681	1618
	Std dev					340	827
	CV					50	51

Table A6 – Cover Depths of FL Bridge

Span	**Location**	**ID**	**Segment**	**Coordinate**		**Bar Size**	**Cover Depth**
			(From South)	*Long. (ft)*	*Trans. (ft)*	*(US #)*	*(inch)*
1	Right lane (North)	7E	10	2296	29	4	2
1	Right lane (North)	8E	12	2256	29	4	1.65
1	Right lane (North)	9E	14	2222.5	29	4	1.75
2	Right lane (North)	1E	2	2130	26	4	1.92
2	Right lane (North)	2E	4	2110	25	4	2.08
2	Right lane (North)	3E	6	2082.5	25	4	2.15
3	Right lane (North)	4E	11	1770	27	4	2.1
3	Right lane (North)	5E	14	1740	26.5	4	2.1
3	Right lane (North)	6E	17	1700	23	4	2.25
1	Left Shoulder (South)	13E	3	2290	1	4	2.4
1	Left Shoulder (South)	14E	6	2256	2	4	2.05
1	Left Shoulder (South)	15E	9	2216	1	4	2.25
2	Left Shoulder (South)	10E	8	2058	2	4	2.05
2	Left Shoulder (South)	11E	10	2035	2	4	2
2	Left Shoulder (South)	12E	12	2010	2	4	2.2
3	Left Shoulder (South)	16E	8	1810	1	4	1.6
3	Left Shoulder (South)	17E	10	1791	2	4	1.95
3	Left Shoulder (South)	18E	12	1760	1	4	2.35
	Mean						2.05
	Std. dev.						0.22
	C.V.						11

NEW JERSEY PILOT BRIDGE

Table A7 – CCD and Corrosion Potentials of NJ Bridge

ID	Coordinates		Static Potentials (mV)	icorr Values (mA/ft²)	icorr Values (μA/cm²)
	Long. (ft)	*Trans. (ft)*			
1	8	5	-200	1.07	1.16
2	14	3	-158	1.09	1.17
3	22	7	-102	0.55	0.59
4	32	5	-128	1.31	1.42
5	36	11	-84	0.60	0.65
6	48	5	-87	0.52	0.56
7	60	3	-184	2.05	2.21
8	62	11	-116	1.48	1.60
9	72	3	-213	3.39	3.66
10	84	7	-239	0.98	1.06
11	6	17	-192	1.16	1.26
12	10	22	-166	0.88	0.95
13	18	13	-107	0.63	0.68
14	24	19	-189	1.59	1.71
15	40	17	-112	1.46	1.58
16	46	15	-103	1.32	1.42
17	56	21	-102	0.26	0.29
18	62	21	-105	0.22	0.24
19	78	19	-141	0.55	0.59
20	86	17	-218	1.21	1.30
21	6	37	-337	3.72	4.01
22	12	25	-202	3.83	4.13
23	28	27	-210	1.91	2.06
24	34	35	-193	1.69	1.82
25	40	25	-160	3.87	4.17
26	42	29	-152	1.79	1.93
27	58	33	-150	1.97	2.13
28	68	37	-246	2.43	2.63
29	78	25	-178	3.31	3.58
30	80	29	-172	1.91	2.06
31	15	21	-124	0.44	0.48
32	64	27	-179	1.97	2.12
Mean			-164	1.60	1.73
Std dev			55	1.05	1.14
CV			34	66	66

Table A8 –OPR and FPWR Values of NJ Bridge

ID	Coordinates		One-Point Resistivity (Ohm-m)	Four-Point Resistivity (Ohm-m)
	Long. (ft)	*Trans. (ft)*		
1	8	5	179	1492
2	14	3	118	1974
3	22	7	233	1872
4	32	5	167	1388
5	36	11		1934
6	48	5	223	
7	60	3	119	1497
8	62	11	204	1809
9	72	3	179	2027
10	84	7	273	1936
11	6	17	221	2048
12	10	22	322	2032
13	18	13	162	1896
14	24	19	204	2069
15	40	17	257	1606
16	46	15	88	1556
17	56	21	277	1809
18	62	21	212	1692
19	78	19	253	1673
20	86	17	236	1303
21	6	37	91	473
22	12	25	132	476
23	28	27	185	646
24	34	35	146	774
25	40	25	105	519
26	42	29	182	840
27	58	33	192	1141
28	68	37	96	495
29	78	25	85	513
30	80	29	218	931
31	15	21	224	1479
32	64	27	199	814
Mean			187	1378
Std dev			62	566
CV			33	41

Table A9 – Cover Depths of NJ Bridge

ID	Coordinates		Transverse Bar Depth	Longitudinal Bar Depth
	Long. (ft)	*Trans. (ft)*		
1	8	5	2.70	2.80
2	14	3	3.20	3.20
3	22	7	2.85	2.90
4	32	5	2.80	2.80
5	36	11	2.85	2.85
6	48	5	2.75	2.75
7	60	3	3.00	3.15
8	62	11	2.95	2.95
9	72	3	2.90	3.00
10	84	7	2.45	2.45
11	6	17	2.85	
12	10	22	2.25	
13	18	13	2.45	2.60
14	24	19	2.15	2.15
15	40	17	2.55	2.60
16	46	15	2.55	2.60
17	56	21	2.60	2.50
18	62	21	2.65	2.65
19	78	19	2.45	2.50
20	86	17	2.20	
21	6	37	2.45	
22	12	25	2.40	
23	28	27	2.70	
24	34	35	2.40	
25	40	25	2.60	
26	42	29	2.45	
27	58	33	2.40	
28	68	37	2.30	
29	78	25	2.85	
30	80	29	2.40	
31	15	21	2.25	
32	64	27	2.30	
Mean			2.58	2.73
Std dev			0.26	0.27
CV			10	10

NEW YORK PILOT BRIDGE

Table A10 – CCD and Corrosion Potentials of NY Bridge

ID	Longitude (ft)	Transverse (ft)	icorr mA/ft²	icorr µA/cm²	Static Potentials (mV)
22	58	21			-295
21	60	23	2.50	2.69	-486
26	64	20	1.14	1.22	-284
29	70	20	1.06	1.14	-282
27	75	17	1.78	1.91	-277
30	78	15	1.60	1.73	-372
35	105	21	1.41	1.52	-479
34	93	23	1.40	1.50	-267
33	104	17	1.61	1.73	-278
TC4	82	15	2.86	3.08	-471
TC5	78	24	4.49	4.83	-480
TC6	76	25	2.22	2.39	-399
NC5 (31)	90	19	2.43	2.62	-303
NC6 (32)	110	21	1.52	1.64	-429
NC 4	30	22	1.97	2.12	-272
LC 4	20	24	2.85	3.07	-436
LC 5	120	21	2.24	2.41	-498
LC 6	146	17	1.66	1.78	-245
LC1	12	8	1.27	1.36	-261
LC2	70.0	8.0	2.55	2.75	-401
LC3	142.0	4.0	3.33	3.59	-521
TC1	86.0	6.0	1.79	1.93	-372
TC2	86.0	8.0	3.95	4.25	-458
TC3	85.0	5.0	2.15	2.32	-380
1NC	12.0	10.0	1.04	1.12	-274
2NC	70.0	7.0	1.09	1.18	-368
3NC	142.0	5.0	1.61	1.73	-351
C2	60	8	1.14	1.23	-352
C3	117	9	1.44	1.55	-345
T1	67	10	1.47	1.58	-345

3	76	8	3.19	3.43	-343
6	81	2	1.74	1.87	-354
7	81	6	1.38	1.49	-363
10	86	2	3.66	3.94	-463
12	90	2	1.26	1.36	-256
15	98	4	1.84	1.98	-308
18	105	4	1.16	1.25	-328
17	106	6	1.25	1.34	-383
20	108	8	1.18	1.27	-311
Mean			1.95	2.10	-361
Std dev			0.87	0.94	79
CV			45%	45%	22%

Table A11 –OPR and FPWR Values of NY Bridge

ID	Longitude (ft)	Transverse (ft)	Resistivity 1 - Probe (ohm-m)	Resistivity 4 - Probe (ohm-m)
22	58	21		579
21	60	23	791	350
26	64	20	1138	321
29	70	20	996	311
27	75	17	862	340
30	78	15	936	412
35	105	21	907	488
34	93	23	738	335
33	104	17	463	354
TC4	82	15	578	375
TC5	78	24	614	226
TC6	76	25	1013	280
NC5 (31)	90	19	935	328
NC6 (32)	110	21	1654	498
NC 4	30	22	208	702
LC 4	20	24	223	418
LC 5	120	21	149	428
LC 6	146	17	179	568
LC1	12	8	1923	311
LC2	70.0	8.0	1038	287
LC3	142.0	4.0	1696	249
TC1	86.0	6.0	683	347
TC2	86.0	8.0	465	350
TC3	85.0	5.0	530	280
1NC	12.0	10.0	1824	565
2NC	70.0	7.0	1104	345
3NC	142.0	5.0	1169	359
C2	60	8		
C3	117	9		
T1	67	10		

3	76	8		
6	81	2		
7	81	6		
10	86	2		
12	90	2		
15	98	4		
18	105	4		
17	106	6		
20	108	8		
Mean			877	385
Std dev			495	114
CV			56%	30%

Table A12 – Cover Depths of NY Bridge

ID	Longitude (ft)	Transverse (ft)	Cover Depths (inch)
22	58	21	1.29
21	60	23	1.90
26	64	20	2.05
29	70	20	1.95
27	75	17	1.95
30	78	15	2.15
35	105	21	2.15
34	93	23	1.90
33	104	17	1.40
TC4	82	15	2.25
TC5	78	24	2.15
TC6	76	25	2.40
NC5 (31)	90	19	1.90
NC6 (32)	110	21	2.60
NC 4	30	22	2.64
LC 4	20	24	2.36
LC 5	120	21	1.8
LC 6	146	17	2.64
LC1	12	8	2.70
LC2	70.0	8.0	2.30
LC3	142.0	4.0	2.55
TC1	86.0	6.0	2.50
TC2	86.0	8.0	2.30
TC3	85.0	5.0	2.40
1NC	12.0	10.0	2.90
2NC	70.0	7.0	2.20
3NC	142.0	5.0	2.40
C2	60	8	
C3	117	9	
T1	67	10	
3	76	8	2.40

6	81	2	2.25
7	81	6	2.40
10	86	2	2.10
12	90	2	2.10
15	98	4	2.15
18	105	4	1.85
17	106	6	2.55
20	108	8	2.05
Mean			2.21
Std dev			0.34
CV			15%

MINNESOTA PILOT BRIDGE

Table A13 – CCD and Corrosion Potentials of MN Bridge

Span	Location ID	Half-Cell Potential (mV)	Linear Polarization ($\mu A/cm^2$)
1	B8	-298	0.288
1	E54	-333	0.192
1	C54	-309	0.218
1	E66	-324	0.160
1	F82	-310	0.293
2	A104	-284	0.283
2	F118	-321	0.286
2	A152	-334	0.257
2	F182	-318	0.189
2	C180	-417	0.432
2	B186	-269	0.264
2	E226	-300	0.244
2	D244	-302	0.211
2	B250	-437	0.684
2	D280	-296	0.244
3	B308	-300	0.276
3	E354	-355	0.282
3	D354	-360	0.256
3	D366	-308	0.189
3	E382	-309	0.173
Mean		-324	0.271
Std dev		41	0.114
C.V.		13%	42%

Table A14 –OPR and FPWR Values of MN Bridge

Span	ID	2-Probe Resistivity (Ohm-m)	4-Probe Resistivity (Ohm-m)
1	B8	516	755
1	E54	793	1135
1	C54	444	465
1	E66	967	2210
1	F82	343	940
2	A104	876	530
2	F118	321	715
2	A152	311	210
2	F182	364	420
2	C180	480	305
2	B186	540	1015
2	E226	346	620
2	D244	542	1315
2	B250	164	150
2	D280	358	785
3	B308	185	330
3	E354	289	1060
3	D354	295	195
3	D366	419	520
3	E382	614	445
Mean		458	706
Std dev		217	487
C.V.		47%	69%

Table A15 – Cover Depths of MN Bridge

Span	ID	Longitudinal Cover Depth (inch)	Transverse Cover Depth (inch)
1	B8	2.12	1.92
1	E54	2.05	1.76
1	C54	2.03	1.88
1	E66	2.2	1.82
1	F82	2.13	2.03
2	A104	2.48	2.05
2	F118	2.17	1.92
2	A152	2.13	2.05
2	F182	2.28	2.07
2	C180	2.25	2.2
2	B186	1.95	1.83
2	E226	2.38	2.15
2	D244	2.27	1.93
2	B250	1.78	1.5
2	D280	2.3	2.24
3	B308	2.38	2.07
3	E354	2.47	1.93
3	D354	2.37	2.2
3	D366	2.33	2.17
3	E382	2.08	1.73
Mean		2.21	1.97
Std dev		0.18	0.19
C.V.		8%	10%

Appendix B
Chloride Measurements of Pilot Bridges

VIRGINIA PILOT BRIDGE

Table B1 – Chloride Concentrations of VA Bridge

Location ID	Concentration at Depth (lbs of Cl^-/yd^3 concrete) [Background Removed = 0.3 lb/yd^3]						
	0.25 - 0.75	*0.75 - 1.25*	*1.25 - 1.75*	*1.75 - 2.25*	*2.25 - 2.75*	*2.75 - 3.25*	*3.25 - 3.75*
G12	3.11	0.48	1.90	1.11	0.84	0.21	0.01
B22	10.85	8.00	3.90	2.98	1.57	0.96	0.39
G38	5.51	3.98	2.25	0.76	0.09		
C52	14.50	8.14	6.37	4.65	3.19	2.17	0.80
H60	5.71	5.12	2.82	1.78	1.07	0.83	0.58
B80	10.59	15.18	10.54	7.88	5.74	3.47	2.78
H92	6.61	5.71	3.74	2.76	1.94	1.19	0.56
C108	7.32	7.63	8.49	6.33	4.06	4.17	3.19
G120	7.43	5.12	3.31	1.43	1.96	0.83	
D126	8.60	7.20	3.85	3.54	3.49	4.15	
Q48	5.64	4.85	3.07	2.14	1.62	0.86	0.74
N72	5.54	2.07	0.83	0.22	0.08		0.02
Q92	9.83	6.79	5.02	2.81	2.00	1.12	1.12
O112	8.06	3.27	3.02	1.55	0.97	0.20	0.08
Q128	8.66	6.87	3.75	3.00	2.03	1.25	0.68
G142	9.31	7.47	3.71	5.00	3.29	2.31	2.87
C152	13.66	10.12	7.54	5.48	6.14	4.61	4.09
G164	5.23	3.94	2.33	1.67	0.99	0.63	0.29
D178	15.08	10.85	7.09	5.75	4.76	2.41	2.17
G190	9.10	6.34	4.04	2.21	1.99	1.31	0.65
C202	7.57	5.73	3.66	3.23	2.27	1.33	0.92
G216	11.13	7.05	4.05	3.36	2.52	1.00	0.52
C248	12.28	12.83	8.77	5.58	3.88	2.25	1.87
G254	9.83	6.66	4.69	3.22	1.71	1.11	1.27
A264	5.17	6.07	5.19	3.43	2.08	1.85	1.28
Q172	7.21	4.51	3.31	1.57	1.09	0.59	0.31
N184	5.15	4.72	2.98	1.51	1.11	0.46	0.14
R202	10.08	8.09	4.83	3.45	2.66	2.19	1.99
N232	7.13	4.88	2.96	2.45	1.55	0.50	0.61
Q256	13.40	11.59	6.32	5.91	4.28	4.41	4.25
Mean	8.64	6.71	4.48	3.22	2.37	1.73	1.27
Std dev	3.07	3.11	2.22	1.86	1.53	1.32	1.22
CV	36%	46%	50%	58%	65%	77%	97%

Table B2 – Diffusion Coefficients of VA Bridge

Location ID	**Diffusion Coeff. Without Background (0.3 lb/yd³)**	
	(in2/year)	*(mm2/year)*
G12	0.031	20
B22	0.028	18
G38	0.021	13
C52	0.034	22
H60	0.044	28
B80	0.046	30
H92	0.058	37
C108	0.154	99
G120	0.027	18
D126	0.088	57
Q48	0.055	35
N72	0.006	4
Q92	0.038	25
O112	0.016	10
Q128	0.042	27
G142	0.077	50
C152	0.090	58
G164	0.037	24
D178	0.051	33
G190	0.034	22
C202	0.054	35
G216	0.030	19
C248	0.034	22
G254	0.037	24
A264	0.057	36
Q172	0.027	18
N184	0.044	28
R202	0.053	34
N232	0.035	23
Q256	0.081	52
Mean	0.048	31
Std dev	0.028	18
CV	60%	60%

FLORIDA PILOT BRIDGE

Table B3 – Chloride Concentrations of FL Bridge

ID	Chloride Contents at Average Depths including Background = 0.15 lb/yd³ (lb/yd³)				
	0.5	*1*	*1.5*	*2*	*2.5*
1E		0.94	0.29	0.25	0.16
2E	0.46	0.11	0.10	0.26	0.19
3E	0.57	0.19	0.14	0.18	0.22
4E	1.11	0.19	0.12	0.12	0.15
5E	0.81	0.45	0.22	0.22	0.16
6E	0.75	0.15	0.16	0.10	0.25
13E	0.69	0.28	0.26	0.22	0.26
15E	0.54	0.17	0.22	0.15	0.13
10E	0.92	0.34	0.20	0.21	0.24
12E	0.99	0.17	0.46	0.26	0.31
16E	0.96		0.22	0.31	
18E	0.59	0.33	0.17	0.15	0.15
Mean	0.76	0.30	0.21	0.20	0.20
Std dev	0.21	0.24	0.10	0.06	0.06
CV	28%	78%	45%	31%	29%

Table B4 - Diffusion Coefficients of FL Bridge

ID	Diffusion Coeff. Without Background = 0.15 lb/yd³	
	inch²/year	*mm²/year*
1E	0.009	6
2E	0.005	3
3E	0.005	3
4E	0.002	1
5E	0.014	9
6E	0.004	3
13E	0.007	5
15E	0.004	3
10E	0.006	4
12E	0.005	3
16E	0.017	11
18E	0.010	6
Mean	0.007	5
Std dev	0.004	3
CV	61%	61%

NEW JERSEY PILOT BRIDGE

Table B5 – Chloride Concentrations of NJ Bridge

ID	Chloride Contents at Avg. Depths including Background = 0.35 lb/yd³ (lb/yd³)							
	0.5"	*1.0"*	*1.5"*	*2.0"*	*2.5"*	*3.0"*	*3.5"*	*4.0"*
1	6.14	4.91	4.32	3.39	2.07	1.48	1.25	0.80
2	5.16	3.77	3.63	3.55	3.06	2.33	2.11	1.66
3	4.10	2.92		1.09	1.07	1.08	0.70	0.28
4	3.87	5.36	3.60	1.65	1.16	0.85	0.71	0.60
5	6.66	4.50	4.21	2.70	1.68	1.02	0.67	0.40
6	5.72	4.01		2.32	1.66	1.04	0.45	0.41
7	4.48	4.05	3.23	2.83	1.64	1.69	1.54	1.04
8	5.77	3.99	3.33	1.49	1.36	1.14	0.45	0.04
9	2.72	2.76	1.87	1.98	2.51	1.13	1.18	0.82
10	9.73	5.93	4.03	2.45	1.28	0.89	0.53	0.25
11	4.85	3.50	2.01	0.85	0.24	0.13	0.00	0.00
12	4.88	2.50	1.65	0.85	0.60	0.50	0.31	0.00
13	6.31	4.60	3.70	1.56	1.27	1.27	1.12	0.71
14	5.32	3.04	1.81	0.79	0.28	0.05	0.00	0.01
15	5.20	3.26	2.76	1.55	0.86	0.41	0.35	0.16
16	5.92	4.04	2.45	1.44	0.61	0.47	0.26	0.03
17	6.54	4.18	3.30	1.24	0.59	0.40	0.28	0.18
18	7.55	5.28	3.92	2.07	0.99	0.66	0.25	0.04
19	5.28	3.03	1.91	0.68	0.12	0.10	0.08	0.05
20	6.64	4.88	4.16	2.10	0.89	0.57	0.19	0.00
21	6.77	6.97	3.80	2.56	2.20	1.51	1.26	1.18
22	6.12	4.47	3.12	2.47	0.95	0.75	0.57	0.34
23	6.36	4.06	1.83	0.59	0.31	0.00	0.12	0.00
24	7.57	7.22	3.87	0.55	0.93	0.28	0.10	0.00
25	6.53	4.90	3.34	1.06	0.49	0.34	0.27	0.07
26	6.51	4.28	2.33	0.66	0.29	0.04		0.00
27	6.29	4.14	1.72	0.68	0.58	0.16	0.00	0.00
28	5.59	3.55	2.66	0.97	0.76	0.57	0.34	0.22
29	5.64	4.63	3.42	1.66	1.15	0.82	0.82	0.62
30	7.47	5.26	3.41	1.30	1.01	0.51	0.26	0.28
31	6.05	2.93	1.84	0.79	0.46	0.32		0.00
32	6.65	4.38	2.74	1.26	0.91	0.73	0.50	0.46
Mean	5.95	4.29	3.00	1.60	1.06	0.73	0.56	0.33
Std dev	1.28	1.11	0.87	0.84	0.69	0.54	0.51	0.41
CV	21%	26%	29%	52%	65%	75%	91%	123%

Table B6 – Diffusion Coefficients of NJ Bridge

ID	Dc - All Depths (mm^2/year) 41 years	Dc - All Depths ($inch^2$/year) 41 years
1	41	0.063
2	93	0.144
3	25	0.038
4	48	0.074
5	25	0.039
6	26	0.040
7	63	0.098
8	20	0.031
9	128	0.198
10	12	0.019
11	11	0.017
12	8	0.013
13	22	0.034
14	8	0.012
15	16	0.025
16	12	0.019
17	12	0.019
18	15	0.024
19	8	0.012
20	19	0.029
21	35	0.054
22	20	0.031
23	7	0.011
24	14	0.021
25	13	0.020
26	8	0.013
27	8	0.012
28	13	0.020
29	23	0.036
30	13	0.020
31	6	0.010
32	12	0.019
Mean	24	0.038
Std dev	26	0.041
CV	107%	107%

NEW YORK PILOT BRIDGE

Table B7 – Chloride Concentrations of NY Bridge

ID	Chloride Contents at Avg. Depths including Background = 0.60 lb/yd³ (lb/yd³)							
	0.5	*1*	*1.5*	*2*	*2.5*	*3*	*3.5*	*4*
TC4	37.26	17.64	10.31	4.28	4.48	4.51		
TC5	24.21	10.94	10.71	4.49	4.15	4.29	3.28	1.44
TC6	17.30	10.99	10.26	4.47	4.35	5.82		
NC 4	15.84	13.30	10.39	7.11	4.88	4.52	5.66	6.46
NC5 (31)	13.81	17.64	4.34	4.28	3.22	0.44		
NC6 (32)	17.67	11.49	3.31	0.63	0.19			
LC 4	17.87	11.30	9.44	4.70	2.62	0.27		
LC 5	17.68	16.15	10.85	11.13	12.11	10.96		
LC 6	24.22	10.96	4.39	4.46	3.51	0.53		
LC1	17.33	11.09	4.45		4.58	3.89	2.21	1.25
LC2	20.35	11.13	4.87	5.85	4.64	2.83	1.30	0.02
LC3	17.73	11.10	11.09	4.56	4.53	4.46	4.49	
TC1	21.26	14.30	9.70	9.96	7.58	7.07	5.89	5.90
TC2	23.54	17.51	10.67	8.87	7.94	4.99	4.10	2.43
TC3	24.36	17.69	11.11	11.15	11.10	4.53	4.50	
1NC	17.76	11.16	4.54	4.57	1.57			0.02
2NC	17.58	10.97	4.52	3.99	2.00			
3NC	24.39	11.28	10.74	6.36	3.30	1.01		
Mean	20.6	13.1	8.1	5.9	4.8	4.0	3.9	2.5
Std dev	5.3	2.8	3.1	2.8	3.1	2.8	1.6	2.7
CV	26%	21%	39%	48%	64%	71%	41%	106%

Table B8 – Diffusion Coefficients of NY Bridge

ID	Diffusion Coeff. Without Background = 0.60 lb/yd³	
	(inch²/yr)	*(mm²/yr)*
TC4	0.019	12
TC5	0.036	23
TC6	0.075	48
NC5 (31)	0.063	41
NC6 (32)	0.018	12
NC 4	0.171	110
LC 4	0.045	29
LC 5	0.406	262
LC 6	0.016	10
LC1	0.046	30
LC2	0.034	22
LC3	0.081	52
TC1	0.131	85
TC2	0.086	55
TC3	0.101	65
1NC	0.028	18
2NC	0.028	18
3NC	0.035	23
Mean	0.079	51
Std dev	0.092	59
CV	117%	117%

MINNESOTA PILOT BRIDGE

Table B9 – Chloride Concentrations of MN Bridge

Span	Location ID	Chloride Contents Minus Background Values = 0.25 lb/cy at Average Depths (lb/yd^3)							
		0.25	**0.75**	**1.25**	**1.75**	**2.25**	**2.75**	**3.25**	**3.75**
1	B8	19.47	12.87	10.99	9.04	8.34	10.33	7.37	3.45
1	E54	18.40	13.14	7.07	2.77	1.90	1.66	0.48	1.17
1	C54	20.03	13.36	6.48	2.07	0.19	0.34	0.73	0.44
1	E66	16.67	15.06	11.75	10.41	4.66	2.00	0.25	0.09
1	F82	19.78	12.29	3.84	1.06	0.09	0.10	0.06	
2	A104	16.46	13.05	8.17	4.32	2.04	0.48	0.00	0.02
2	F118	18.72	10.61	4.15	0.78	0.18	0.52	0.06	0.00
2	A152	14.78	12.40	12.01	11.92	11.41	12.96	10.33	8.10
2	F182	20.05	14.28	3.95	0.86				
2	C180	18.55	14.82	10.61	5.40	3.30	0.98	0.10	
2	B186	17.44	16.40	11.84	10.44	6.87	3.97	2.34	0.72
2	E226	19.99	11.07	8.81	3.63	1.52	0.31		0.29
2	D244	20.14	18.19	11.55	11.20	6.11	1.92	0.65	
2	B250	18.94	14.06	13.38	10.27	9.91	7.94	0.61	
2	D280	17.82	13.32	6.11	3.58	2.04	0.60		
3	B308	16.74	14.86	11.69	11.81	11.00	6.01	2.73	0.99
3	E354	18.39	15.81	11.64	7.78	6.52	4.96	4.63	2.98
3	D354	18.46	18.38	13.80	12.28	8.82	7.72	4.95	2.64
3	D366	21.77	14.03	10.31	3.84	0.51	0.12	0.05	0.11
3	E382	25.53	22.19	18.15	13.08	6.69	2.72	1.14	0.36
Mean		18.91	14.51	9.82	6.83	4.85	3.46	2.15	1.53
Stddev		2.24	2.71	3.71	4.38	3.87	3.85	3.01	2.22
C.V.		12%	19%	38%	64%	80%	111%	140%	145%

Table B10 – Diffusion Coefficients of MN Bridge

Span	Location ID	Diffusion Coeff. (inch²/year)	Diffusion Coeff. (mm²/year)
1	B8	0.142	92
1	E54	0.027	17
1	C54	0.019	12
1	E66	0.077	50
1	F82	0.014	9
2	A104	0.037	24
2	F118	0.013	8
2	A152	x	X
2	F182	0.016	10
2	C180	0.044	28
2	B186	0.099	64
2	E226	0.024	15
2	D244	0.070	45
2	B250	0.118	76
2	D280	0.027	17
3	B308	0.147	95
3	E354	0.098	63
3	D354	0.161	104
3	D366	0.026	17
3	E382	0.070	45
Mean		0.061	42
Std dev		0.050	32
C.V.		82%	77%